UNIVERSITY OF SOUTHAMPTON
FACULTY OF PHYSICAL SCIENCES AND ENGINEERING
SCHOOL OF ELECTRONICS AND COMPUTER SCIENCE

Layered Turbo Trellis-Coded Modulation for Cooperative Communications

by

Hua Sun
B. Eng., MSc.

A doctoral thesis report submitted in partial fulfilment of
the requirements for the award of Doctor of Philosophy
at the University of Southampton

Mar 2016

SUPERVISOR:
Dr. Soon Xin Ng
PhD, SMIEEE, MIET, CEng, FHEA
Department of Electronics and Computer Science
and
Professor Lajos Hanzo
FREng, FIEEE, FIEE, DSc, EIC IEEE Press
Chair of Southampton Wireless Group
University of Southampton
Southampton SO17 1BJ
United Kingdom

Dedicated to my family and friends

UNIVERSITY OF SOUTHAMPTON

ABSTRACT

FACULTY OF PHYSICAL SCIENCES AND ENGINEERING
SCHOOL OF ELECTRONICS AND COMPUTER SCIENCE

Doctor of Philosophy

Layered Turbo Trellis-Coded Modulation for Cooperative Communications

by Hua Sun

In this thesis, we propose a suite of Turbo Trellis Coded Modulation (TTCM) aided transmission schemes designed for cooperative communications. Our objective is to combine Coded Modulation (CM) schemes with layered modulation arrangements in the context of cooperative communications for the sake of improving both the flexibility and power-efficiency of the entire system, while maintaining a moderate system complexity. Our investigations are focussed on the physical layer and on the network layer.

Specifically, we firstly introduce and study the family of Trellis-Coded Modulation (TCM) and TTCM schemes. The encoder, decoder, as well as the structure of both CM schemes is investigated in detail. The BER performance of four popular CM schemes, namely of TCM, of TTCM, of Bit-Interleaved Coded Modulation (BICM) and of BICM with Iterative Decoding (BICM-ID) is investigated, when communicating over both Additive-White-Gaussian-Noise (AWGN) and uncorrelated Rayleigh fading channels. By analysing the performance of the four CM schemes, we show that the TTCM scheme performs better than the other three CM schemes not only for transmission over AWGN but also over uncorrelated Rayleigh fading channels. When employing the TTCM scheme in Decode-and-Forward (DAF) relaying assisted cooperative communications, the BER performance of the system is substantially improved.

Then, we proposed two possible solutions for reducing the complexity of the TTCM scheme in the context of cooperative communications. The first one is based on Superposition Modulation (SPM) and the other relies on Hierarchical Modulation (HM). The transmitter may employ multiple low code-rate encoders, and the coded signal streams may be merged together by the SPM scheme to form a super-signal, so that they may be transmitted simultaneously without requiring extra transmit antennas. In this situation, the different signals exhibiting different error sensitivities may be mapped into specific SPM layers for transmissions. By contrast, a similar layered modulation scheme, namely HM may also be used, which is capable of reducing the complexity of the system. By employing the HM concept, the information in the different HM layers may be demodulated/decoded separately. Therefore, when the system is communicating based on the HM concept, it becomes quite flexible. When the relay node is capable of receiving all layers' information in the HM signal, it may opt for forwarding either all of its received streams, or only the specifically required streams, instead of fully retransmitting all information received from the source. In this way, the processing burden imposed on the relay node may be reduced.

Furthermore, the HM scheme may also be employed for improving the power-efficiency of the entire cooperative communication system. The original design objective of the HM scheme was that of providing Unequal Error Protection (UEP), while maintaining a high data rate. However, in cooperative communications, we may 're-purpose' the HM scheme for reducing the power dissipation of all the nodes in the cooperative networks. Hence, our research was then focussed on finding the appropriate HM aided cooperative strategy, which is capable of reducing the power consumption of the entire system. As a further contribution, the Discrete-input Continuous-output-Memoryless-Channel's (DCMC) capacity was also quantified. We relied on the DCMC capacity metric to find a lower-bound for the performance of HM aided cooperative communication, when assuming that a 'Perfect' capacity-achieving channel code is used. Additionally, a hybrid cooperative communication system relying on TTCM, SPM, as well as HM has also been proposed and investigated.

Finally, we employed our HM aided TTCM cooperative communication strategy in wireless *ad hoc* networks. A realistic system architecture and practical channels were considered, where the coded HM scheme was combined with an Opportunistic Routing (OR) algorithm for reducing the transmit power of each node in the cooperative network, as well as for the sake of reducing the average power consumption of the entire system. The results showed that if the system appropriately utilized the sophisticated modulation/demodulation capability of the layered modulation schemes, the flexibility of the OR algorithm may be improved, while the power consumption of the cooperative communication system may be reduced without increasing the outage probability.

Declaration of Authorship

I, **Hua Sun**, declare that the thesis entitled **Layered Turbo Trellis-Coded Modulation for Cooperative Communications** and the work presented in it are my own and has been generated by me as the result of my own original research. I confirm that:

- This work was done wholly or mainly while in candidature for a research degree at this University;
- Where any part of this thesis has previously been submitted for a degree or any other qualification at this University or any other institution, this has been clearly stated;
- Where I have consulted the published work of others, this is always clearly attributed;
- Where I have quoted from the work of others, the source is always given. With the exception of such quotations, this thesis is entirely my own work;
- I have acknowledged all main sources of help;
- Where the thesis is based on work done by myself jointly with others, I have made clear exactly what was done by others and what I have contributed myself;
- Parts of this work have been published.

Signed: ..... Date: .....

Acknowledgements

Firstly, I would like to express my heartfelt gratitude to my supervisor Dr. Soon Xin Ng and Prof. Lajos Hanzo for their outstanding supervision and support throughout my Ph.D study and related research. Their patient guidance, kind inspiration and encouragement have greatly benefited me not only in research but also in life.

Besides my supervisor, I would like to give my special thanks to my colleague Dr. Chen Dong, for his support, help and discussions throughout my research. The collaborate work with Dong is one of the most significant milestones in my Ph.D study. My sincere thanks also goes to Dr. Shaoshi Yang and Dr. Yongkai Huo for all their unconditional help and support. I would also thank all my colleagues and the staff of the Communications Group, both past and present, the big family gives me an unforgettable memory full of happiness and joy.

I would also like to thank my family, my parents: Han Ping Tong, Song Bai Sun, parents-in-law: Man Xia Gao, Da Hua Li, and all my relatives. Their love and support make me brave and strong, let me become more and more confident when facing the challenges in my life.

Last but not the least, sincere thanks to my lovely wife Dr. Zhujun Li for her love, support and care for me since 2008.

List of Publications

Journals:

1. **H. Sun**, S. X. Ng and L. Hanzo,“Turbo Trellis-Coded Hierarchical Modulation Assisted Decode-and-Forward Cooperation”, IEEE Transactions on Vehicular Technology, vol. 64, no. 9, pp. 3971-3981, Oct. 2014.

2. **H. Sun**, S. X. Ng, C. Dong and L. Hanzo, “Decode-and-Forward Cooperation-Aided Triple-Layer Turbo-Trellis-Coded Hierarchical Modulation”, IEEE Transactions on Communications, vol. 63, no. 4, pp. 1136-1148, Jan. 2015.

3. **H. Sun**, S. X. Ng and L. Hanzo, “The Discrete-Input Continuous-Output Memoryless Channel Capacity of Cooperative Hierarchical Modulation”. IET communications, vol. 10, no. 1, pp. 65-71, Jan. 2016

4. **H. Sun**, C. Dong, S. X. Ng and L. Hanzo, “Five Decades of Hierarchical Modulation and Its Benefits in Relay-Aided Networking”. IEEE Access, vol. 3, pp 2891-2921, Dec. 2015.

Conferences:

1. **H. Sun**, S. X. Ng and L. Hanzo, “Superposition Coded Modulation for Cooperative Communications”, 2012 IEEE Vehicular Technology Conference (VTC Fall), pp.1-5, Quebec City, Canada, 3-6 Sept. 2012.

2. **H. Sun**, Y. R. Shen, S. X. Ng and L. Hanzo, “Turbo Trellis Coded hierarchical modulation for cooperative communications”, 2013 IEEE Wireless Communications and Networking Conference (WCNC), pp.2789-2794, Shanghai, China, 7-10 Apr. 2013.

3. A. J. Aljohani, **H. Sun**, S. X. Ng and L. Hanzo, “Joint source and Turbo Trellis Coded Hierarchical Modulation for context-aware medical image transmission”, 2013 IEEE 15th International Conference on e-Health Networking, Applications & Services (Healthcom), pp.1-5, Lisbon, Portugal, 3-6 Sept. 2013.

Contents

Glossary

3D	three-dimensional
AAF	Amplify-and-Forward
APP	*A Posteriori* Probability
AWGN	Additive White Gaussian Noise
BER	Bit Error Rate
BICM	Bit-Interleaved Coded Modulation
BICM-ID	Bit-Interleaved Coded Modulation with Iterative Decoding
BPS	Bits Per Symbol
bps	bits per symbol per TS
CDF	Cumulative Distribution Function
CIR	Channel Impulse Response
CM	Coded Modulation
CSI	Channel State Information
D-BLAST	Diagonal Bell Laboratories Layered Space-Time
DAF	Decode-and-Forward
DAPSK	Differential Amplitude Phase Shift Keying
DARPA	Advanced Research Project Agency
DCMC	Discrete-input Continuous-output Memoryless Channel
DN	Destination Node
DVB-T/-H	Digital Video Broadcasting for Terrestrial Television/Handhelds
ECL	Effective Code Length
EXIT	Extrinsic Information Transfer
ExOR	Extremely Opportunistic Routing

FEC Forward Error Correction
FED Free Euclidean Distance
FESR Fish-Eye State Routing

GeRaF Geographic random forwarding

HM Hierarchical Modulation
HMOR Hierarchical Modulated Opportunistic Routing

ICI Inter Channel Interference

LDPC Low-Density Parity-Check
LTE Long Term Evolution

MAP Maximum A Posteriori
MIMO Multiple-Input-Multiple-Output
MLC Multi-Level Coding

OR Opportunistic Routing

PDF Probability Density Function
PMF Probability Mass Function
PS Power Sharing

QoS Quality of Service

RDRPLR Reduced-Distance-Related-Pathloss-Reduction
RM Reed-Muller code
RN Relay Node
RSC Recursive Systematic Convolutional

SDMA Space-Division Multiple Access
SER Symbol Error Rate
SISO Single-Input-Single-Output
SN Source Node
SNR Signal-to-Noise Ratio
SOVA Soft-Output Viterbi Algorithm
SP Set Partitioning
SPM Superposition Modulation

TC	Turbo Codes
TCM	Trellis-Coded Modulation
TDMA	Time Division Multi Access
TOR	Traditional OR
TR	Traditional Routing
TS	Time Slot
TTCHM	Turbo Trellis-Coded Hierarchical Modulation
TTCM	Turbo Trellis-Coded Modulation
TuCM	Trubo Coded Modulation
UEP	Unequal Error Protection
V-BLAST	Vertical BLAST
VA	Viterbi Algorithm
VANETs	Vehicular *Ad Hoc* Networks
VLC	Variable Length Code

List of Symbols

Special Symbols

α: The path-loss exponent (**Chapter 5**, **Chapter 6**).

(α, β): The twin-layer SPM-16QAM weighting factor pair.

$\widetilde{\alpha}$: The normalization parameter of the twin-layer HM-16QAM ratio.

$\widetilde{\beta}$: The normalization parameter of the triple-layer HM-64QAM ratio.

γ: The signal to noise ratio for digital transmission (**Chapter 3-5**).
The instantaneous receive signal to noise ratio, which is give by $\gamma = \widetilde{h}\overline{\gamma}$ (**Chapter 6**).
The path-loss exponent (**Appendix**).

$\overline{\gamma}$: The average receive signal to noise ratio, which is defined as $\overline{\gamma} = \frac{¶_t \kappa}{N_0 d^\alpha}$ (**Chapter 6**).

ζ: The number of iterations in the CM decoder.

ζ_m: The number of iterations between the CM decoder and the soft demapper.

η: The block size of the CM encoder/decoder.

κ: A constant, which is defined to be $\kappa = \left(\frac{c}{4\pi f_c}\right)^2$.

π: The CM encoder/decoder interleaver.

π^{-1}: The CM encoder/decoder de-interleaver.

π_c: The channel interleaver.

π_c^{-1}: The channel de-interleaver.

ρ: The pre-coding parameters for SPM.

σ: The CSI error variance (**Chapter 5**).

Δ: The CSI errore (**Chapter 5**).
The constant for curve-fitting schemes (**Chapter 6**).

Φ: The average throughput of the entire system and the unit is packets per TS.

Ω: The mean square value of the uncorrelated Rayleigh fading h.

$A_{k,m}$: *a posteriori* Probability of the k_{th} transition of the MAP algorithm when assuming the data word transmitted is m.

c: The speed of light, which is $C = 3 \times 10^8 m/s$.

C: The channel capacity and the unit is bit per symbol.

f_c: The carrier frequency, which is $f_c = 2.4\ GHz$ in **Chapter 6**.

G: The path gain or reduced path-loss.

h: The uncorrelated Rayleigh fading coefficient.

$\widetilde{h}$: The instantaneous channel fading value (**Chapter 6**).

h_v^j: The element in $H(D)$, which denotes the connection status between the informations and the modulo-2 adders.

$H(D)$: The generator polynomial (in octal) of the CM schemes.

$H(X,Y)$: The joint entropy.

I: The mutual information.

I_A: The *apriori* information.

I_E: The *extrnsic* information.

k: The Boltzmann's constant, which is $k = 1.38e^{-23}$ (**Appendix**).

n: The AWGN for digital transmission (**Chapter 3-5**).

N_0: The power of the AWGN noise for digital transmission (**Chapter 2-5**).
The noise power at the receiver and the unit is (dBm) (**Appendix**).

N_p: The noise power according to the transmission bandwidth and the unit (dBm/Hz) (**Appendix**).

N_r: The number of maximum retransmission attempts for each node, which equals to $N_t - 1$ (**Chapter 6**).

N_{state}: The number of the total system states (**Chapter 6**).

N_t: The number of maximum transmission attempts for each node in the cooperative network (**Chapter 6**).

p: Probability density function.

P: Probability (**Chapter 6**).

$\overline{P}$: $\overline{P} = 1 - P$ (**Chapter 6**).

P_a: *apriori* probability.

P_e: *extrinsic* probability.

P_o: *aposteriori* probability.

P_L: Path loss in dB (**Appendix**).

Pr: Probability (**Chapter 2-5**).

P_r: The receive signal power (**Appendix**).

P_t: The transmit signal power (**Appendix**).

$¶_t$: The transmit signal power (**Chapter 6**).

$\overline{PWC}$: The average packet power consumption (**Chapter 6**).

R_1: The twin-layer HM-16QAM ratio.

(R_1, R_2): The triple-layer HM-64QAM ratio pair.

R_c: The code rate of the CM schemes.

R_m: The number of bits per symbol.

R_o: The number of bits per TS.

R_s: The number of symbols per TS.

T: The temperature measured in Kelvin (**Appendix**).

u_k: The k_{th} transition of the data word.

Special Operations

$\sum$: The summation of all elements.

$\prod$: The product of all elements.

$\int$: The integration function.

Chapter 1

Introduction

During recent decades, wireless communication technology has been dramatically improved as part of this "information and telecommunication revolution". Sophisticated wireless products and services have been invented and employed in almost every activity of people's daily lives, which facilitates remarkable convenience. With the continued growth of the wireless communication industry, the demand for reliable wireless access is ever increasing. Therefore, more efficient coding schemes, modulation schemes, as well as detection algorithms are developed. A basic wireless digital communication system is seen in Figure 1.1. We considered both Additive White Gaussian Noise (AWGN) and uncorrelated Rayleigh flat fading channels [1–4] in our investigations. In digital communications [2, 3], the input of the system is a bit sequence of '0' and '1'. Source coding and channel coding schemes are employed for assisting the transmissions through hostile wireless channels, which are capable of improving the robustness of communication systems against both noise and channel fading. Note that the output of the source coding and channel coding block in Figure 1.1 is still a signal sequence formed by bits. The Modulator block converts the bit-sequence into a complex-valued symbol-sequence, which may be modulated onto an analogue signal associated with specific voltage levels and phases. The investigations in this treatise are mainly focussed on the performance of channel coding schemes and layered modulation schemes conceived for cooperative communications.

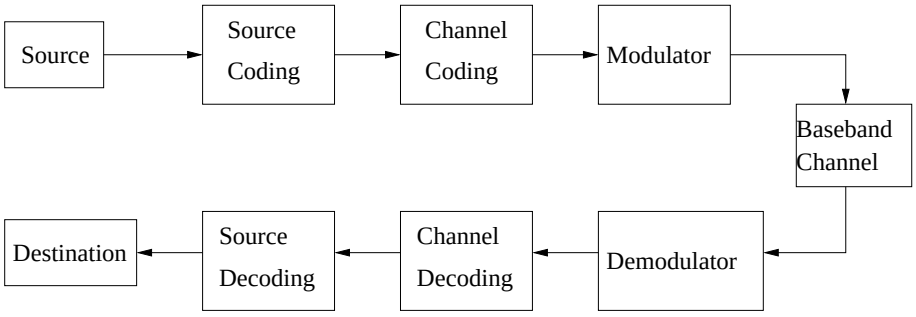

Figure 1.1: The general architecture of a wireless communication system.

1.1 Coded Modulation Scheme

Coded Modulation (CM) intrinsically amalgamates channel coding and modulation [5, 6]. Four popular CM schemes including Trellis-Coded Modulation (TCM) [7], Turbo Trellis-Coded Modulation (TTCM) [8], Bit-Interleaved Coded Modulation (BICM) [9] and Bit-Interleaved Coded Modulation with Iterative Decoding (BICM-ID) [10] have been discussed and compared to each other in detail in [6]. When encoding a signal stream formed by m-bit data words, the CM scheme will introduce an extra parity bit for each uncoded data word by invoking a finite-state Forward Error Correction (FEC) encoder. Therefore, the codeword produced by the FEC encoder will contain $(m+1)$ bits. Consequently, the number of signal constellation points are doubled, but the signalling rate (or bandwidth) remains unchanged. Hence, a coding gain may be achieved without bandwidth expansion. Figure 1.2 illustrates the simplified diagram of a wireless communication system assisted by CM schemes.

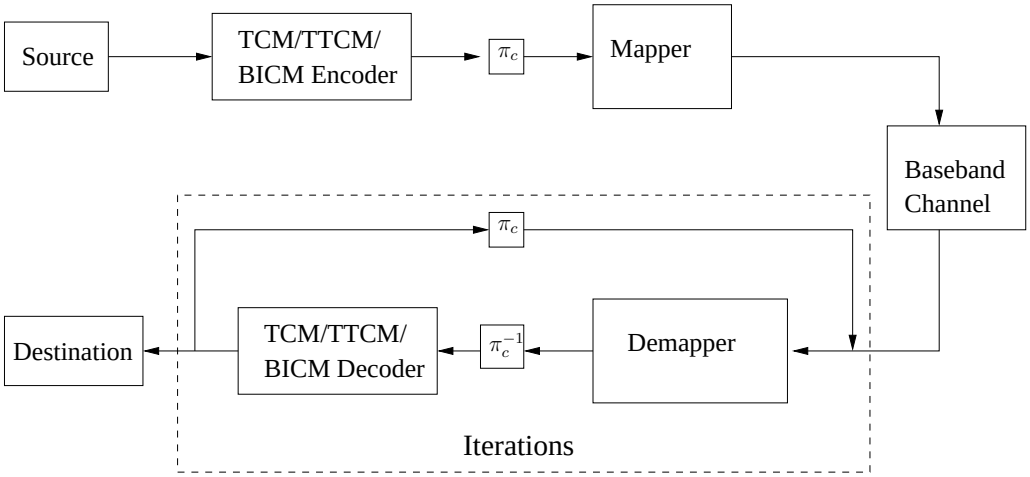

Figure 1.2: The general Coded Modulation schematic.

As shown in Figure 1.2, the CM encoder generates coded words based on the information bit sequence of the source, where the block π_c denotes the symbol-based channel interleaver and π_c^{-1} represents the symbol-based channel de-interleaver. The channel interleaver employed for the sake of dispersing the error burst imposed by the fading channel [6, 8]. Based on specifically designed iterative detection algorithms, extrinsic soft-information is exchanged between the CM channel decoder and symbol-to-bit demapper, as well as between the component codes within the CM decoder block. In this treatise, we mainly focus our attention on the performance of layered modulation schemes relying on TTCM designed for cooperative communications. The relevant details of the TCM and TTCM schemes will be discussed in Chapter 2, while the historical evolution of the CM schemes over the past 60 years is summarized at a glance in Table 1.1 and Table 1.2.

After Shannon outlined the foundations of information theory and derived the channel capacity (which is also referred to as the Shannon limit) in 1948, various channel coding schemes have been developed and investigated by researchers for improving the performance of wireless communica-

Year	**Author(s)**	**Contribution**
1948	Shannon [11]	Information theory and channel capacity
1950	Hamming [12]	Hamming codes was proposed
1954	Reed [13]	Reed-Muller code (RM) was introduced
1955	Elias [14]	Convolutional code
1962	Gallager [15]	Low-Density Parity-Check (LDPC) codes
1972	Bahl *et al.* [16]	Maximum A Posteriori (MAP) algorithm
1974	Bahl *et al.* [17]	The symbol based MAP algorithm
1977	MacWilliams [18]	Monograph on the theory of error correcting codes
	Imai and Hirawaki [19]	Bandwidth-efficient Multi-Level Coding (MLC)
1978	Wolf [20]	Trellis-decoding of block codes
1982	Ungerböck [21]	Trellis-Coded Modulation (TCM)
1987	Wei [22]	Rotationally invariant differentially encoded multidimensional constellation for the design of TCM
1988	Blahut [23]	Multiple trellis-coded modulation
1989	Pottie and Taylor [24]	Multilevel codes based on partitioning
	Calderbank [25]	Multilevel codes and multistage decoding
	Hagenauer *et al.* [26]	Soft-Output Viterbi Algorithm (SOVA)
1990	Koch and Baier [27]	Classic Log-MAP algorithm and sub-optimal Max-Log-MAP algorithm
1991	Webb *et al.* [28]	Hard-decision Star QAM/Differential Differential Amplitude Phase Shift Keying (DAPSK)
1992	Zehavi [29]	Bit-Interleaved Coded Modulation (BICM)
1993	Berrou [30]	Turbo codes
1994	Kofman *et al.* [31]	Performances of a multilevel coded modulation
	Huber and Wachsmann [32]	Capacity of equivalent channels of multilevel coding
	Le Goff *et al.* [33]	BICM-based Trubo Coded Modulation (TuCM)
1995	Robertson *et al.* [34]	Approx-Log-MAP algorithm
1996	Raphaeli [35]	Noncoherent coded modulation
1997	Li and Ritcey [10]	Bit-Interleaved Coded Modulation with Iterative Decoding (BICM-ID)
1998	Robertson and Wörz [36]	Turbo Trellis-Coded Modulation (TTCM)
	Li and Ritcey [10]	BICM-ID using soft feedback
	Caire *et al.* [37]	The theoretical error bound of BICM
	ten Brink *et al.* [38, 39]	Soft-decision demodulation techniques
1999	Li and Ritcey [40]	Combining TCM with BICM-ID
2000	Morelos-Zaragoza *et al.* [41]	Multilevel coded modulation (symmetric constellation)
	Isaka *et al.* [42]	Multilevel coded modulation (asymmetric constellation)

Table 1.1: Milestones in Coded Modulation (1948-2000).

Year	Author(s)	Contribution
2001	Chindapol and Ritcey [43]	Bit-to-symbol mapping for BICM-ID
2004	Hanzo *et al.* [6]	TCM, TTCM, BICM and BICM-ID schemes
	Hou and Lee [44]	Multilevel LDPC code design for semi-BICM
	Lampe *et al.* [45]	Multilevel coding for multiple-antenna transmission
2005	Sikora and Costello [46]	Proposed a new algorithm for turbo equalization
	Nysaeter and Otnes [47]	Turbo equalization with trellis coded modulation
2006	Nana *et al.* [48]	Improved decoding of LDPC coded modulations
2008	Ng *et al.* [49]	Near-capacity TTCM design based on EXIT-chart
2009	Ng *et al.* [50]	Distributed turbo trellis coded modulation for Cooperative communications
2010	Yang *et al.* [51]	Labelling optimization for BICM-ID systems
2011	Nguyen and Lampe [52]	BICM with mismatched decoding metrics
	Islam *et al.* [53]	Analysis and design of cooperative BICM-OFDM systems
2012	Cheng *et al.* [54]	Improve the performance of the LTE turbo-coded modulation by irregular mapping
2013	Vladeanu [55]	Turbo trellis coding is combined with spatial modulation
2014	Liang *et al.* [56]	TTCM is employed by cognitive radio networks
2015	Sun *et al.* [57]	TTCM is combined with hierarchical modulation in cooperative communications

Table 1.2: Milestones in Coded Modulation (2001-2015).

tions. The achievable rate of the communication systems relying on powerful coding schemes has been gradually approaching the Shannon limit. Furthermore, the concept of layered modulation schemes has been proposed for supporting the transmission of multiple independent streams. In this treatise, we investigate various TTCM aided layered modulation schemes conceived for cooperative communications.

1.2 Layered Modulation Schemes

The family of layered modulation schemes was developed by combining multiple independent bit-sequences or symbol-sequences in order to form an expanded constellation diagram, which guarantees that all information may be transmitted and received simultaneously without requiring extra transmit or receive antennas. By employing layered modulation schemes, the achievable rate of the entire communication system may be increased, while the complexity of the system may remain modest. The two most popular layered modulation schemes proposed in recent decades are Superposition Modulation (SPM) and Hierarchical Modulation (HM).

1.2.1 Superposition Modulation

SPM is a modulation technique developed to simultaneously transmit/receive multiple symbol sequences with the aid of linear symbol-based superposition instead of forming their bijective mapping [58]. In 1932, Roder proposed a detection algorithm for receiving a pair of radio frequencies [59], where the two analogue signals may be detected simultaneously from their superposition. Roder's algorithm may be considered to be the first SPM technique. A few decades later, Bergmans and Cover [60] proposed a more sophisticated technique for cooperative broadcasting in 1974. It had been formally shown in [61, 62] that the SPM scheme is capable of approaching the AWGN channel's capacity, while maintaining a relatively low complexity.

Year	**Author(s)**	**Contribution**
1932	Roder [59]	Superposition of two radio frequencies
1974	Bergmans and Cover [60]	Cooperative broadcasting
1986	Laurent [61]	Construction of digital phase modulation by SPM
1997	Duan *et al.* [62]	Algorithms for approaching the AWGN capacity
1999	Gadkari and Rose [63]	Time-division versus SPM for UPE
2000	Pellen and Portugheis [64]	SPM aided multistage turbo code
2001	Wang and Orchard [65]	Design of coded SPM for UPE
2003	Karabulut *et al.* [66]	SPM aided block coding scheme
2004	Karabulut *et al.* [67]	Rate design rule for SPM
	Sun *et al.* [68]	SPM aided TTCM for multirate broadcast
2005	Larsson and Vojcic [69]	Cooperative diversity of SPM
2006	Ding *et al.* [70]	SPM for cooperative multiple access system
2007	Ishii [71]	Diversity utilizing of cooperative SPM
2009	Hasan and Aygolu [72]	Incremental relaying SPM cooperative transmission
	Huan *et al.* [73]	High order SPM cooperative transmission
	Ping *et al.* [74]	Iterative MMSE detection of coded SPM
	Tong *et al.* [75]	Peak-power limitation of SPM
2010	Zhang and Hanzo [76]	Unified treatment of SPM aided transmission
	Wo and Hoeher [58]	SPM aided BICM code
2011	Hoeher and Wo [77]	Survey on SPM
2012	Sun *et al.* [78]	TTCM aided SPM in cooperative communications
	Noemm *et al.* [79]	SPM aided irregular convolutional code
2013	Xi *et al.* [80]	Demodulation for modified SPM
	Chen *et al.* [81]	Orthogonal SPM aided LDPC adaptive cooperative
2014	Zhao *et al.* [82]	Decoding algorithms of LDPC coded SPM
2015	Zein Eldin *et al.* [83]	Multi rate coded SPM for multi user transmission

Table 1.3: Milestones in Superposition Modulation (1932-2015).

Table 1.3 represents the SPM scheme's history and milestones. Observe in Table 1.3 that most of the SPM research was published after the 1990s. More specifically, the investigations were mainly focussed on the performance of the SPM based channel coding or source coding schemes

conceived for cooperative communications after 2005. Numerous powerful coding schemes, such as Turbo Codes (TC), BICM, TCM, TTCM and LDPC codes have been combined with SPM in [58, 64, 66, 68, 78, 81, 82], where both the demapping/decoding algorithms and the attainable performance of the related systems have been discussed in detail. Furthermore, the SPM scheme may be beneficially employed for providing Unequal Error Protection (UEP) for the multiple independent information streams of the different SPM layers [63, 65]. In this treatise, the SPM concept is invoked for improving the efficiency of the cooperative communication system designed in Chapter 3 and Chapter 5. Explicitly, the design of the SPM constellation is detailed both in Chapter 3 and in Chapter 5 according to the specific system requirements considered.

1.2.2 Hierarchical Modulation

As an integral part of the Digital Video Broadcasting for Terrestrial Television/Handhelds (DVB-T/-H) standard [84], HM is widely employed by the IT industry for upgrading diverse telecommunication services [85, 86]. Compared to a system using conventional single-layer modulation, the system employing HM has higher flexibility, while being capable of maintaining backward compatibility. Explicitly, both the original and the upgraded new services may be combined by the HM scheme and broadcast to the receivers without requiring any additional bandwidth. Hence, although the services have been upgraded to a higher data rate, the original devices are still supported by the upgraded broadcast system without requiring any software or hardware upgrade [87].

HM has been developed for combining independent information streams layer-by-layer, which are then mapped onto HM constellations. The information contained in the different layers may also be demapped/detected separately. The general performance of the HM scheme has been detailed in [88–91]. It can be observed from the simulation results of [88, 89] that the different layers of the HM constellation exhibit different protection levels. Consequently, the Signal-to-Noise Ratio (SNR) required for receiving the layer having a higher protection level requires a lower SNR_r than that of the less well protected layers. The author of [92] employed HM in his system to provide UEP for the information contained in the different layers, which stimulated substantial research interests [93–98]. More specifically, the authors of [96, 97] invoked a HM scheme for providing UEP for video and image encoding, where the information bits are mapped to specific protection layers according to their error-sensitivity-based priority. The evolution and milestones of the HM scheme's research are summarized in Table 1.4 at a glance. In this treatise, the HM constellation design is discussed in detail according to the cooperative communication protocol detailed in Chapter 3, Chapter 4 and Chapter 5.

1.3 Opportunistic Routing

In wireless communications, multiple Relay Nodes (RNs) may be activated for assisting the transmissions between the pair of communicating nodes. Hence, there may be multiple possible trans-

Year	Author(s)	Contribution
1993	Fazel and Ruf [99]	Multiresolution modulation is combined with multilevel coding
1995	Morimoto *et al.* [100]	HM for satellite communication
1996	Morimoto *et al.* [101]	Hierarchical image transmission for multimedia mobile communications
1997	O'Leary [102]	HM transmission in COFDM system
1998	Engels and Rohling [103]	64-DAPSK in hierarchical COFDM system
1999	Schill *et al.* [104]	HM for broadcasting based on multilevel codes
2000	Seegert [105]	Coded HM for broadcast communication over fading channel
2001	Vitthaladevuni and Alouini [106]	BER computation of 4/M-QAM HM
2003	Vitthaladevuni and Alouini [107]	BER computation of generalized HM QAM
2004	Pons *et al.* [108]	Enhanced TCM coded HM
2005	Barmada *et al.* [109] Jiang and Wilford [87]	HM QAM based H.246 video transmission HM for upgrading digital broadcasting
2006	Hossain *et al.* [110–112] Chang *et al.* [113]	Adaptive HM for multiclass data transmission Adaptive HM QAM based low-complexity H.264/AVC video transmission
2007	Hausl and Hagenauer [114]	Relay aided Turbo coded HM communication
2008	Wang and Yi [115]	Enhanced HM optimization
2009	Chang and Lee [88] Hellge *et al.* [84]	Analysis of HM aided cooperative communication over Rayleigh fading channel HM for DVB-H broadcast services
2010	Park [116]	HM aided network coding for two-way relay transmission
2011	Arslan *et al.* [97] Peng *et al.* [117]	Coded HM for progressive image transmission Hierarchical cooperative relay aided heterogeneous networks
2012	Chang *et al.* [118]	Optimized UEP for Multiplexed HM
	Hu and Liu [119]	Low-complexity LDPC coded HM aided broadcasting system design and implementation
2013	Wang and Cai [120] Meric *et al.* [121] Mouhouche *et al.* [122]	Fair scheduling of the HM in wireless communications Adaptive CM aided HM in satcom system Throughput of HM aided precoded OFDM
2014	Saeed *et al.* [123]	Space-time coded aided HM with MRC reception in Nakagami-m channel
2015	Sun *et al.* [57]	HM aided TTCM for cooperative communications

Table 1.4: Milestones in Hierarchical Modulation (1993-2015).

mission links between the Source Node (SN) and the Destination Node (DN). Hence, there is a need to find an optimum route, which is capable of conveying the packets to their destinations at a lower power consumption as well as at the lowest delay. The route selection algorithm in the network layer of wireless communications is referred to as the routing algorithm. Traditional Routing (TR) algorithms, such as dynamic source routing and *ad hoc* on-demand distance vector routing [124–127], may select one or more optimized fixed routes before transmissions. Once the transmissions commence, the selected route must not be changed until the next transmission Time Slot (TS). The TR algorithm may select the route based on the quality of the current channel states or based on the geographic distance among the candidate RNs, which may not adapt sufficiently promptly to dynamic wireless environments due to the rapid fluctuation of the channel conditions [128] in high-velocity scenarios, such as Vehicular *Ad Hoc* Networks (VANETs), for example. Nonetheless, the TR algorithm may result in a preponderance of retransmissions in wireless communications, which may lead to a waste of network resources or even to dropped sessions [129].

With the exponential growth of the number of wireless communication devices, new routing algorithms are required for supporting heterogeneous networks and wireless devices in order to overcome the limitations of the TR algorithms. Hence, Opportunistic Routing (OR) algorithms have been developed [126, 130–136], which typically rely on the following four steps:

1. Candidate relay selection;
2. Packet broadcast to the candidate relays;
3. Relay selection for packet forwarding;
4. Packet forwarding.

Unlike the TR algorithms, the OR algorithms typically exploit the broadcast nature of wireless communications, where the receiver may be chosen from the full set of nodes in the network, which are capable of flawlessly receiving the packets. Note that among all the candidate relay nodes, the one which is geographically closest to the DN is most likely to be chosen for forwarding the packet during the next transmission [135]. Since multiple candidates are available for receiving the broadcast packet, the probability of at least one candidate correctly receiving the packets may be improved. Hence, the reliability, the throughput, as well as the power efficiency of the entire system may be improved with the aid of OR algorithms. The evolution and history of the OR algorithms is summarized in Table 1.5.

Furthermore, the Extremely Opportunistic Routing (ExOR) concept was proposed by Biswas in 2005, which is considered to be the seminal OR algorithm in the literature [132]. A list of forwarder nodes may be stored in the header of the packets of the ExOR algorithm, which may be used for beneficially selecting the specific receiver among all candidates. With the rapid development of multi-hop wireless networks, increasingly more OR algorithms have been proposed in recent

Year	Author(s)	Contribution
2003	Zorzi and Rao [126]	Geographic random forwarding (GeRaF) algorithm
	Fussler *et al.* [137]	Contention-based forwarding for mobile networks
2004	Zhao *et al.* [138]	GeRaF aided hybrid-ARQ for *ad hoc* networks
	Biswas and Morris [139]	OR algorithm in multi-hop wireless networks
2005	Yuan *et al.* [140]	Resilient opportunistic mesh routing algorithm
	LeBrun *et al.* [141]	Knowledge-based OR in wireless *ad hoc* networks
	Biswas and Morris [132]	Extremely Opportunistic Routing (ExOR) algorithm
2006	Westphal [142]	OR algorithm in dynamic *ad hoc* networks
	Rozner *et al.* [143]	Simple OR protocol for wireless mesh networks
	Zhong *et al.* [144]	Candidates selection for opportunistic path forwarding
2007	Zeng *et al.* [145]	Throughput of geographic OR algorithm
	Nassr *et al.* [146]	Scalable and reliable sensor network routing
	Chachulski *et al.* [133]	Trading structure for randomness OR algorithm
2008	Lin *et al.* [147]	OR with segmented network coding (CodeOR)
	Koutsonikolas *et al.* [148]	Synergistic interflow network coding and OR
	Conan *et al.* [149]	Fixed point OR in delay tolerant networks
2009	Zeng *et al.* [150]	Location-aided OR in multirate and multihop networks
	Yang *et al.* [151]	Position based OR algorithm
	Laufer *et al.* [152]	Multirate routing in wireless mesh networks
2010	Lin *et al.* [153]	Online opportunistic network coding aided by SlideOR
	Naghshvar and Javidi [154]	OR with congestion diversity in multi-hop networks
	Bletsas *et al.* [155]	Interference limited OR in reactive sensing
2011	Mao *et al.* [156]	Energy-efficient OR in wireless sensor networks
	Lee and Hwang [157]	Minimum energy cost design of a two-hop networks
	Lee and Haas [135]	OR for short-haul multi-hop networks
	Fang *et al.* [158]	Node-constrained OR in wireless mesh networks
2012	Bhorkar *et al.* [159]	Adaptive OR for wireless *ad hoc* networks
	Lampin *et al.* [160]	QoS oriented OR protocol for sensor networks
	Wang *et al.* [161]	Cooperative OR in mobile *ad hoc* networks
2013	Guo *et al.* [162]	Opportunistic flooding with unreliable links
	Xiao *et al.* [163]	Time-sensitive OR in delay tolerant networks
	Shin *et al.* [164]	Parallel OR in wireless networks
2014	Zuo *et al.* [129]	Cross-layer energy-efficient OR algorithm
	Zhong *et al.* [165]	Coding-aware OR in cognitive radio networks
	Xiao *et al.* [166]	Community-aware OR in mobile social networks
2015	Chen *et al.* [167]	Theoretical analysis of buffer-aided OR
	Wu *et al.* [168]	Game-theoretic based OR in wireless networks
	Elias *et al.* [169]	Contest-aware OR for stationary sensor networks

Table 1.5: Milestones in Hierarchical Modulation (2003-2015).

decades. More specifically, the performance of the OR algorithms in multi-hop wireless networks has been investigated, in terms of their energy consumption [129,156,170], their system delay [129, 171] as well as their system capacity/throughput bound [131]. In [129], Jin has investigated the energy-efficiency of the OR algorithm in a four-hop network. In this treatise, we will employ a system architecture similar to that of [129], albeit as a substantial distinguishing feature, our packets are formed by the layered-modulated symbols. To be more specific, the OR algorithm is combined with a TTCM-aided HM scheme for cooperative communications in Chapter 6, where the packets transmitted throughout the four-node *ad hoc* network are the coded twin-layer HM signals. Unlike in the Traditional OR (TOR) algorithm, the packets transmitted through an *ad hoc* network may follow different routes by exploiting the specific feature of the HM scheme which is in contrast to the TOR algorithms, as detailed in Chapter 6. The achievable throughput, the delay distribution, the outage probability and the power consumption of our four-node *ad hoc* network will be discussed in detail in Chapter 6.

1.4 Motivation and Thesis Outline

Cooperative communication has drawn significant research attention [172–174], where the broadcast nature of the wireless channel may be exploited for user cooperation. Cooperative communications substantially improve the robustness of the system against the hostile fading effects of the environment. Recently, cooperative communication techniques have also been introduced in some of the standards, including the IEEE 802.16j WiMAX and Long Term Evolution (LTE) Advanced standard [172]. Additionally, a range of other sophisticated techniques have also been introduced into cooperative communications, including CM schemes (TC, TCM, TTCM, BICM) [50, 175–177], as well as layered modulation schemes (SPM, HM) [70, 73, 88, 117]. However, even though the CM schemes are indeed capable of reliable transmissions over noisy fading channels, their detection complexity may be relatively high, especially when a higher code-rate encoder is employed. This complexity problem becomes even more severe for channels subjected to the deleterious effects of interference [74]. Hence, conceiving efficient cooperative communications solutions having a relatively low system complexity becomes an attractive research problem.

A relay-aided coded HM scheme was introduced in [114], where Hausl and Hagenauer combined turbo coding [6] with a HM scheme conceived for cooperative communications. The original signal sequence was broadcast by the SN by ensuring that the layer having a higher protection level was received by the DN directly, while the less strongly protected layer was flawlessly received and retransmitted by the RN. However, the authors of [114] only considered a specific scenario, when the position of the RN is right in the middle of the SN-DN link and invoked a specific bit-to-symbol mapping scheme. The performance of coded HM schemes was then further explored in [116, 178–180] in the context of cooperative communications, where the common choice is to employ multiple encoders at the SN and combine all the coded bit sequences layer-by-layer to create a HM signal sequence. Again, the less well-protected layers are assisted by the RN in the

cooperative network. The bit-to-symbol mapping optimization of the HM scheme was considered in [116, 181]. More specifically, by appropriately designing the constellation mapping, the HM scheme becomes capable of enhancing the protection of the higher-priority information at the expense of providing a weaker protection for the other layers. In [180], the impact of the RN's specific position was explicitly considered in terms of the attainable Bit Error Rate (BER). For a specific coded HM scheme, the power received at the RN should be sufficiently high for guaranteeing that the RN still becomes capable of receiving the information in the lower protected layer at an acceptable integrity. Therefore, the position of the RN directly influences the power allocation of the entire system. Several parameters have to be taken into consideration when optimizing a coded HM aided cooperative communication system. On one hand, distorting the HM constellation for the sake of improving the BER of its high-priority layers at the detriment of its low-priority layers degrades its average BER compared to conventional modulation schemes. On the other hand, sophisticated channel coding schemes, such as TCM, TTCM and BICM [6, 36, 182, 183] are required for protecting each HM layer at the expense of an increased complexity. Hence, giving cognizance both to the complexity and to the power efficiency of the overall system, while maintaining its flexibility becomes a challenging task.

In this treatise, the TTCM scheme is employed for cooperative communications. With the aid of Decode-and-Forward (DAF) based relaying, the HM is invoked for supporting multiple independent information streams, while reducing both the complexity and the transmission power of the system. Additionally, the SPM scheme is also employed for improving the time-efficiency of the entire system. Finally, the coded layered modulation scheme is also combined with OR algorithms in the network layer of cooperative multi-hop wireless networks for improving the performance of the system. The organization of the thesis is listed bellow with reference to Figure 1.3:

Chapter 1: We briefly introduce the evolution and history of the CM, SPM and HM schemes, as well as of the family of OR algorithms. The outline, motivation, research methodology and contribution of the thesis are also summarized.

Chapter 2: The TCM scheme is introduced in Section 2.2, where the encoder and decoder of the TCM, the Set Partitioning (SP) concept and the symbol-based MAP algorithm are discussed. Then, in Section 2.3, the encoder and decoder of the TTCM scheme are discussed, while the Extrinsic Information Transfer (EXIT) charts are illustrated in Section 2.4. In Section 2.5, we first investigated the performance of the classic TCM, TTCM, BICM and BICM-ID schemes when communicating over both AWGN and uncorrelated Rayleigh fading channels in Section 2.5.1, where the performance of four CM schemes is compared. Then, the performance of the TTCM scheme employing different code-rate, modulation-level, block size and number of iterations has been investigated in Section 2.5.2, when communicating over Rayleigh fading channels. Section 2.5.3 illustrates the EXIT chart analysis of the TTCM decoder, while Section 2.6 concludes the chapter.

Chapter 3: A TTCM aided SPM based three-node cooperative communication arrangement has

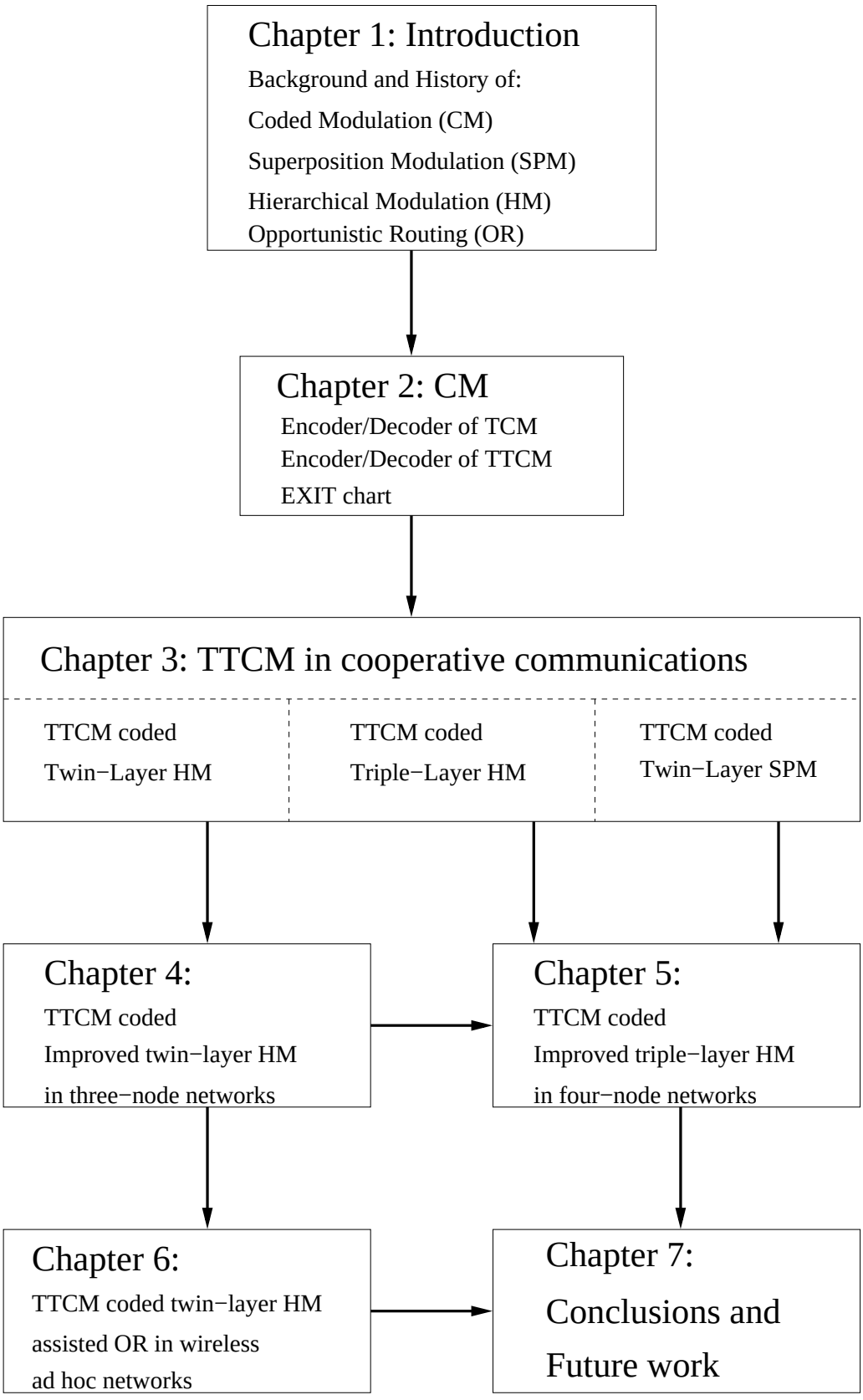

Figure 1.3: The outline of the thesis.

been proposed in Section 3.2, where the demodulation and decoding of the TTCM aided SPM symbol is illustrated in Section 3.2.4 while the performance of the TTCM-SPM aided cooperative communications is characterized in Section 3.2.7. Then, a TTCM aided HM based scheme is proposed for cooperation in Section 3.3, where the specifically designed HM constellations designed for supporting a single user's transmissions is illustrated in Section 3.3.3. Section 3.3.4 details both the system's block diagram as well as our communications protocol, while the corresponding simulation results are provided in Section 3.3.5. Furthermore in Section 3.4, we amalgamated both SPM and HM for the sake of supporting cooperative communications in a five-node network, where the communication protocol is detailed in Section 3.4.3. Section 3.4.4 represents our simulation results and Section 3.5 concludes Chapter 3.

Chapter 4: An improved twin-layer HM aided cooperative system is proposed in this chapter, while the system architecture and the communication protocol employed are presented in Section 4.3. Section 4.4 details the BER performance limits of the coded twin-layer HM scheme based on the Discrete-input Continuous-output Memoryless Channel (DCMC) capacity. Our TTCM aided twin-layer HM based cooperative communication system design is discussed in Section 4.5. While, Section 4.6 offers our conclusions. Additionally, in Appendix A.1, we compare our simplified path-loss model employed in Chapter 4 and the simplified free-space path-loss model of [1].

Chapter 5: An improved triple-layer TTCM aided HM based cooperative system is proposed in this chapter. The system model and the cooperative communication protocol, as well as the path-loss model, are detailed in Section 5.2. Section 5.3 investigated the HM constellations employed, where the demodulation procedure of the TTCM aided triple-layer HM-64QAM arrangement is discussed in Section 5.4. Section 5.5 outlines the BER performance limits of the system based on the DCMC capacity analysis. The performance of the TTCM aided triple-layer HM based cooperative communications scheme is investigated in Section 5.6. Meanwhile, in Section 5.7 we amalgamate the triple-layer HM and twin-layer SPM in a five-node cooperative communication system, where the system's performance is optimized based on the relay's position as well as on the transmit power of the nodes, in addition to a number of other system parameters. Section 5.8 summarizes the findings of this chapter.

Chapter 6: The TTCM aided twin-layer HM based cooperation communication scheme discussed in Chapter 4 is incorporated into multi-hop wireless networks in this chapter. Our design objectives and our system model are illustrated in Section 6.2, while Section 6.3 details the theoretical analysis of the TTCM-HM aided OR algorithm. Section 6.3.2 defines the legitimate system states of the layered modulation aided OR based system and the corresponding state-transition probabilities are presented in Section 6.3.3. The algorithms used for theoretically analysing our OR based cooperative communication networks are discussed in Section 6.3.4. The investigations characterising the OR based multi-hop networks are detailed

in Section 6.4. Finally, in Section 6.5 we discuss our simulation results, while Section 6.5 concludes the chapter.

Chapter 7: Section 7 summarizes the findings of our investigations. Our design guidelines are presented in Section 7.2 and the limitations and challenges of our investigations are discussed in Section 7.3, while our future research ideas are discussed in Section 7.4.

1.5 Research Methodology

In this treatise, all the channel coding related simulations of Chapter 2, Chapter 3, Chapter 4 and Chapter 5 are carried out by IT++, which is a C++ library of classes and functions designed for signal processing and communications. The BER versus SNR simulation results of the basic CM schemes provided in Chapter 2 were verified in [6]. In Chapter 3, Chapter 4 and Chapter 5, the TTCM scheme of Chapter 2 is employed. In the context of the HM scheme, we focus on manipulating the transmitter's constellation map. The key results of Chapter 3, Chapter 4 and Chapter 5 were verified with the aid of EXIT-charts. Additionally, we also evaluated the Discrete-Input Continuous-Output Memoryless Channel (DCMC) capacity of the system.

Finally, the simulations of Chapter 6 are carried out by Matlab, which confirmed our theoretical analysis. Explicitly, the simulation results are based on packet-by-packet transmissions, while the theoretical analysis relies on random processes based on the single-step state transition probability matrices.

1.6 Novel Contributions

Based on the following publications [57, 78, 184–187], the novel contributions of the thesis are summarised as follows:

- A TTCM aided SPM based system is conceived for cooperative communication in [78]. More explicitly, the cooperative communication protocol, the SPM modulation and demodulation procedure, as well as an efficient power-sharing method are proposed for cooperative communications in [78].
- A TTCM aided HM based scheme is proposed for cooperative communications in [184]. In contrast to the conventional HM scheme, we employ a specifically designed HM scheme for reducing the transmit power of the source node in the context of a cooperative communication system. The generation of HM constellations and the related communication protocols are detailed in [184].
- Based on the TTCM aided twin-layer HM based cooperative communication scheme proposed in [184], our system is further improved in [185]. The cooperative communication

protocol is designed with an increased flexibility in mind. Furthermore, the BER performance limits of the coded twin-layer HM based cooperative system are derived based on our DCMC capacity analysis. The performance of the TTCM assisted twin-layer HM aided cooperative communication system is optimized based on the specific position of the relay node and a new parameter termed as the HM ratio [185].

- An improved TTCM aided triple-layer HM cooperative communication scheme is proposed in [57, 186], where the cooperative network is extended to a four-node network and the SPM concept is also invoked for increasing the efficiency of the entire system. The BER performance limits of the coded triple-layer HM scheme are derived according to the DCMC capacity. The performance of both the TTCM aided triple-layer HM and of the twin-layer SPM based cooperative system are optimized based on the above-mentioned HM ratio, the SPM weighting factor, the positions of the relay nodes, as well as the transmit power of the nodes in the network [57, 186].

- The HM scheme is employed in wireless *ad hoc* networks for reducing the power consumption of the entire cooperative system in [187]. The achievable FER performance of the TTCM aided twin-layer HM based scheme is characterized as a function of the instantaneous receive SNR, when communicating over Rayleigh-distributed block fading channels. More explicitly, the BER, the delay, the outage probability and the power consumption of the cooperative networks are analysed theoretically. Our simulation results closely match our theoretical analysis. Furthermore, the simulation results also demonstrate that by incorporating the layered modulation scheme into our OR algorithms, the outage probability and power consumption of the entire system is reduced [187].

Chapter 2

Turbo Trellis-Coded Modulation

2.1 Introduction

In this chapter, we will discuss the theory and performance of the Turbo Trellis-Coded Modulation (TTCM) scheme. As described in Chapter 1, the main contribution of this treatise is centred around the intrinsic amalgamation of the layered modulation schemes with TTCM for the sake of improving the efficiency of cooperative communication systems at the cost of a moderate system complexity. The rationale of opting for TTCM is that it outperforms Trellis Coded Modulation (TCM) as well as Bit-Interleaved Coded Modulation (BICM) and Bit-Interleaved Coded Modulation with Iterative Detection (BICM-ID) both for transmission over Additive-White-Gaussian-Noise (AWGN) and uncorrelated Rayleigh fading channels [6].

Coded Modulation (CM) schemes have been conceived for achieving reliable performance, while maintaining a high bandwidth efficiency in wireless communications. The TCM scheme combined with symbol-based channel interleaving was proposed by Ungerböck [7] for transmission over Gaussian channels. By contrast, Divsalar had further developed the family of CM schemes for mobile communications over fading channels [188, 189]. The concept of TTCM was proposed by Robertson *et al*. [8], which has a similar structure to binary turbo code [190], but instead of convolutional codes, TCM schemes were employed as component codes. Both the TCM and TTCM schemes employ Set-Partition mapping instead of Gray mapping for the sake of achieving the lowest possible Symbol Error Rate (SER). Apart from the symbol-based CM schemes, bit-based CM schemes, such as BICM [9] and BICM-ID [10] have also been developed and investigated in the late twentieth century.

In this chapter, we introduce the TCM as well as TTCM schemes and compare the CM schemes of TCM, TTCM, BICM and BICM-ID. The decoding convergence of the iterative TTCM decoder is studied based on Extrinsic-Information-Transfer (EXIT) charts [49, 191]. The organization of the chapter is as follows. The classic TCM scheme and the Maximum A Posteriori (MAP) algorithm are introduced in Section 2.2. Section 2.3 outlines the encoder and decoder of the TTCM scheme,

while Section 2.4 introduces the concept of EXIT charts. Our simulation results and the related discussions are provided in Section 2.5. The conclusions of the chapter are offered in Section 2.6

2.2 Trellis-Coded Modulation

The tutorial paper of Ungerböck [7] eloquently describes the TCM scheme. Instead of transmitting a m-bit uncoded symbol, the TCM scheme will employ a finite state Forward Error Correction (FEC) encoder to expand the original symbol set by adding an extra bit. This extra bit is generated by a convolutional encoder, which restricts the legitimate state transitions amongst the consecutive phasor. The number of constellation points is doubled in order to absorb the extra redundancy bit. Hence, the number of bits contained in the transmitted symbol will be increased to $m+1$ and as a benefit - a beneficial coding gain may be achieved without increasing the symbol-rate and the bandwidth.

2.2.1 TCM Encoder

Again, the TCM encoder introduced by Ungerböck in [7] relies on a Recursive Systematic Convolutional (RSC) code [21], which attaches an extra parity bit to each of the original information symbol. When communicating the eight-state TCM encoder of Ungerböck seen in Figure 2.1 for instance, the 2-bit input data word may be expanded to a 3-bit coded word by adding a parity bit, which is generated by the RSC encoder. Then, the encoded 3-bit coded words may be interleaved by a symbol-based interleaver, which is invoked for the sake of dispersing the probability of bursty symbol errors caused by the hostile fading channel. Then, the interleaved coded words will be mapped onto complex symbols by the Set-Partitioning (SP) based 8-PSK modulator.

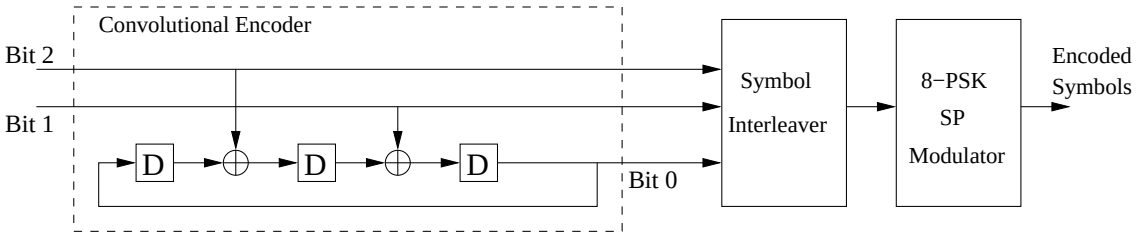

Figure 2.1: The eight-state Ungerböck TCM encoder [7].

The block D seen in Figure 2.1 denotes the delay introduced by a register stage, where the eight states are defined by the outputs of the three registers. The parity bit generated by the convolutional encoder shown in Figure 2.1 may be expressed as:

$$H^j(D) = h_\nu^j \cdot D^\nu + h_{\nu-1}^j \cdot D^{\nu-1} + ... + h_1^j \cdot D + h_0^j \,, \tag{2.1}$$

where $h_\nu^j \in \{0,1\}$ denotes the presence or absence of a connection between the information bits and the modulo-2 adders are shown in Figure 2.1. Explicitly, when we have $h_\nu^j = 1$, there is

a connection at the specific encoder stage. By contrast, when there is no connection, we have $h_\nu^j = 0$. The generator polynomial coefficient $H^j(D)$ is associated with the jth information bit. When considering the TCM encoder of Figure 2.1 for instance, the generator polynomial may be expressed as:

$$H^0(D) = 1001\ , \tag{2.2}$$

$$H^1(D) = 0010\ , \tag{2.3}$$

$$H^2(D) = 0100\ , \tag{2.4}$$

where normally we represent the generator polynomials in octal format as follows:

$$\mathbf{H(D)} = [H^0(D)\ \ H^1(D)\ \ H^2(D)] = [11\ \ 02\ \ 04]\ . \tag{2.5}$$

In [7], Ungerböck defined $h_\nu^0 = h_0^0 = 1$, which guarantees the realisability of the encoder. Meanwhile, the generator polynomials should also obey $h_\nu^j = h_0^j = 0$ for $j > 0$, as detailed in [6, 7]. By defining the values of h_ν^j, we can guarantee that whenever two paths diverge from or merge into a common state in the trellis, the parity bit will be the same for these transitions. When designing the generator polynomials, the parameters referred to as the Free Euclidean Distance (FED) and the Effective Code Length (ECL) should be taken into consideration. Again, the generator polynomials of a range of TCM codes are discussed in detail in [6, 7].

2.2.2 Set Partitioning

In general, Gray coding is applied in wireless communications in order to map the bits to the symbols by ensuring that the adjacent symbols only differ by a single bit for the sake of minimizing the bit error probability. However, as described in [6], when higher-order modulation schemes are employed, parallel transitions may occur in the trellis diagram of the TCM decoder. In order to prevent the TCM decoder from having high error probability, we have to increase the Euclidean distance associated with the parallel transitions. Therefore, the so called Set Partitioning (SP) philosophy was introduced by Ungerböck to overcome this problem. As seen for the 8PSK SP constellation map displayed in Figure 2.2, the SP may divide the coded word into multiple subsets, where the minimum Euclidean distance of the new subset points will be extended at every new partitioning step.

As shown in Figure 2.2, the rate-2/3 8PSK TCM encoder will produce a signal stream formed by 3-bit coded words. The length of the signal stream is defined as the transmission block size η of the TCM encoder, where in the 3-bit coded word (b_2, b_1, b_0), b_2, b_1 are the original information bits and b_0 is the parity bit generated by the encoder relying on the generator polynomial of Eq. (2.5). Based on the partitioning tree shown in Figure 2.2, it can be observed that the Euclidean distance of the partitioned subsets is gradually increased. Note that the parity bit b_0 is used for protecting the information bits b_1 and b_2, but b_0 itself receives the lowest protection, because the Euclidean distance between the constellation point sets corresponding to $b_0 = 0$ and $b_0 = 1$ is the lowest

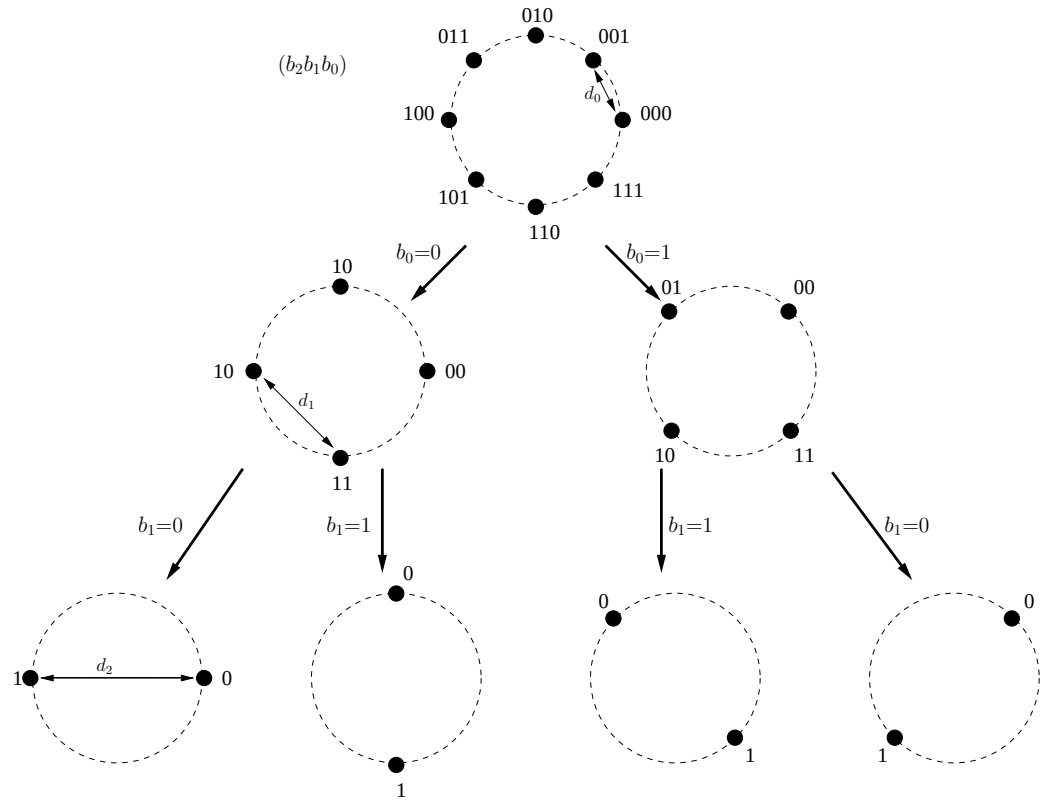

Figure 2.2: The 8PSK set partitioning [6].

possible one in the 8PSK set. By contrast, b_2 has the highest Euclidean distance, therefore it is the most error-resilient bit, which indicates a low probability of corruption.

2.2.3 Symbol Based MAP Algorithm

Both the TCM scheme, as well as the TTCM scheme employ the symbol-based Maxi *A Posteriori* (MAP) algorithm to demodulate/decode the received signal stream. The symbol-based MAP algorithm is detailed in [36]. In contrast to the maximum likelihood sequence estimation based Viterbi Algorithm (VA), the MAP algorithm guarantees that the SER is minimized. However, the complexity of the MAP algorithm is higher than that of the VA. As the terminology of the MAP algorithm suggests, the core idea of the MAP algorithm is to find the encoded sequence that maximizes the entire *A Posteriori* Probability (APP). Both the bit-based and symbol-based MAP decoding procedures are discussed in [6]. In this section, we will briefly introduce the MAP algorithm. The APP of a specific transition from state $\grave{s}$ to state s may be expressed as:

$$A_{k,m} = \Pr\left(u_k = m \mid y_k\right) = \sum_{all\ \grave{s},s} \Pr\left(u_k = m \wedge S_{k-1} = \grave{s} \wedge S_k = s \mid y_k\right) \ , \tag{2.6}$$

where, y_k denotes the kth received symbol in the signal streams, while the transmitted data word is given by $u_k = m$ and the coded word transmitted is x_k. In [6], the APP $A_{k,m}$ is formulated as

$$A_{k,m} = C_k \cdot \Pr_{apr}(k,m) \cdot \sum_{\substack{(\grave{s},s)\Rightarrow \\ u_k=m}} \alpha_{k-1}(\grave{s})\, \eta_k(\grave{s},s)\, \beta_k(s)\ , \tag{2.7}$$

where C_k is a common scaling factor at the kth input, which may be omitted because it affects all calculations the same way. Hence the APP may be simplified as:

$$\bar{A}_{k,m} = \Pr_{apr}(k,m) \cdot \sum_{\substack{(\grave{s},s)\Rightarrow \\ u_k=m}} \alpha_{k-1}(\grave{s})\, \eta_k(\grave{s},s)\, \beta_k(s)\ . \tag{2.8}$$

Here we have

$$\eta_k(\grave{s},s) = \exp\left(-\frac{|y_k - h_k x_k|^2}{N_0}\right)\ , \tag{2.9}$$

where h_k is the channel's fading coefficient and N_0 is the variance of the AWGN. Additionally, $\Pr_{apr}(k,m)$ is the *a priori* probability, which is equi-probable during the very first decoding:

$$\Pr_{apr}(k,m) = \frac{1}{M}\ , \tag{2.10}$$

where M denotes the modulation-order. Explicitly, the forward recursion may be derived as:

$$\alpha_k(s) = \sum_{all\ \grave{s}} \Pr_{apr}(k,m) \cdot \eta_k(\grave{s},s) \cdot \alpha_{k-1}(\grave{s})\ , \tag{2.11}$$

while the backward recursion can be formulated as:

$$\beta_{k-1}(\grave{s}) = \sum_{all\ s} \Pr_{apr}(k,m) \cdot \eta_k(\grave{s},s) \cdot \beta_k(s)\ . \tag{2.12}$$

In order to simplify the calculation of the APP, Robertson introduced the Log-MAP algorithm in [36]. The APP calculation has hence been converted to the logarithmic domain using the Jacobian logarithm as follows:

$$\begin{aligned} g(s_1,s_2) &= \ln\left(e^{s_1} + e^{s_2}\right) \\ &= \max(s_1,s_2) + \ln\left(1 + e^{-|s_1-s_2|}\right) \\ &= \max(s_1,s_2) + f_c\left(|s_1 - s_2|\right)\ . \end{aligned} \tag{2.13}$$

Based on the Log-MAP algorithm, Robertson also conceived a simplified Log-MAP algorithm in [8], which was termed as the Max-Log-MAP algorithm formulated as:

$$\ln\left(\sum_n e^{s_n}\right) \approx \max_n(s_n)\ , \tag{2.14}$$

where $\max_n(s_n)$ denotes the maximum value of $\{s_n\}$ for all n. Although, the complexity of the Max-Log-MAP algorithm is relatively low, it imposes a performance penalty owing to the above-mentioned simplification. In order to improve the performance of the Max-Log-MAP algorithm, while maintaining a relatively low complexity, the Approx-Log-MAP algorithm was developed [6],

which stores the values of the function f_c in Eq. (2.13) in a look-up table introduced in [8]. Hence Eq. (2.14) may be converted to:

$$\ln\left(\sum_n e^{s_n}\right) = g\left\{s_n, g\left(s_{n-1}, \cdots g\left[s_3, g\left(s_1, s_2\right)\right]\cdots\right)\right\} \ . \tag{2.15}$$

By applying a look-up table, the Approx-Log-MAP algorithm's complexity is reduced. Hence, it is only slightly more complex than the Max-Log-MAP, and yet has a similar performance to that of the MAP algorithm. In the simulations conducted throughout this treatise, the Approx-Log-MAP algorithm is employed by the TTCM decoder for decoding the received signal stream.

2.3 Turbo Trellis-Coded Modulation

The TTCM scheme is detailed in [6, 36]. Again, its encoder and decoder have a similar structure to that of the turbo code, but TCM schemes are employed as its component codes. The encoder and decoder as well as the iterative decoding of the TTCM scheme will be discussed in this section, assuming familiarity with the turbo-decoding principles detailed for example in [6].

2.3.1 TTCM Encoder

As shown in Figure 2.3, the TTCM encoder consists of a pair of TCM encoders developed by Ungerböck [7]. The symbol-based interleaver π and de-interleaver π^{-1} [192] guarantees that the ordering of the coded symbols in the two paths is harmonized, and that the bursty errors are dispersed. The puncturing process carried out by the Selector of Figure 2.3 only allows the original information bits to be sent once, rather than twice. Hence, the parity information in the coded symbols is generated alternatively by each of the two TCM encoders. Observe furthermore in Figure 2.3 that a channel interleaver is used for dispersing the bursty symbol errors imposed by the fading channel.

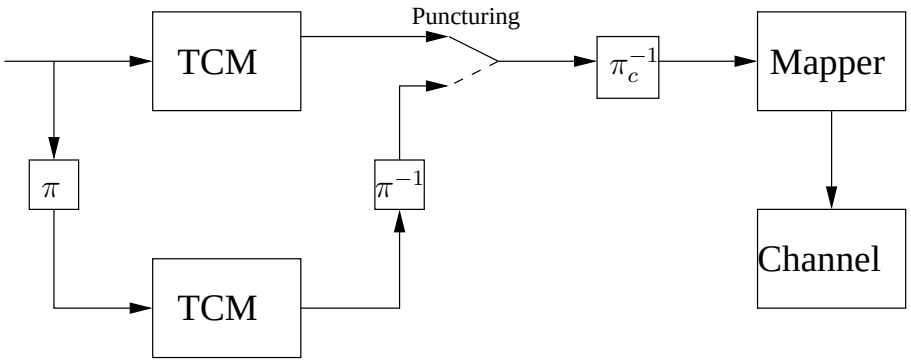

Figure 2.3: Schematic of the TTCM encoder [36].

Additionally, the generator polynomials proposed by Robertson and Wörz for the TCM components of the TTCM encoder are illustrated in Table 2.1. Note that in our simulations all the

generator polynomials we choose for the TTCM encoders are the 8-state generator polynomials.

Code	States	$H^0(D)$	$H^1(D)$	$H^2(D)$	$H^3(D)$
4QAM	8	13	06	-	-
8PSK	4	07	02	04	-
8PSK	8	11	02	04	-
16QAM	8	11	02	04	10
16QAM	16	21	02	04	10
64QAM	8	11	04	02	-
64QAM	16	21	04	10	-

Table 2.1: 'Punctured' TCM codes exhibiting the best minimum distance for 4QAM, 8PSK, 16QAM and 64QAM, where octal format is used for specifying the generator polynomials [36].

2.3.2 TTCM Dencoder

Similar to the classic turbo codes, the TTCM decoder also employs iterative decoding. The number of decoding iterations between the two TCM codes is denoted as ζ. The information flow within a single TCM decoder is illustrated in Figure 2.4.

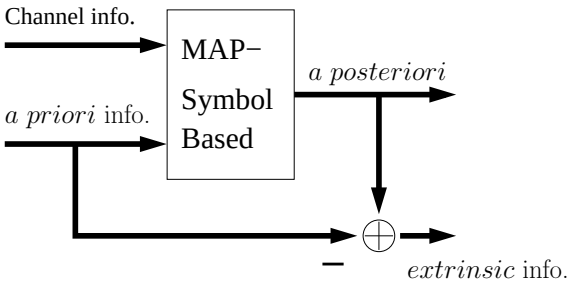

Figure 2.4: The TCM decoder [6] constitutes a MAP algorithm based decoder.

The schematic of the TTCM decoder is represented in Figure 2.5. It may be observed from Figure 2.5 that the TTCM decoder consists of two TCM decoders. The details of the TTCM decoding procedure are discussed in [6].

As shown in Figure 2.4, for each TCM decoder, there are two inputs, which are referred to as the channel information and *a priori* information. As seen in Figure 2.5, $P_a(c)$ is the *a priori* information of the codeword received from the channel (from the demapper), while $P_a(d)$ is the *a priori* information of the data word gleaned from the other TCM decoder component. Furthermore, $P_o(d)$ is the *a posteriori* information generated by the TCM decoder. By extracting $P_a(d)$ from $P_o(d)$, the *extrinsic* information of the data word $P_e(d)$ may be derived, which will become $P_a(d)$ for the other TCM decoder. Additionally, it may also be observed from Figure 2.5 that we

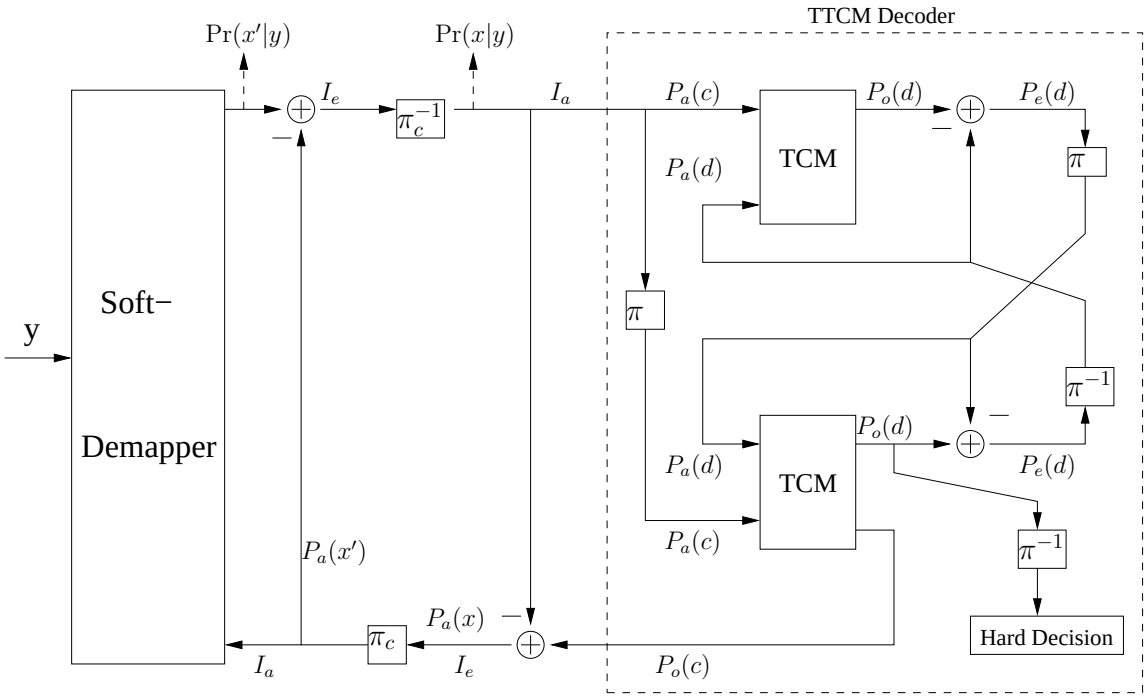

Figure 2.5: The iterative decoding structure of the TTCM decoder.

can also invoke iterations between the soft-demapper and the TTCM decoder. The soft-demapper may firstly derive the $(\eta \times M)$-element probability matrix storing the probabilities of receiving y, when the coded word c is transmitted, where the elements of the matrix may be expressed as:

$$p\left(y_k|x_k^{(i)}\right) = \frac{1}{\pi N_0} \exp\left(-\frac{\left|y_k - h_k x_k^{(i)}\right|^2}{N_0}\right) , \tag{2.16}$$

where $x^{(i)} = \mu\left(c^{(i)}\right)$ is the phasor representing the coded word $c^{(i)}$ that was mapped to $k \in \{0,1,\ldots,\eta\}$ and $i \in \{0,1,\ldots,M-1\}$. Furthermore, y_k here denotes the signal received from the channel, which is formulated as $y_k = hx_k + n_k$, where x_k is the transmitted signal, h_k denotes the complex-valued Rayleigh fading envelop and n_k is the AWGN noise. Hence, the conditional PDF of $p\left(y_k|x_k^{(i)}\right)$ obeys the Gaussian distribution. Furthermore, η is the block size of the TTCM encoder and M is the modulation-order. Based on the above probability matrix, the $(\eta \times M)$-element probability matrix of $\Pr(x|y)$ may also be derived, which is the soft-input of the TTCM decoder. The elements of this second probability matrix may be formulated as [6]

$$\Pr\left(x_k^{(i)}|y_k\right) = p\left(y_k|x_k^{(i)}\right) \Pr\left(x^{(i)}\right) , \tag{2.17}$$

where we have $Pr\left(x^{(i)}\right) = Pr\left(c^{(i)}\right)$ due to the one-to-one mapping. If we assume that there are no iterations between the soft-demapper and the TTCM decoder, the values of $\Pr\left(c^{(i)}\right)$ may be $1/M$, which are equi-probable. By contrast, when there is information exchange between the soft-demapper and the TTCM decoder, $\Pr\left(c^{(i)}\right)$ will represent the *a priori* information $P_a(c)$, which is the feedback gleaned from the TTCM decoder to the soft-demapper, as shown in Figure 2.5.

Hence, the values of Pr $\left(c^{(i)}\right)$ will no longer be equi-probable and they will be different after every iteration. The iterations between the soft-demapper and the TTCM decoder are typically capable of improving the decoding performance. Again, for further details on the TTCM principles please refer to [6].

2.4 Extrinsic Information Transfer Charts

The Extrinsic Information Transfer (EXIT) chart concept was introduced by ten Brink and it was discussed in detail in [193–195]. It was developed for analysing the convergence behaviour of iterative decoding schemes, as detailed in [196]. The mutual information exchange between the component decoders, as well as the mutual information exchange between the decoder and the soft-demapper may be conveniently visualized by the EXIT charts, which assists the designer in characterising the decoder's ability to approach the channel capacity [195]. The bit-based EXIT chart concept was discussed in [193–195], while the symbol-based EXIT chart concept was introduced in [191, 197]. When analysing the performance of the symbol-based TTCM scheme, the symbol-based EXIT chart scheme is employed.

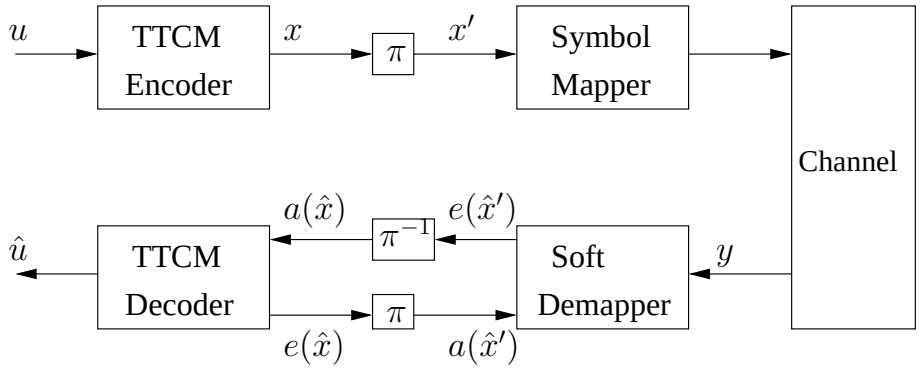

Figure 2.6: The general block diagram of the iterations between the soft demapper and the TTCM decoder.

The block diagram of the information flow within the TTCM decoder is shown in Figure 2.6. It illustrates the iterations between the TTCM decoder and the Soft-Demapper. Note that u is the uncoded data word and x is the encoded codeword, while y is the complex-valued signal received by the Soft-Demapper from the wireless channel. The EXIT curves visualize the 'per-symbol mutual information' [198] exchange. To elaborate a little further, we divide the mutual information exchanged during the iterations into two parts, namely the 'Inner' part, which enters the *a priori* information $I_A^{(i)}$ into the Soft-Demapper, and outputs the *extrinsic* information $I_E^{(i)}$ by the Soft-Demapper. The 'Outer' part, relies on the input *a priori* information $I_A^{(o)}$ of the TTCM decoder and outputs the *extrinsic* information $I_E^{(o)}$ of the TTCM decoder. The calculations of I_A and I_E of the

'Inner' and 'Outer' parts are detailed in [6, 197, 198]. According to Figure 2.6, we have:

$$I_A^{(i)} = I_E^{(o)} , \tag{2.18}$$

$$I_E^{(i)} = I_A^{(o)} , \tag{2.19}$$

where we have:

$$I_E^{(i)}\left(\hat{x_k}'^{(m)}\right) = \log_2(M) - \frac{1}{N}\sum_{k=1}^{N} E\left[\sum_{m=1}^{M} e\left(\hat{x_k}'^{(m)}\right)\log_2\left(e\left(\hat{x_k}'^{(m)}\right)\right)\right] , \tag{2.20}$$

with N being the block size and M being the modulation-order. Provided that N is sufficiently large, we have:

$$I_E^{(i)}\left(\hat{x_k}'^{(m)}\right) = \log_2(M) - \frac{1}{N}\sum_{k=1}^{N}\sum_{m=1}^{M} e\left(\hat{x_k}'^{(m)}\right)\log_2\left(e\left(\hat{x_k}'^{(m)}\right)\right) , \tag{2.21}$$

where, $e\left(\hat{x_k}'^{(m)}\right) = \Pr\left(\hat{x_k}'^{(m)} \mid y_k\right)$, which is the *extrinsic* probability of the transmitted symbol $\hat{x_k}'^{(m)}$ generated by the Soft-Demapper. Similarly, we have

$$I_E^{(o)}\left(\hat{x_k}^{(m)}\right) = \log_2(M) - \frac{1}{N}\sum_{k=1}^{N}\sum_{m=1}^{M} e\left(\hat{x_k}^{(m)}\right)\log_2\left(e\left(\hat{x_k}^{(m)}\right)\right) , \tag{2.22}$$

where again, $e\left(\hat{x_k}^{(m)}\right) = \Pr\left(\hat{x_k}^{(m)} \mid y_k\right)$, which is the *extrinsic* probability of the transmitted symbol $\hat{x_k}^{(m)}$ estimated by the TTCM decoder. The EXIT chart analysis results of the TTCM scheme will be represented and discussed in Section 2.5. Again, for more details on EXIT-charts, please refer to [196] and to [199].

2.5 Simulation Results

In this section, we will characterize the performance of the TCM, TTCM, BICM and BICM-ID schemes communicating over both AWGN and uncorrelated Rayleigh fading channels. The simulation parameters of this study are shown in Table 2.2. Additionally, the EXIT chart analysis of the TTCM scheme is also discussed in this section.

2.5.1 Comparison of TCM, TTCM, BICM and BICM-ID

Figure 2.7 and Figure 2.8 illustrate the BER versus SNR performance of the TCM, TTCM, BICM and BICM-ID schemes communicating over AWGN and uncorrelated Rayleigh fading channels, respectively. The generator polynomials used are given in Table 2.1. Throughout this treatise we employ the 8-state CM code generator. The related performance summary is recorded in Table 2.3. It can be observed from these two figures that at the same encoder/decoder complexity characterized by 64 trellis-states, the TTCM scheme performances better than the remaining CM schemes. When communicating over the uncorrelated Rayleigh fading channel, the receive SNR required for achieving a 10^{-6} BER performance for the rate-1/2 4QAM TTCM scheme is about 4.23 dB, while

Coded Modulation	**TCM, TTCM, BICM, BICM-ID**
Modulation Scheme	4PSK, 8PSK, 16QAM, 64QAM
Mapper type	Set-Partitioned
Number of iterations	$\zeta_{TTCM} = \{2,4,6,8\}$, $\zeta_{BICM-ID} = 8$
Code Rate	1/2, 2/3, 3/4, 5/6
Code Memory	3 for TTCM and BICM-ID
	6 for TCM and BICM
Decoder type	Approximate Log-MAP
Symbols per frame	12,000
Number of frames	10,000
Channel	AWGN, Uncorrelated Rayleigh fading channel

Table 2.2: Simulation parameters used in the simulation results of Figure 2.7 to Figure 2.13.

that for the rate-1/2 TCM scheme is 16.42 dB, for the rate-1/2 BICM scheme is 11.65 dB and finally, for the BICM-ID scheme it is 10.47 dB. Hence in this treatise, we mainly focus our attention on the performance of the TTCM scheme invoked for cooperative communications, as a benefit of its superior performance.

When evaluating the BER performance of a CM scheme, both the required E_b/N_0 and the SNR should be taken into consideration, where E_b is the average power per information bit, while $SNR = E_s/N_0$ and E_s is the average power per symbol transmitted. For a code rate of:

$$R_c = \frac{k}{n}\,, \tag{2.23}$$

the CM encoder generates n-bit codewords based on every k information bits. When an M-ary modulation scheme is employed for producing transmitted symbols having m Bits Per Symbol (BPS), we have:

$$R_m = \log_2(M) = m\,. \tag{2.24}$$

If we assume that the symbol rate of the scheme is R_s symbols per timeslot, then the throughput of the system may be expressed as:

$$R_o = R_c \cdot R_m \cdot R_s\,. \tag{2.25}$$

Therefore, we can derive the relationship between E_b/N_0 (ratio) and SNR (ratio) as:

$$E_b/N_0 = \frac{E_b}{N_0} = \frac{1}{R_o}\frac{E_s}{N_0} = \frac{1}{R_o}SNR\,. \tag{2.26}$$

Hence we have:

$$E_b/N_0\ [dB] = SNR\ [dB] - 10\log_{10}(R_o)\ . \tag{2.27}$$

In order to avoid the ambiguity between E_b/N_0 and SNR, in the majority of our simulations, we opt for using the SNR, when evaluating the BER performance of our system. Additionally, in our simulations, we mainly focus our attention on cooperative communications over uncorrelated Rayleigh fading channels.

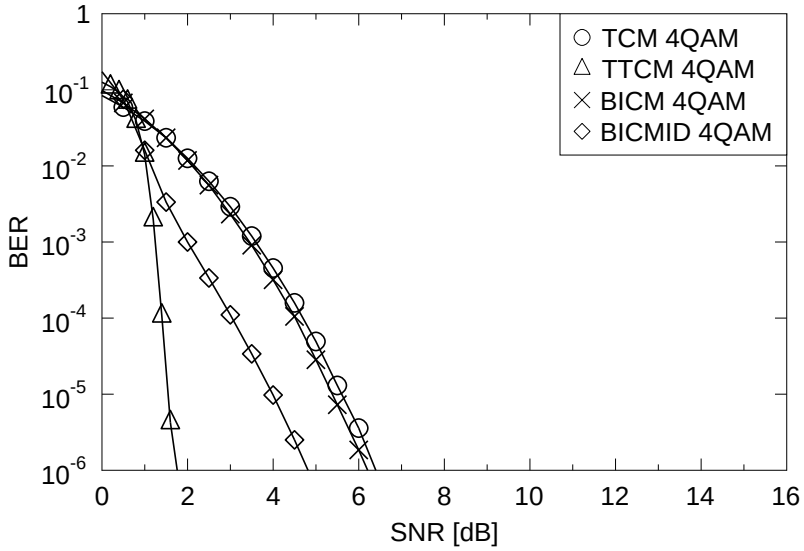

Figure 2.7: The BER versus SNR performance of TCM, TTCM, BICM and BICM-ID communicating over AWGN channels. The code rate of all the four CM schemes is $R_c = 1/2$, where 4QAM using set-partitioning is employed. The related simulation parameters are shown in Table 2.1 and Table 2.2. The block size of the CM schemes is $\eta = 12,000$, the number of iterations at the decoder of TTCM is $\zeta_{TTCM} = 4$ and of BICM-ID is $\zeta_{BICM-ID} = 8$, the memory length of the schemes in the table is 3, where the simulation results are summarized in Table 2.3.

CM R_c**=1/2, 4QAM**	**BER**	E_b/N_0**[dB] (AWGN)**	**SNR[dB] (AWGN)**	E_b/N_0**[dB] (Rayleigh)**	**SNR[dB] (Rayleigh)**
TCM	10^{-6}	6.40	6.40	16.42	16.42
TTCM	10^{-6}	1.74	1.74	4.23	4.23
BICM	10^{-6}	6.21	6.21	11.65	11.65
BICM-ID	10^{-6}	4.82	4.82	10.47	10.47

Table 2.3: The E_b/N_0 and SNR values required for achieving BER of 10^{-6} by the CM schemes when communicating over both AWGN and uncorrelated Rayleigh fading channels. These values are based on the simulation results of Figure 2.7 and Figure 2.8. The related simulation parameters are shown in Table 2.1 and Table 2.2. The block size of the CM schemes is $\eta = 12,000$, the number of iterations at the decoder of TTCM is $\zeta_{TTCM} = 4$ and of BICM-ID is $\zeta_{BICM-ID} = 8$ and the memory length of the schemes in the table is 3.

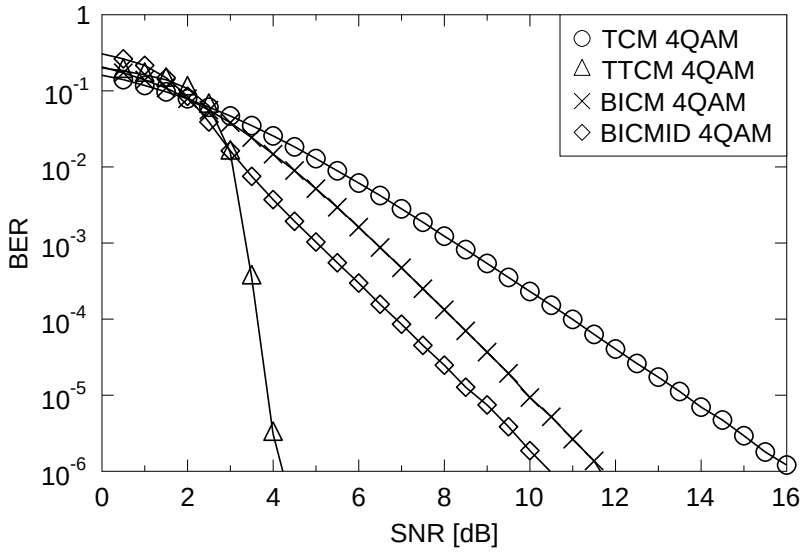

Figure 2.8: The BER versus SNR performance of TCM, TTCM, BICM and BICM-ID communicating over uncorrelated Rayleigh fading channels. The code rate of all the four CM schemes is $R_c = 1/2$, where 4QAM using set-partitioning is employed. The related simulation parameters are shown in Table 2.1 and Table 2.2. The block size of the CM schemes is $\eta = 12,000$, the number of iterations at the decoder of TTCM is $\zeta_{TTCM} = 4$ and of BICM-ID is $\zeta_{BICM-ID} = 8$, the memory length of the schemes in the table is 3, where the simulation results are summarized in Table 2.3.

2.5.2 BER Performance of TTCM over Uncorrelated Rayleigh Channel

Figure 2.9 portrays the SNR versus BER performance of the TTCM scheme for different code rates R_c for transmission over an uncorrelated Rayleigh fading channel, while the related performance results are summarized at a glance in Table 2.4. It can be observed that upon increasing the code rate, as well as the modulation-orders, the SNR required for achieving a BER of 10^{-6} by the TTCM aided system is also increased. Note that a higher code rate R_c results in a higher decoding complexity. We used an 8-state generator polynomial and opted for a rate-5/6 64QAM TTCM encoder, where two of the information bits within the encoded symbol are not protected. This is directly reflected by the specific slope of the BER versus SNR performance curve recorded for $R_c = 5/6$ at the SNR values greater than 21 dB, when communicating over Rayleigh fading channels.

Figure 2.10 illustrates the BER versus SNR performance of the rate-1/2 TTCM 4QAM scheme for different number of TTCM decoding iterations ζ, when communicating over an uncorrelated Rayleigh fading channel. The related results are recorded at a glance in Table 2.5. It can be observed that upon increasing the number of TTCM decoder iterations, the attainable BER performance is substantially improved. However, for $\zeta > 6$, any further increase of ζ only results in marginal improvement of the BER performance, despite increasing the complexity of the TTCM decoder. For example, when increasing the number of iterations ζ from 4 to 6, the SNR required is only reduced

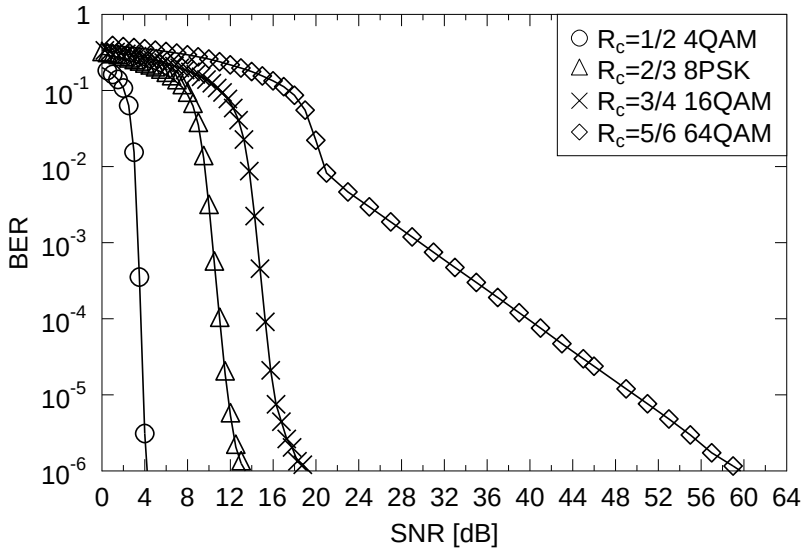

Figure 2.9: The BER versus SNR performance of TTCM communicating over an uncorrelated Rayleigh fading channel. The code rates are $R_c \in \{1/2(4QAM), 2/3(8PSK), 3/4(16QAM), 5/6(64QAM)\}$, where set-partitioning is employed. The related simulation parameters are shown in Table 2.1 and Table 2.2. The number of iterations at the decoder of TTCM is $\zeta_{TTCM} = 4$, the memory length of the TTCM encoder is 3 and the block size is $\eta = 12,000$, where the simulation results are summarized in Table 2.4.

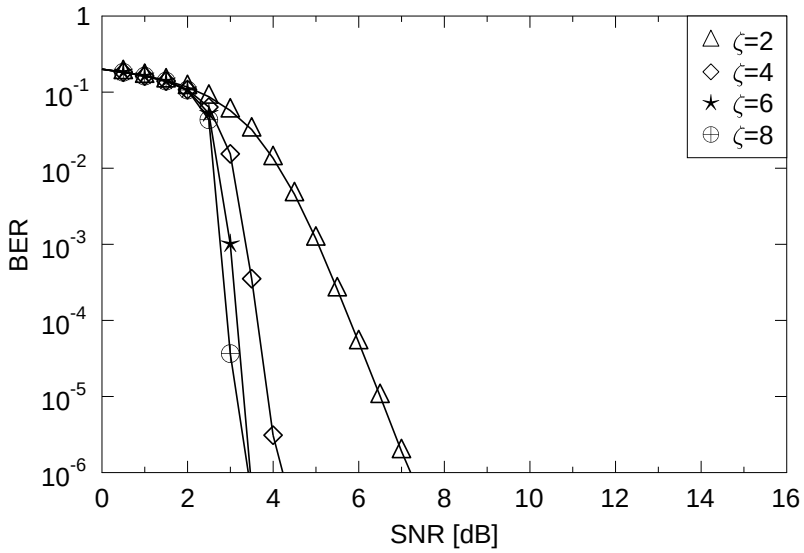

Figure 2.10: The BER versus SNR performance of TTCM schemes communicating over an uncorrelated Rayleigh fading channel. The code rate of the TTCM encoder is $R_c = 1/2$, where 4QAM with set-partitioning is employed. The number of iterations are $\zeta \in \{2, 4, 6, 8\}$ and the related simulation parameters are shown in Table 2.1 and Table 2.2. The memory length of the TTCM encoder is 3, the block size is $\eta = 12,000$ and the simulation results are summarized in Table 2.5.

TTCM Rate R_c	Modulation	BER	E_b/N_0[dB] (Rayleigh)	SNR[dB] (Rayleigh)
1/2	4QAM	10^{-6}	4.23	4.23
2/3	8PSK	10^{-6}	10.40	13.40
3/4	16QAM	10^{-6}	14.47	19.24
5/6	64QAM	10^{-6}	52.70	59.69

Table 2.4: The E_b/N_0 and SNR values required for achieving BER of 10^{-6} by the TTCM scheme communicating over an uncorrelated Rayleigh fading channel. These values are based on the simulation results showed in Figure 2.9. The code rates are $R_c \in \{1/2(4QAM), 2/3(8PSK), 3/4(16QAM), 5/6(64QAM)\}$, where set-partitioning is employed, the related simulation parameters are shown in Table 2.1 and Table 2.2, where the number of iterations at the decoder for TTCM is $\zeta_{TTCM} = 4$, the block size is $\eta = 12,000$ and the memory length of the TTCM encoder is 3.

TTCM R_c=1/2, 4QAM	SNR[dB] (Rayleigh)	TTCM R_c=1/2, 4QAM	SNR[dB] (Rayleigh)
$(\eta = 12000, \zeta = 2)$	7.22	$(\eta = 1200, \zeta = 4)$	5.62
$(\eta = 12000, \zeta = 4)$	4.23	$(\eta = 2400, \zeta = 4)$	4.92
$(\eta = 12000, \zeta = 6)$	3.47	$(\eta = 12000, \zeta = 4)$	4.23
$(\eta = 12000, \zeta = 8)$	3.42	$(\eta = 24000, \zeta = 4)$	4.06

Table 2.5: The SNR values required for achieving BER of 10^{-6} of the TTCM scheme communicating over an uncorrelated Rayleigh fading channel. These values are based on the simulation results showed in Figure 2.10 and Figure 2.11. The related simulation parameters are shown in Table 2.1 and Table 2.2. The number of block size η and the number of iterations ζ are detailed in the table and the memory length of the TTCM encoder is 3.

by about 0.76 dB, which is not as remarkable as that when increasing ζ from 2 to 4. Therefore, in order to achieve a better BER performance, while maintaining a low decoding complexity, we prefer $\zeta = 4$ for the TTCM decoder. Additionally, Figure 2.11 represent the BER versus SNR performance of the rate-1/2 TTCM 4QAM scheme employing different block sizes η given the number of iterations at the TTCM decoder is $\zeta = 4$. It may be observed that a higher block size of the TTCM scheme may provide a better performance. Hence, based on the simulation results of Figure 2.11, we predominantly opted for $\eta = 12,000$ in this treatise. However, in Chapter 3 and Chapter 6, due to the high complexity of the system, the value of η is set to 1,200 in the simulations and the specific reason for this choice is also justified in these two chapters.

2.5.3 EXIT Charts Analysis of TTCM

Outer Curve of the EXIT Charts

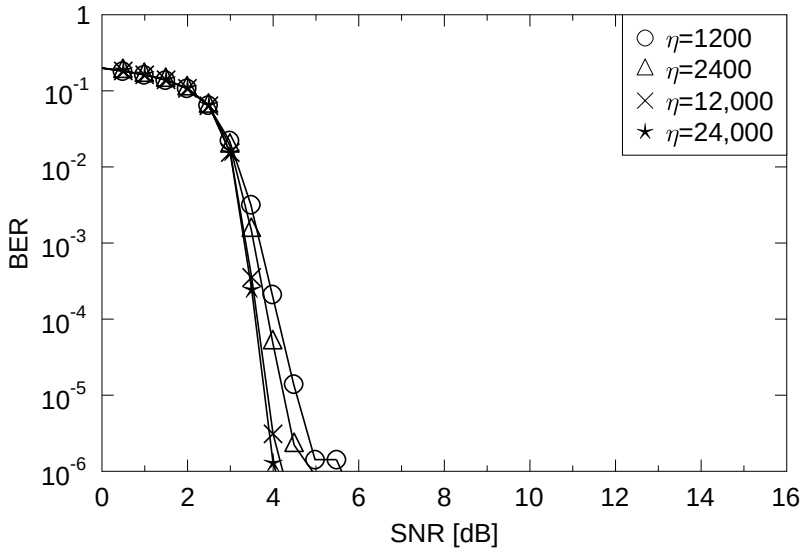

Figure 2.11: The BER versus SNR performance of TTCM schemes communicating over an uncorrelated Rayleigh fading channel. The code rate of the TTCM encoder is $R_c = 1/2$, where 4QAM with set-partitioning is employed. The block sizes used for the TTCM schemes are $\eta \in \{1200, 2400, 12000, 24000\}$ and the related simulation parameters are shown in Table 2.1 and Table 2.2. The memory length of the TTCM encoder is 3, the number of iterations is $\zeta = 4$ and the simulation results are summarized in Table 2.5.

Again, in this section familiarity with the EXIT-chart principles is assumed, as detailed in [6]. As described in Section 2.4, the EXIT chart technique relies on the interplay of the 'Outer' and the 'Inner' decoder components of a serially concatenated scheme seen in Figure 2.6. Figure 2.12 represents our simulation results for the 'Outer' decoder curve of the rate-1/2 TTCM 4QAM scheme. It is worth mentioning that due to the symbol-based nature of the TTCM scheme, the two bits contained in the coded symbol cannot be separated and hence the maximum value of the mutual information $I^{(o)}$ and $I^{(i)}$ will be '2'. The 'Outer' decoder curve of the EXIT chart characterizes the outer decoder based on the mutual information (per symbol) received from the inner soft-demapper. If no iterations are invoked between the soft-demapper and the decoder, the equivalent 'Inner' decoder curve is a flat horizontal curve.

B Inner Curve and Trajectory of the EXIT Charts

The 'Inner' decoder's mutual information curve $I^{(i)}$ of the EXIT chart represents the soft mutual information that the soft demapper is capable of producing based on combining the channel's output at a given SNR and the *a priori* information provided by the 'Outer' decoder. Note that the area under the 'Inner' decoder's curve is proportional to the DCMC capacity [49, 195] at a specific SNR. In this section we assume that the number of iterations between the soft demapper and TTCM decoder is $\zeta_m = 4$, where the Monte-Carlo simulation-based staircase-shaped decoding trajectory is used for visualizing the exchange of mutual information between the soft demapper and the

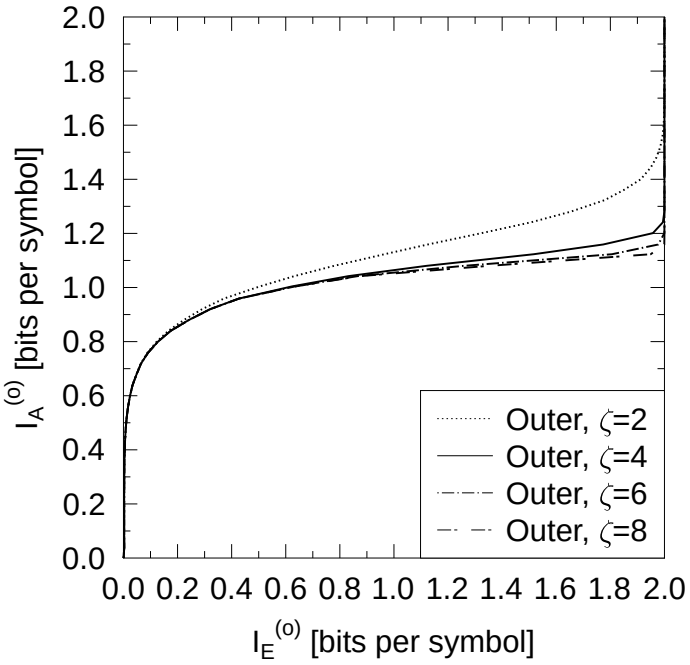

Figure 2.12: The EXIT curve of the TTCM decoder, which constitutes the 'Outer' decoder of the TTCM aided MIMO-2 $\times$ 1 scheme. The code rate is $R_c = 1/2$ and the 4QAM modulation scheme associated with set-partitioning is employed. The number of iterations of the TTCM decoder is $\zeta \in \{2,4,6,8\}$ and the related simulation parameters are shown in Table 2.1 and Table 2.2, where the memory length of the TTCM decoder is 3 and the simulation results are summarized in Table 2.6.

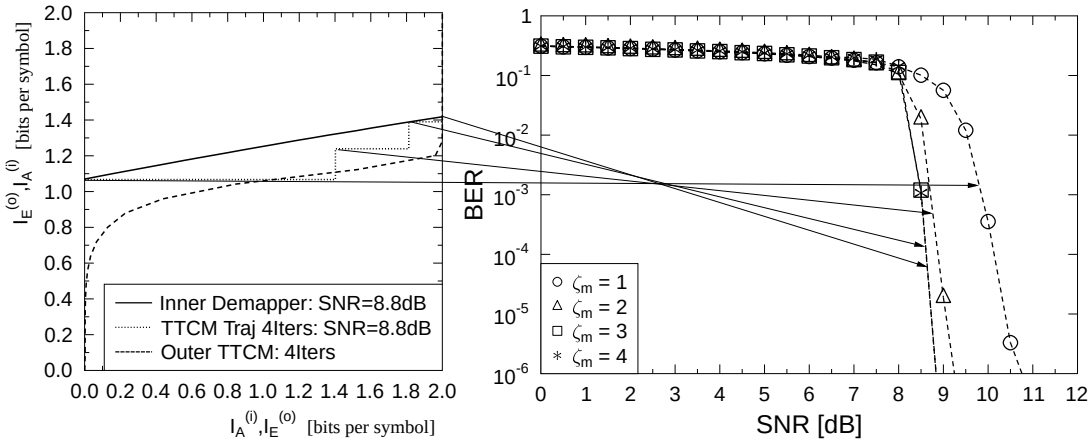

Figure 2.13: The EXIT charts of the TTCM aided MIMO-2 $\times$ 1 scheme. The code rate $R_c = 1/2$ and 4QAM modulation associated with set-partitioning is employed. The number of iterations between the soft demapper and the TTCM decoder is $\zeta_m = 4$, the number of iterations of the TTCM decoder is $\zeta = 4$ and the memory length of the TTCM decoder is 3, where the related simulation parameters are shown in Table 2.1 and Table 2.2.

ζ	$I_E^{(o)}$ [BPS]	$I_A^{(o)}$ [BPS]
2	2.000	1.760
4	2.000	1.323
6	2.000	1.241
8	2.000	1.201

Table 2.6: The statistics of the 'Outer' curve of the EXIT charts analysis of the TTCM aided MIMO-2 $\times$ 1 scheme, based on the simulation results of Figure 2.12. The code rate is $R_c = 1/2$ and the 4QAM modulation scheme associated with set-partitioning is employed. The number of iterations of the TTCM decoder is $\zeta \in \{2,4,6,8\}$, where the related simulation parameters are shown in Table 2.1 and Table 2.2, the memory length of the TTCM decoder is 3 and the related results are shown in Figure 2.12.

TTCM decoder on an iteration-by-iteration basis. Figure 2.13 represents the EXIT chart of the TTCM scheme aided MIMO-2 $\times$ 1 arrangement of Figure 2.6. To elaborate a little further, in Figure 2.6, the 'Inner Demapper' curve represents the information received from the channel, when the receive SNR is 8.8 dB, which may be interpreted as the soft information input to the decoder from the demapper. Furthermore, the label 'Outer TTCM' characterizes the decoding capability of the TTCM decoder, where the 'TTCM Traj 4 Iters' curve shows the information exchange between the decoder and the soft demapper, when the receive SNR is 8.8 dB, for $\zeta = 4$ iterations. In order to decode the signal received at an arbitrarily low BER, the SNR has to be sufficiently high for guaranteeing an open 'tunnel' between the 'Inner' decoder's curve and the 'Outer' decoder's curve of the EXIT chart. The terminology of 'tunnel' defines the gap between the Inner and Outer decoder's curve, which characterizes the relationship between the information received from the channel and the decoding capability of the decoder. If the tunnel is wide enough, the information received from the channel is sufficient for the decoder to correctly decode the signal and the stair-case-shaped Monte-Carlo simulation based trajectory curve is capable of travelling through this open tunnel. However, if the received SNR is low, the tunnel will be closed that the bit-by-bit simulation based decoding trajectory fails to travel through the tunnel. Hence, the decoder fails to flawlessly decode the signal received [6]. Hence, the EXIT chart is often used for finding the minimum SNR required for a concatenated scheme to achieve a vanishingly low BER. Therefore, this technique has been widely employed both for overall system design and for channel code design. It can be observed from Figure 2.13 that when the SNR is 8.8 dB, the soft demapper may 'just' guarantee the presence of an open tunnel for the decoder, since the decoding trajectory reaches $I_E^{(o)} = 2$ after four iterations. Note that any SNR lower than 8.8 dB may lead to the closure of the tunnel, hence the decoder becomes unable to decode the information with an arbitrarily low BER. In a nutshell, the basic EXIT-chart properties are as follows:

1 In order to have an infinitesimally low BER, the Monte-Carlo simulation-based stair-case-shaped decoding trajectory has to reach the top right corner of the EXIT-chart. This requires

that the inner- and outer- decoder's EXIT curves do not have an intercept point, hence creating an open EXIT-tunnel all the way to the top-right conner.

2 If the top-right conner of the EXIT-chart is not reached by the stair-case-shaped decoding trajectory, a residual BER floor is expected, as exemplified in Figure 2.13.

3 Given a specific SNR, the normalized area under the corresponding inner-decoder EXIT-curve is proportional to the DCMC capacity at that SNR.

2.6 Summary and Conclusions

In Section 2.2, we have introduced the classic TCM scheme, including the TCM encoder and decoder, the set partitioning principles, as well as the symbol-based MAP algorithm. The TTCM scheme is discussed in Section 2.3, where the iterations between the two TCM components in the TTCM decoder are further elaborated on. Furthermore, the EXIT chart principles as well as the iterations between the soft demapper and the TTCM decoder are detailed in Section 2.4. The comparison of the four CM schemes, namely of TCM, TTCM, BICM and BICM-ID have been presented in Section 2.5.1. Explicitly, the results of Figure 2.7 and Figure 2.8 show that the TTCM scheme has a better BER performance than the TCM, BICM and BICM-ID schemes, when communicating over both AWGN as well as uncorrelated Rayleigh fading channels. The simulation results shown in Section 2.5.2 illustrated that a higher number of iterations ζ and a larger block size η is capable of improving the attainable BER performance. However, in order to achieve a better BER performance, while maintaining a moderate TTCM decoding complexity, we prefer to opt for $\eta = 12,000$ and $\zeta_{TTCM} = 4$ in our simulations. Additionally, the results of our EXIT charts analysis was provided in Section 2.5.3. In the following chapters, TTCM scheme will be combined with layered modulation schemes for cooperative communications. Our motivation is to improve the performance of the TTCM aided cooperative communication system while maintaining a moderate system complexity relying on the layered modulations, such as Superposition Modulation (SPM) or Hierarchical Modulation (HM).

Chapter 3

Amalgamation of Superposition- and Hierarchical- Modulation with Turbo Trellis-Coded Modulation for Cooperative Communications

3.1 Introduction

In this chapter, we investigate an intrinsic amalgam of Turbo Trellis-Coded Modulation (TTCM) with both Superposition Modulation (SPM) and with Hierarchical Modulation (HM) in the context of a Decode-and-Forward (DAF) cooperative communication system. Our simulation results show that by combining the layered modulation with the TTCM, we are capable of increasing the flexibility of cooperative communications when supporting multiple users' transmissions, while the complexity and the power consumption of the cooperative communications may be reduced. We will demonstrate that this regime is capable of reducing the transmit power of the nodes in the context of cooperative networks. This chapter is divided into three parts, which deal with SPM based TTCM aided cooperative communications, with HM based TTCM assisted cooperative communications, as well as with embedded SPM and HM assisted TTCM aided cooperative communications.

3.2 SPM based TTCM aided Cooperative Communications

3.2.1 Introduction

Coded Modulation (CM) [5, 6] relies on a joint design of channel coding and modulation, which absorbs the parity bits by increasing the number of bits per symbol rather than the bandwidth, as in Trellis-Coded Modulation (TCM) and Turbo Trellis-Coded Modulation (TTCM). TCM is a

bandwidth efficient scheme relying on symbol-based interleaving and the classic set partitioning technique, as detailed in [5, 6, 200]. TTCM has a similar structure to turbo codes, but employs two TCM encoder/decoder blocks as its components and it performs better than TCM in both Gaussian and uncorrelated Rayleigh fading channels. The comparison of TCM, TTCM and other CM schemes such as Bit-Interleaved Coded Modulation (BICM) and BICM using Iterative Detection (BICM-ID) were discussed in [201]. In this section, TTCM is invoked due to its superior performance in uncorrelated Rayleigh fading channels.

Cooperative communications [202,203] constitute another effective method of combating channel fading. In this section, a TTCM aided Decode-and-Forward (DAF) scheme is proposed. Symbol-based Super-Position Modulation (SPM) is employed at the relay node for generating a new symbol sequence, which contains all the information received from both source nodes. Hence the communication between the Relay Node (RN) and the Destination Node (DN) would only require a single timeslot. Therefore, the slot efficiency is increased and precious transmission power can be saved.

Additionally, in order to increase the attainable power efficiency of the entire DAF system, a sophisticated Power Sharing (PS) technique based on Extrinsic Information Transfer (EXIT) charts [49] is introduced. The area under the EXIT curve is related to the normalized throughput that the decoder could reach at a given Signal-to-Noise Ratio (SNR) [198]. Hence, the EXIT chart can be used to determine the minimum SNR requited for achieving an infinitesimally low Bit Error Ratio (BER). In this section, the entire relaying system is divided into two links, namely the source-to-relay (SR) link and the relay-to-destination (RD) link. The minimum required SNR of each link is different. Hence, if the transmission power of the Source Nodes (SNs) and that of the RN were constrained to be identical, this would degrade the power efficiency of the whole system. An appropriate PS technique is capable of rearranging the transmission power of each SN and RN node, so that both the RN and DN simultaneously achieve an infinitesimally low BER. Hence, the BER performance of the system can be improved at a given average transmission power, when the appropriate PS technique is employed. The contributions of this section are:

1. The TTCM channel coding scheme was combined with the SPM technique to improve the performance of a two-user cooperative communication system and the detailed design was presented.

2. The PS technique was brought in and the power efficiency of the entire system had been improved.

The organisation of this section is as follows. Section 3.2.2 presents the system model and our motivation. Section 3.2.3 illustrates the SPM mapping at the RN, while Section 3.2.5 details the detection of the super-symbols. The pathloss reduction and our PS technique are detailed in Section 3.2.6. Our simulation results and analysis are provided in Section 3.2.7.

3.2.2 System Model

Figure 3.1 shows our system model. Two SNs, namely A and B, communicate with the DN labelled as D using the RN denoted as R. At the first Time Slot (TS), the SN A and B will transmit two signal frames namely $\{x_1\}$ and $\{x_2\}$, which are coded by TTCM rate-1/2 4QAM encoder, simultaneously to the RN R, where the signal received at the RN may be expressed as:

$$y = h_1 x_1 + h_2 x_2 + n_{RN} \,, \tag{3.1}$$

here h is the complex-valued channel fading coefficient and n is the Additive White Gaussian Noise (AWGN) having a variance of $N_0/2$ per dimension. Whilst, the RN R may produce a signal sequence $\{x\}$ for transmitting the information contained in the two signal frames $\{x_1\}$ and $\{x_2\}$ during the following TS. The $\{x\}$ is the SPM super-symbol generated from x_1 and x_2, and the generation rule is detailed in Eq. (3.3). Hence, the signal received by the DN may be:

$$y = hx + n_{DN} \,. \tag{3.2}$$

When compared to the network coding scheme of [204], the main benefit of our relaying scheme is that the RN may still be able to broadcast the information to the other nodes, which does not receive the information $\{x_1\}$ or $\{x_2\}$. In the network coding scheme of [204], the relay is invoked for exchanging information between two even or possibly multiple nodes. The pair of signal sequences $\{x_1\}$ and $\{x_2\}$ may be combined at the RN by an XOR function, therefore the two signal sequences may be inherently combined without expanding the constellation size of the signal, i.e. without requiring extra bandwidth. But in order to receive the original information $\{x_1\}$ broadcast by the RN, the receiver should have already obtained the information $\{x_2\}$. However, even though our relaying algorithm may increase the constellation size of the broadcast signal, both $\{x_1\}$ and $\{x_2\}$ may be received by any node without the requirement of receiving $\{x_1\}$ or $\{x_2\}$.

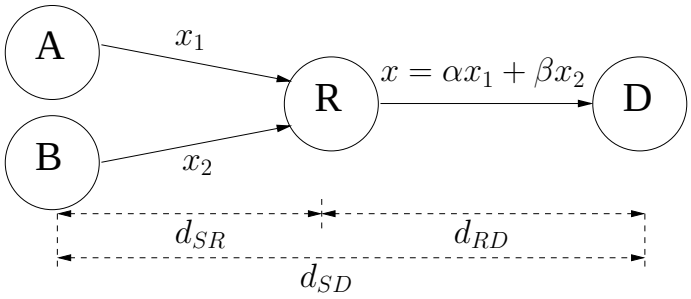

Figure 3.1: The model of a system relying on two SNs, one RN and one DN.

Note that, the entire cooperative communication system may require 2 TSs for the delivery of the pair of independent signal frames. Meanwhile, there are two information bits for a pair of rate-1/2 TTCM 4QAM coded symbols. Therefore, we let the RN to absorb these two information bits for producing an 8PSK symbol using a rate-2/3 TTCM encoder. As a benefit, the RN only

requires a single TS for the following transmission. However, a higher order modulation scheme typically imposes a higher complexity and a reduced fading resistance, while the flexibility of the system may also be reduced. Hence we conceive a SPM aided MIMO technique for the RN, where the RN first simultaneously receives the signals from the two SNs during the first timeslot based on our MIMO2×1 scheme with the aid of powerful maximum likelihood detection. Then, the RN decodes and separately re-encodes the two signal sequences using the same number of modulation levels. As shown is Eq. (3.3), the pair of signal frames would then be linearly combined using different weighting factors to generate a super-symbol frame, which would be transmitted to the DN during the second timeslot. In this case, it would only require two timeslots for transmitting two information frames from the two SNs to the DN. In these investigations, we assume that the entire system benefits from perfect Channel State Information (CSI).

3.2.3 Low-Order Linear Superposition

The SPM scheme was introduced in [202, 205]. Figure 3.2 shows the generation of the super-symbols. It can be seen that the constellation map of the super-symbol is similar to that of a 16QAM scheme. An SPM weighting factor pair (α,β) is defined, where α is assigned to $\{x_1\}$, which is the symbol received from SN A, while β is assigned to $\{x_2\}$, which is the symbol received from SN B.

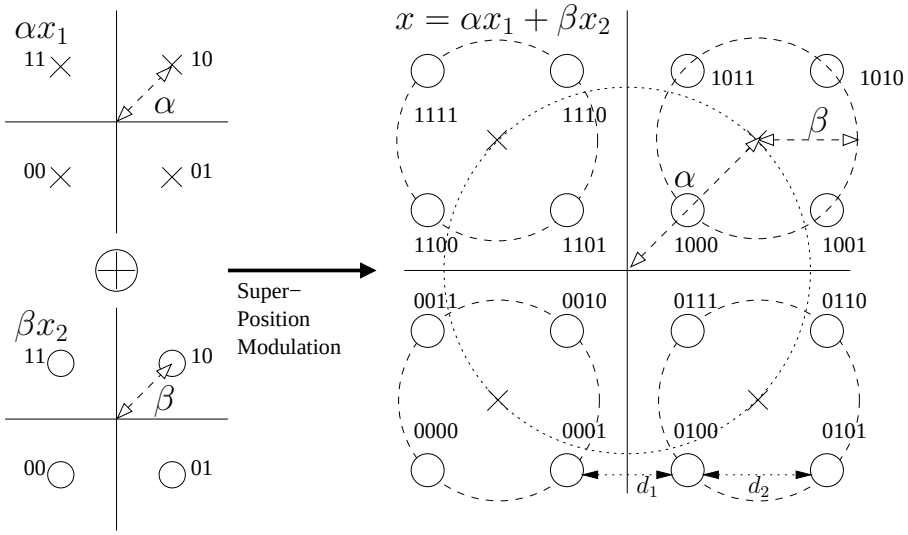

Figure 3.2: The generation of a 16-level super symbol set from two 4QAM symbol sets. We assume $\alpha > \beta$ in this figure.

Note that, the symbols contained in both of the signal frames $\{x_1\}$ and $\{x_2\}$ are set-partition modulated square 4QAM symbols. Then the SPM symbol can be written as:

$$x = \alpha x_1 + \beta x_2 \,, \tag{3.3}$$

where we have $E[|x_1|^2] = 1$ and $E[|x_2|^2] = 1$, since the average symbol power is assumed to be unity. When the two 4QAM symbols are multiplied using their SPM weighting factors, their

average power becomes:

$$E\left[\mid \alpha x_1 \mid^2\right] = \alpha^2 E\left[\mid x_1 \mid^2\right] = \alpha^2 \,, \tag{3.4}$$

$$E\left[\mid \beta x_2 \mid^2\right] = \beta^2 E\left[\mid x_2 \mid^2\right] = \beta^2 \,. \tag{3.5}$$

Since the average symbol power of the super-symbol should also be unity, we have:

$$\begin{aligned} E\left[\mid x \mid^2\right] &= E\left[\mid \alpha x_1 + \beta x_2 \mid^2\right] \\ &= E\left[\alpha^2 x_1^2 + \beta^2 x_2^2 + 2\alpha\beta x_1 x_2\right] \\ &= \alpha^2 E\left[\mid x_1 \mid^2\right] + \beta^2 E\left[\mid x_2 \mid^2\right] + 2\alpha\beta E\left[x_1 x_2\right] \\ &= \alpha^2 + \beta^2 + 2\alpha\beta E\left[x_1 x_2\right] \\ &= 1 \,. \end{aligned} \tag{3.6}$$

Furthermore, the two 4QAM symbol streams are independent of each other, yielding:

$$E\left[x_1 x_2\right] = E\left[x_1\right] E\left[x_2\right] = 0 \,, \tag{3.7}$$

where we have $E\left[x_1\right] = E\left[x_2\right] = 0$. Hence, it can be seen that the SPM weighting factor pair should satisfy:

$$\alpha^2 + \beta^2 = 1 \,. \tag{3.8}$$

It may be observed from the Figure 3.2 that if the factor α is larger than β, the constellation map of the super-symbol would be the expansion of the constellation map of x_2 based on the constellation map of x_1. Here we define the signal stream with larger SPM factor to be the dominant symbol and the signal stream with smaller SPM factor to be the auxiliary symbol. As shown in Figure 3.2, the minimal Euclidean distance d among the super-symbols is decided by the distance of d_1 and d_2 in Figure 3.2, which may be derived based on the value of α, where d is given by:

$$d = \begin{cases} \frac{1}{\sqrt{2}} \min\left(2\sqrt{1-\alpha^2}, 2\left(\alpha - \sqrt{1-\alpha^2}\right)\right) & \left(\alpha \geq \sqrt{1/2}\right) \\ \frac{1}{\sqrt{2}} \min\left(2\alpha, 2\left(\sqrt{1-\alpha^2} - \alpha\right)\right) & \left(\alpha < \sqrt{1/2}\right) \,. \end{cases} \tag{3.9}$$

If $\alpha \geq \sqrt{1/2}$, the maximum minimal Euclidean distance $d_{\max}$ is achieved for $2\sqrt{1-\alpha^2} = 2(\alpha - \sqrt{1-\alpha^2})$, which gives $\alpha = \sqrt{4/5}$. By contrast, if $\alpha < \sqrt{1/2}$, then $d_{\max}$ is attained for $2\alpha = 2(\sqrt{1-\alpha^2} - \alpha)$, which gives $\alpha = \sqrt{1/5}$. The minimal Euclidean distance $d_{\max}$ within the constellation map of the superposition symbols would be maximised, when α equals to $\sqrt{1/5} = 0.4472$ or $\sqrt{4/5} = 0.8944$, as shown in Figure 3.3. The weighting factor pair (0.4472, 0.8944) also obeys Eq. (3.8), which is the optimum choice in terms of maximising the minimal Euclidean distance.

Naturally, having a higher minimal Euclidean distance in a constellation set implies a higher resistance against both channel fading and noise. However, when considering the constellation map of a combined channel coding and modulation scheme, a larger Euclidean may not necessarily result in an improved BER performance. In this section, we did not optimize the SPM ratio pair for achieving the lowest overall BER performance. More specifically, we considered a SPM ratio of

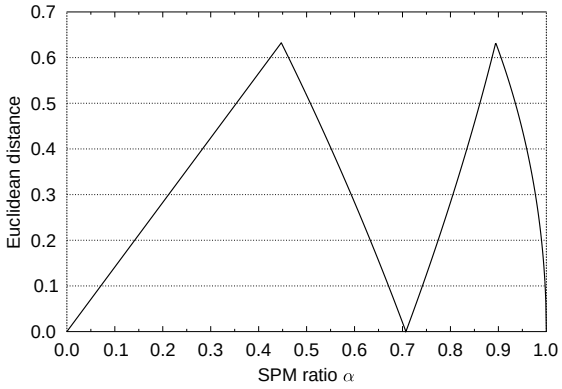

Figure 3.3: The relationship between the SPM ratio α and the Euclidean distance of the corresponding SPM-16QAM constellations.

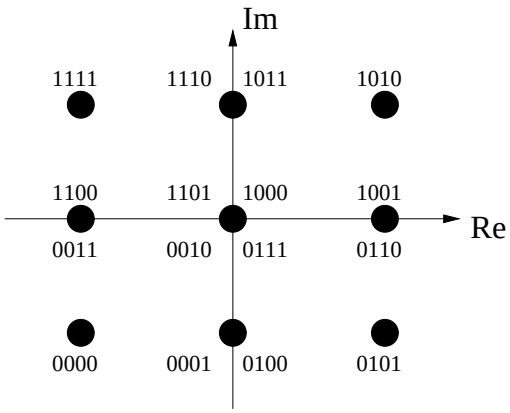

Figure 3.4: The SPM constellation map when the SPM ratio pair is $(\alpha = \sqrt{1/2}, \beta = \sqrt{1/2})$.

$(\alpha = 0.8944, \beta = 0.4472)$ because here we aim for maximizing the Euclidean distance of our CM scheme. Note that a super-symbol is constituted by the combination of the primary symbol and the auxiliary symbol, where the primary symbol has a larger minimal Euclidean distance, hence exhibiting an improved BER performance compared to that of the auxiliary symbol. Therefore, a beneficial strategy is proposed in Section 3.2.7 for balancing these two BERs.

Additionally, the SPM ratio pair should not be set to $(\alpha = \sqrt{1/2}, \beta = \sqrt{1/2})$, where the two symbols forming the super-symbol may have the same weights, since this would collapse the original 16-point constellation into a 9-point constellation, as shown in Figure 3.4. The details of the twin-layer SPM constellation map associated with $(\alpha = \sqrt{1/2}, \beta = \sqrt{1/2})$ are summarized in Table 3.1. It may be observed that when we choose $(\alpha = \sqrt{1/2}, \beta = \sqrt{1/2})$, the SPM super-symbols may not remain equi-probable. Furthermore, the signal power of four constellation points becomes zero. Finally, there are also overlaps among the constituent constellations. This will lead to SPM symbol detection errors.

(x_1, x_2)	SPM symbol	Pro.
(00, 00)	(-0.5, -0.5j)	1/16
(01, 01)	(0.5, -0.5j)	1/16
(10, 10)	(0.5, 0.5j)	1/16
(11, 11)	(-0.5, 0.5j)	1/16
(00, 01), (01, 00)	(0, -0.5j)	1/8
(01, 10), (10, 01)	(0.5, 0j)	1/8
(10, 11), (11, 10)	(0, 0.5j)	1/8
(00, 11), (11, 00)	(-0.5, 0j)	1/8
(00, 10), (01, 11), (10, 00), (11, 01)	(0, 0j)	1/4

Table 3.1: The table of constellation points of the twin layer SPM symbols when ($\alpha = \sqrt{1/2}, \beta = \sqrt{1/2}$).

3.2.4 Detection of the Super-symbols

At the RN, two 4QAM symbol sequences are merged in order to form a SPM signal sequence. Although the new super-symbol contains the information of two 4QAM symbols and the constellation map of the superposition signal is similar to that of classic 16QAM, the decoding block of the receiver is still based on 4QAM symbols. To decode the SPM symbols received from the RN, the first step is to compute the symbol probabilities of the SPM symbol and then to calculate the symbol probabilities of the two 4QAM symbol sequences. The output of the demapper at instant k is the Probability Density Function (PDF) of receiving y_n at the DN, given that the super-symbol $x_k = \alpha x_{1,k} + \beta x_{2,k}$ was transmitted, which can be expressed as:

$$p\left(y_k | x_{1,k}, x_{2,k}\right) = \frac{1}{\pi N_0} \exp\left(-\frac{\left|y_k - h\left(\alpha x_{1,k} + \beta x_{2,k}\right)\right|^2}{N_0}\right), \tag{3.10}$$

where y_k is the signal received at the DN, which is formulated as $y_k = h_k(\alpha x_{1,k} + \beta x_{2,k}) + n_k$, while h_k is the fast Rayleigh fading and n_k is the AWGN noise. Hence, the conditional PDF $p\left(y_k | x_{1,k}, x_{2,k}\right)$ obeys the Gaussian distribution. The PDF of receiving y_k, given $x_{1,k}$ or $x_{2,k}$ may be derived from Eq. (3.10) as:

$$p\left(y_k | x_{1,k} = x^{(i)}\right) = \sum_{j=0}^{3} p\left(y_k | x_{1,k} = x^{(i)}, x_{2,k} = x^{(j)}\right), \tag{3.11}$$

$$p\left(y_k | x_{2,k} = x^{(j)}\right) = \sum_{i=0}^{3} p\left(y_k | x_{2,k} = x^{(j)}, x_{1,k} = x^{(i)}\right), \tag{3.12}$$

where $x^{(i)}$ and $x^{(j)}$ are the hypothetically transmitted set-partition labeled 4QAM symbols for $\{i, j\} \in \{0, 1, 2, 3\}$, as shown in Figure 3.2, and $k \in \{1, 2, \ldots, \eta\}$ is the order of the current symbol in the received signal stream. Furthermore, η is the block size of the TTCM encoder/decoder, which is 12,000 in this study. The input of the TTCM decoder is a $(\eta \times M)$-element probability matrix, where $M = 4$ is considered. Based on Eq. (3.11) and Eq. (3.12), the elements in the pair of probability matrices Pr_{x_1} and Pr_{x_2} required for decoding $\{x_1\}$ and $\{x_2\}$ will be expressed as:

$$\mathrm{Pr}_{x_1}(k, i) = \mathrm{Pr}\left(x_{1,k} = x^{(i)} \mid y_k\right) = p\left(y_k \mid x_{1,k} = x^{(i)}\right) \times \mathrm{Pr}\left(x^{(i)}\right), \tag{3.13}$$

$$\Pr_{x_2}(k,j) = \Pr\left(x_{2,k} = x^{(j)} \mid y_k\right) = p\left(y_k \mid x_{2,k} = x^{(j)}\right) \times \Pr\left(x^{(j)}\right) . \quad (3.14)$$

We note that in order to reduce the complexity of the entire system, we do not invoke any iterations between the demapper and the TTCM decoder at the DN. Hence the elements of the probability matrices $\Pr\left(x^{(i)}\right)$ and $\Pr\left(x^{(j)}\right)$ are all equi-probable, associated with 1/4. Then, the TTCM decoder used at the DN may decode both information sequences $\{x_1\}$ and $\{x_2\}$ based on the pair of probability matrix using the classic Approx-log MAP scheme of [6].

3.2.5 Iterative Decoding Based on MIMO-2 × 1 at the RN

The iterative decoding of TTCM was detailed in [6, 36]. A TTCM decoder is constituted by a pair of TCM decoders, as shown in Figure 3.5. Figure 3.6 shows the iterative information exchange between the TTCM decoder and the demapper at the RN.

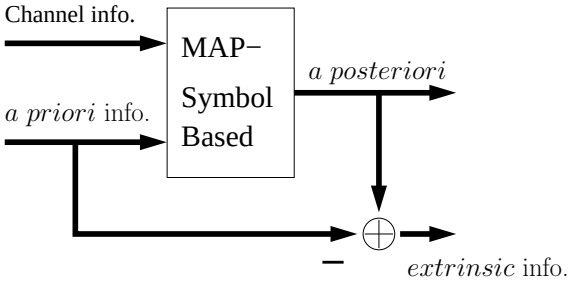

Figure 3.5: The TCM decoder [6] constitutes a MAP algorithm based decoder.

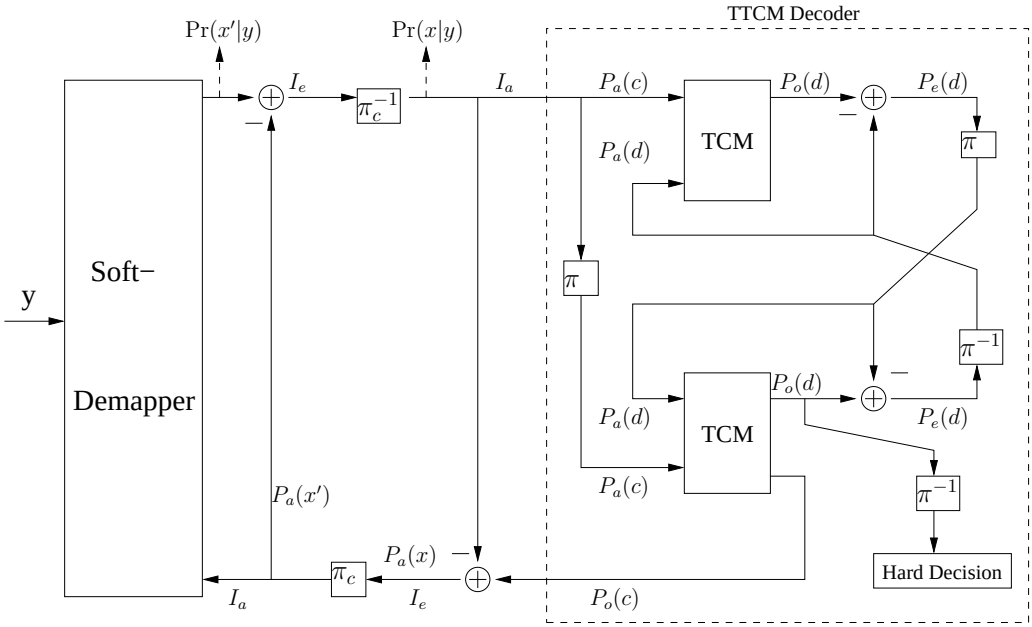

Figure 3.6: The iterative decoding at the RN.

The detection is based on an equivalent two-transmitter one-receiver system. The EXIT chart

visualises the *extrinsic* information flow between the two TCM decoders and the Soft-Demapper [49, 191]. The two TCM decoders are identical. As observed in Figure 3.6 that the *a priori* information of the codeword $P_a(c)$ gleaned from the Soft-Demapper is not the only input. The other input $P_a(d)$ is received from the lower TCM decoder, which is the *a priori* information of the data word. Both $P_a(c)$ and $P_a(d)$ are used for generating the *a posteriori* information (APP) of the data word $P_o(d)$. After subtracting the *a priori* information $P_a(d)$ from the *a posteriori* information $P_o(d)$, the *extrinsic* probability of the dataword $P_e(d)$ is obtained. Then, $P_e(d)$ is interleaved to generate the *a priori* information $P_a(d)$ for the lower TCM decoder. The same process is repeated at the lower TCM decoder, except that the lower TCM decoder would additionally compute the *a posteriori* information of the codeword $P_o(c)$ during the last TCM iteration. The interleaver and de-interleaver between the two TCM decoders will not influence the amount of mutual information, its role is to keep the sequence of the two data streams in the right order. As shown in Figure 3.6, the probability of the codeword $P_o(c)$ at the output of the lower TCM decoder would be fed to the Soft-Demapper, while $P_o(d)$ would be forwarded to the decision block.

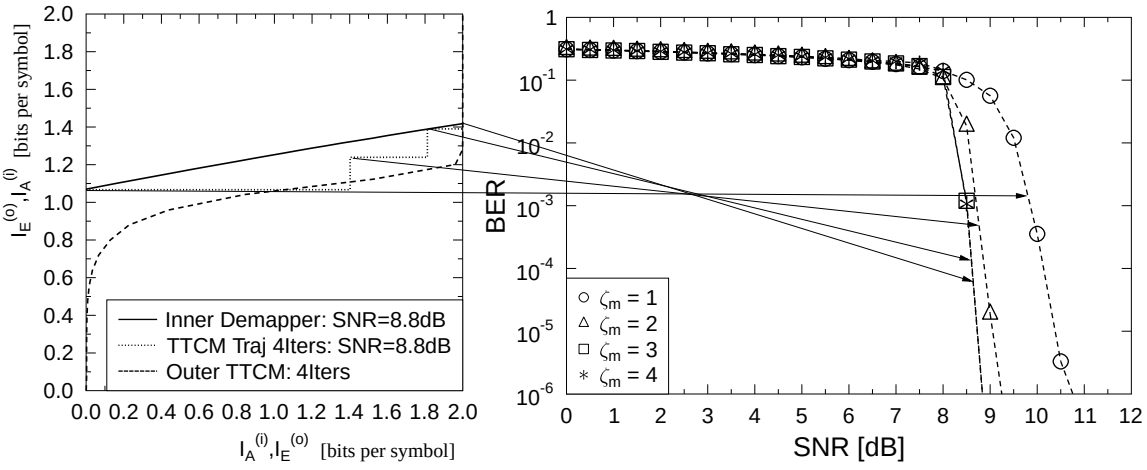

Figure 3.7: The EXIT-chart based on a (2×1)-element MIMO assisted TTCM 4QAM scheme (as the first transmission TS of the system of Figure 3.1), when communicating over an uncorrelated Rayleigh fading channel. The number of iterations between the TTCM decoder and the soft-decoder at the RN is $\zeta_m = 4$ and the related simulation parameters are shown in Table 3.2.

Figure 3.7 shows the EXIT chart characterising the *extrinsic* information exchange between the TTCM decoder and the MIMO-2×1 scheme's demapper. The 'Inner Demapper' curve represents the information received from the channel when the receive SNR is 8.8 dB, which represents the soft information input to the decoder by the demapper of Figure 3.6. Meanwhile, the 'Outer TTCM' curve characterizes the decoding capability of the TTCM decoder, where the 'TTCM Traj 4 Iters' curve portrays the information exchange between the decoder and the soft demapper, when the receive SNR is 8.8 dB, for $\zeta = 4$ iterations. More specifically, the outer decoder's EXIT curve is based on the *a priori* information $P_a(c)$, while the *extrinsic* information is $[P_o(d) - P_a(d)]$, which represents the input and output of the TTCM decoder block in Figure 3.6. Hence, the shape

of this curve depends on the number of TTCM iterations and on the choice of the component TCM decoder. By contrast, the inner decoder's EXIT curve is based on the *a priori* information in $P_a(x')$ and on the *extrinsic* information $[P(x'|y) - P_a(x')]$. The shape of the inner decoder's EXIT curve is only dependent on the receive SNR.

Based on a given number of modulation levels , on the SNR and on the number of iterations, an open EXIT tunnel leading to the (2,y) bound of Figure 3.7 might be formed. When this is the case, decoding convergence to an infinitesimally low BER is possible. The step-wise linear decoding trajectory traversing through the open EXIT chart tunnel of Figure 3.7 is based on Monte-Carlo simulations. It depicts the information exchange during each iteration between the MIMO-2X1 demapper and the TTCM decoder. The variables I_a and I_e in the EXIT charts represent all the mutual information terms in units of bits per symbol. The maximum mutual information value in the EXIT chart is $I_e = 2$, because 4QAM modulation is employed. Again, the EXIT charts can be used to find the minimum SNR required for achieving an infinitesimally low BER. The PS technique can be invoked to reduce the overall transmission power. According to the EXIT-chart shown in Figure 3.7, we find that in order to receive the two rate-1/2 TTCM coded signal frames form the two SNs, the required receive SNR should be 8.8 dB, which may guarantee an open tunnel for TTCM decoder.

3.2.6 Path Gain and Power Sharing

A. Path Gain

As shown in Figure 3.1, when relying on a RN, the propagation distance d_{SD} is divided into two parts, namely d_{SR} and d_{RD}, hence the path loss is reduced and the performance of the system may be improved. When considering an inverse-square-power free-space path loss model, the reduced-distance-related pathloss reduction (path gain) between the SN and RN can be expressed as [206]:

$$G_{SR} = \frac{d_{SD}^2}{d_{SR}^2}\,, \tag{3.15}$$

By contrast, the path gain of the link between the RN and the DN is

$$G_{RD} = \frac{d_{SD}^2}{d_{RD}^2}\,, \tag{3.16}$$

If the RN is located right in the middle, then we have $d_{SR} = d_{RD} = d_{SD}/2$ and $G_{sr} = G_{rd} = 4$, which is about 6.02 dB.

B. Power Sharing

In this section optimum PS is proposed for reducing the overall transmission power of the whole system. To achieve an infinitesimally low BER (eg. 10^{-6}), the required receive SNR (dB) of the RN is different from that of the DN. In this situation, optimally sharing the overall average transmission power between the SNs and RN based on the difference between the receive SNR

required at the RN and at the DN is capable of reducing the required average receive power of the entire system. When considering the path gain, if the transmission power ratio (SNR ratio) required to get a low BER at the SN is denoted as $\gamma_{T,s}$ and that of the RN is as $\gamma_{T,r}$, then we have:

$$\mathrm{Y}_{R,r} = 10\log_{10}(\gamma_{T,s}) + G_{sr}[dB]\,, \tag{3.17}$$

$$\mathrm{Y}_{R,d} = 10\log_{10}(\gamma_{T,r}) + G_{rd}[dB]\,, \tag{3.18}$$

where, $\mathrm{Y}_{R,r}$ and $\mathrm{Y}_{R,d}$ is the receive SNR (dB) required at the RN and DN, respectively. Based on Eq. (3.17) and Eq. (3.18), if the difference of the receive SNR (dB) required between the RN and DN is represented by $\mathrm{Y}_{R,\Delta}$, then we have:

$$\begin{aligned}\mathrm{Y}_{R,\Delta} &= \mathrm{Y}_{R,d} - \mathrm{Y}_{R,r} \\ &= 10\log_{10}(\gamma_{T,r}) - 10\log_{10}(\gamma_{T,s}) \\ &= 10\log_{10}\left(\frac{\gamma_{T,r}}{\gamma_{T,s}}\right)\,. \end{aligned} \tag{3.19}$$

If $\mathrm{Y}_{R,\Delta} = 10\log_{10}(\gamma_{R,\Delta})$, then the receive SNR ratio between the RN and DN may be formulated as:

$$\gamma_{R,\Delta} = \frac{\gamma_{T,r}}{\gamma_{T,s}}\,, \tag{3.20}$$

where the average transmission power ratio per timeslot of the overall system is given by:

$$\bar{\gamma}_T = \frac{\gamma_{T,s} + \gamma_{T,r}}{2}\,. \tag{3.21}$$

Hence, the transmission power ratio at the SNs can be formulated as:

$$\gamma_{T,s} = \frac{2\bar{\gamma}_T}{1+\gamma_{R,\Delta}}\,, \tag{3.22}$$

while, the transmission power ratio at the RN is given by:

$$\gamma_{T,r} = \frac{2\bar{\gamma}_T\gamma_{R,\Delta}}{1+\gamma_{R,\Delta}}\,. \tag{3.23}$$

3.2.7 Simulation Results

The BER versus SNR performance of the SPM aided TTCM-4QAM scheme communicating over uncorrelated Rayleigh fading channels is shown in Figure 3.8 and Figure 3.9. The performance of the first user is studied when using an SPM weighting factor α ranging from 0.1 to 0.95. As seen in Figure 3.8 and Figure 3.9, when α increases, the performance of the first user improves, except for $\alpha = 0.707$. When we have $\alpha = 0.707$, the 16-point SPM constellation of Figure 3.2 will collapse into a 9-point SPM constellation, because some of the constellation points are at the same location. This would make detection impossible and a high BER floor will emerge. Note that for $\alpha > 0.7071$ the first user's signal x_1 becomes the dominant signal, while x_2 becomes the auxiliary signal, where we have $\beta < 0.707$, and vice versa. The higher α , the stronger protection the dominant symbol x_1 will have, which directly leads to a performance loss for the auxiliary symbol x_2. As seen in

Coded Modulation	**TTCM**
Modulation Scheme	4QAM, SPM-16QAM
Mapper type	Set-Partitioned
Number of iterations	$\zeta = 4, \zeta_m = 4$
Code Rate	1/2
Code Memory	3
Code Polynomial (octal)	$H = [13\ 06]$
Decoder type	Approximate Log-MAP
Symbols per frame	12,000
Number of frames	10,000
Channel	Uncorrelated Rayleigh fading channel
Path-loss exponent	2

Table 3.2: Simulation parameters used in the schematic of Figure 3.1, which are employed in the simulations in Figure 3.8 to Figure 3.11.

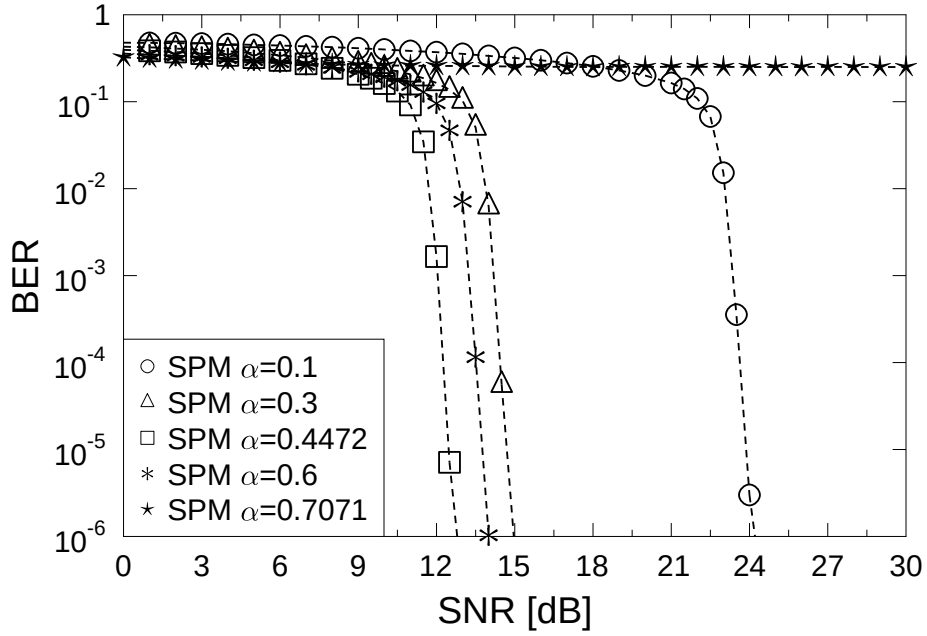

Figure 3.8: The BER versus SNR performance of the twin-layer SPM aided TTCM-4QAM scheme (as the second transmission TS of the system of Figure 3.1), when communicating over uncorrelated Rayleigh fading channels. The performance of the first user is studied when using $\alpha = \{0.1, 0.3, 0.4472, 0.6, 0.707\}$. The simulation parameters are shown in Table 3.2.

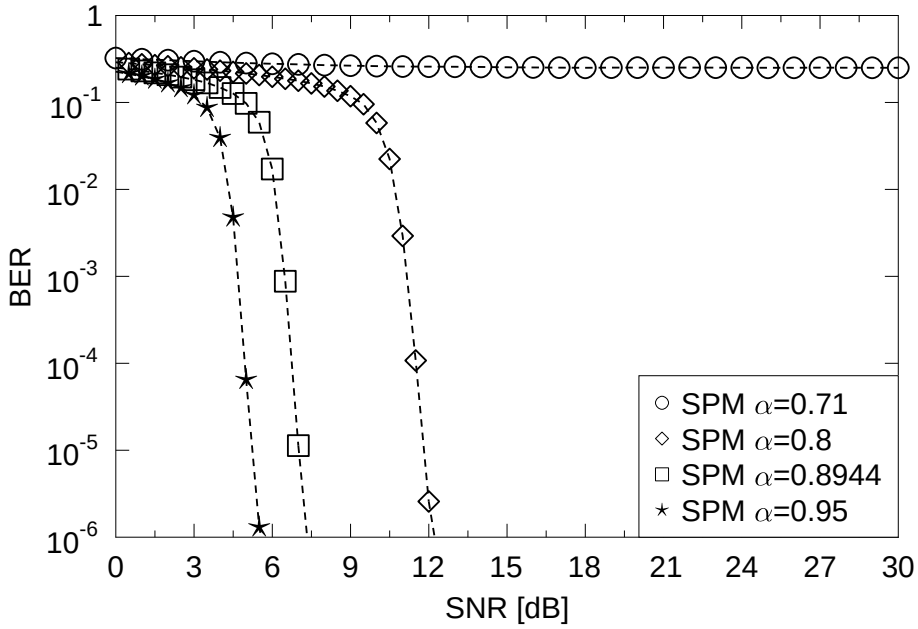

Figure 3.9: The BER versus SNR performance of the twin-layer SPM aided TTCM-4QAM scheme (as the second transmission TS of the system of Figure 3.1), when communicating over uncorrelated Rayleigh fading channels. The performance of the first user is studied when using $\alpha = \{0.707, 0.8, 0.8944, 0.95\}$. The simulation parameters are shown in Table 3.2.

Figure 3.8, the best ratio for the auxiliary signal is given by 0.4472. According to the analysis of Section 3.2.3, we decide to set the SPM weighting factor pair to be $(\alpha = 0.8944, \beta = 0.4472)$. While the simulation parameters are shown in Table 3.2.

We have proposed the 'Equal BER' method to achieve the same BER for both users by using $(\alpha = 0.8944, \beta = 0.4472)$ for all even symbol periods, while swapping the weighting factor to $(\alpha = 0.4472, \beta = 0.8944)$ for all odd symbol periods. The performance of the Equal BER scheme is shown in Figure 3.10 in comparison to the user 1 and user 2 performance curves based on the fixed ratio factor pair of $(\alpha = 0.8944, \beta = 0.4472)$. As seen in Figure 3.10, the performance of the Equal BER method is approximately 2.4 dB better than that of user 2, but approximately 3 dB worse than that of user 1 for the conventional method at a BER of 10^{-6}. Moreover, the RN could also absorb the two information bits contained in the two 4QAM symbols and communicate with DN by 8PSK symbol with code rate 2/3. In this situation, the modulation level at the RN and the DN is increased from 4 to 8, while its BER performance is approximately 3 dB worse than that of our equal BER scheme at a BER of 10^{-6}, as shown in Figure 3.10.

Figure 3.7 shows the EXIT chart of the detection process at the RN, where two SNs simultaneously transmit their 4QAM-based frames to the RN. This is equivalent to a (2×1)-element MIMO scheme, where two transmit antennas are used for conveying two independent signals to a receiver having a single antenna. The number of TTCM decoding iterations was fixed to four. As

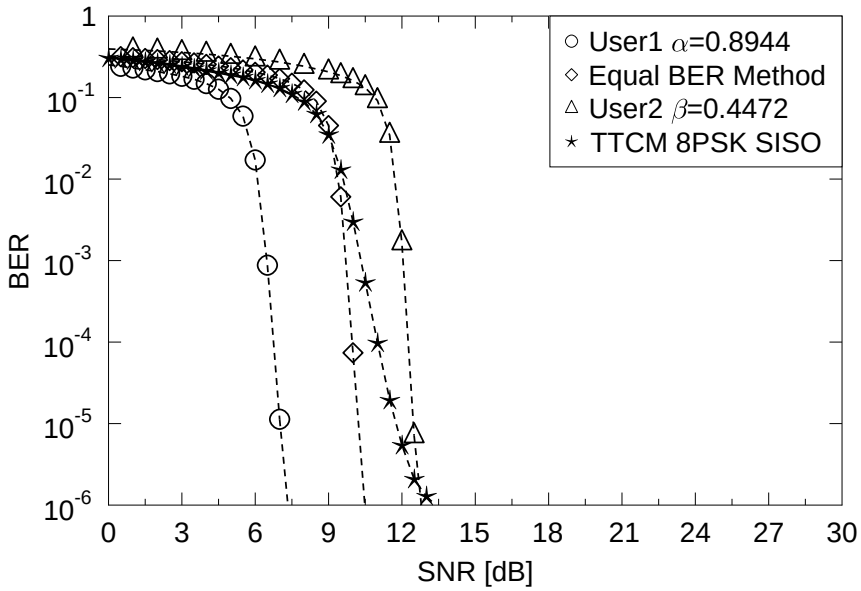

Figure 3.10: The BER versus SNR performance of the twin-layer SPM aided TTCM-4QAM scheme (as the second transmission TS of the system of Figure 3.1). The first and second users are based on the ratio factors of $\alpha = 0.8944$ and $\beta = 0.4472$, respectively. The equal BER method is also considered for comparison. The simulation parameters are shown in Table 3.2 and the simulation results are summarized in Table 3.3.

seen in Figure 3.7, the link between the SNs and the RN requires an SNR of 8.8 dB in order to achieve a low BER at the RN. By contrast, as seen in Figure 3.10, the RN to DN link requires an SNR of 10.5 dB to achieve a BER below 10^{-6}. The difference between these two SNRs is given by $Y_{R,\Delta} = 10.5 - 8.8 = 1.7$ dB. Hence, according to the Eq. (3.22) and Eq. (3.23), the total transmit power at the SNs (A and B) is 3.17 dB, and the transmit power at the RN is 4.77 dB. Our simulation results recorded for the TTCM-4QAM aided SPM based cooperative schemes are depicted in Figure 3.11. When a RN located at the midway position between the SNs and DN is employed, the PS based scheme performs approximately 0.5 dB better than the equal-power scheme at a BER of 10^{-6}. As seen in Figure 3.11, it can be stated that the PS-based SPM cooperative scheme requires approximately $10.5 - 4.0 = 6.5$ dB lower SNR than the non-cooperative SPM scheme. It is also $8.8 - 4.0 = 4.8$ dB more power-efficient than the two-transmitter one-receiver TTCM-4QAM scheme. The simulation results of this section are summarized in Table 3.3, where we use bits per symbol per TS (bps), when considering the throughput of the cooperative communication system.

3.3 HM based TTCM aided Cooperative Communications

3.3.1 Introduction

Having investigated the SPM based scheme in Section 3.2, we now study the HM based scheme in this section. The existing wireless networks support in excess of 4 billion subscribers, hence it

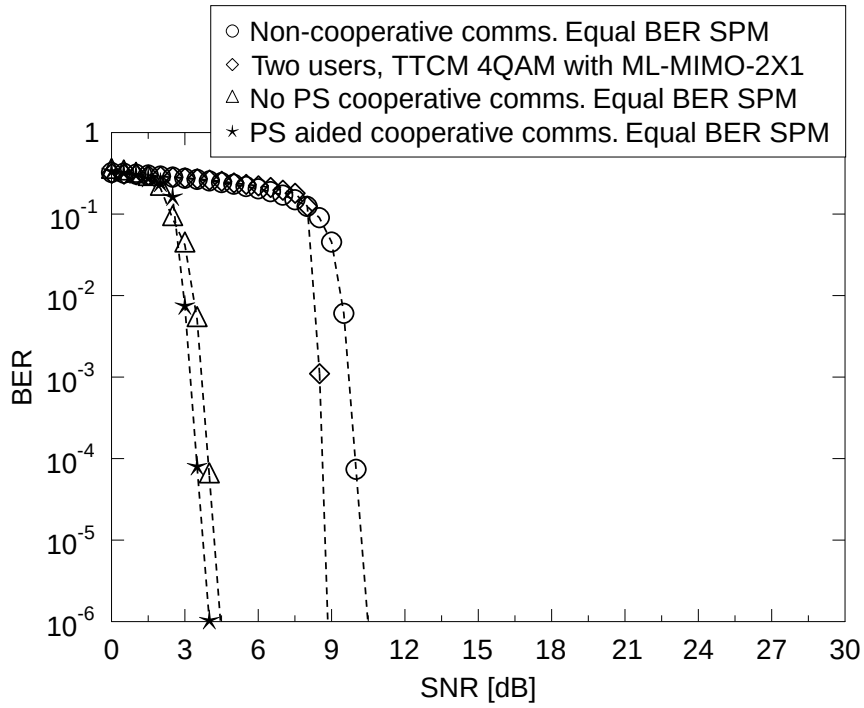

Figure 3.11: The BER versus SNR performance of the SPM aided TTCM-4QAM based cooperative communication schemes. The performance curves of the non-cooperative SPM aided TTCM-4QAM scheme and of the (2×1)-element MIMO aided TTCM-4QAM scheme (as seen in Figure 3.1) are also considered for comparisons. The simulation parameters are shown in Table 3.2 and the simulation results are summarized in Table 3.3.

Channel		**Uncorrelated Rayleigh**	
Memory		3	
Decoder Type		Approximate Log-MAP	
Code	Designed bps	SNR (dB) at	
		BER of 10^{-3}	BER of 10^{-6}
TTCM-SPM User1 $\alpha = 0.8944$	1	6.48	7.34
TTCM-SPM User2 $\beta = 0.4472$	1	12.04	12.80
Equal-TTCM-SPM User1	1	9.70	10.39
Equal-TTCM-SPM User2	1	9.63	10.48
TTCM 8PSK Rate-2/3	2	10.32	13.40
TTCM 4QAM MISO2 $\times$ 1	2	8.50	8.84
No PS Coop. system in Figure 3.1	1	3.68	4.45
PS aided Coop. system in Figure 3.1	1	3.21	4.00

Table 3.3: The SNR threshold values of various CM schemes, when transmitting over uncorrelated Rayleigh fading channels. These values are based on Figure 3.8 to Figure 3.11. The related simulation parameters are shown in Table 3.2.

would be impossible to replace all the personal devices or base stations in upgrading their services. Furthermore, maintaining the Quality of Service (QoS) for all subscribers, while aiming for an increased QoS for the upgraded new services would require strict backward compatibility [86, 207]. Hierarchical Modulation (HM), which is also often referred to as layered modulation may be considered as an efficient solution to the above-mentioned upgrading problems. The benefit of HM is that it is capable of manipulating multiple simultaneous data streams by modulating them on to a number of different layers, while the information in the different layers may be demodulated separately [207]. In this way, the upgraded new services may be merged with the already available services, where the original devices may simply switch to a higher number of modulation levels or to a higher coding rate in the upgraded broadcast devices [4].

The HM scheme is well investigated by Alouini in [110, 208] in terms of the general mapping model, the complexity analysis and the BER performance. HM scheme has also been incorporated in cooperative communication systems by Hausl [114] and Li [209]. It is shown that by employing HM scheme, the destination node could only demap part of the received signal from the source, while the relay node could provide the rest of the information to assist the entire transmission. Their results illustrated that the performance of the system could be improved without enlarging the complexity of the entire system. On the other hand, we note that the majority research work on the HM scheme nowadays focuses on its capacity features. The HM scheme always appears in rate-adaptive systems to support multiple users. However, with the development of cooperative communication theory, the HM scheme would have other potential benefits, for instance, improving a single user's performance, while maintaining a high data/code rate at a low transmit power level.

In this section, we propose a single relay aided cooperative communication system. The TTCM channel coding scheme and HM scheme are introduced to improve the performance of the entire system. More specifically, a special designed HM scheme aided soft-decoding TTCM (TTCHM) scheme is implied. The assumption is that the destination node (DN) could only receive 4QAM signal from the source node due to the hostile fading channel, our simulation results had shown that with the TTCHM scheme and the relay, it is possible for the SN to transmit 16QAM symbol or even 64QAM symbol while maintaining an acceptable BER performance. The contributions of this section are:

1. We propose a newly designed HM scheme for cooperative communications when communicating over Rayleigh fading channels.

2. A novel Turbo Trellis-Coded Hierarchical Modulation (TTCHM) scheme was conceived for improving the performance of the entire system.

The organization of this section is as follows. Section 3.3.2 illustrates the system model and the section's rationale. Section 3.3.3 presents the HM's layering method, while Section 3.3.4 details the system's block diagram and our communications protocol. Our simulation results and analysis are provided in Section 3.3.5.

3.3.2 System Model

In this section we introduce our TTCHM assisted Decode-And-Forward (DAF) based cooperative communication scheme of Figure 3.12. Compared to the system shown in Figure 3.1, our cooperative communication system of Figure 3.12 also needs two TSs for completing its transmissions. However, instead of assuming that the DN is incapable of receiving the information in Figure 3.1, the DN of the newly designed system of Figure 3.12 is capable of receiving part of the soft information broadcast by the SN, which is an explicit benefit of our HM scheme. To be more specific, during the first communication Time Slot (TS), the SN would transmit a frame of TTCHM symbols $\{x_1\}$ to both the Relay Node (RN) and the DN. Then the RN decodes the stream $\{x_1\}$ in order to produce the frame $\{x_2\}$, which would be forwarded to the DN during the second TS. The DN would then recover the frame $\{x_1\}$ based on the pair of frames received from the SN and RN.

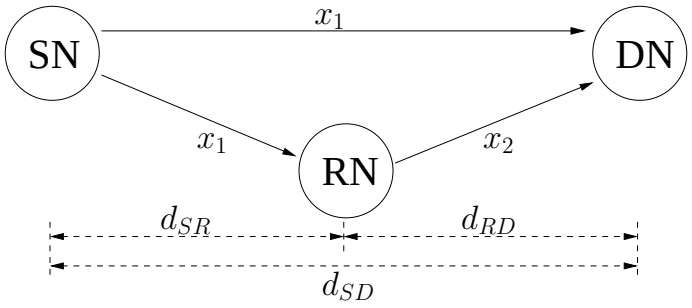

Figure 3.12: The model of a single-relay cooperative system.

We consider an uncorrelated Rayleigh flat-fading channel and the receivers are assumed to acquire perfect Channel State Information (CSI). After the first TS, the symbol received by the DN may be expressed as:

$$y_{SD} = \sqrt{G_{SD}} h_{SD} x_1 + n_{SD} \,, \tag{3.24}$$

while the symbol received by the RN is:

$$y_{SR} = \sqrt{G_{SR}} h_{SR} x_1 + n_{SR} \,, \tag{3.25}$$

where the subscript SD denotes the SN-DN link and the subscript SR represents the SN-RN link. By contrast, the symbols received at the DN during the 2nd TS, which are sent by the RN, may be expressed as:

$$y_{RD} = \sqrt{G_{RD}} h_{RD} x_2 + n_{RD} \,, \tag{3.26}$$

where the subscript RD represents the RN-DN link. Additionally, the notations h_{SD}, h_{SR} and h_{RD} denote the complex-valued coefficients of the uncorrelated Rayleigh fading for the different links, while n_{SD}, n_{SR} and n_{SR} denote the Additive White Gaussian Noise (AWGN) having a variance of $N_0/2$ per dimension. Moreover, the terms G_{SD}, G_{SR} and G_{SR} represent the reduced-distance-related-pathloss-reduction for each link, which we also refer to as the path-gain. We consider an inverse-second-power law based free-space path-loss model [206] and naturally, the path-gain G_{SD}

of the SD link is assumed to be unity. The position of the RN in our simulations is assumed to be right in the middle between the SN and DN. Therefore the path-gain of the SR link is:

$$G_{SR} = \left(\frac{d_{SD}}{d_{SR}}\right)^2 = 4\,, \tag{3.27}$$

and similarly, the path-gain of the RD link is:

$$G_{RD} = \left(\frac{d_{SD}}{d_{RD}}\right)^2 = 4\,. \tag{3.28}$$

The HM scheme and our communication protocol will be discussed in the following two sections.

3.3.3 Hierarchical Modulation

The general hierarchical constellation strategy was detailed in [208]. In contrast to the conventional HM scheme, the HM scheme used in our communication protocol has the following two main differences:

1. A new bit-to-symbol mapping method is defined, where the signal constellation is optimized according to the position of the RN.
2. The classic Set-Partitioning (SP) technique is employed in our TTCHM scheme and the symbol-based MAP algorithm is used for guaranteeing a minimum Symbol Error Rate (SER).

However, the SP scheme would assign the parity bit to the least protected constellation-position, which would lead to a high BER for the parity bit. Fortunately, we will demonstrate that this does not jeopardize the overall BER of the information bits.

Figure 3.13 shows our twin-layer HM-16QAM mapping scheme. Similar to the conventional HM scheme, we partition the coded symbols into different layers and map two data bits to each layer. The most important two bits represent the base layer. Their constellation points are defined by the set S_{4QAM}, which are represented by the four shaded circles in Figure 3.13, note that the positions of the points in the constellation map of the S_{4QAM} here is the same with the conventional 4QAM modulation scheme. Based on the base layer, the twin-layer HM-16QAM symbols are generated using a parameter δ_1:

$$S_{HM-16QAM} = \widetilde{\alpha}\left[S_{4QAM} \pm \sqrt{2}\delta_1 e^{\pm\frac{\pi}{4}j}\right]\,, \tag{3.29}$$

where $\widetilde{\alpha} = 1/\sqrt{1+2\delta_1^2}$ is the normalization parameter, which maintains the average symbol power of the $S_{HM-16QAM}$ constellation to be unity. Furthermore, we define a HM parameter R_1, which equals to d_1/d_0 relying on the distances d_0 and d_1 seen in Figure 3.13. The value of δ_1 (also seen in Figure 3.13) depends on this R_1. When we change the value of R_1, the positions of the constellation points in the HM-16QAM would be changed. To be more specific, before the normalization, we have $\delta_1 = d_0/2$ and $d_0 + d_1 = \sqrt{2}$. The relationship between the δ_1 and R_1 can be expressed by:

$$\delta_1 = \frac{d_0}{\sqrt{2}\sqrt{2}} = \frac{d_0}{\sqrt{2}\,(d_0+d_1)} = \frac{1}{\sqrt{2}\,(1+R_1)}\,, \tag{3.30}$$

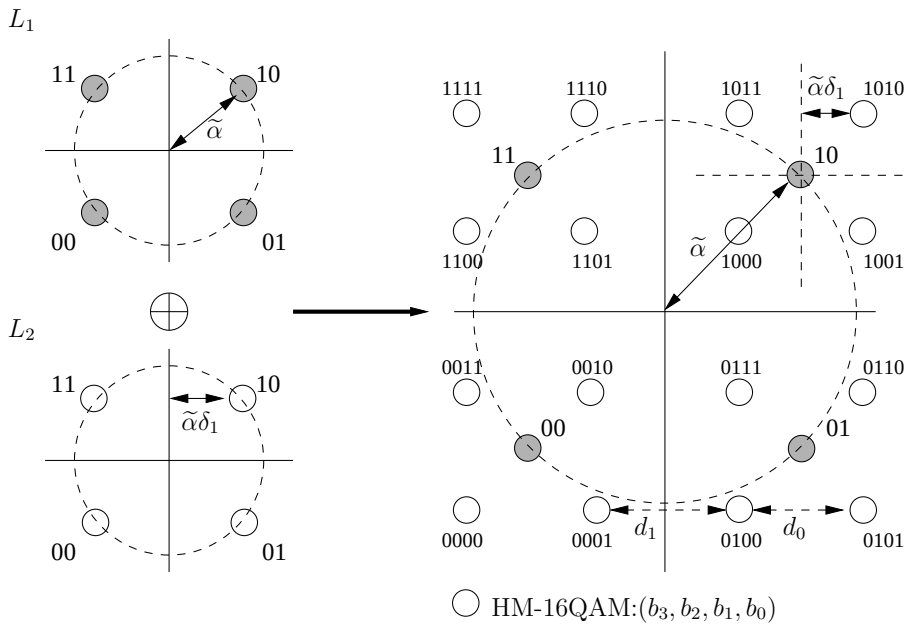

Figure 3.13: The constellation map of the twin-layer HM-16QAM scheme.

here, it also can be observed that:

$$R_{1\max} = \frac{d_{1\max}}{d_{0\min}} = \frac{\sqrt{2}}{0} \Rightarrow \infty \,, \tag{3.31}$$

$$R_{1\min} = \frac{d_{1\min}}{d_{0\max}} = \frac{0}{\sqrt{2}} \Rightarrow 0 \,, \tag{3.32}$$

to sum up, we have $0 < R_1 < \infty$.

Furthermore, as shown in Figure 3.14 the triple-layer HM-64QAM constellations may be generated by adding a third layer to the twin-layer HM-16QAM signals upon introducing the HM parameter δ_2, which can be formulated as:

$$S_{HM-64QAM} = \widetilde{\beta}\left[S_{4QAM} \pm \sqrt{2}\delta_1 e^{\pm\frac{\pi}{4}j} \pm \sqrt{2}\delta_2 e^{\pm\frac{\pi}{4}j}\right] \,, \tag{3.33}$$

where, δ_2 depends on the ratio of d_3/d_2, as shown in Figure 3.14. We define $R_2 = d_3/d_2$ and the normalization parameter in Eq. (3.33) is given by $\widetilde{\beta} = 1/\sqrt{1+2\delta_1^2+2\delta_2^2}$. Again, also before the normalization, it can be observed in Figure 3.14 that we have $\delta_2 = (d_1 - d_3)/2$, which can be further written as:

$$\begin{aligned} \delta_2 &= \frac{d_0 R_1 - d_2 R_2}{2} \\ &= \frac{d_0 R_1 - (d_0 + 2\delta_2) R_2}{2} \\ &= \frac{d_0 (R_1 - R_2)}{2(1+R_2)} = \frac{R_1 - R_2}{\sqrt{2}(1+R_1)(1+R_2)} \,. \end{aligned} \tag{3.34}$$

Note that the value of R_2 is directly restricted by the value of R_1, we have:

$$R_{2\max} = \frac{d_{3\max}}{d_{2\min}} = \frac{d_1}{d_0} \Rightarrow R_1 \,, \tag{3.35}$$

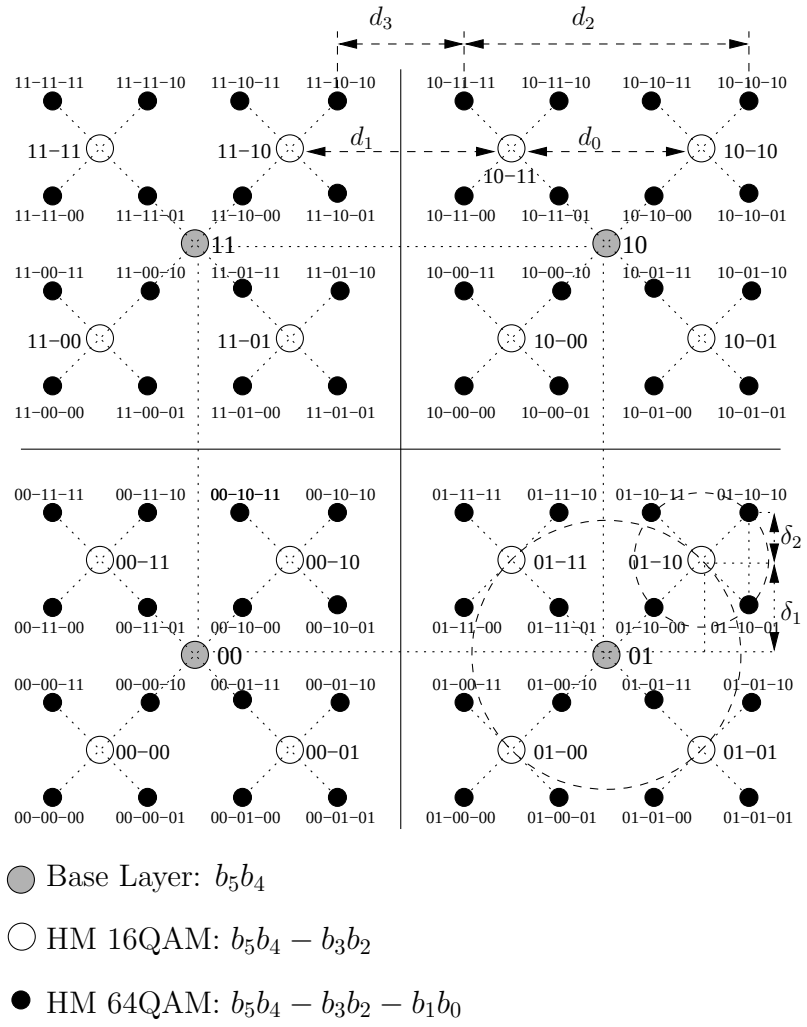

Figure 3.14: The constellation map of the triple-layer HM-64QAM scheme.

if $R_1 > 1$, $\max(\delta_2) \to d_0/2$, we have:

$$R_{2\min} = \frac{d_{3\min}}{d_{2\max}} = \frac{d_1 - d_0}{2d_0} \Rightarrow \frac{1}{2}\left(\frac{d_1}{d_0} - 1\right) = \frac{1}{2}(R_1 - 1) \ , \tag{3.36}$$

if $R_1 < 1$, $\max(\delta_2) \to d_3/2$, so:

$$R_{2\min} = \frac{d_{3\min}}{d_{2\max}} = \frac{0}{d_0 + d_3} \Rightarrow 0 \ . \tag{3.37}$$

In all, when generating the HM-64QAM symbol, the relationship between the R_1 and R_2 is:

$$\begin{cases} 0 < R_2 < R_1 & \text{if} \quad R_1 \leqslant 1 \\ \dfrac{1}{2}(R_1 - 1) < R_2 < R_1 & \text{if} \quad R_1 > 1 \end{cases} \tag{3.38}$$

In the simulations, our HM mapping is controlled by the ratio R_1 and R_2, these two parameters will be tested to optimize the performance of the system.

3.3.4 Communication Protocol

We denote the bits in the codeword of the HM-16QAM symbol as $(b_3b_2 - b_1b_0)$, where (b_3b_2) occupy the base layer, which are also related to L_1, and (b_1b_0) belong to the second layer L_2. By contrast, as shown in Figure 3.13, the bits in the HM-64QAM symbol are grouped as $(b_5b_4 - b_3b_2 - b_1b_0)$, where the base layer L_1 contains (b_5b_4), the second layer L_2 includes (b_3b_2), while (b_1b_0) are in the third layer L_3.

A. When x_1 is a TTCHM-16QAM symbol stream

When the SN generates the TTCHM-16QAM signal frames, the HM scheme divides the 16QAM symbol into two layers, namely L_1 (b_3b_2) and L_2 (b_1b_0). As seen in Figure 3.13, the two information bits in L_1 decide, which particular quadrant the transmitted symbol comes from, while the pair of bits contained in L_2 illustrate the exact location of the transmitted symbol in each quadrant.

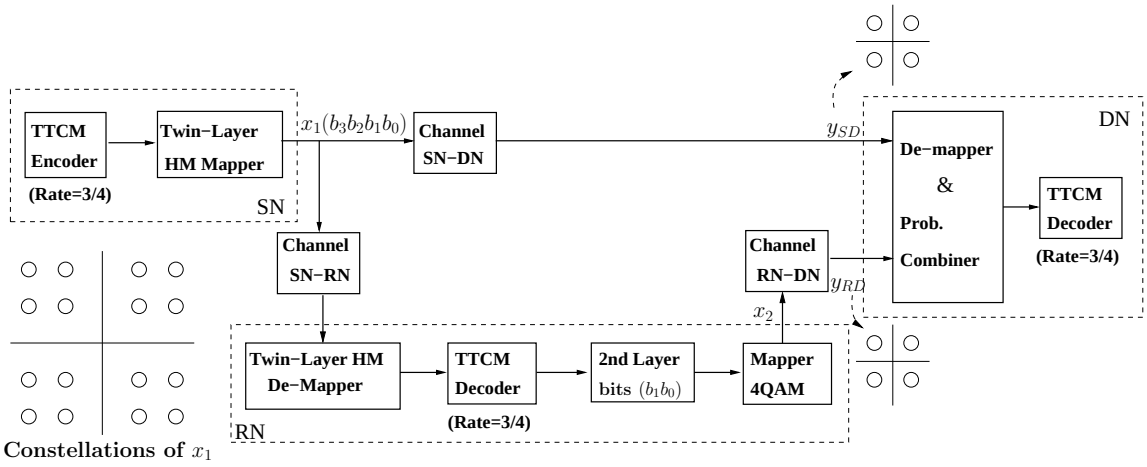

Figure 3.15: Twin-layer TTCHM-16QAM aided cooperative system.

The system's schematic is shown in Figure 3.15, where the DN demaps x_1 as a 4QAM symbol for recovering the two-bit information contained in L_1 during the first TS. The output of the demapper at the DN is the PDF of detecting L_1, when y_{SD} was received, which may be expressed as:

$$p\left(y_{SD,n}|L_{1,n}^{(i)}\right) = \frac{1}{\pi N_0}\exp\left(-\frac{\left|y_{SD,n} - \sqrt{G_{SD}}h_{SD}\widetilde{\alpha}S_{4QAM}^{(i)}\right|^2}{N_0}\right)$$
$$i \in \{0,1,2,3\}\,, \tag{3.39}$$

where, $n \in \{1,2,\ldots,\eta\}$, which is the position of the current symbol in the signal frame received and η is the block length of the TTCM decoder/encoder. Note that due to the higher complexity of our cooperative communication system, in this section we opted for a shorter block size, which is $\eta = 1,200$. More explicitly, the RN will decode the entire frame $\{x_1\}$ from the SN for detecting

	b_3	b_2		b_1	b_0
$L_1^{(0)}$	0	0	$L_2^{(0)}$	0	0
$L_1^{(1)}$	0	1	$L_2^{(1)}$	0	1
$L_1^{(2)}$	1	0	$L_2^{(2)}$	1	0
$L_1^{(3)}$	1	1	$L_2^{(3)}$	1	1

Table 3.4: Mapping rule of the HM-16QAM of Figure 3.15.

both $L_1(b_3b_2)$ and $L_2(b_1b_0)$, where only the bit-pair $L_2(b_1b_0)$ is mapped to the general set-partition modulated 4QAM symbols for transmission to the DN within the frame $\{x_2\}$. During a symbol period in the second TS, the DN will demap x_2 and will produce the PDF of receiving y_{RD}, when L_2 was transmitted:

$$p\left(y_{RD,n}|L_{2,n}^{(j)}\right) = \frac{1}{\pi N_0}\exp\left(-\frac{\left|y_{RD,n}-\sqrt{G_{RD}}h_{RD}x_{2,n}^{(j)}\right|^2}{N_0}\right)$$
$$j \in \{0,1,2,3\}\ . \tag{3.40}$$

More specifically, the corresponding mapping rule is shown in Table 3.4, where the bit-positions in the constellation map are shown in Figure 3.13. Finally, the elements in the $(\eta \times 16)$ probability matrix $\mathrm{Pr}_{HM-16QAM}$ required for decoding the rate-3/4 TTCHM signal frame at the DN may be expressed as:

$$\begin{aligned}\mathrm{Pr}_{HM-16QAM}(n,k) &= \mathrm{Pr}\left(x_{1,n}^{(k=4i+j)} \mid y_n\right) = \mathrm{Pr}\left(L_{1,n}^{(i)} \mid y_{SD,n}\right) \times \mathrm{Pr}\left(L_{2,n}^{(j)} \mid y_{RD,n}\right) \\ &= p\left(y_{SD,n} \mid L_{1,n}^{(i)}\right) \times \mathrm{Pr}\left(L_{1,n}^{(i)}\right) \times p\left(y_{RD,n} \mid L_{2,n}^{(j)}\right) \times \mathrm{Pr}\left(L_{2,n}^{(j)}\right) \\ & i,j \in \{0,1,2,3\},\ \ k \in \{0,1,\ldots,15\}\ . \end{aligned} \tag{3.41}$$

Note that the DN would demap the signals x_1 and x_2 as a pair of 4QAM symbols, but the number of modulation levels in the TTCHM decoding block of Figure 3.15 is 16. Since we do not invoke any iterations between the demapper and the TTCM decoder for the sake of maintaining a reduced decoding complexity, we have $\mathrm{Pr}\left(L_{1,n}^{(i)}\right) = 1/4$ and $\mathrm{Pr}\left(L_{2,n}^{(j)}\right) = 1/4$, which are equiprobable. Explicitly, we employ a rate-3/4 convolutional code as the constituent code of the TTCM encoder [8]. The constraint length was chosen to be $k = 4$ and the generator polynomials expressed in octal format are $\mathbf{H}(\mathbf{D}) = [11\ \ 02\ \ 04\ \ 10]$. In our forthcoming investigations, we will adapt the parameter R_1 for the sake of optimizing the performance of the system. The related simulation results will be discussed in Section 3.3.5.

B. When x_1 is a TTCHM-64QAM symbol stream

When the SN generates HM-64QAM signal frames, there would be three layers in each HM symbol, namely L_1 (b_5b_4), L_2 (b_3b_2) and L_3 (b_1b_0). We employ a single RN in our cooperative communication system and we also divide the HM-64QAM symbol into two layers, namely L_H and L_L. The layer L_H is identical to layer L_1 of the HM-16QAM scheme, but layer L_L contains

both L_2 and L_3. In this way, both L_H and L_L would assume similar roles as L_1 and L_2 in HM-16QAM.

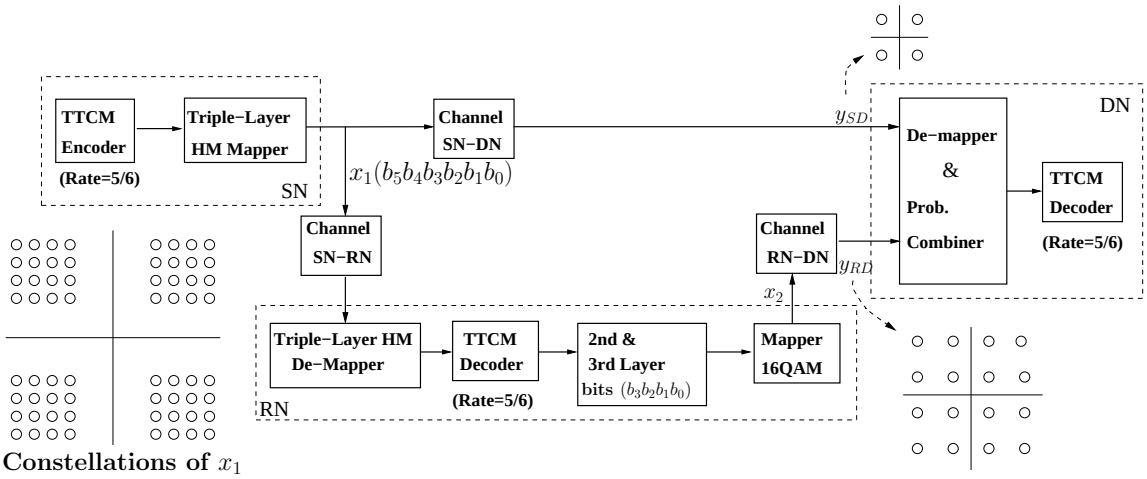

Figure 3.16: Triple-layer TTCHM-64QAM aided cooperative system, which is similar to its twin-layer counterpart in Figure 3.15.

As shown in Figure 3.16, the DN would demap x_1 as a 4QAM symbol and the PDF of receiving y_{SD} - conditioned on L_H being transmitted - may be calculated as:

$$p\left(y_{SD,n} \mid L_{H,n}^{(i)}\right) = \frac{1}{\pi N_0} \exp\left(-\frac{\left|y_{SD,n} - \sqrt{G_{SD}} h_{SD} \widetilde{\beta} S_{4QAM}^{(i)}\right|^2}{N_0}\right)$$
$$i \in \{0,1,2,3\}\ . \tag{3.42}$$

Then, x_1 would be decoded by the RN for detecting the six data bits $(b_5b_4b_3b_2b_1b_0)$. However, only $(b_3b_2b_1b_0)$ of each 6-bit symbol would be mapped to a set-partition modulated 4-bit 16QAM symbol for transmission to the DN in form of the symbol x_2 during the second TS. Based on the symbol x_2, the PDF of receiving y_{RD} - given L_L is transmitted - may be expressed at the DN as:

$$p\left(y_{RD,n} \mid L_{L,n}^{(j)}\right) = \frac{1}{\pi N_0} \exp\left(-\frac{\left|y_{RD,n} - \sqrt{G_{RD}} h_{RD} x_{2,n}^{(j)}\right|^2}{N_0}\right)$$
$$j \in \{0,1,\ldots,15\}\ , \tag{3.43}$$

where the mapping rule is seen in Table 3.5. Again, the position of each point in the constellation map is illustrated in Figure 3.13. Therefore, the $(\eta \times 64)$-element probability matrix $\mathrm{Pr}_{HM-64QAM}$ required for decoding the rate-5/6 TTCHM signal frame may be expressed as:

$$\begin{aligned}\mathrm{Pr}_{HM-16QAM}(n,k) &= \mathrm{Pr}\left(x_{1,n}^{(k=16i+j)} \mid y_n\right) = \mathrm{Pr}\left(L_{H,n}^{(i)} \mid y_{SD,n}\right) \times \mathrm{Pr}\left(L_{L,n}^{(j)} \mid y_{RD,n}\right) \\ &= p\left(y_{SD,n} \mid L_{H,n}^{(i)}\right) \times \mathrm{Pr}\left(L_{H,n}^{(i)}\right) \times p\left(y_{RD,n} \mid L_{L,n}^{(j)}\right) \times \mathrm{Pr}\left(L_{L,n}^{(j)}\right) \\ & i \in \{0,1,2,3\},\ \ j \in \{0,1,\ldots,15\},\ \ k \in \{0,1,\ldots,63\}\ . \end{aligned} \tag{3.44}$$

	$b_3b_2b_1b_0$		$b_3b_2b_1b_0$
$L_L^{(0)}$	0000	$L_L^{(8)}$	1000
$L_L^{(1)}$	0001	$L_L^{(9)}$	1001
$L_L^{(2)}$	0010	$L_L^{(10)}$	1010
$L_L^{(3)}$	0011	$L_L^{(11)}$	1011
$L_L^{(4)}$	0100	$L_L^{(12)}$	1100
$L_L^{(5)}$	0101	$L_L^{(13)}$	1101
$L_L^{(6)}$	0110	$L_L^{(14)}$	1110
$L_L^{(7)}$	0111	$L_L^{(15)}$	1111

Table 3.5: Mapping rule of the HM-64QAM of Figure 3.16.

Note that when the number of modulation levels of the HM scheme is 64, the six data bits in each codeword are still divided into two layers, namely into L_H and L_L, where there are two bits in layer L_H, while the layer L_L contains the remaining four bits. In this situation, there are two different symbol-to-bit demapper blocks at the DN, the first one is a 4QAM demapper, which is activated during the first TS, while the second one is a 16QAM demapper, which is activated during the second TS at the DN. The rate 5/6 encoder of the 64QAM-based TTCM scheme [8] is used in our TTCHM scheme. The constraint length was chosen to be $k = 6$ and the generator polynomials expressed in octal format are $\mathbf{H}_{64QAM}(\mathbf{D}) = [11\ \ 04\ \ 02]$. The parameters R_1 and R_2 will be jointly adapted for optimizing the performance of the entire system, and the related results and discussions would be provided in Section 3.3.5.

3.3.5 Simulation Results

In this section, we provide our simulation results for characterizing the proposed TTCHM assisted cooperative communication systems. Again, our channel model is the uncorrelated Rayleigh fading channel and the receiver has the perfect CSI. Firstly, the performance of the TTCHM-16QAM scheme is presented and the related simulation results are displayed in Figure 3.17 to Figure 3.19. While the related parameters are shown in Table 3.6

Figure 3.17 characterizes the relationship between the BER performance of the TTCHM-16QAM and the ratio R_1. We considered the BER performance of the system to be a function of the ratio R_1, while considering four different average bit power to noise ratio of E_b/N_0. It can be observed from Figure 3.17 that when $E_b/N_0 = 6$ dB, the best BER performance is attained at $R_1 = 1.6$, while at $R_1 = 1.7$ for $E_b/N_0 = 8$ dB, $R_1 = 2.0$ for $E_b/N_0 = 10$ dB and $R_1 = 2.5$ for $E_b/N_0 = 12$ dB.

Figure 3.18 compares the BER performance of our TTCHM-16QAM schemes for different R_1 values. Four of the five R_1 values are based on the simulation results shown in Figure 3.17, while $R_1 = 1$ is also included, which represents the general square 16QAM mapping. It was found that the performance of our TTCHM-16QAM aided cooperative system is optimized at $R_1 = 1.6$. As seen in Figure 3.18, the performance of the entire system associated with the ratio of $R_1 = 1.6$ is

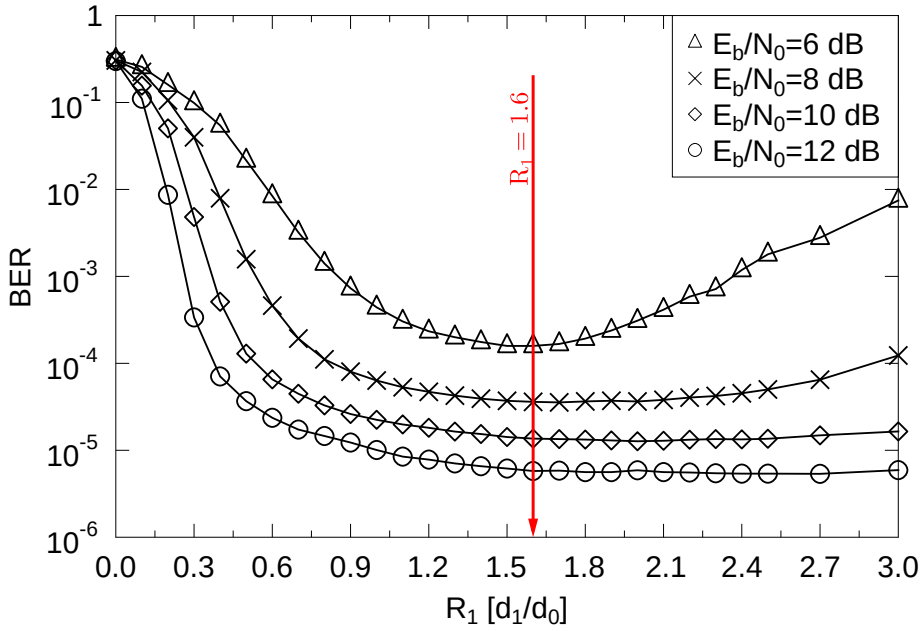

Figure 3.17: The BER versus R_1 performance of the TTCHM-16QAM aided cooperative system of Figure 3.15 communicating over uncorrelated Rayleigh fading channels. The results are based on different HM ratios R_1 at E_b/N_0 $[dB] = \{6, 8, 10, 12\}$. The simulation parameters are shown in Table 3.6.

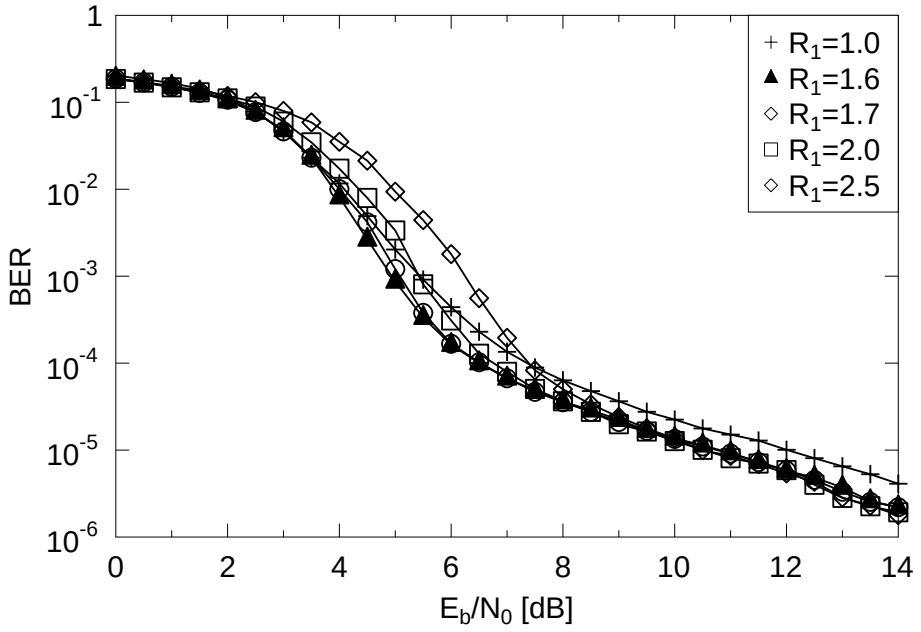

Figure 3.18: The BER versus E_b/N_0 performance of the TTCHM-16QAM aided cooperative system of Figure 3.15 communicating over uncorrelated Rayleigh fading channels. The results are based on different HM ratio R_1 at $R_1 = \{1.0, 1.6, 1.7, 2.0, 2.5\}$. The simulation parameters are shown in Table 3.6.

Coded Modulation	**TTCM**
Modulation Scheme	16QAM, 64QAM, SPM
Mapper type	Set-Partitioned
Number of iterations	4
Code Rate	R_c^{16QAM}=3/4, R_c^{64QAM}=5/6
Code Memory	3
Code Polynomial (octal)	$H_{16QAM} = [11\ 02\ 04\ 10]$, $H_{64QAM} = [11\ 04\ 02]$
Decoder type	Approximate Log-MAP
Symbols per frame	1,200
Number of frames	10,000
Channel	Uncorrelated Rayleigh fading channel
Path-loss exponent	2

Table 3.6: Simulation parameters used in the schematics of Figure 3.15 and Figure 3.16, which are employed in the simulations in Figure 3.17 to Figure 3.24.

about 1.5 dB better than that of the general square mapping HM scheme at BER=10^{-5}.

Furthermore, we compared the BER performance of every single bit in the codeword symbol of the optimized TTCHM-16QAM scheme in Figure 3.19. It can be stated that the BER of b_3 is similar to the overall BER performance of the three information bits and it is about 1.5 dB worse than that of b_1, but about 1.2 dB better than that of b_2, as recorded at BER=10^{-6}. Note that the BER performance of the three information bits is within a $\pm$1.5 dB range of the overall BER performance of the three information bits at a BER of 10^{-6}. However, as mentioned in Section 3.3.3, when the signal power is low, the BER performance of the parity bit b_0 is at least 2 dB worse than that of the information bits. This is mainly because the parity bit in the SP scheme has the lowest minimum Euclidean distance. Fortunately, the performance of the parity bit does not degrade the performance of the three information bits.

Next, we investigated the attainable performance of our TTCHM-64QAM scheme. The related simulation results are displayed in Figure 3.20 to Figure 3.22. Since the TTCHM-64QAM scheme is controlled by the pair of HM ratios R_1 and R_2, we have used two typical values of R_1, namely 1.0 and 1.6. When $R_1 = 1$, the HM-16QAM becomes the original square mapping and $R_1 = 1.6$ represents the best configuration of the TTCHM-16QAM scheme in cooperative communications according to our results in Figure 3.18. The comparisons are carried out separately based on these two R_1 values.

It can be observed in Figure 3.20 and Figure 3.21 that when choosing $R_1 = 1.6$, the best performance is achieved for $R_2 = 0.6$. By contrast, the system attained its best performance for $R_2 = 0.33$ at $R_1 = 1$. Note that when the HM-64QAM ratio pair is $(R_1 = 1.0, R_2 = 0.33)$, the constellations will be turned into the original square 64QAM mapping. In Figure 3.22, we picked the HM ratio parameter pairs of $(R_1 = 1.0, R_2 = 0.33)$, $(R_1 = 1.0, R_2 = 0.4)$, $(R_1 =$

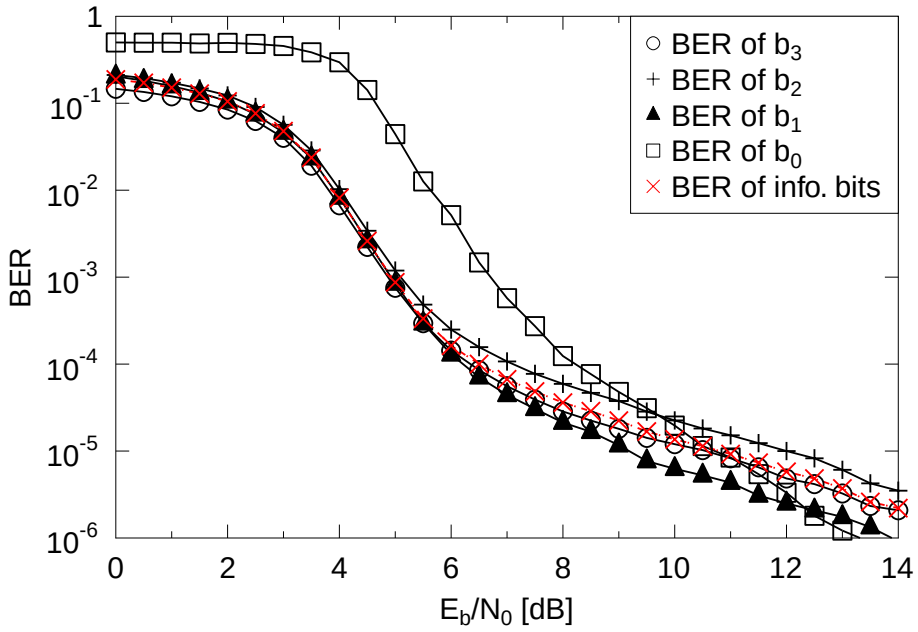

Figure 3.19: The BER versus E_b/N_0 performance of the TTCHM-16QAM aided cooperative system of Figure 3.15 communicating over uncorrelated Rayleigh fading channels. The results are based on HM ratio $R_1 = 1.6$, and each single bit in the codeword symbol namely b_3, b_2, b_1 and b_0. While, b_3, b_2 and b_1 are information bits, b_0 is the parity bit. The simulation parameters are shown in Table 3.6.

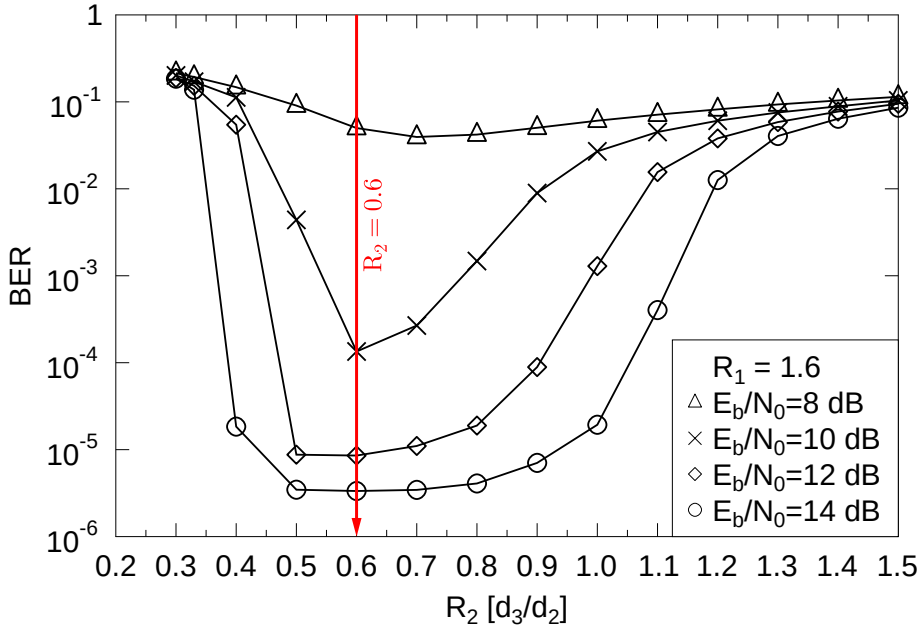

Figure 3.20: The BER versus R_2 performance of the TTCHM-64QAM aided cooperative system of Figure 3.16 communicating over uncorrelated Rayleigh fading channels. The results are based on different HM ratios R_2 at $R_1 = 1.6$ and $E_b/N_0\ [dB] = \{8, 10, 12, 14\}$. The simulation parameters are shown in Table 3.6.

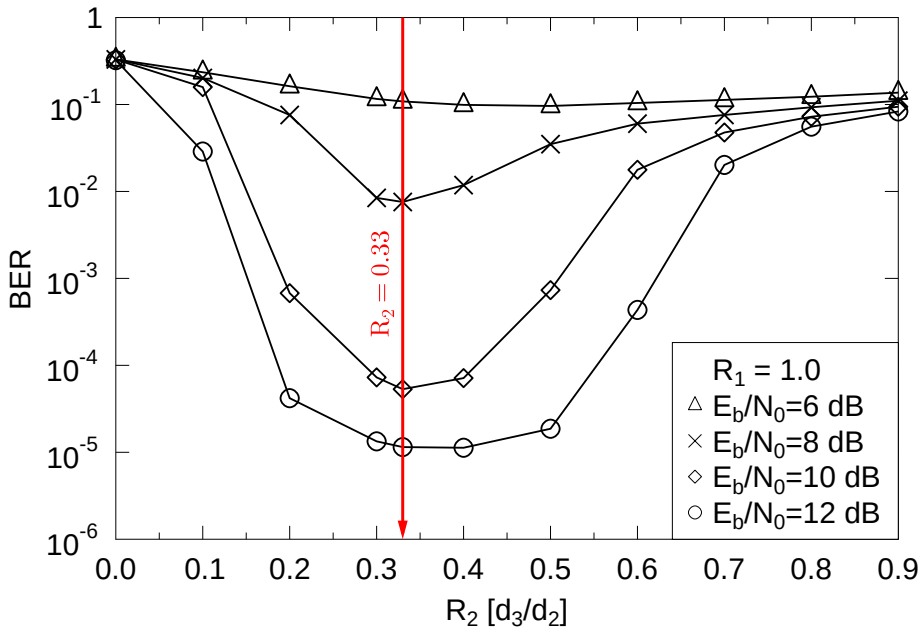

Figure 3.21: The BER versus R_2 performance of the TTCHM-64QAM aided cooperative system of Figure 3.16 communicating over uncorrelated Rayleigh fading channels. The results are based on different HM ratios R_2 at $R_1 = 1.0$ and E_b/N_0 $[dB] = \{8, 10, 12, 14\}$. The simulation parameters are shown in Table 3.6.

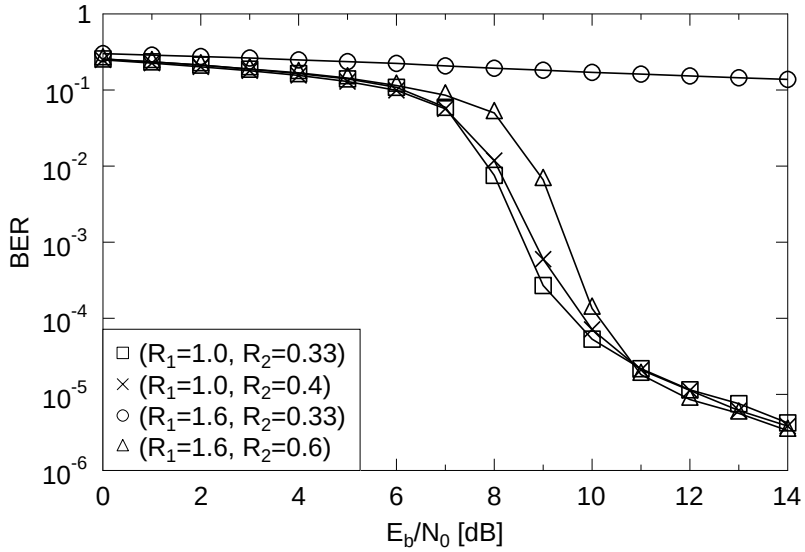

Figure 3.22: The BER versus E_b/N_0 performance of the TTCHM-64QAM aided cooperative system of Figure 3.16 communicating over uncorrelated Rayleigh fading channels. The results are based on different HM ratio pair at $(R_1, R_2) = \{(1.0, 0.33), (1.0, 0.4), (1.6, 0.33), (1.6, 0.6)\}$. The simulation parameters are shown in Table 3.6.

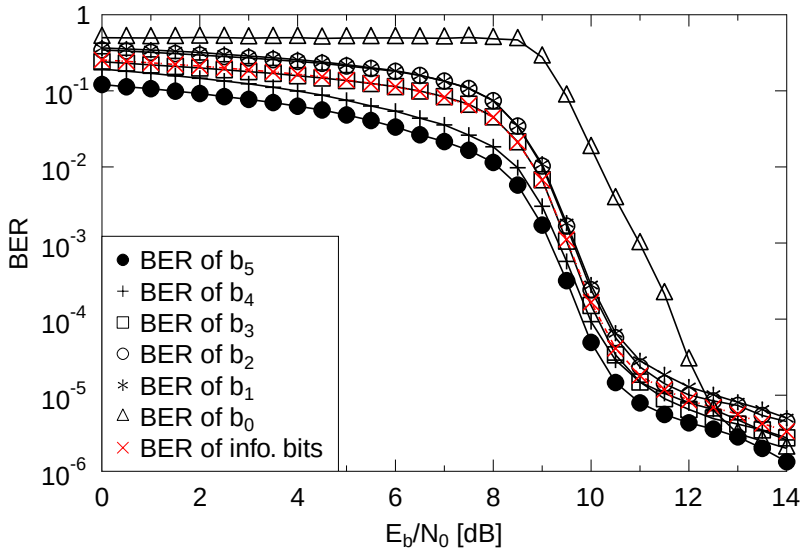

Figure 3.23: The BER versus E_b/N_0 of the TTCHM-64QAM aided cooperative system of Figure 3.16 communicating over uncorrelated Rayleigh fading channels. The results are based on HM ratio pair ($R_1 = 1.6$, $R_2 = 0.6$), and each single bit in the codeword symbol namely b_5, b_4, b_3, b_2, b_1 and b_0. While, b_5, b_4, b_3, b_2 and b_1 are information bits, b_0 is the parity bit. The simulation parameters are shown in Table 3.6.

$1.6, R_2 = 0.33)$ and $(R_1 = 1.6, R_2 = 0.6)$ to perform a BER versus E_b/N_0 comparison. The results show that when the E_b/N_0 value is between 8 dB and 10 dB, the system associated with the ratio parameter pair of $(R_1 = 1.0, R_2 = 0.33)$ performs about 1 dB better than that with the ratio pair $(R_1 = 1.6, R_2 = 0.6)$. However, when E_b/N_0 is higher than 11 dB, the system relying on the ratio pair of $(R_1 = 1.6, R_2 = 0.6)$ turns out to be better. More explicitly, it is about 0.5 dB better than that associated with the ratio pair of $(R_1 = 1.0, R_2 = 0.33)$ at BER=10^{-5}.

Similar to the investigations reported in Figure 3.19, the BER recorded for each of the six coded bits in our TTCHM-64QAM scheme are shown in Figure 3.23. It can be stated that the BER performance of the two bits contained in the first layer (b_5b_4) is better than the average BER performance of the other information bits ($b_3b_4b_5b_6$). On the other hand, there are only moderate differences among the performances of the three information bits contained in the second layer. Furthermore, they are all close to the average BER performance of the five information bits. At a BER of 10^{-5}, the required E_b/N_0 of the first bit (b_5) in the codeword is about 11.5 dB, which is about 1.5 dB better than that of the average BER of the five information bits. The E_b/N_0 differences among the other four information bits are within a ± 1 dB range. Although the BER performance of the parity bit b_0 is not as good as that of the others, this does not degrade the overall performance of the information bit. The simulation results of Figure 3.23 show that the BER of each information bit in the TTCHM-64QAM scheme is similar with other.

Compared to the non-cooperative Single-Input-Single-Output (SISO) TTCM schemes, our so-

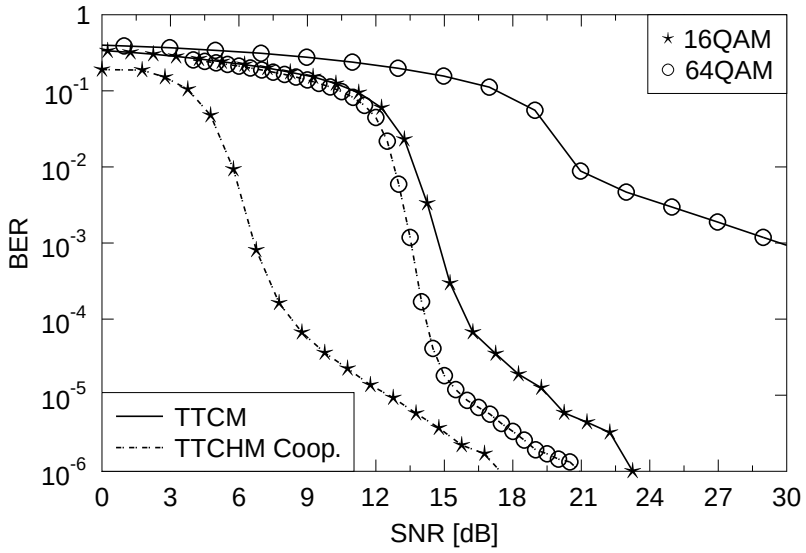

Figure 3.24: The BER versus SNR curves of the TTCHM aided cooperative communications against the non-cooperative communications non-HM aided TTCM schemes. The HM-16QAM scheme of Figure 3.15 is using a HM ratio $R_1 = 1.6$, and the HM ratio pair for the HM-64QAM scheme of Figure 3.16 is $(R_1 = 1.6, R_2 = 0.6)$. The simulation parameters are shown in Table 3.6 and the simulation results are summarized in Table 3.7.

lution attains a substantial improvement. In the cooperative system of Figure 3.15, we use two TSs to transmit a single rate-3/4 TTCM coded symbol having three information bits. Hence, the relationship between the SNR and E_b/N_0 of the TTCHM-16QAM cooperative scheme may be expressed as:

$$SNR_{TTCHM-16QAM}\,[dB] = (E_b/N_0)_{TTCHM-16QAM} + 10\log_{10}\left(\frac{3}{2}\right) . \tag{3.45}$$

Similarly, the cooperative scheme shown in Figure 3.16 requires two TSs for conveying a single rate-5/6 TTCM coded symbol having five information bits. Here we have:

$$SNR_{TTCHM-64QAM}\,[dB] = (E_b/N_0)_{TTCHM-64QAM} + 10\log_{10}\left(\frac{5}{2}\right) . \tag{3.46}$$

Therefore, we may convert our BER versus E_b/N_0 results into BER versus SNR curves. The related simulation results are shown in Figure 3.24. Observe in the figure that our cooperative TTCHM-16QAM aided system performs about $23.25 - 17.47 = 5.78$ dB better than the non-cooperative conventional TTCM-16QAM scheme at a BER of 10^{-6}. By comparison, the original non-cooperative system relying on the conventional TTCM-64QAM scheme requires about 29.70 dB for approaching the BER of 10^{-3}, which is increased to 59.39 dB for the BER of 10^{-6}. By contrast, our cooperative TTCHM-64QAM communication scheme exhibited a BER of 10^{-6} at $SNR = 20.93$ dB, which is about $23.25 - 20.93 = 2.32$ dB better than that of the non-cooperative conventional TTCM-16QAM scheme, when choosing the block size of the TTCM scheme to be $\eta = 1200$. The simulation results of this section are summarized in Table 3.7. Note that, according to the LTE standard, the receive signal power of the mobile device should be between -60 dBm and

Channel				**Uncorrelated Rayleigh**		
Memory				3		
Decoder Type				Approximate Log-MAP		
Code	R_1	R_2	Designed bps	SNR (dB) at		
				BER of 10^{-3}	BER of 10^{-6}	FER of 10^{-1}
Coop. TTCHM 16QAM	1.6	–	1.5	6.67	17.47	6.71
Coop. TTCHM 64QAM	1.6	0.6	2.5	13.52	20.93	14.32
TTCM 16QAM SISO	–	–	3	14.75	23.25	16.18
TTCM 64QAM SISO	–	–	5	29.70	59.39	54.96

Table 3.7: The SNR threshold values of various CM schemes, when transmitting over uncorrelated Rayleigh fading channels. These values are based on Figure 3.24, while the simulation parameters are shown in Table 3.6.

-110 dBm, while the acceptable receive SNR range should be in the range of -5 dB to 30 dB, when aiming for a packet error rate no higher than 0.1.

3.4 SPM and HM Based TTCM Aided Cooperative Communications

3.4.1 Introduction

In this section, we amalgamate the SPM and HM schemes for attaining an attractive cooperative communication scheme. The system is designed for assisting the transmissions of a pair of independent links. The system model is detailed in Section 3.4.2 and the corresponding communication protocol is defined in Section 3.4.3, while Section 3.4.4 presents our simulation results.

3.4.2 System Model

The general system model is detailed in Figure 3.25, where the SN_A is forwarding $\{x_1\}$ to DN_A, while, SN_B is transmitting $\{x_2\}$ to DN_B, simultaneously. A single RN is activated for assisting the two independent streams. Both of the two SNs employ a twin-layer HM-16QAM aided rate-3/4 TTCM encoder, as shown in Section 3.3.4. During the first TS, DN_A will receive L_1 of $\{x_1\}$, while, DN_B will receive L_1 of $\{x_2\}$. The L_2 of $\{x_1\}$ ($\{x_2\}$) may be conveyed to the DN_A (DN_B) by the RN using the twin-layer SPM scheme, as shown in Section 3.2, during the second TS. Note that during the first TS, the RN may simultaneously receive the two information streams $\{x_1\}$ and $\{x_2\}$ using an Space-Division Multiple Access (SDMA) Multiple-Input-Multiple-Output (MIMO) scheme, where the streams are distinguished with the aid of their unique, stream-specific Channel Impulse Response (CIR), as described in the Section 3.2 and Section 3.3.

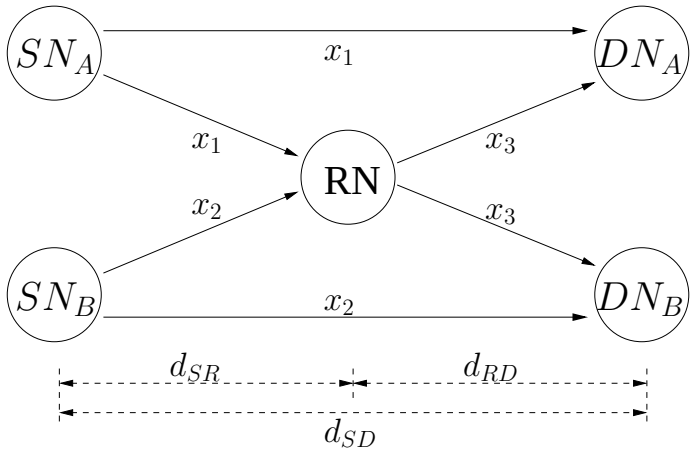

Figure 3.25: The general system model

3.4.3 Communication Protocol

To be more specific, the schematic of our communication scheme is depicted in Figure 3.26. It can be considered as the combination of the schematic proposed in Figure 3.1 of Section 3.2 and the schematic of Figure 3.15 in Section 3.3. Firstly, the two SNs will broadcast their TTCM aided twin-layer HM-16QAM based signal streams to the RN as well as both of the two DNs, which is similar to the first transmission TS of the schematic of Figure 3.15. The RN will receive the two independent signal streams simultaneously and will extract the L_2 information contained in the two twin-layer HM-16QAM modulated signal sequences. Then a twin-layer SPM signal formed by the two L_2 information from the two SNs will be forwarded to both of the two DNs, which is similar to the second transmission TS of the schematic of Figure 3.1. By employing the detection method discussed in Section 3.2 and Section 3.3, both of the two DNs may be capable of receiving the information from the two SNs. Therefore, the single RN in Figure 3.26 is capable of assisting the transmissions among four communication nodes.

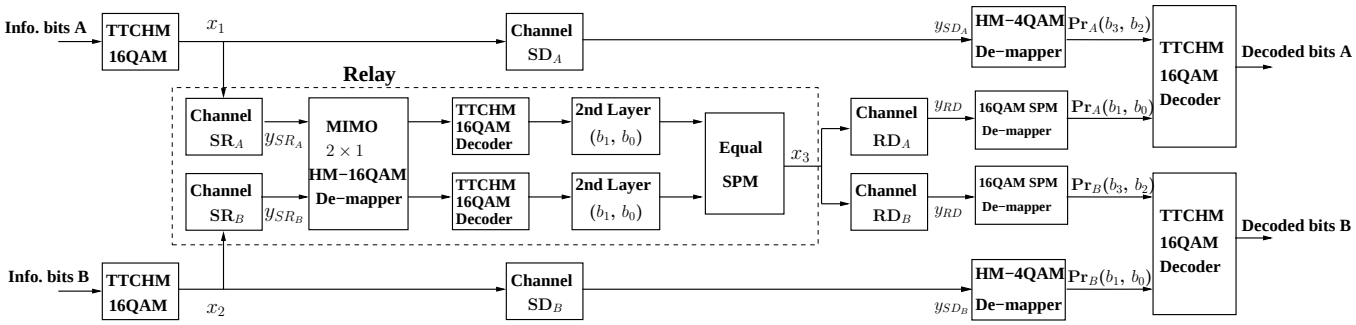

Figure 3.26: The block diagram of the cooperative communication system.

We denote the bits in the codeword of the HM-16QAM symbol as $(b_3b_2b_1b_0)$, where (b_3b_2) occupy the base layer (L_1), and (b_1b_0) belong to the second layer L_2. Both of the two SNs produce

rate-3/4 TTCM encoded HM-16QAM symbols. During the first TS, the signal frames $\{x_1\}$ and $\{x_2\}$ would be demapped as 4QAM symbols at DN for conveying the information contained in their first layer L_{1,x_1}, L_{1,x_2}, due to the relatively low receive SNR at the DN. The PDF of receiving L_1, when x_1 or x_2 was transmitted at the DN may be expressed as:

$$p\left(y_{SD_A} \mid L_{1,x_1}^{(i)}\right) = \frac{1}{\pi N_0} \exp\left(-\frac{\left|y_{SD_A} - \sqrt{G_{SD_A}} h_{SD_A} \widetilde{\alpha} S_{4QAM}^{(i)}\right|^2}{N_0}\right), \tag{3.47}$$

$$p\left(y_{SD_B} \mid L_{1,x_2}^{(j)}\right) = \frac{1}{\pi N_0} \exp\left(-\frac{\left|y_{SD_B} - \sqrt{G_{SD_B}} h_{SD_B} \widetilde{\alpha} S_{4QAM}^{(j)}\right|^2}{N_0}\right), \tag{3.48}$$

where, we have $\{i, j\} \in \{0, 1, 2, 3\}$. Note that the HM ratio $R_1 = 1.6$ is used and uncorrelated Rayleigh fading is considered, where the block size of the TTCM encoder/decoder is $\eta = 1,200$ and the number of iterations in the decoder is $\zeta = 4$. The RN may decode the layer L_2 of $\{x_1\}$ and $\{x_2\}$ from the signal it received, and the layers L_{2,x_1} and L_{2,x_2} may be merged by SPM scheme, using the SPM ratio pair $(\alpha = 0.8972, \beta = 0.4472)$, where the SPM signal stream $\{x_3\}$ may be expressed as:

$$x_3 = \alpha L_{2,x_1} + \beta L_{2,x_2}. \tag{3.49}$$

Then, $\{x_3\}$ would be broadcast to both DN_A and DN_B. Additionally, as described in Section 3.2, we employ an identical-BER based SPM scheme at the RN. By employing a twin-layer 16QAM SPM De-mapper at the DN, the PDF of receiving y_{RD}, provided x_3 is transmitted, may be expressed as:

$$p\left(y_{RD} \mid L_{2,x_1}^{(i)}, L_{2,x_2}^{(j)}\right) = \frac{1}{\pi N_0} \exp\left(-\frac{\left|y_{RD} - h_{RD}\left(\alpha L_{2,x_1}^{(i)} + \beta L_{2,x_2}^{(j)}\right)\right|^2}{N_0}\right). \tag{3.50}$$

Hence, we have:

$$p\left(y_{RD} \mid L_{2,x_1}^{(i)}\right) = \sum_{j=0}^{3} p\left(y_{RD} \mid L_{2,x_1}^{(i)}, L_{2,x_2}^{(j)}\right), \tag{3.51}$$

$$p\left(y_{RD} \mid L_{2,x_2}^{(j)}\right) = \sum_{i=0}^{3} p\left(y_{RD} \mid L_{2,x_1}^{(i)}, L_{2,x_2}^{(j)}\right). \tag{3.52}$$

Therefore, the $(\eta \times M)$-element probability matrix required for decoding $\{x_1\}$ ($\{x_2\}$) at DN_A (DN_B) may be expressed as

$$\begin{aligned}\mathrm{Pr}_{x_1}(n,k) &= \mathrm{Pr}\left(x_{1,n}^{(k=4i+j)} \mid y\right) = \mathrm{Pr}\left(L_{1,x_{1,n}}^{(i)} \mid y_{SD_A}\right) \times \mathrm{Pr}\left(L_{2,x_{1,n}}^{(j)} \mid y_{RD}\right) \\ &= p\left(y_{SD_A} \mid L_{1,x_{1,n}}^{(i)}\right) \times \mathrm{Pr}\left(L_{1,x_{1,n}}^{(i)}\right) \times p\left(y_{RD} \mid L_{2,x_{1,n}}^{(i)}\right) \times \mathrm{Pr}\left(L_{2,x_{1,n}}^{(i)}\right),\end{aligned} \tag{3.53}$$

and

$$\begin{aligned}\mathrm{Pr}_{x_2}(n,k) &= \mathrm{Pr}\left(x_{2,n}^{(k=4i+j)} \mid y\right) = \mathrm{Pr}\left(L_{1,x_{2,n}}^{(i)} \mid y_{SD_B}\right) \times \mathrm{Pr}\left(L_{2,x_{2,n}}^{(j)} \mid y_{RD}\right) \\ &= p\left(y_{SD_B} \mid L_{1,x_{2,n}}^{(i)}\right) \times \mathrm{Pr}\left(L_{1,x_{2,n}}^{(i)}\right) \times p\left(y_{RD} \mid L_{2,x_{2,n}}^{(i)}\right) \times \mathrm{Pr}\left(L_{2,x_{2,n}}^{(i)}\right),\end{aligned} \tag{3.54}$$

where we have $\{i, j\} \in \{0, 1, 2, 3\}$ and $k \in \{0, 1, \ldots, 15\}$. Since no iterations are invoked between the demapper and the TTCM decoder at the DN, we have $\Pr\left(L^{(i)}_{1,x_{1,n}}\right) = \Pr\left(L^{(i)}_{2,x_{1,n}}\right) = 1/4$ and $\Pr\left(L^{(i)}_{1,x_{2,n}}\right) = \Pr\left(L^{(i)}_{2,x_{2,n}}\right) = 1/4$.

3.4.4 Simulation Results

Our simulation results are displayed in Figure 3.27. In order to make explicit comparisons, we consider two different iteration numbers ($\zeta = 1$ and $zeta = 4$) between the MIMO demapper and the rate-3/4 TTCM decoder at the RN, as well as three different RN positions. Furthermore, we assume that SN_A and SN_B are close to each other, whilst DN_A is close to DN_B. The position of the RN is located right in the direct link between the two SNs and the two DNs. The results shown in Figure 3.27 are summarized in Table 3.8.

It may be observed from Figure 3.27 that in the context of our DAF cooperative communication system the BER performance of the entire system will be improved by moving the position of the RN closer to the SN. To achieve a BER of 10^{-6}, when the number of iterations between the MIMO demapper and the TTCM decoder is $\zeta_{MIMO} = 1$, and we have $d_{SR}/d_{SD} = 0.25$, the required receive SNR is about 20.26 dB, where the receive SNR required to achieve the same BER performance as for $d_{SR}/d_{SD} = 0.5$ is about 26.26 dB, while it is 29.76 dB for the system associated with $d_{SR}/d_{SD} = 0.75$. It may also be observed from Figure 3.27 that by increasing the number of iterations between the MIMO demapper and the TTCM decoder at the RN from $\zeta_{MIMO} = 1$ to $\zeta_{MIMO} = 4$, the BER performance of the cooperative system attains an approximately 9 dB SNR improvement.

Channel	**Uncorrelated Rayleigh**		
Modulation	MIMO, HM-16QAM, SPM-16QAM		
BPS	3		
Distance of RN	d_{SR}/d_{SD}=0.25	d_{SR}/d_{SD}=0.50	d_{SR}/d_{SD}=0.75
	SNR (dB) at BER of 10^{-3}		
$\zeta^{SR}_{MIMO} = 1$	11.78	17.80	21.32
$\zeta^{SR}_{MIMO} = 4$	9.35	15.36	18.89
	SNR (dB) at BER of 10^{-6}		
$\zeta^{SR}_{MIMO} = 1$	20.26	26.26	29.76
$\zeta^{SR}_{MIMO} = 4$	10.95	17.69	21.16

Table 3.8: The SNR threshold of our SPM and HM based TTCM aided cooperative system of Figure 3.26, when transmitting over uncorrelated Rayleigh fading channels. These values are based on the simulation results shown Figure 3.27. The related parameters are shown in Table 3.6.

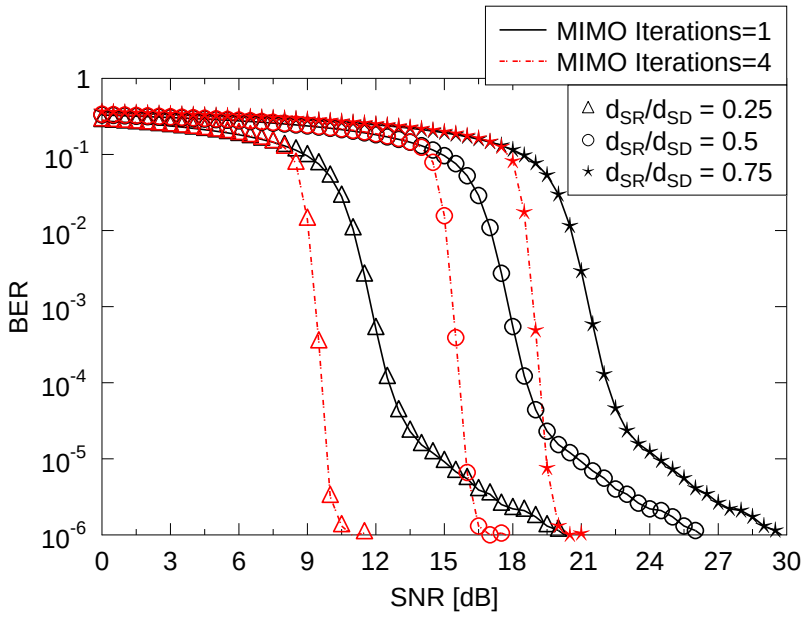

Figure 3.27: The BER versus SNR performance of our SPM and HM based TTCM aided cooperative system of Figure 3.26 communicating over uncorrelated Rayleigh fading channels. The simulation parameters and the simulation results are shown in Table 3.8.

3.5 Summary and Conclusions

In this chapter, we have focussed our investigations on the combination of layered modulation schemes with TTCM conceived for cooperative communications. The key results in this chapter are summarized in Table 3.9.

System Employed	Parameters Used	Designed for minimized power consumption						Max bps
		Modulation Employed	Modulation Parameter	SNR [dB] at BER		TS	bps	
				10^{-3}	10^{-6}			
Figure 3.1	Table 3.2	Twin-layer SPM	$(\alpha = 0.89, \beta = 0.45)$	3.21	4.00	2	1	2
Figure 3.15	Table 3.6	Twin-layer HM	$R_1 = 1.6$	6.67	17.47	2	1.5	3
Figure 3.16	Table 3.6	Triple-layer HM	$(R_1 = 1.6, R_2 = 0.6)$	13.52	20.93	2	2.5	5
Figure 3.26	Table 3.8	Twin-layer HM Twin-layer SPM	$R_1 = 1.6$ $(\alpha = 0.89, \beta = 0.45)$	15.36	17.69	2	3	6

Table 3.9: The SNR threshold values of various TTCM aided cooperative communication systems when transmitting over uncorrelated Rayleigh fading channels. We assume that the RN of each cooperative system is located right in the middle of the SN-DN link. The number of iterations between the soft-demapper and TTCM decoder at the RN of the systems of Figure 3.1 and Figure 3.26 is assumed to be $\zeta_m = 4$.

In Section 3.2, we have conceived a SPM based TTCM cooperative communication scheme. The proposed scheme only requires two TSs for conveying two information frames from two SNs to the DN. Both EXIT charts and PS techniques were employed for increasing the power efficiency

of the entire cooperative communication system. We demonstrated that the proposed scheme only requires approximately 4.0 dB to achieve a BER of 10^{-6}, which is about 6.5 dB lower than the SNR required by the non-cooperative equal-SPM scheme proposed in Section 3.2.7. By contrast, a TTCHM aided cooperative communication scheme was proposed in Section 3.3. We amalgamated cooperative communication, TTCM channel coding and a HM scheme for attaining further performance gains. However, the higher code-rates of 3/4 and 5/6 of the TTCM encoder resulted in an increased computational complexity. To compensate for this, the block size of the TTCM decoder in Section 3.3 was set $\eta = 1,200$, instead of $\eta = 12,000$ as in Section 3.2. The shorter block size of the TTCM encoder/decoder may however erode its decoding capability, as expected at a reduced computational complexity. Our simulation results have demonstrated that the BER performance of the entire system can be improved without reducing the coding rate or without requiring extra transmission power, as discussed in Section 3.3.5 and detailed in Table 3.7. However, optimum choice of the HM ratio depends on the position of the RN. Specifically, the optimum ratio pairs found for our TTCHM scheme have to be updated using a position-based look-up table, when the RN is not located in the mid-point between the SN and DN. Finally, we have amalgamated the SPM and HM schemes with TTCM in Section 3.4 for cooperative communications. We found that although the receive SNR required for achieving a BER of 10^{-6} in the twin-layer HM-16QAM aided system of Figure 3.15 in Section 3.3 is similar to that of the system advocated in Figure 3.26 of Section 3.4, the system of Figure 3.26 assists the transmissions among four nodes and conveys two rate-3/4 TTCM coded signal in two transmission TSs, while that of Figure 3.15 in Section 3.3 only conveys a single signal sequence during the two TSs.

However, the drawbacks of the schemes proposed in this chapter are also obvious. None of the four schematics conceived is particularly flexible. Explicitly, the DN may only be capable of starting the decoding process after the SN and RN finished their transmissions. Therefore, regardless of how important the information received from the SN is, it will only be received at the end of the second transmission TS. For the schematics of Figure 3.15 and Figure 3.16, the transmission from the RN to DN is only used for conveying the soft information of layer L_2 of the HM aided signal from SN, hence it is not possible to derive the BER versus SNR performance for the transmissions from the RN to DN. Therefore, we may not able to derive the minimum SNR required for the DN to receive the signal from the RN. Consequently, in the simulations, we have to set the signal power transmitted from the RN to be always identical to that of the SN. Therefore, the power efficient scheme of Section 3.2 may not be directly invoked for the schematics of Section 3.3. Furthermore, the flexible modulation/demodulation nature of the HM scheme is not fully exploited by the cooperative schemes proposed in Section 3.3. Motivated by eliminating these limitations, in Chapter 4, we will focus our attention on improving the performance of the twin-layer HM aided TTCM scheme conceived for cooperative communications. The flexibility as well as the power-efficiency will be carefully taken into consideration, while in Chapter 5, we will construct an improved hybrid system based on HM, SPM as well as the TTCM.

Chapter 4

Twin-layer Hierarchical Modulation Aided Turbo Trellis-Coded Modulation for Cooperative Communications

4.1 Introduction

Hierarchical Modulation (HM), which is also known as layered modulation, has been widely adopted across the telecommunication industry. Its strict backwards compatibility with conventional single-layer modems and its low complexity facilitate the seamless upgrading of wireless communication services. The potential employment of HM schemes in cooperative communications has the promise of increasing the achievable throughput at a low power consumption. In this chapter, we propose a single-relay aided hierarchical modulation based cooperative communication system. The Source Node (SN) employs Turbo Trellis-Coded Modulation (TTCM) schemes relying on specifically designed HM, while the Relay Node (RN) invokes the Decode-and-Forward protocol. We have analysed the system's achievable rate as well as its bit error ratio using Monte-Carlo simulations. The results demonstrate that the power consumption of the entire system may be reduced by our cooperative communication scheme. In this chapter, familiarity with the turbo-detection principles and with EXIT-charts is assumed, as detailed in [6].

In Chapter 3, we have conceived a cooperative communication system assisted by a HM aided TTCH scheme. The transmission protocol is detailed in Section 3.3 and in [184], where the underlying idea is to rely on the HM scheme for reducing the transmit SNR[1] (SNR_t) of the SN in cooperative communications. However, we observe that the system advocated in Section 3.3 has three drawbacks. Firstly, the Destination Node (DN) will only be able to decode the information it received from the SN and RN, after all the nodes in the cooperative network have completed

[1]The definition of transmit SNR was proposed in [206], which is convenient for simplifying the discussions, although this is not a physically measurable quantity, because it relates the power at the transmitter to the noise at the receiver.

their transmission. Secondly, the power-efficiency of the system may be further improved, because in Section 3.3 we assumed that SNR_t of the RN (SNR_t^{RN}) is identical to SNR_t of the SN (SNR_t^{SN}). The reduced path-loss facilitated by the RN was not taken into consideration in the simulations, where the RN was located right in the middle of the SN to DN link. Thirdly, we distorted the HM constellation for the sake of improving the BER performance of its high-priority layers at the detriment of its low-priority layers, which degrades its average BER compared to that of conventional modulation schemes.

Against this background, we circumvented the above-mentioned limitations by proposing a new cooperative communication system in this chapter, where the RN position is no longer a fixed position. Instead, similar to the user-cooperation philosophy of [210], we will find the optimum RN position. The design goal of the system in this chapter is to combine the TTCM channel coding scheme and HM scheme in the context of cooperative communications for the sake of increasing its time-efficiency and for reducing the total power dissipation of the entire system, while maintaining a low complexity and guaranteeing reliable transmission in each link of the cooperative network. The HM constellations and the position of the RN are also taken into consideration, when optimizing the system. To be more specific, the SN will employ two independent rate-1/2 TTCM encoders and HM is used for combining the two independent codewords into HM symbols. According to the symbol-to-bit demapping of the HM scheme, the SNR_r required for decoding the information contained in the higher protection layers is lower than that of the information in the lower protection layers. Therefore, by employing the HM scheme, the SNR_t^{SN} may be reduced to the minimum required value that can 'just' guarantee the successful detection of the base layer (highest priority) of the entire HM based symbol stream at the DN. By contrast, the information in the lower priority layer may be received and retransmitted by the Decode-and-Forward (DAF) based RN. Hence, the entire system requires two Time Slots (TS) for conveying the information from the SN to the DN. Note that each transmission between the SN (or RN) and the DN only deals with a single layer of the twin-layer HM-16QAM signals. In this way, not only the SNR_t^{SN} and SNR_t^{RN} may be reduced, but also the processing complexity of the system may be mitigated.

The TTCM scheme of [6], is a joint coding and modulation arrangement scheme employing a similar structure to that of turbo codes, but employs Trellis-Coded-Modulation (TCM) [5] as its components. Specifically, TTCM is invoked as the coding and modulation scheme in our communication system, because it has a better performance when communicating over Rayleigh fading channels than that of other joint coding and modulation schemes, such as TCM and Bit-Interleaved Coded Modulation (BICM), as well as iteratively detected BICM (BICM-ID) [6]. An excellent performance is achieved without expanding the bandwidth for the sake of accommodating channel coding. Furthermore, our rate-1/2 TTCM is compatible with HM, since for each HM layer we have two bits, and similarly, the output codeword of the rate-1/2 TTCM encoder also contains two bits. Hence, if we want to reserve one bit of a HM layer for the redundancy bit to protect the original information bits, the TTCM encoder directly satisfies this requirement.

The main contributions of this chapter are as follows:

- A new HM scheme is designed for DAF based cooperative communications, which is intrinsically amalgamated with TTCM and we refer to it as Turbo Trellis-Coded Hierarchical Modulation (TTCHM);
- The capacity lower bound of our DAF cooperative system is derived based on the Discrete-input Continuous-output Memoryless Channel (DCMC) capacity analysis, as well as on the DCMC capacity of each individual layer of the twin-layer HM-16QAM symbol sequence;
- Based on the DCMC capacity analysis and on our Monte-Carlo simulations, a power allocation plan is provided and it is demonstrated that the power dissipation of the entire system may be readily optimized by relying on just two variables, namely the HM ratio R_1 and the DAF RN's position.

The rest of the chapter is organized as follows: Section 4.2 introduces both our system model and our cooperative communication strategy. Section 4.3 illustrates the HM scheme proposed for cooperative communications, and details the symbol-to-bit demapper of the HM symbols. The DCMC capacity analysis and our optimization procedure are described in Sections 4.4. In Section 4.5, the proposed TTCHM aided cooperative system is investigated and our power-allocation plan is characterized. Our conclusions and future research are discussed in Section 4.6. While Appendix A.1 compares our simplified path-loss model to the simplified free-space path-loss model in [1].

4.2 System Model

The general model of our TTCHM aided DAF RN based cooperative communication system is depicted in Figure 4.1. During the first transmission TS, a sequence of TTCHM symbols $\{x_s\}$ is broadcast by the SN to both the RN and the DN. The SNR_t^{SN} is set to the minimal value for enabling the DN to decode only the information contained in the first layer L_1 (base layer) of the TTCHM signals $\{x_s\}$. Then in the following TS, another signal frame, namely $\{x_r\}$ is forwarded to the DN by the RN. The DN would then be capable of recovering the second layer L_2 of the signal frame $\{x_s\}$ based on the signal sequence received from the RN. In order to simplify the system, we consider that the position of the RN is located between the direct SN-DN path.

We considered an uncorrelated Rayleigh flat-fading channel, where the receivers were assumed to acquire perfect Channel State Information (CSI). After the first TS, each symbol received by the DN may be expressed as:

$$y_{SD} = \sqrt{G_{SD}} h_{SD} x_s + n_{SD} \,, \tag{4.1}$$

while each of the symbols received by the RN is:

$$y_{SR} = \sqrt{G_{SR}} h_{SR} x_s + n_{SR} \,, \tag{4.2}$$

where the subscript SD denotes the SN-DN link and the subscript SR represents the SN-RN link. By contrast, each of the symbols received at the DN during the second TS, which are sent by the

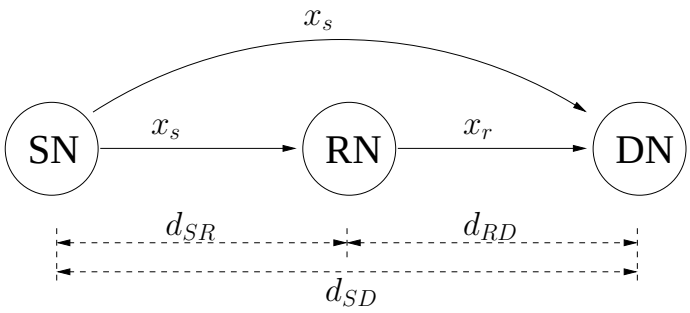

Figure 4.1: The model of a single-relay aided cooperative system.

RN, may be expressed as:

$$y_{RD} = \sqrt{G_{RD}} h_{RD} x_r + n_{RD} \,, \tag{4.3}$$

where the subscript RD represents the RN-DN link. Additionally, the notations h_{SD}, h_{SR} and h_{RD} denote the complex-valued coefficients of the uncorrelated Rayleigh fading for the different links, while n_{SD}, n_{SR} and n_{RD} denote the Additive White Gaussian Noise (AWGN) having a variance of $N_0/2$ per dimension. Moreover, the variables G_{SD}, G_{SR} and G_{RD} represent the Reduced-Distance-Related-Pathloss-Reduction (RDRPLR) for each link, which we also refer to as the path-gain. We consider an inverse-second-power law based free-space path-loss model [1, 206] and naturally, the path-gain G_{SD} of the SD link is assumed to be unity. Therefore the path-gain of the SR link is [211]:

$$G_{SR} = \left(\frac{d_{SD}}{d_{SR}}\right)^2 \,, \tag{4.4}$$

and similarly, the path-gain of the RD link is:

$$G_{RD} = \left(\frac{d_{SD}}{d_{RD}}\right)^2 \,, \tag{4.5}$$

while, we also have:

$$d_{SD} = d_{SR} + d_{RD} \,. \tag{4.6}$$

In a realistic situation, there is always a path-loss between the SN and DN, but in order to simplify the system model, in our simulations, we normalized this path-loss to 0 dB. Hence, when considering the channel is uncorrelated Rayleigh flat fading channel, the transmit power at the SN (which is also referred to as the signal power) would be identical to the power received at the DN. If the transmissions between the SN and DN are on a frame-by-frame basis over the uncorrelated Rayleigh fading channel, the average received SNR$_r$ ($\overline{SNR_r^{DN}}$) at the DN would be given by:

$$\overline{SNR_r^{DN}} = E(|h|^2 \, SNR_t) = E(|h|^2) SNR_t^{SN} \,, \tag{4.7}$$

where SNR_t^{SN} is the transmit SNR defined as the ratio of the transmit power at the SN to the noise power at the DN:

$$SNR_t^{SN} = \frac{E(|x|^2)}{N_0} = \frac{1}{N_0} \,, \tag{4.8}$$

with $E(|x|^2) = 1$. Furthermore, the uncorrelated Rayleigh fading coefficient h is generated by the complex-valued Gaussian distribution having a zero mean and a variance of one. When the number of uncorrelated Rayleigh fading coefficients we generated is large, we have [212]:

$$E(|h|^2) = \frac{1}{N}\sum_{k=1}^{N}|h_k|^2 \approx 1\,. \tag{4.9}$$

Hence, for a large frame size of N symbols, we may assume that SNR_r at the DN (SNR_r^{DN}) is equal to SNR_t^{SN}, or equivalently we have $\overline{SNR_r^{DN}} = SNR_t^{SN}$. At this stage, we note that we have proved in Appendix A.1, that the channel model we employed in this study may be directly converted into the actual channel encountered by taking the path-loss into consideration.

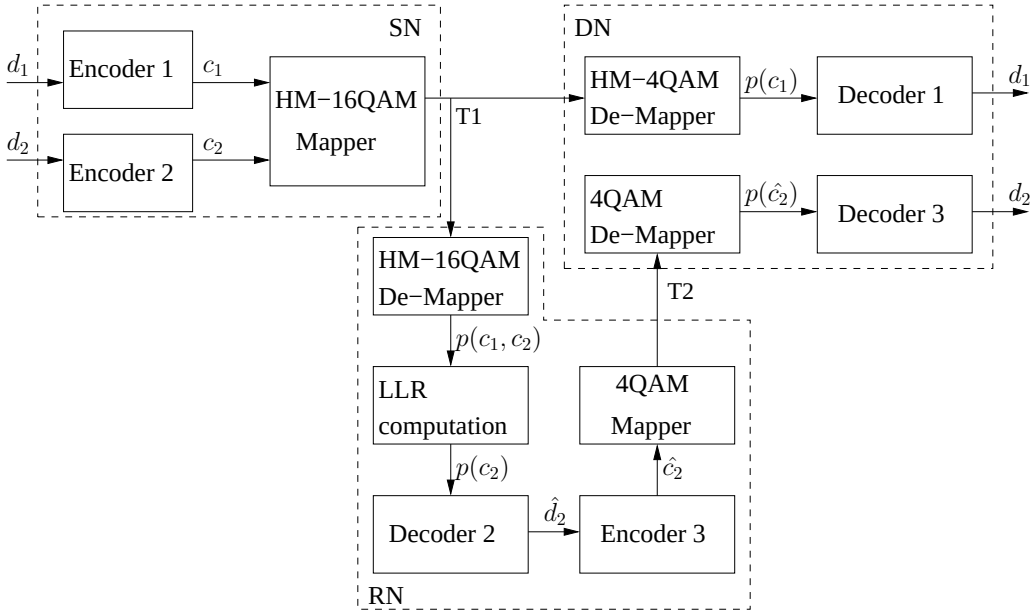

Figure 4.2: The system diagram of a single-relay aided cooperative system, which relies on the HM scheme of Figure 3.15.

To be more specific, the block diagram of the entire system is shown in Figure 4.2 which relies on the original HM scheme of Figure 3.15. If SNR_r at DN (SNR_r^{DN}) is not high enough, the DN may opt for decoding the information only from Encoder 1 during the first TS. During the second TS, the RN is expected to send the information from Encoder 2 to the DN. Additionally, the RN here would demodulate all bits of the HM-16QAM symbols, but it only has to decode the information received from Encoder 2, regardless of the information gleaned from Encoder 1 and encapsulated in the HM-16QAM symbol. The RN would hence re-encode the information corresponding to Encoder 2, and then the encoded signal would be mapped onto a conventional square 4QAM symbol for transmission to the DN. Note that, in contrast to the schematics of Figure 3.15 and Figure 3.16, the cooperative system is capable of guaranteeing that the DN may immediately decode the information contained in the base layer, based on the signal it has received from the SN. By contrast, the schematics of Figure 3.15 and Figure 3.16 may only commence decoding the information after receiving two TSs' transmission. Explicitly, the schematics of Figure 3.15 and

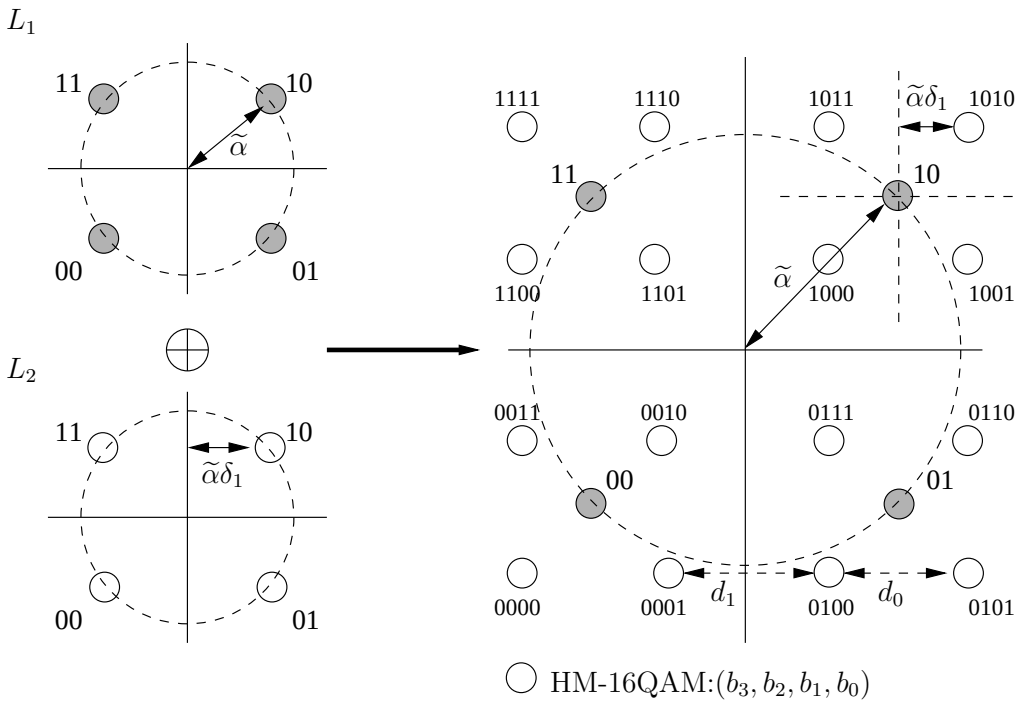

Figure 4.3: The constellation map of the HM scheme used in Figure 4.2, where we have $R_1 = d_1/d_0$.

Figure 3.16 fail to fully benefit from the modulation/demodulation flexibility of the HM scheme as the schematic in this treatise.

4.3 Twin-Layer HM Constellation

Our twin-layer model of the HM-16QAM constellation seen in Figure 4.3 was originally introduced in [184]. Since TTCM is employed, where the symbol-based decoder's performance is determined by the Symbol Error Ratio (SER) [6], set-partition based bit-to-symbol mapping is invoked by the HM constellation instead of Gray mapping.

We define the four bits in a HM-16QAM symbol as $(b_3b_2b_1b_0)$, where L_1 is occupied by (b_3b_2), while (b_1b_0) are contained in L_2. The generation rule of the twin-layer HM-16QAM symbols may be expressed as:

$$S_{HM-16QAM} = \widetilde{\alpha}\left[S_{4QAM} \pm \sqrt{2}\delta_1 e^{\pm\frac{\pi}{4}j}\right] , \tag{4.10}$$

where S_{4QAM} denotes the conventional square 4QAM constellations, while the parameter $\widetilde{\alpha}$ is used for normalizing the average symbol energy to unity. Furthermore, the ratio $R_1 = d_1/d_0$ is defined for controlling the shape of the HM-16QAM constellations, as shown in Figure 4.3, where both the parameters $\widetilde{\alpha}$ and δ_1 are directly controlled by the HM ratio R_1 and their relationship may be

expressed as follows:

$$\delta_1 = \frac{1}{\sqrt{2}\,(1+R_1)}\,. \tag{4.11}$$

$$\widetilde{\alpha} = \frac{1}{\sqrt{1+2\delta_1^2}} = \frac{1+R_1}{\sqrt{1+(1+R_1)^2}}\,. \tag{4.12}$$

Finally, another constraint is imposed on the HM ratio R_1 in the simulations, namely that we have $R_1 > 0$, as detailed in Section 3.3. The entire HM-16QAM constellation point arrangement is directly controlled by the HM ratio R_1. Upon increasing the value of R_1, the four constellation points in each quadrant would move closer to each other. Hence it is necessary to have a higher SNR_r at the RN (SNR_r^{RN}) in order to adequately detect the information contained in L_2. However, we only need a lower SNR_r^{DN} for a reliable[2] detection of the two bits in L_1 at DN. Note that by applying a pair of independent TTCM encoders at the SN, the twin-layer information received from the SN can now be demapped and decoded separately. Therefore, the DN now may become capable of receiving the information in both L_1 and L_2. If the receive SNR at the DN is high enough for the DN to decode the information in L_1, the DN may immediately activate the decoding process after the first TS, instead of waiting until the end of the second transmission TS, which was not possible for the cooperative schematics of Figure 3.15 and Figure 3.16 proposed in Section 3.3. Again, in this chapter, our objective is to find both the optimum HM ratio and the related RN position.

4.3.1 Detection L_1 at DN

When SNR_t^{SN} is relatively low, the DN is only capable of receiving the information contained in L_1 of the signal sequence it received from the SN. Hence, DN may demap the HM-16QAM signal frames as 4QAM symbols for detecting L_1. The input of the TTCM decoder is an $(\eta \times M)$-element probability matrix, where η is the block size of the encoder and M is the number of modulation levels. The elements of this matrix are given by the probability of $\Pr\left(x_n^{(i)} \middle| y\right)$, where y is the received signal, while $x_n^{(i)}$ is the hypothetically transmitted M-ray symbol for $i \in \{0, 1, \cdots, M-1\}$ and n is the time index, which represents the position of the current received symbol in the signal frame received. In order to decode L_1 at the DN, the demapper should produce an $(\eta \times 4)$-element probability matrix containing $p(y|x_n^{(i)})$. Explicitly, according to Eq. (4.10), the elements of the PDF matrix may be expressed as:

$$p\left(y_{SD}|x_{q,n}^{(i)}\right) = \frac{1}{\pi N_0}\exp\left(-\frac{|y_{SD}-\sqrt{G_{SD}}hx_{q,n}^{(i)}|^2}{N_0}\right)$$
$$x_{q,n}^{(i)} \in \{\widetilde{\alpha}e^{j-3\pi/4}, \widetilde{\alpha}e^{j-\pi/4}, \widetilde{\alpha}e^{j\pi/4}, \widetilde{\alpha}e^{j3\pi/4}\}. \tag{4.13}$$

This $(\eta \times 4)$-element PDF matrix $\text{Pr}_{L1}(n,i)$ is used for computing the input of Decoder 1 as [6]:

$$\text{Pr}_{L1}(n,i) = \Pr\left(L_{1,n}^i|y_{SD}\right) = p\left(y_{SD}|x_{q,n}^{(i)}\right)\Pr\left(x_{q,n}^{(i)}\right)\,, \tag{4.14}$$

[2]We define a 'reliable detection' as a detection that gives a BER lower than 10^{-6}.

where $i \in \{0,1,2,3\}$ and $n \in \{0,1,\cdots,\eta-1\}$, while $\Pr\left(x_{q,n}^{(i)}\right) = 1/4$, which represents equi-probable symbols, because in the interests of having a low complexity, we assumed the schematic of Figure 4.2 using non-iterative detection operating without exchanging extrinsic information with the demapper in our symbol-based scheme. When demapping the HM-16QAM signal to 4QAM symbols for calculating the conditional PDF of receiving L_1, we will assume that the signal sequence that DN received during the first TS is based on 4QAM symbols. Let L_1^0 represent the pair of bits (00) in L_1, where we have L_1^1 for (01), L_1^2 for (10) and L_1^3 for (11), while the positions of the constellation points of x_q here are the four center points in each quadrant, of Figure 4.3.

4.3.2 Detection L_2 at RN

As shown in Figure 4.2, the RN receives and retransmits the information in L_2, where SNR_r^{RN} has to be sufficiently high for guaranteeing that the RN is capable of receiving the entire HM-16QAM signal sequence from the SN. During the first TS, the RN will firstly demap the HM-16QAM signal received from SN to produce an $(\eta \times 16)$-element probability matrix, where according to the HM-16QAM generation rule, the elements in the $(\eta \times 16)$ probability matrix may be expressed as:

$$p\left(y_{SR}|\, x_{s,n}^{(i)}\right) = \frac{1}{\pi N_0}\exp\left(-\frac{|y_{SR}-\sqrt{G_{SR}}hx_{s,n}^{(i)}|^2}{N_0}\right)$$
$$x_{s,n}^{(i)} \in \left\{\widetilde{\alpha}\left[S_{4QAM} \pm \sqrt{2}\delta_1 e^{\pm\frac{\pi}{4}j}\right]\right\}\ . \tag{4.15}$$

Then, the $(\eta \times 16)$-element probability matrix of $\mathrm{Pr}_{HM-16QAM}(n,i) = \Pr(x_{s,n}^{(i)}|y_{SR})$ may be formulated as:

$$\Pr\left(x_{s,n}^{(i)}\middle|\, y_{SR}\right) = p\left(y_{SR}|\, x_{s,n}^{(i)}\right)\Pr\left(x_{s,n}^{(i)}\right)\ , \tag{4.16}$$

where $i \in \{0,1,2,\cdots,15\},\ n \in \{0,1,\cdots,\eta-1\}$, while $\Pr\left(x_{s,n}^{(i)}\right) = 1/16$, which represents equi-probable symbols. The Log Likelihood Ratio (LLR) computation block of Figure 4.2 will generate the probability matrix of the information in L_2 gleaned from the HM-16QAM symbol it received. The resultant generation rule is given by:

$$\begin{aligned}\mathrm{Pr}_{L2}(n,l) =& \Pr\left(L_{2,n}^{l}\middle|\, y_{SR}\right)\\ =& \Pr\left(x_{s,n}^{(l)}\middle|\, y_{SR}\right) + \Pr\left(x_{s,n}^{(l+4)}\middle|\, y_{SR}\right) +\\ & \Pr\left(x_{s,n}^{(l+8)}\middle|\, y_{SR}\right) + \Pr\left(x_{s,n}^{(l+12)}\middle|\, y_{SR}\right)\\ & l \in \{0,1,2,3\},\ \ n \in \{0,1,\cdots,\eta-1\}\ ,\end{aligned} \tag{4.17}$$

where the $(\eta \times 4)$-element probability matrix Pr_{L2} is the input of Decoder 2, generating L_2. After decoding the information in L_2, the RN will then re-encode the information and retransmit it to DN in the following TS using the rate-1/2 TTCM 4QAM scheme.

4.4 DCMC Based System Analysis

The achievable DCMC capacity will be used for calculating both the bound of our cooperative communication system, as well as the achievable rate of receiving L_1 and L_2 from the twin-layer HM-16QAM symbols. When considering the DCMC capacity with input $X = \{x^{(0)}, x^{(1)}, \ldots, x^{(M-1)}\}$ (M is constellation size) and output $Y = \mathbb{C}$, the PDF of receiving y given that $x^{(k)}$ is transmitted may be expressed as [213]:

$$p\left(y|x^{(k)}\right) = \frac{1}{\pi N_0} \exp\left(\frac{-\left|y - hx^{(k)}\right|^2}{N_0}\right), \tag{4.18}$$

where we have:

$$p(y) = \sum_{k=0}^{M-1} p\left(y \mid x^{(k)}\right) \Pr\left(x^{(k)}\right), \tag{4.19}$$

here Pr is for probability. To elaborate further, the mutual information of receiving y when $x^{(k)}$ is transmitted is given by $\log_2[p(y \mid x^{(k)})/p(y)]$, hence the average mutual information of receiving the output Y due to the input X may be derived as [213, 214]:

$$I(X;Y) = \sum_{i=0}^{M-1} \int_{-\infty}^{+\infty} p\left(y|x^{(i)}\right) \Pr\left(x^{(i)}\right) \log_2\left(\frac{p\left(y|x^{(i)}\right)}{\sum_{k=0}^{M-1} p\left(y|x^{(k)}\right) \Pr\left(x^{(k)}\right)}\right) \mathrm{d}y\,. \tag{4.20}$$

So the DCMC capacity can be formulated as:

$$C_{DCMC}^{ML} = \max_{\Pr(x^{(i)})} I(X;Y)\,, \tag{4.21}$$

where ML is short for maximum likelihood, $I(X;Y)$ is maximized when we have $\Pr(x^{(i)}) = 1/M$ $(i \in \{0 \sim M-1\})$ and Eq. (4.21) may be simplified as [213]:

$$C_{DCMC}^{ML} = \log_2(M) - \frac{1}{M} \sum_{i=0}^{M-1} E\left[\log_2 \sum_{k=0}^{M-1} \exp(\Phi_{i,k}) \mid x^{(i)}\right], \tag{4.22}$$

where the unit of C is bits per symbol (BPS). Furthermore, $E[A \mid x^{(i)}]$ is the expectation of A conditioned on $x^{(i)}$, whereas the term $\Phi_{i,k}$ may be expressed similarly to that in [213]:

$$\Phi_{i,k} = \frac{-\left|\sqrt{G}h(x^{(i)} - x^{(k)}) + n\right|^2 + |n|^2}{N_0}, \tag{4.23}$$

where h is the fading coefficient, G is the path-gain and n is the AWGN at the receiver. In this chapter, the DCMC capacity will be used for deriving the lower bound of the entire cooperative communication system, as well as the achievable performance of receiving each layer of the HM signals. The E_s/N_0 difference between the simulation results and the DCMC capacity is our key performance metric, because it explicitly characterizes the ability of our TTCHM scheme to approach the idealized DCMC capacity.

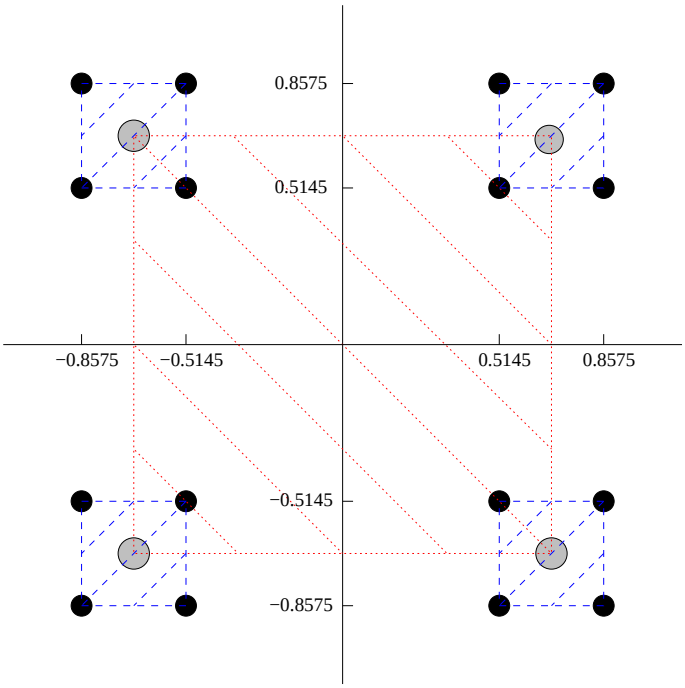

Figure 4.4: The decision area for L_1 and L_2 of the HM-16QAM symbols of Figure 4.3, when the twin-layer HM-16QAM ratio $R_1 = 3.0$.

4.4.1 Channel Capacity of the SN-DN Link

In our communication protocol, the DN demaps the HM-16QAM symbols received from the SN during the first TS as 4QAM symbols for decoding the information contained in L_1 of the HM signals. Therefore, when calculating the DCMC capacity of the SN-DN link, the constellation size here would be set to $M = 4$, rather than to $M = 16$. By contrast, the signal received over the SN-DN link is the HM-16QAM symbol stream. Therefore we have to evaluate the DCMC capacity of the 4QAM partition of our HM-16QAM constellation. We choose those four center points ($\widetilde{\alpha} S_{4QAM}$), as shown in Figure 4.3, in each quadrant to calculate the DCMC capacity lower bound of receiving L_1 from the HM-16QAM symbols, which hence will be referred to as the capacity of L_1.

Figure 4.4 portrays our general constellation map for the HM ratio of $R = 3$. The four constellation points in each quadrant represented by a square printed using dashed lines defines the two bits contained in the first layer of the HM-16QAM symbols. Decision errors would occur if the corruption imposed by the noise and fading exceeds the decision boundary among the four quadrants, which is illustrated by the larger square of Figure 4.4 printed in dotted line. We choose those four center points ($\widetilde{\alpha} S_{4QAM}$) in each quadrant to calculate the DCMC capacity of receiving L_1 from the HM-16QAM symbols, which hence will be referred to as the capacity of L_1:

$$C^{L_1}_{HM-16QAM} = 2 - \frac{1}{4}\sum_{i=0}^{3} E\left[\log_2 \sum_{k=0}^{3} \exp\left(\Phi_{i,k}\right) \mid x_q^{(i)}\right], \tag{4.24}$$

where we have $x_q^{(i)} \in \{\widetilde{\alpha}e^{j\pi/4}, \widetilde{\alpha}e^{j3\pi/4}, \widetilde{\alpha}e^{j-3\pi/4}, \widetilde{\alpha}e^{j-\pi/4}\}$, $i \in \{0,1,2,3\}$ and $\widetilde{\alpha}$ is the normalized polynomial of the HM-16QAM symbols based on the current HM ratio.

4.4.2 Channel Capacity of the SN-RN Link

The RN would demap the signal received from the SN by the HM-16QAM demapper of Figure 4.2 and calculates a $(N \times 16)$-element symbol probability matrix, if the RN is used for receiving both of the two layers' information in the HM symbol, the channel capacity may be expressed as:

$$C_{HM-16QAM} = 4 - \frac{1}{16}\sum_{i=0}^{15} E\left[\log_2 \sum_{k=0}^{15} \exp(\Phi_{i,k}) \mid x_s^{(i)}\right] , \tag{4.25}$$

where we have $x_s^{(i)} \in \left\{\widetilde{\alpha}\left[S_{4QAM} \pm \sqrt{2}\delta_1 e^{\pm\frac{\pi}{4}j}\right]\right\}$ and $i \in \{0,1,2,\cdots,15\}$. However, the RN will only deal with the information in L_2, while the $(N \times 16)$-element probability matrix will be converted into a $(N \times 4)$-element matrix for decoding the information in L_2 of the HM symbols. When considering the DCMC capacity of receiving L_2 of the HM signal, we also have to subtract two bits from the DCMC capacity of the HM-16QAM constellation. Hence, based on the chain-rule of mutual information [6, 214], we have:

$$\begin{aligned}
&I(b_3,b_2,b_1,b_0;y)\\
&= I(b_3;y) + I(b_2;y \mid b_3) + I(b_1;y \mid b_3,b_2) + I(b_0;y \mid b_3,b_2,b_1)\\
&= H(b_3) - H(b_3 \mid y) + H(b_2 \mid b_3) - H(b_2 \mid b_3,y) + H(b_1 \mid b_3,b_2)\\
&\quad - H(b_1 \mid b_3,b_2,y) + H(b_0 \mid b_3,b_2,b_1) - H(b_0 \mid b_3,b_2,b_1,y)\\
&= [H(b_3) + H(b_2 \mid b_3)] - [H(b_3 \mid y) + H(b_2 \mid b_3,y)] +\\
&\quad [H(b_1 \mid b_3,b_2) + H(b_0 \mid b_3,b_2,b_1)] -\\
&\quad [H(b_1 \mid b_3,b_2,y) + H(b_0 \mid b_3,b_2,b_1,y)]\\
&= H(b_3,b_2) - H(b_3,b_2 \mid y) + H(b_1,b_0 \mid b_3,b_2) -\\
&\quad H(b_1,b_0 \mid b_3,b_2,y)\\
&= I(b_3,b_2;y) + I(b_1,b_0;y \mid b_3,b_2) ,
\end{aligned} \tag{4.26}$$

while $H(X,Y)$ is the joint entropy given by

$$H(X,Y) = -\sum_{x\in X}\sum_{y\in Y} p(x,y)\log_2 p(x,y). \tag{4.27}$$

It can be stated that:

$$I(b_1,b_0;y \mid b_3,b_2) = I(b_3,b_2,b_1,b_0;y) - I(b_3,b_2;y) , \tag{4.28}$$

where we have $C_{HM-16QAM} = \max_{\Pr(x_s)}\{I(b_3,b_2,b_1,b_0;y)\}$, which is the DCMC capacity of receiving HM-16QAM signals, while $C_{HM-16QAM}^{L_1} = \max_{\Pr(x_q)}\{I(b_3,b_2;y)\}$, which is the DCMC capacity of receiving L_1 from the twin-layer HM-16QAM signal. When considering $I(b_1,b_0;y \mid b_3,b_2)$,

we found that the detection of L_2 is not entirely independent from the information contained in L_1. However, the achievable DCMC capacity of receiving L_2 will only be approached, when L_1 is perfectly received. Hence, we may define the DCMC capacity of receiving L_2 to be $C^{L_2}_{HM-16QAM} = \max_{\Pr(x_s)}\{I(b_1, b_0; y \mid b_3, b_2)\}$, which may be expressed as:

$$C^{L_2}_{HM-16QAM} = C_{HM-16QAM} - C^{L_1}_{HM-16QAM} \,. \tag{4.29}$$

Note that the average symbol power is normalized to unity, and the HM-16QAM symbols are equiprobable, hence $\Pr(x_q) = 1/4$ and $\Pr(x_s) = 1/16$.

4.4.3 Statistics of the DCMC in Each Link and Overall System Optimization

In our simulations, the coding rate R_c of the two encoders employed by the SN is 1/2, hence we only focus our attention on the specific SNR values, where the DCMC capacity reaches 1 bit per symbol. Multiple values of the HM ratio had been tested and the relative statistics are recorded in Table. 4.1. At a given HM ratio, both the minimum $SNR_r^{L_1}$ required for decoding the first layer at the DN and $SNR_r^{L_2}$ of the second layer at the RN may be found. The SNR difference between the two layers is:

$$\mathcal{G}_{SNR} = SNR_r^{L_2} - SNR_r^{L_1} \text{ [dB]} \,. \tag{4.30}$$

If we set SNR_t^{SN} to be identical to the specific SNR_r value, which is required for the reliable detection of L_1 in the HM-16QAM symbol, we may have $SNR_t^{SN} = SNR_r^{L_1}$. This would guarantee that the BER of decoding L_1 would reach an arbitrarily low value. In this situation, if we want the BER performance of receiving L_2 to become sufficiently low, the channel gain G_{SR} of the SN-RN link should satisfy:

$$10\log_{10} G_{SR} + SNR_r^{L_1} = SNR_r^{L_2} \,. \tag{4.31}$$

If we use the ratio d_{SR}/d_{SD} for representing the position of the RN, we arrive at:

$$\mathcal{G}_{SNR} = 10\log_{10}\left(\frac{d_{SD}}{d_{SR}}\right)^2 \,, \tag{4.32}$$

where $\mathcal{G}_{SNR}$ is given by Eq. (4.30) and hence we have:

$$\frac{d_{SR}}{d_{SD}} = 10^{-\frac{\mathcal{G}_{SNR}}{20}} \,. \tag{4.33}$$

Once the position of the RN becomes known, the path gain between the RN and DN is formulated as:

$$G_{RD} = \left(1 - \frac{d_{SR}}{d_{SD}}\right)^{-2} \,. \tag{4.34}$$

In the capacity analysis, we observe that a system employing a rate-1/2 channel coding scheme and 4QAM modulation for communication over uncorrelated Rayleigh fading channels requires $SNR_r = 1.81$ dB to reach a DCMC capacity of 1 BPS. Hence the SNR_t^{RN} has to satisfy:

$$SNR_t^{RN} = 1.81 - 10\log G_{RD} \quad \text{[dB]} \,. \tag{4.35}$$

HM Ratio	DCMC 1 BPS	$\text{SNR}_r^{L^1}$ [dB]	$\text{SNR}_r^{L^2}$ [dB]	G_{SR} [dB]	Pos. RN [d_{SR}/d_{SD}]	G_{RD} [dB]	SNR_t^{RN} [dB]	$\overline{\text{SNR}_t}$ [dB]
0.5	1	3.41	10.76	7.35	0.43	4.87	-3.05	1.28
1.0	1	2.78	10.64	7.86	0.41	4.50	-2.69	0.86
1.5	1	2.46	11.41	8.95	0.36	3.83	-2.02	0.77
2.0	1	2.27	12.39	10.12	0.31	3.25	-1.43	0.80
2.5	1	2.15	13.39	11.23	0.27	2.79	-0.97	0.87
3.0	1	2.08	14.35	12.27	0.24	2.42	-0.61	0.94
3.5	1	2.02	15.24	13.22	0.22	2.14	-0.33	1.00
4.0	1	1.98	16.07	14.09	0.20	1.91	-0.10	1.07
4.5	1	1.95	16.84	14.89	0.18	1.72	0.09	1.12
5.0	1	1.93	17.56	15.63	0.17	1.57	0.24	1.17
5.5	1	1.91	18.22	16.31	0.15	1.44	0.37	1.21
6.0	1	1.90	18.84	16.94	0.14	1.33	0.48	1.25
6.5	1	1.89	19.42	17.54	0.13	1.24	0.58	1.28
7.0	1	1.88	19.97	18.09	0.12	1.16	0.66	1.31
7.5	1	1.87	20.49	18.62	0.12	1.08	0.73	1.34
8.0	1	1.87	20.98	19.11	0.11	1.02	0.79	1.36
8.5	1	1.86	21.44	19.58	0.11	0.96	0.85	1.38
9.0	1	1.86	21.88	20.02	0.10	0.91	0.90	1.40
9.5	1	1.85	22.30	20.44	0.10	0.87	0.95	1.42
10.0	1	1.85	22.69	20.85	0.10	0.83	0.99	1.44

Table 4.1: The DCMC statistics of the average transmission power of the HM-16QAM cooperative system shown in Figure 4.2. The uncorrelated Rayleigh fading channel is considered, while the number of samples when calculating the DCMC capacity is 10^5, and the related results are showed in Figure 4.6. Compared to Table 4.3, the target SNR threshold here is given by the SNR, when the capacity reaches 1 BPS.

Likewise, the SNR_t^{SN} of the SN should guarantee that:

$$SNR_t^{SN} = SNR_r^{L_1} \, . \tag{4.36}$$

Hence, the average SNR_t of the entire system is given by:

$$\overline{SNR_t} = 10\log_{10}\left(\frac{10^{(SNR_t^{SN}/10)} + 10^{(SNR_t^{RN}/10)}}{2}\right) \ [\text{dB}] \, . \tag{4.37}$$

Let us now consider the DCMC capacity at the HM ratio of $R_1 = 1.5$ for instance. Based on Eq. (4.24) and Eq. (4.29), the DCMC capacity of receiving L_1, L_2 and conventional 4QAM relying on Gray mapping for transmission over uncorrelated Rayleigh fading channels are shown in Figure 4.5a. Observe from Figure 4.5a that the SNR_r values required for the reliable detection of L_1 and L_2 of our rate-1/2 coded HM-16QAM scheme are 2.46 dB and 11.41 dB, respectively. Hence, SNR_t^{SN} should be set to 2.46 dB and the path-loss reduction of the SN-RN link is $11.41 - 2.46 = 8.95$ dB. Given the path gains G_{SR} and G_{RD}, the DCMC capacity based on the SNR_t of L_1 and L_2 is portrayed in Figure 4.5b. Observe in Figure 4.5b that there is an intersection between the

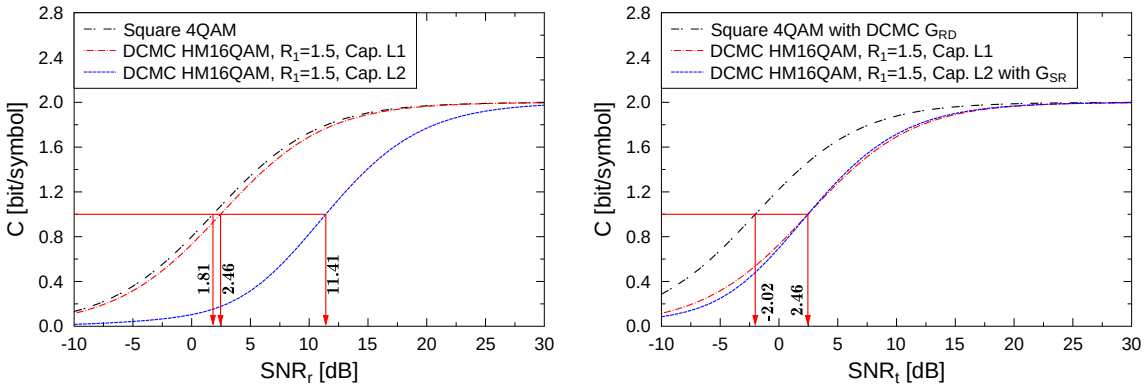

(a) The DCMC capacity versus SNR_r of L_1 and L_2 of our HM-16QAM scheme when the HM ratio R_1 is 1.5, and conventional 4QAM with Gray mapping.

(b) The DCMC capacity versus transmit SNR_t of L_1 and L_2 of our HM-16QAM scheme when the HM ratio R_1 is 1.5, and conventional 4QAM with Gray mapping.

Figure 4.5: DCMC capacity versus SNR for the schematic of Figure 4.2 based on Eq. (4.24), Eq. (4.25) and Eq. (4.29). The number of samples when calculating the DCMC capacity is 10^5. The channel is an uncorrelated Rayleigh fading channel.

DCMC capacity curves of L_1 and L_2. This intersection indicates that an arbitrarily low BER can be achieved at the DN (for L_1) and at the RN (for L_2), provided that the SNR_t^{SN} is at least 2.46 dB. Note furthermore that with the benefit of having the above-mentioned path gain of 3.88 dB for the RN-DN link, SNR_t^{RN} should be set to $1.81 - 3.88 = -2.07$ dB, in order to achieve a DCMC capacity of 1 BPS at the DN. Hence, in this situation, $\overline{SNR_t}$ of the system would be 0.77 dB according to Eq. (4.37). This $\overline{SNR_t}$ value determines the lower bound of the power consumption for our communication strategy based on the current value of the HM ratio R_1, provided that a perfect capacity-achieving channel coding scheme is used.

4.4.4 DCMC Capacity Based Results

By calculating the $\overline{SNR_t}$ of multiple HM ratios and on different RN positions, the resultant three-dimensional $\overline{SNR_t}$ versus R_1 and d_{SR}/d_{SD} plot shown in Figure 4.6 may be generated. The dashed-line curve seen at the 'valley' in the figure represents the optimized solution based on the current HM ratio R_1, which is indeed at the lowest point of the power-dissipation surface, confirming that based on a given HM ratio R_1, our power-allocation regime has found the optimum RN position for ensuring that the power efficiency of the entire system is optimized. Moreover, the value of the HM ratio R_1 will be adjusted according to the current SNR_t^{SN} in order to guarantee the required target BER performance of receiving the information contained in L_1 of the HM-16QAM signal frame. Explicitly, the resultant system is dynamically optimized based on the current SNR_t^{SN}.

Based on the optimum power consumption curve seen in Figure 4.6, we have generated Fig-

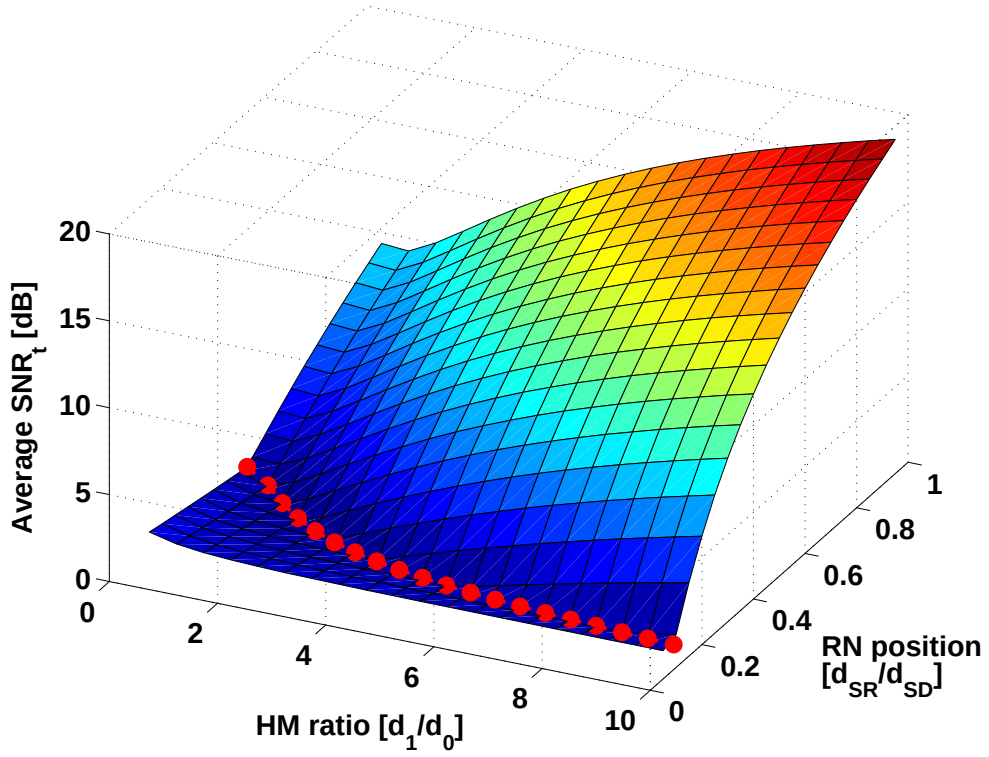

Figure 4.6: The three-dimensional (3D) plot of the power consumption surface of the entire system shown in Figure 4.2, when perfect capacity-achieving codes are assumed to be used. Hence, the system operates exactly at the DCMC capacity. The results are based on Eq. (4.24), Eq. (4.29) and Eq. (4.30), and the number of samples when calculating the DCMC capacity is 10^5. The channel is an uncorrelated Rayleigh fading channel. The related simulation results are summarized in Table 4.1.

ure 4.7a to Figure 4.7c. It can be observed from Figure 4.7a that when the value of the HM ratio is $R_1 = 1.5$, the $\overline{SNR_t}$ value of the entire system will be 0.77 dB per TS, which is the lowest possible value. This shows that if a perfect capacity-achieving rate-1/2 channel coding scheme is invoked, the optimum power consumption of the entire system will translate into $\overline{SNR_t} = 0.77$ dB per TS, which is considered to be the lower bound of our cooperative communication system. At the same point the optimum position for the RN is at the normalized distance of $d_{SR}/d_{SD} = 0.36$, as also seen in Figure 4.7b. Hence the RDRPLR G_{RD} is 3.88 dB. Furthermore, Figure 4.7c illustrates that upon increasing the HM ratio R_1, the optimum position of the RN is moved closer to the SN, which is due to the increase of the SNR$_r^{RN}$ required for adequately receiving L_2, and hence the SNR$_t^{RN}$ required for high-integrity transmissions in the RN-DN link will consequently be increased.

Figure 4.7d shows the relationship between the required SNR$_r$ and the HM ratios, where we observe that for a reliable detection of the information contained in L_1 of the HM-16QAM scheme, the minimum SNR$_r$ should be higher than 1.81 dB. On the other hand, the lowest SNR$_r$ required for a reliable detection of L_2 is 11.41 dB. Hence, provided that SNR$_t^{SN}$ is higher than 1.81 dB, the

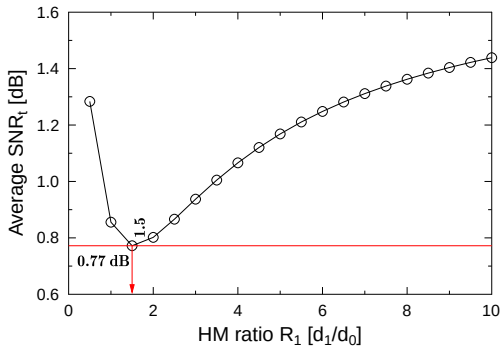

(a) The DCMC based $\overline{SNR_t}$ of the entire system versus HM ratio based on the optimized curve in Figure 4.6.

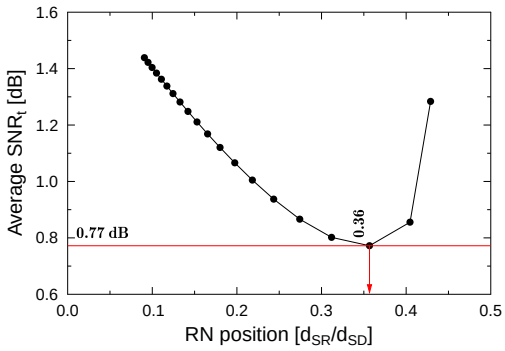

(b) The DCMC based $\overline{SNR_t}$ of the entire system versus RN position based on the optimized curve in Figure 4.6.

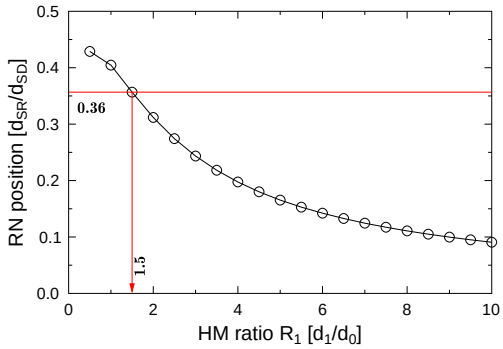

(c) The DCMC based RN position versus HM ratio based on the optimized curve in Figure 4.6.

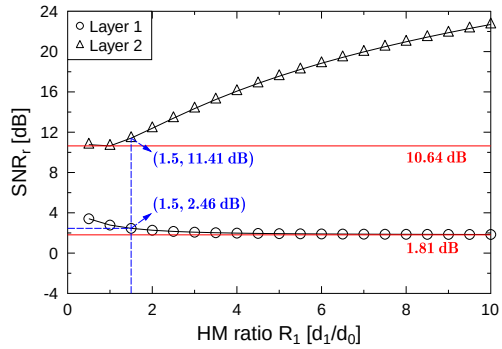

(d) The SNR versus HM ratio figure for decoding L_1 and L_2, the SNR$_r$ here is the value when the DCMC capacity reaches to 1 BPS.

Figure 4.7: The DCMC capacity analysis based results of the cooperative schematic shown in Figure 4.2. The simulation results are based on Eq. (4.24), Eq. (4.29) and Eq. (4.30), and the number of samples when calculating the DCMC capacity is 10^5. The channel is an uncorrelated Rayleigh fading channel, while the related results are summarized in Table 4.1.

system is capable of operating at a vanishingly low BER. Additionally, if SNR_t^{SN} is higher than 11.41 dB, the DN becomes capable of detecting the information received from the SN without the need of employing a RN.

4.5 TTCHM-16QAM Cooperative System Design

4.5.1 The SNR$_t$ of the RN

In Section 4.4, we have detailed the DCMC capacity analysis of our cooperative communication strategy and we have found both the minimum power consumption and the optimum RN position. In practice, we do not have any control over the position of mobile relays, but the relay-selection

algorithm would appoint a relay close to the optimum location. In this section, the SN will employ a pair of rate-1/2 TTCM encoders, rather than assuming a perfect capacity-achieving channel code, and we will optimize this practical system. The related parameters are shown in Table 4.2.

Coded Modulation	**TTCM**
Modulation Scheme	4QAM, HM-16QAM
Mapper type	Set-Partitioned
Number of iterations	4
Code Rate	1/2
Code Memory	3
Code Polynomial (octal)	$H_{4QAM} = [13\ 06]$
Decoder type	Approximate Log-MAP
Symbols per frame	12,000
Number of frames	10,000
Channel	Uncorrelated Rayleigh fading channel
Path-loss exponent	2

Table 4.2: Simulation parameters used in the schematic of Figure 4.2 and employed in the simulation results of Figure 4.8 to Figure 4.10d.

In order to establish a database for the system, we firstly simulated the BER versus SNR performance of both L_1 and L_2 of the HM-16QAM scheme based on different values of the HM ratio R_1. The results of four typical HM ratio values are shown in Figure 4.8. In this investigation, the simulations are carried out in a C++ platform, the number of iterations of our rate-1/2 TTCM decoder is $\zeta = 4$, while the block size is $\eta = 12,000$. Using a large number of iterations allows the TTCM decoder to more closely approach capacity, while a large block length assists in avoiding error propagation, but also imposes an increased complexity. When simulating the BER versus SNR results, we find that no substantial BER performance improvement is achieved for more than four iterations or for block sizes above 12,000 symbols.

The constraint of the system is to guarantee the BER performance of each link should be no higher than 10^{-6}. The TTCHM-16QAM aided cooperative communication system optimized in Section 4.4 is used and our simulation results are discussed in the following section. Note however that since Encoder 2 of Figure 4.2 used at the RN is linked with a conventional 4QAM modem with rate-1/2 TTCM channel coding scheme, SNR$_t^{RN}$ is given by:

$$SNR_t^{RN} = 4.23 - 10\log_{10} G_{RD} \quad [\text{dB}]\,, \tag{4.38}$$

where a SNR$_r$ of 4.23 dB is required for achieving a BER of 10^{-6} for our TTCM/4QAM single link, while the simulation results are recorded in Table. 4.3.

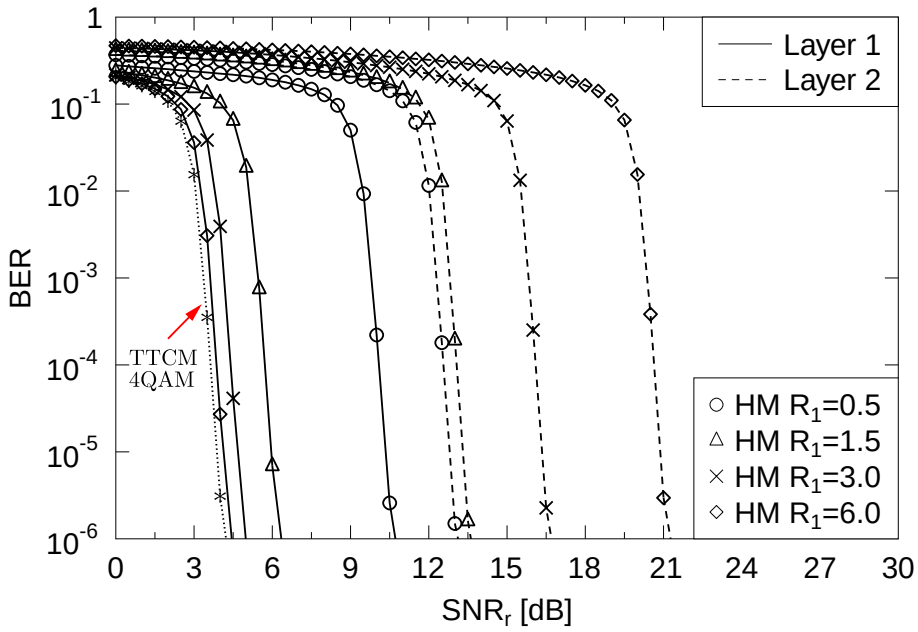

Figure 4.8: The BER versus SNR of decoding the information contained in L_1 and L_2 of the HM-16QAM symbols based on different HM ratios R_1. The SN employs two independent rate-1/2 TTCM encoders along with the HM-16QAM scheme, while the simulation parameters are shown in Table 4.2 and the system's architecture is portrayed in Figure 4.2.

4.5.2 Simulation Results

Similar to Figure 4.6, the three-dimensional plot of the power consumption surface recorded for our TTCHM aided cooperative communication system is depicted in Figure 4.9. The dashed line seen at the valley of the surface represents our optimized TTCHM-16QAM system. Based on the dashed line in Figure 4.9, three two-dimensional plots are generated, as seen in Figure 4.10a to Figure 4.10c. Observe that for achieving BER of 10^{-6}, the TTCHM aided cooperative communication system requires at least $\overline{SNR_t} = 3.62$ dB per TS. The optimum RN position is at $d_{SR} = 0.26 d_{SD}$ and the optimum HM ratio is 3.0, while the throughput of our system is 1 bps . Due to employing a realistic channel coding scheme, our TTCHM system would require a $3.62 - 0.77 = 2.85$ dB higher SNR$_t$ than the idealized system of Section 4.4, which relied on a perfect capacity-achieving channel code operating exactly at the DCMC capacity of each link.

Upon focusing our attention on the BER performance of decoding the information contained in L_1 and L_2 separately, we generated Figure 4.10d. Explicitly, Figure 4.10d illustrates the relationship between the SNR$_r$ and the related HM ratios required for detecting L_1 and L_2. Based on our optimization regime of Section 4.4, the discrepancy between the two curves at a given HM ratio may be exploited for deciding upon the required position of the RN. We could also infer two important limits from Figure 4.10d, where the minimum SNR$_r$ required for a reliable detection of the information contained in L_1 is 4.23 dB. This means that based on our communication protocol, it would be impossible for the DN to receive the information of L_1 from the SN at a BER lower

HM Ratio	**SNR**$_r^{L^1}$ **[dB]**	**SNR**$_r^{L^2}$ **[dB]**	**BER**	**G**$_{SR}$ **[dB]**	**Pos. RN [**d_{SR}/d_{SD}**]**	**G**$_{RD}$ **[dB]**	**SNR**$_t^{RN}$ **[dB]**	$\overline{\textbf{SNR}_t}$ **[dB]**
0.5	10.72	13.12	1e-6	2.40	0.76	12.34	-8.11	7.77
1.0	7.58	12.85	1e-6	5.27	0.55	6.85	-2.62	4.97
1.5	6.35	13.61	1e-6	7.27	0.43	4.93	-0.70	4.12
2.0	5.66	14.68	1e-6	9.02	0.35	3.80	0.43	3.79
2.5	5.28	15.70	1e-6	10.41	0.30	3.12	1.11	3.68
3.0	4.98	16.71	1e-6	11.72	0.26	2.61	1.62	3.62
3.5	4.86	17.59	1e-6	12.73	0.23	2.28	1.94	3.64
4.0	4.73	18.48	1e-6	13.75	0.21	2.00	2.23	3.66
4.5	4.64	19.26	1e-6	14.62	0.19	1.79	2.44	3.68
5.0	4.53	19.97	1e-6	15.44	0.17	1.61	2.62	3.68
5.5	4.48	20.63	1e-6	16.15	0.16	1.47	2.76	3.70
6.0	4.45	21.27	1e-6	16.83	0.14	1.35	2.87	3.73
6.5	4.42	21.87	1e-6	17.45	0.13	1.25	2.97	3.77
7.0	4.39	22.41	1e-6	18.02	0.13	1.17	3.06	3.78
7.5	4.37	22.94	1e-6	18.57	0.12	1.09	3.14	3.80
8.0	4.37	23.42	1e-6	19.06	0.11	1.03	3.20	3.82
8.5	4.34	23.87	1e-6	19.53	0.11	0.97	3.26	3.83
9.0	4.33	24.31	1e-6	19.98	0.10	0.92	3.31	3.85
9.5	4.32	24.72	1e-6	20.40	0.10	0.87	3.35	3.86
10.0	4.30	25.11	1e-6	20.81	0.10	0.83	3.40	3.87

Table 4.3: The statistics of the average transmission power of the HM-16QAM aided cooperative system of Figure 4.2. The related results are shown in Figure 4.9, where the simulation parameters are shown in Table 4.2. Compared to Table 4.1, the target SNR threshold here is defined as the value when the BER performance of the Monte-Carlo simulations reaches 10^{-6}.

than 10^{-6} if SNR$_r^{DN}$ is lower than 4.23 dB. Hence, in this situation the RN would have to be activated to transmit the information of both L_1 and L_2 to the DN. On the other hand, for a reliable detection of L_2, the minimum SNR$_r$ has to be above 12.85 dB, as highlighted in Figure 4.10d. If the SNR$_r$ recorded at the DN is higher than 12.85 dB, the entire system would be turned into a non-cooperative system, because the DN would be capable of decoding the whole HM-16QAM symbol stream at a BER lower than 10^{-6} without invoking a RN.

Note that the throughput of a single link assisted by a rate-1/2 TTCM encoder using 4QAM constellations is also 1 bps, as mentioned at the end of Section 4.5, while the SNR$_r$ required for achieving a BER performance of 10^{-6} by the rate-1/2 TTCM and 4QAM aided scheme is 4.23 dB when communicating over uncorrelated Rayleigh fading channels. Hence, in order to transmit two frames of 4QAM signals, the rate-1/2 TTCM aided single link system will require two TSs, while the $\overline{SNR_t}$ per TS is 4.23 dB, which is 4.23-3.62=0.61 dB higher than that of our TTCHM aided cooperative communication system. Moreover, when the SNR$_t^{SN}$ is higher than 12.85 dB, the throughput of our TTCHM aided cooperative system may be doubled to 2 bps.

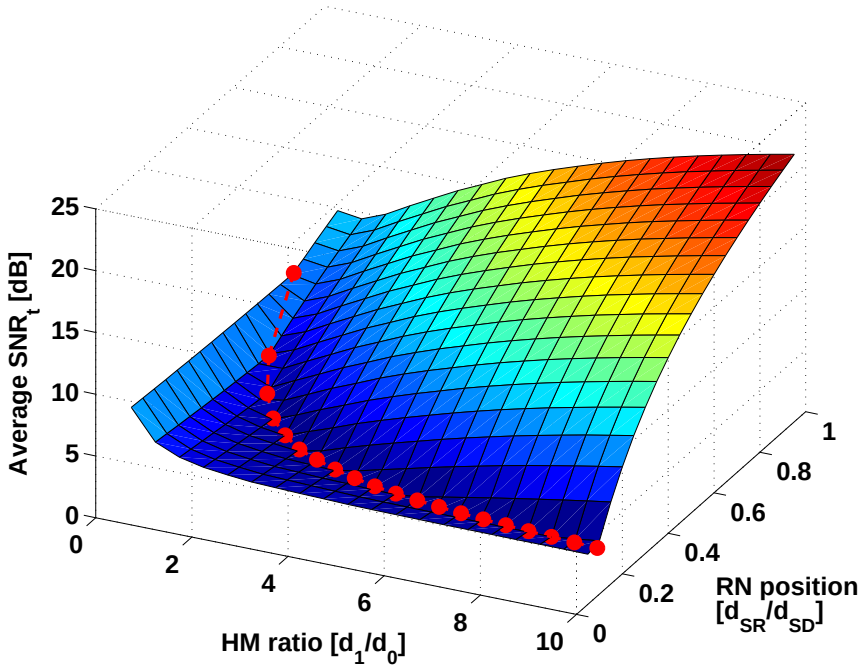

Figure 4.9: The 3D plot of the simulation based power consumption surface of the entire system of Figure 4.2, when the SN employs two independent rate-1/2 TTCM encoders along with a HM-16QAM scheme, while the simulation parameters are shown in Table 4.2 and the related results are summarized in Table 4.3.

The HM-16QAM aided system of Figure 3.15 detailed in Section 3.3 has a similar structure to the scheme proposed in this chapter and both schemes have to rely on two TSs. However, the scheme advocated in Section 3.3 employed a single rate-3/4 TTCM encoder at SN, while at the end of each TS, the DN will only receive two probability matrices. This arrangement does not directly facilitate the high-quality detection of both layers. Furthermore, the DN of the system advocated in Figure 3.15 in Section 3.3 can only activate the decoding procedure at the end of the second TS. When comparing the scheme advocated in Section 3.3 and that proposed in this chapter, it can be observed that even though the throughput of the system designed in Section 3.3 is 1.5 bps, which is higher than the 1 bps throughput of the system conceived in this chapter, the system proposed in this chapter guarantees that the more important L_1 information can be decoded immediately after the first TS. As a further difference, the simulations of Section 3.3 were carried out for a fixed RN position (right in the middle of the SN-DN link) and in order to guarantee a BER lower than 10^{-6}, $\overline{SNR_t}$ had to be at least 12.09 dB for the TTCM block size of $\eta = 12,000$, as shown in Figure 4.11. By contrast, the system optimized in this chapter requires $\overline{SNR_t} = 3.62$ dB for achieving a BER of 10^{-6}, while the optimum RN position is also taken into consideration in the proposed scheme. Furthermore, the higher code rate of $R_c = 3/4$ and the long block size of $\eta = 12,000$ for the schematic of Figure 3.15 in Section 3.3 will lead to an increased system complexity, by contrast, the complexity of the schematic of Figure 4.2 remains moderate when given the same block size η.

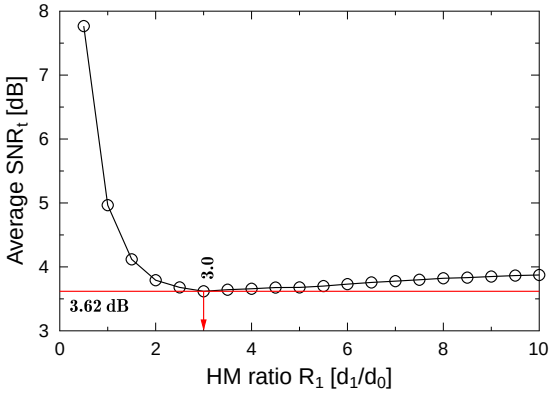

(a) The simulation based average SNR$_t$ of the entire system versus HM ratio based on the optimized curve in Figure 4.9.

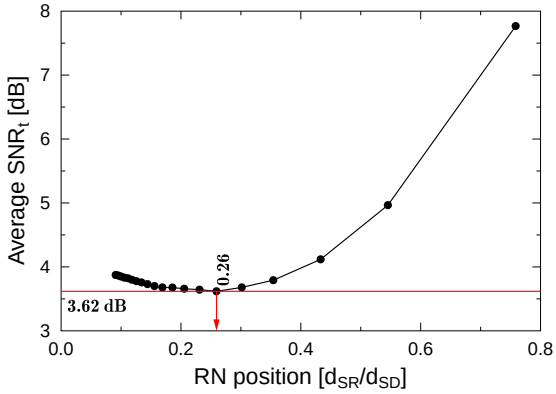

(b) The simulation based average SNR$_t$ of the entire system versus RN position based on the optimized curve in Figure 4.9.

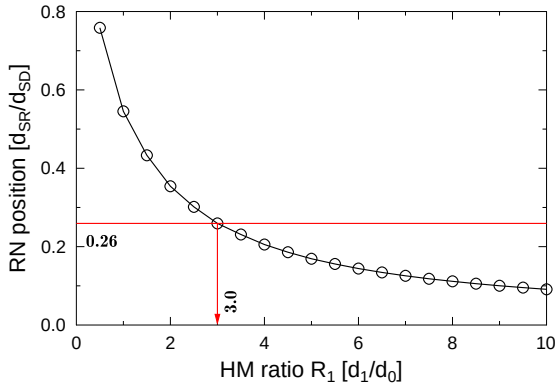

(c) The simulation based RN position versus HM ratio based on the optimized curve in Figure 4.9.

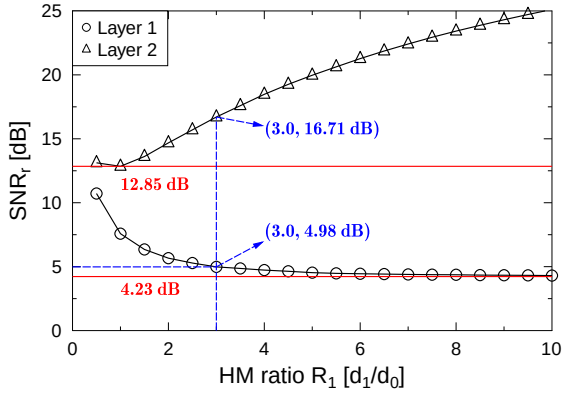

(d) The SNR$_r$ versus HM ratio figure for decoding L_1 and L_2, while the value of the SNR_r here is the required SNR$_r$ for each layer to achieve 10^{-6} BER performance.

Figure 4.10: The simulation results for our TTCHM-16QAM aided cooperative communication system of Figure 4.2. The figure is based on the doted curve seen in Figure 4.9 and the simulation parameters are shown in Table 4.2.

When comparing our optimized TTCHM scheme to the conventional HM using uncoded 16QAM relying on Gray mapping, the related simulation results are shown in Figure 4.11. It can be observed that for the system using an uncoded HM-16QAM scheme for transmission over the uncorrelated Rayleigh fading channel, the SNR_r^{DN} required for receiving L_1 is above 60 dB, which is approximately 55 dB higher than that of our TTCHM scheme. By contrast, our optimized cooperative TTCHM scheme requires a SNR_t^{SN} of approximately 4.98 dB for achieving a reliable transmission. However, the price we paid for achieving an improved BER performance is the reduction of the system's throughput. When the SNR_t^{SN} is higher than 4.23 dB, but lower than 12.85 dB, the throughput of our cooperative TTCHM system is 1 bps, while if the SNR_t^{SN} is higher than 12.85 dB, the throughput of our cooperative system may reach 2 bps. However, the achievable rate of the conventional HM-16QAM scheme is 4 bps.

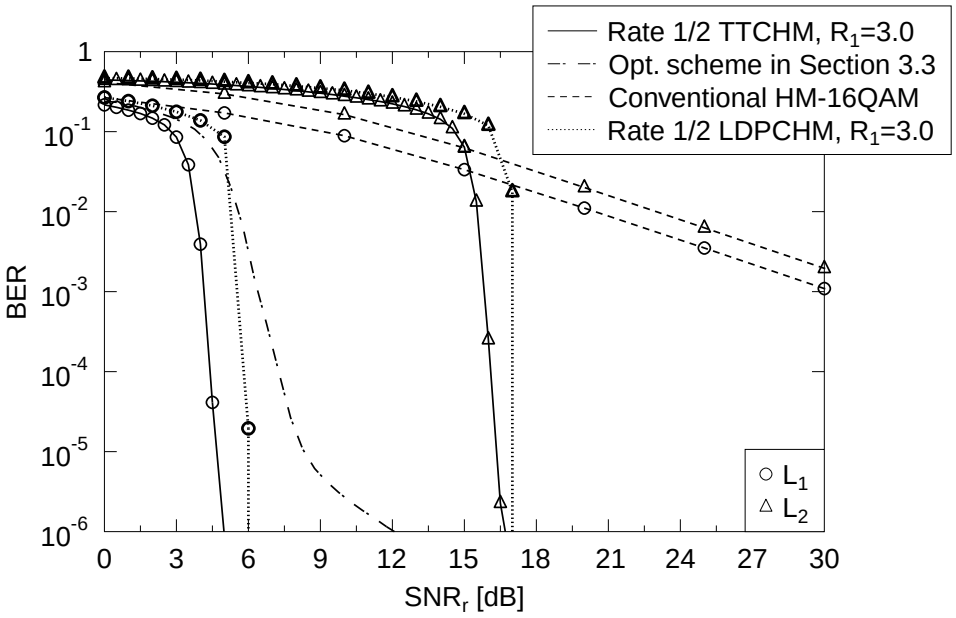

Figure 4.11: The BER versus SNR performance of the transmission between the SN and RN for our optimized TTCHM scheme shown in Figure 4.2, for the optimized scheme of Section 3.3 (as shown in Figure 3.15), for the conventional HM scheme and for our cooperative system using twin rate-1/2 LDPC encoders. For our optimized TTCHM scheme, the HM ratio R_1 is 3.0, and the optimized scheme in Section 3.3 employs a rate-3/4 TTCM encoder using the same ζ and η. The conventional HM scheme represents the uncoded HM scheme using conventional 16QAM with Gray mapping. The Rate 1/2 LDPCH's curve characterizes the performance of our cooperative system when using twin rate-1/2 LDPC encoders. The related parameters are shown in Table 4.4 and Table 4.2, while the simulation results are summarized in Table 4.4.

Additionally, we have also included the BER versus SNR performance of our cooperative communication system, when using the bit-based rate-1/2 regular LDPC encoder of [15, 215] instead of the symbol-based TTCM scheme. We refer to this LDPC code assisted HM scheme as the LDPCHM arrangement. Here the block size of the rate-1/2 LDPC encoder is the same as that of the TTCM encoder in this treatise, while the maximum number of LDPC decoder iterations is set to $\zeta_l = 20$. It can be observed that even though the number of the iterations of the LDPC decoder is significantly higher than that of the TTCM decoder, the BER of L_1 and L_2 of the LDPCHM aided system is still slightly worse than that of the TTCHM scheme. It was also found in [216] that a symbol-based scheme always has a lower convergence threshold than an equivalent bit-based scheme. The simulation results showed in Figure 4.11 have been summarized in Table 4.4.

Channel	**Uncorrelated Rayleigh**			
Code	TTCM, LDPC			
Modulation	HM-16QAM			
Decoder Type	Approximate Log-MAP			
Decoder Iteration	$\zeta_{TTCM} = 4$, $\zeta_{LDPC} = 20$			
Block Size	12,000			
Frame Size	10,000			
	Required SNR_r (dB) at BER of 10^{-6}			Achievable
	Receive L_1	Receive L_2	Receive entire symbol	bps
TTCM aided HM-16QAM	4.98	16.71	16.71	2
LDPC aided HM-16QAM	6.08	17.23	17.23	2
Opt. scheme in Section 3.3	–	–	12.09	1.5
Conventional HM-16QAM	59.96	63.08	62.89	4

Table 4.4: The SNR threshold values of the schematic seen in Figure 4.2 using both TTCM and LDPC schemes, in the schematic of Figure 3.15 with its optimized HM ratio of $R_1 = 1.6$, for the conventional uncoded HM-16QAM scheme using Gray mapping. The values are extracted from Figure 4.11. Note that the number of iterations for the TTCM decoder is identical to that in Table 4.2, which is $\zeta_{TTCM} = 4$, while for the bit-based LDPC decoder is set to $\zeta_{LDPC} = 20$. Additionally, although it increases the system's complexity, in order to make a fair comparison, we set the block size to $\eta = 12,000$ for the optimized scheme of Figure 3.15, instead of the $\eta = 1,200$ choice of Section 3.3.

4.6 Summary and Conclusions

In this chapter, we have proposed a TTCHM aided cooperative communication system. The key results in this chapter as well as in Chapter 2 and Chapter 3 are summarized in Table 4.5. We may observe that the system requires 2 TSs for conveying a pair of rate-1/2 TTCM encoded 4QAM signal frames from SN to DN. The optimum $\overline{SNR_t}$ is 3.62 dB per TS, which is within $3.62 - 0.77 = 2.85$ dB from the capacity lower bound. We demonstrated that at a throughput of 1 bps, cooperative communication is capable of providing reliable transmissions, provided that the SNR_t^{SN} is higher than 4.23 dB. By contrast, when SNR_t^{SN} is higher than 12.85 dB, the throughput of the system will be increased to 2 bps, because SNR_t^{SN} becomes sufficiently high for the DN to receive both L_1 and L_2 from the SN during the first TS.

We may also observe that compared to the cooperative schematic of Figure 3.15 , the achievable throughput of the cooperative schematic of Figure 4.2 remains lower, but it also requires a lower transmit power than that of Figure 3.15. Nonetheless, by fully exploiting the demodulation flexibility of the HM scheme as well as that of the DAF relaying, the SNR_t^{SN} of the system of Figure 4.2 is reduced to about 4.98 dB. Although, the system of Figure 3.15 has a similar structure to that of Figure 4.2, the required SNR_t^{SN} is $17.47 - 4.98 = 12.49$ dB higher than that of Figure 4.2. In Chapter 5 we will further investigate a more sophisticated HM aided cooperative scheme by expanding the twin-layer HM-16QAM constellations to a triple-layer HM-64QAM constellation,

Code Employed	System Employed	Parameters Employed	Designed for minimized power consumption						Max bps
			$\mathbf{SNR}_t^{SN}$	$\mathbf{SNR}_t^{RN}$	Pos. RN	$\overline{\mathbf{SNR}_t}$	TS	bps	
'Perfect'	Figure 4.2	–	2.46 dB	-2.02 dB	0.36	0.77 dB	2	1	2
TTCM	Figure 4.2	Table 4.2	4.98 dB	1.62 dB	0.26	3.62 dB	2	1	2
TTCM	Figure 3.1	Table 3.2	3.17 dB	4.77 dB	0.5	4.00 dB	2	0.5	2
TTCM	Figure 3.15	Table 3.6	17.47 dB	–	0.5	17.47 dB	2	1.5	3
TTCM	Figure 3.16	Table 3.6	20.93 dB	–	0.5	20.93 dB	2	2.5	5
TTCM	Figure 3.27	Table 3.8	17.69 dB	–	0.5	17.69 dB	2	3	6
TTCM	SISO 4QAM	Table 2.2	4.23 dB	–	–	4.23 dB	1	1	1
TTCM	SISO 8PSK	Table 2.2	13.40 dB	–	–	13.40 dB	1	2	2
TTCM	SISO 16QAM	Table 2.2	19.24 dB	–	–	19.24 dB	1	3	3

Table 4.5: The SNR threshold values of the schematics investigated in Chapter 2, Chapter 3 and in this Chapter. The specific simulation parameters for each system are detailed in the table. The target performance of all the simulation based schemes in the table is based on a BER of 10^{-6}. The terminology 'Perfect' in the table indicates that the channel coding scheme employed is 'perfect channel capacity achieving' as discussed in Section 4.4. Note that the block size η for the systems in Figure 3.15, Figure 3.16 and Figure 3.27 is $\eta = 1,200$, while for the other schemes in the table is $\eta = 12,000$.

where more RNs will be employed and additionally the SPM scheme will also be considered for improving the efficiency of the system, as mentioned in Chapter 3.

Code Employed	System Employed	Parameters Employed	Designed end-to-end energy spend per bit for minimized power consumption
'Perfect'	Figure 4.2	–	0.77 dB
TTCM	Figure 4.2	Table 4.2	3.62 dB
TTCM	Figure 3.1	Table 3.2	4.04 dB
TTCM	Figure 3.15	Table 3.6	15.71 dB
TTCM	Figure 3.16	Table 3.6	16.95 dB
TTCM	Figure 3.27	Table 3.8	12.91 dB
TTCM	SISO 4QAM	Table 2.2	4.23 dB
TTCM	SISO 8PSK	Table 2.2	10.29 dB
TTCM	SISO 16QAM	Table 2.2	14.49 dB

Table 4.6: The end-to-end energy per bit requirement of the schematics investigated in Chapter 2, Chapter 3 and in this Chapter. The specific simulation parameters used for each system are also listed in the table.

The values of the end-to-end SNR per bit of our cooperative communication schemes are recorded in Table 4.6. It can be observed that our cooperative communication scheme proposed in this chapter will consume less transmission power than the other cooperative communication schemes of **Chapter 2** and **Chapter 3**.

By invoking more RNs for cooperative communications, the system of Figure 4.2 will furthering approach to the capacity bound, but it would inevitably reduce the attainable throughput and in-

crease the system's complexity. As an attractive design alternative, Spatial Modulation (SM) [217] may be invoked for approaching the channel capacity, where activating one out of N_t transmit antennas allows us to convey $\log_2 N_t$ extra bits. Hence, for the sake of achieving the same throughput, the SM aided transmitter may employ a lower-order modulation scheme for the activated antenna. This would require a lower SNR_t^{SN} for the classic modulation based constituent scheme of SM to achieve the same target BER, whilst additionally requiring only a single RF chain. These solutions will be considered in our future investigations.

However, the system proposed in this chapter still has its pros and cons. First, the attainable performance critically hinges on the specific path-loss exponent. When a lower path-loss exponent is considered, the optimum RN position will be closer to the SN. If the RN is too close to the SN, it is more appropriate to employ either classic MIMO or Spatial Modulation (SM) schemes instead of the HM aided cooperative communication scheme of Figure 4.2. Meanwhile, if there is no RN close to the SN, it is better to use Amplify-and-Forward (AAF), instead of DAF [218] relaying.

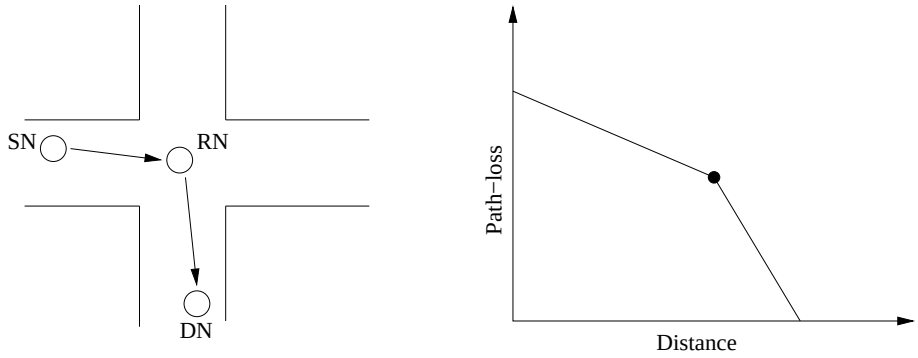

Figure 4.12: A cooperative communication model and the corresponding break-point-based path-loss model.

As seen in Figure 4.12, in practical cooperative communications the positions of the SN, RN and DN are unlikely to be on a straight line. Hence, using a break-point-based path-loss model [219] may be more realistic for analysing the cooperative communications scenario of Figure 4.2. Hence, future research also has to consider the more realistic break-point-based path-loss model of Figure 4.12.

Chapter 5

Triple-layer Hierarchical Modulation Aided Turbo Trellis-Coded Modulation for Cooperative Communications

5.1 Introduction

Hierarchical Modulation (HM) is widely employed across the telecommunication industry. The potential application of the coded HM scheme in cooperative communications has attracted a lot of research interest. In this chapter, a twin-relay aided triple-layer cooperative communication system is proposed. The system amalgamates rate-1/2 TTCM, triple-layer HM-64QAM and twin-layer SPM-16QAM schemes in the context of cooperative communications. We will optimize the entire system based on both the HM ratio pair (R_1, R_2), as well as on the Superposition Modulation (SPM) weighting pair (α, β) and on the positions of the two relays. We will demonstrate that our optimized system is capable of reliably transmitting a triple-layer HM-64QAM signal with the aid of two time slots at an average Signal-to-Noise Ratio (SNR) of 6.94 dB per time slot. In this chapter, familiarity with the turbo-detection principles and with EXIT-charts is assumed, as detailed in [6].

In Section 3.3, the TTCM aided HM based cooperative schematics of Figure 3.15 and Figure 3.16 had been conceived and discussed in detail. For eliminating the limitations of the scheme of Figure 3.15, we introduced the cooperative scheme of Figure 4.2 based on channel coded twin-layer HM-16QAM in Chapter 4. The schematic of Figure 4.2 employs two independent rate-1/2 TTCM encoders, which guarantees that the cooperative system is capable of fully exploiting the demodulation flexibility of the HM scheme, that the information in different layers of the twin-layer HM signal may be decoded separately. The cooperative schematic of Figure 4.2 successfully avoids the efficiency problem of the schematics of Figure 3.15 and Figure 3.16, that the DN may immediately activate the decoding process when after the first TS. In this chapter, we will focus on improving the cooperative schematic proposed in Figure 3.16 by using a similar method to that

proposed in Chapter 4. The SN will employ three rate-1/2 TTCM encoders, instead of a single rate-3/4 TTCM decoder in Figure 3.16. While, in order to further reduce the retransmission burden at the RN, a twin-RN assisted relaying is considered. Additionally, the SPM scheme proposed in Section 3.2 of Chapter 3 may also be considered for improving the efficiency of the transmissions from RNs to DN.

As a further technological evolution of Chapter 4, in this chapter we intrinsically amalgamate triple-layer HM, twin-layer SPM and TTCM for creating an attractive cooperative communication system. Our goal is to increase the efficiency and reduce the total power consumption of the entire system, while maintaining a low complexity. This cooperative communication system model may be readily used for assisting multilayer video transmission for example [96, 220] or for multilayer image transmission [97]. We exploit the idealized simplifying assumption that the system benefits from perfect Channel State Information (CSI), including both the fading and path-loss. Hence, according to the receiver's SNR, we are capable of determining the transmission power required at the transmitter, which we defined as the transmit SNR (SNR_t)[1]. We proposed a Turbo Trellis-Coded Hierarchical Modulation (TTCHM) aided twin-relay based cooperative communication scheme, where three rate-1/2 TTCM encoders are employed at the SN for constructing a 64QAM-based triple-layer HM scheme. The TTCM scheme detailed in [6] has a better performance for transmission over Rayleigh fading channels than other joint coding and modulation schemes, such as TCM and BICM. An excellent performance can be attained by TTCM without expanding the bandwidth. A rate-k/(k+1) TTCM scheme can be used for protecting a k-bit HM layer by expanding the number of constellation points from 2^k to 2^{k+1}. We considered $k = 1$ in this treatise.

Depending on the specific symbol-to-bit demapping arrangement of the HM scheme, different HM layers have different protections. Explicitly, the information in the higher-protection layers may require a lower SNR_r at the DN than that of the information in the lower-protection layers. Hence, when the SN transmits a multi-layer HM signal in our cooperative communication network, the SNR_t at the SN (SNR_t^{SN}) may be reduced to the minimum value that can 'just' guarantee the successful detection of the base layer (highest priority) of the HM signal at the DN. By contrast, the information in the lower priority layers may be received and retransmitted by the RN. Since we proposed a triple-layer HM scheme, two RNs are activated for retransmitting the information of the two lower layers. More specifically, a linear SPM scheme is employed by the two RNs for simultaneously transmitting the two signal frames to the DN during the second time slot (TS). Hence, two TSs are required for the transmission of all the three layers from the SN to the DN. Since the transmissions between the SN and RN (or RN and DN) only deal with a single 4QAM layer of the triple-layer HM-64QAM signals, the decoding complexity imposed on the two RNs (and DN) is reduced. Moreover, the SNR_t at the RN (SNR_t^{RN}) can also be minimized, because both RNs will only retransmit using 4QAM. If only one RN is available for assisting the transmissions, the RN would have to detect both enhancement layers from the HM-64QAM signals. The position of

[1] The definition of transmit SNR was proposed in [206], which is convenient for simplifying the discussions, although this is not a physically measurable quantity, because it relates the power at the transmitter to the noise at the receivers.

this RN would be near to the SN and the transmission between the RN and the DN will be based on 16QAM modulation. This would require a high SNR_t due to the transmission of a higher-order modulation scheme over a longer distance. Due to the flexibility of HM, the lowest-protection layer that contains the least important information can be discarded in the adverse situation, when none of the RNs is capable of detecting it. Nonetheless, the DN can still receive the pair of more important layers of the HM-64QAM. We found that apart from reducing the power dissipation of the entire system, the processing complexity of the twin-relay aided cooperative communication network may also be mitigated, when an appropriate design is invoked.

The main contributions of this chapter are as follows:

- A triple-layer HM-64QAM scheme is designed for aiding a Decode-and-Forward (DAF) based cooperative communications, which involves intrinsically amalgamating TTCM, HM and SPM schemes;
- The capacity analysis of the cooperative system based on the DCMC capacity is provided and the capacity of the individual layers of the HM based scheme is formulated. The lower capacity bound of the DAF cooperative system is also derived;
- Based on our Monte-Carlo simulations, a power-allocation is conceived and it is demonstrated that the power consumption of the entire system may be readily optimized by relying on the related variables, namely by the HM-based symbol-energy ratio pair (R_1, R_2), by the SPM weighting pair (α, β), and by the relay's geographic position.

The rest of the chapter is organized as follows. Section 5.2 introduces both the system model and our cooperative communication strategy. The specific HM-64QAM mapping rule designed for cooperative communication is detailed in Section 5.3. The protocol of the symbol-to-bit demapper of the HM symbols is discussed in Section 5.4. In Section 5.5, both the DCMC capacity and our optimization strategy are characterized, while our TTCHM aided cooperative communication design is discussed in Section 5.6. The SPM aided triple-layer TTCHM-64QAM system is detailed in Section 5.7, as well as the related simulation results. Our conclusions and future research ideas are discussed in Section 5.8.

5.2 System Model

Our TTCHM aided DF RN based cooperative communication system is illustrated in Figure 5.1. During the first transmission TS, the SN will broadcast a sequence of TTCHM symbols $\{x_1\}$ to RN_1, RN_2 and DN. In the following TSs, RN_1 will transmit a signal frame $\{x_2\}$ to the DN, another signal frame $\{x_3\}$ will also be sent to the DN by the RN_2. Again, the entire system would require three TSs to convey the triple-layer TTCHM-64QAM symbol based signal frame $\{x_1\}$ to DN.

We consider a simplified path-loss model proposed in [1] and define the path-loss exponent to be 3 which is usually used to simulate the path-loss in urban areas [1]. Note that the path-loss exponent

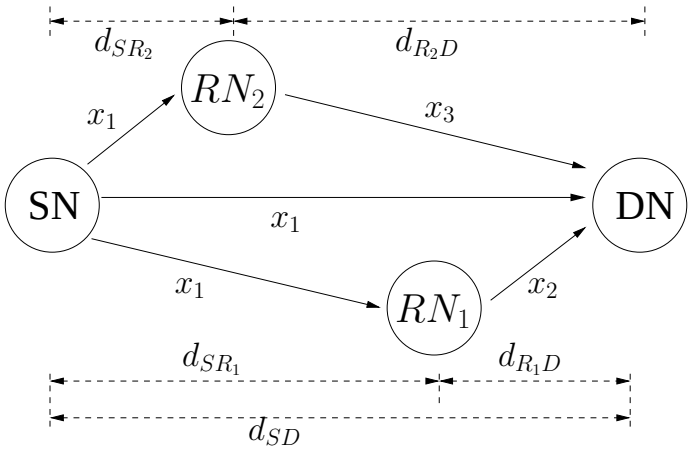

Figure 5.1: The model of a two-relay cooperative system.

is set to 2 in Chapter 3, Chapter 4 and Chapter 6 for simplifying the system model. When simulating the system proposed in Figure 5.1, the triple-layer HM-64QAM signal is more likely to be impeded by the channel fading as well as AWGN compared to the twin-layer HM-16QAM signal. Hence, fully receiving the HM-64QAM signal will require higher receive SNR, consequently the position of the RN which may need to retransmit the lowest protected layer in our system of Figure 5.1 will be much more closer than that of the RN proposed in the cooperative schematic of Figure 4.2 in Chapter 4. If the RNs are very close to the DN, MIMO or simple receive-retransmit DAF relaying may turn out to be more efficient and more simple for the transmission target. Hence, in order to avoid the position of the RNs to be too close to the SN, we set the channel exponent to be 3 for increasing the reduced path-loss between the SN-RNs link. The path-gain G_{SD} of the SD link is assumed to be unity. Therefore the path-gains of the two SR links are:

$$G_{SR_k} = \left(\frac{d_{SD}}{d_{SR_k}}\right)^3 , \tag{5.1}$$

and similarly, the path-gains of the two RD links are:

$$G_{R_kD} = \left(\frac{d_{SD}}{d_{R_kD}}\right)^3 . \tag{5.2}$$

In a realistic situation, there is a path-loss between the SN and DN, but in order to simplify the system model, we normalized this path-loss to 0 dB [2]. Note that, by adding the path-loss between the SN-DN link and considering realistic noise power, our system model could be directly converted into a realistic wireless communication system model [221]. Hence the transmit power at the SN (SNR_t^{SN}) would be identical to the power received at the DN (SNR_r^{DN}). If the transmissions between the SN and DN are on a frame-by-frame basis over an uncorrelated Rayleigh fast fading channel, the average received SNR at DN ($\overline{SNR_r^{DN}}$) would be given by:

$$\overline{SNR_r^{DN}} = E(|h|^2\, SNR_t) = E(|h|^2) SNR_t^{SN} , \tag{5.3}$$

[2] Further details on the path-loss and path-gain issues are given in Appendix A.1

where the SNR_t^{SN} is the transmit SNR defined as the ratio of the transmit power to the noise power at the DN:

$$SNR_t^{SN} = \frac{E(|x|^2)}{N_0} = \frac{1}{N_0}\,, \tag{5.4}$$

where $E(|x|^2) = 1$, while the Additive White Gaussian Noise (AWGN) having a variance of $N_0/2$ per dimension. Furthermore, due to the uncorrelated Rayleigh fading parameter h is generated by Gaussian distribution with zero mean and variance equals to one, when the number of the uncorrelated Rayleigh fading parameter we generated is large, we may have [212]:

$$E(|h|^2) = \frac{1}{N}\sum_{k=1}^{N}|h_k|^2 \approx 1\,. \tag{5.5}$$

Hence, for a large frame size of N symbols, we may assume that SNR_r^{DN} is equal to the SNR_t^{SN}, or equivalently $\overline{SNR_r^{DN}} = SNR_t^{SN}$.

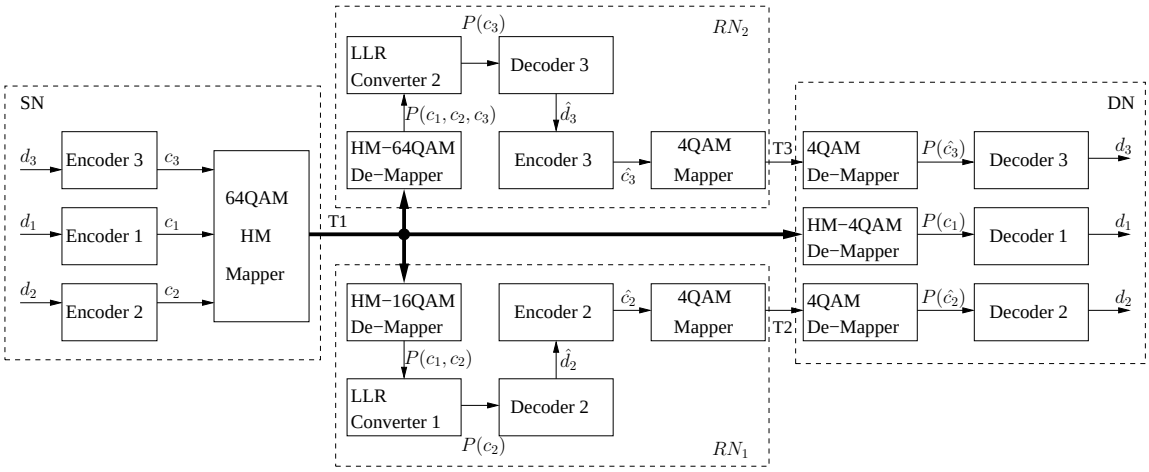

Figure 5.2: The system diagram of a twin-relay aided cooperative system.

The system diagram of our HM aided DAF RN based cooperative communication system is illustrated in Figure 5.2. Similar with the schematic of Figure 4.2, that the SN in Figure 5.2 will now employ multiple low code-rate TTCM encoders, three rate-1/2 TTCM encoders as shown in Figure 5.2, instead of a single high code-rate TTCM encoder (as the rate-5/6 TTCM encoder in Figure 3.16). The resultant three coded words c_1, c_2, c_3 are mapped to the symbol of the triple-layer HM-64QAM scheme, where according to the demodulation flexibility of the HM scheme, the three coded words c_1, c_2, c_3 contained in the HM-64QAM symbol may be demodulated separately during the cooperative communications. T_k represents the k_{th} TS. The entire system requires three TSs for conveying the information from the SN to the DN. We assign c_1 to the base layer (L_1), which is the layer associated with the highest protection, c_2 is in the second layer (L_2) and c_3 is in the third layer (L_3), which is the lowest protection layer. In order to reduce the transmit SNR (SNR_t) of all the three nodes in the cooperative network, we set SNR_t at the SN (SNR_t^{SN}) to a level, which 'just' ensures that DN receives the information at the required target-integrity in L_1, while the rest of the two layers will be received and retransmitted by the two RNs to the DN. In this way, each of the RN

only has to deal with a single layer and the DN only has to receive a single layer during each TS, so that the complexity of the system remains moderate. Let us now focus our attention on designing a specific HM mapping rule that is suitable for cooperative communications and then optimize the system based on its DCMC capacity analysis regarding the positions of the pair of RNs employed.

5.3 Triple Layer HM Constellation

Our triple-layer model of the HM-64QAM constellation seen in Figure 5.3 was originally introduced in Section 3.3. Because the system in Section 3.3 that we have proposed is assisted by the TTCM, so that in order to achieve a lower Symbol-Error-Rate (SER), the mapping we used is set-partition instead of Gray mapping. While, the mapping model we proposed in this chapter is also set-partition.

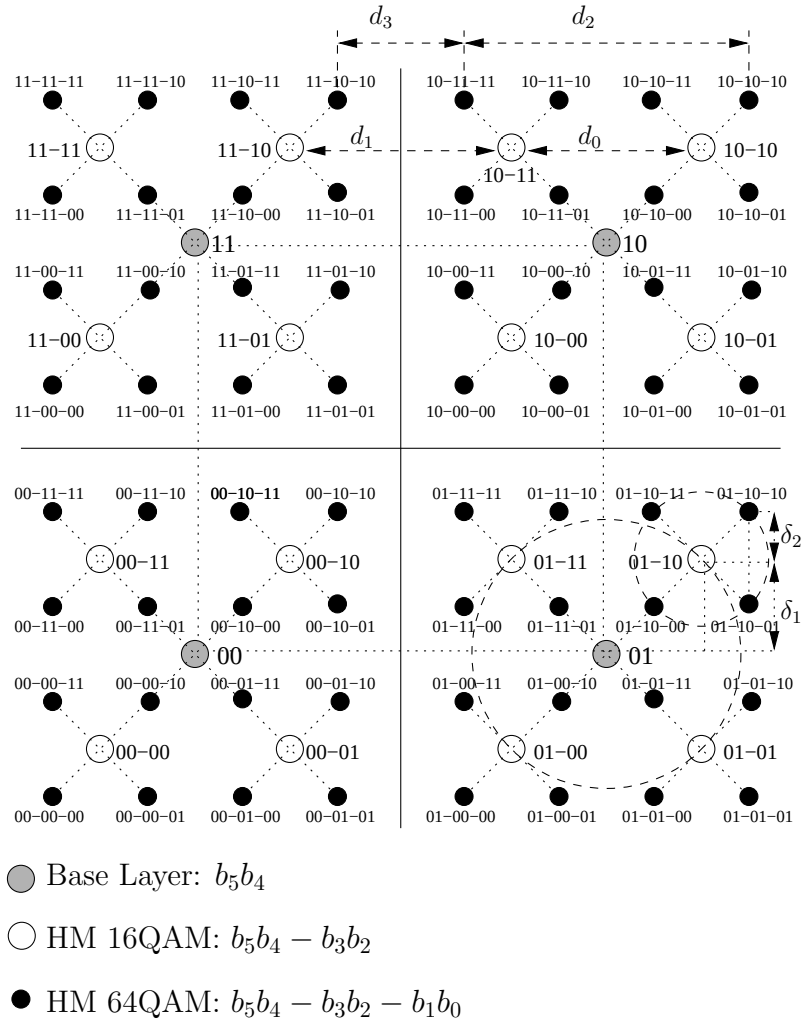

Figure 5.3: The constellation map of the HM scheme used in the schematic of Figure 5.2, where $R_1 = d_1/d_0$, $R_2 = d_3/d_2$.

We denote the six bits of a HM-64QAM symbol as $(b_5b_4b_3b_2b_1b_0)$, where L_1 is occupied by

(b_5b_4), while (b_3b_2) belong to L_2 and (b_1b_0) are contained in L_3. The generation rule of the triple-layer HM-64QAM symbols may be expressed as:

$$S_{HM-64QAM} = \widetilde{\beta}\left[S_{4QAM} \pm \sqrt{2}\delta_1 e^{\pm\frac{\pi}{4}j} \pm \sqrt{2}\delta_2 e^{\pm\frac{\pi}{4}j}\right] . \tag{5.6}$$

A HM ratio pair of ($R_1 = d_1/d_0, R_2 = d_3/d_2$) is defined along with the control parameters $\widetilde{\beta}$, δ_1 and δ_2. The relationships among these parameters are

$$\widetilde{\beta} = 1/\sqrt{1+2\delta_1^2+2\delta_2^2}\,, \tag{5.7}$$

$$\delta_1 = \frac{1}{\sqrt{2}\,(1+R_1)}\,, \tag{5.8}$$

$$\delta_2 = \frac{R_1 - R_2}{\sqrt{2}\,(1+R_1)\,(1+R_2)}\,. \tag{5.9}$$

The HM ratio pair is used for controlling the formation of the constellation map and the restrictions imposed on the HM ratio pair are:

$$\begin{cases} 0 < R_2 < R_1 & \text{if } R_1 < 1 \\ \frac{1}{2}(R_1 - 1) < R_2 < R_1 & \text{if } R_1 > 1\,. \end{cases} \tag{5.10}$$

In the simulations, different HM ratio pairs will be tested and we will optimize the average SNR_t ($\overline{SNR_t}$) of the system based on four factors, namely the HM ratio pair (R_1, R_2), the position of RN_1 and the position of RN_2.

5.4 Demap HM Symbols

The symbol-to-bit Demapper block of Figure 5.2 will produce a $(\eta \times M)$-element Probability Density Function (PDF) matrix of receiving y given $x_n^{(i)}$ transmitted, that the PDF matrix will be used to calculate the input to the TTCM decoder, where η is the number of received symbols, which also refers to the block size of the encoder, and M is the number of modulation levels. $x_n^{(i)}$ is the hypothetically transmitted M-ray symbol for $i \in \{0, 1, \cdots, M-1\}$ and n is the time index denotes the order of current received symbol in the signal frame received. Whilst, the element in the PDF matrix is $p\left(y|x_n^{(i)}\right)$. The general equation of calculating the PDF of receiving y, given that $x_n^{(i)}$ is transmitted may be expressed as:

$$p\left(y|x_n^{(i)}\right) = \frac{1}{\pi N_0}\exp\left(-\frac{\left|y - \sqrt{G}hx_n^{(i)}\right|^2}{N_0}\right)$$
$$i \in \{0, 1, \ldots, M-1\}\,, \tag{5.11}$$

where h is the fading coefficient and G is the path-gain.

5.4.1 Detection of L_1 at DN

The DN of Figure 5.2 will demap the HM-64QAM signal frames received from the SN as 4QAM symbols for detecting the information contained in the base layer of the triple-layer HM-64QAM

constellation. According to the HM-64QAM generation rule of Eq. (5.6), Eq. (5.11) may be rewritten as:

$$p\left(y_{SD}|L_{1,n}^{(i)}\right) = p\left(y_{SD}|x_n^{(i)}\right) = \frac{1}{\pi N_0}\exp\left(-\frac{\left|y_{SD}-\sqrt{G_{SD}}h_{SD}x_n^{(i)}\right|^2}{N_0}\right)$$
$$x_n^{(i)} \in \{\widetilde{\beta}e^{j\pi/4}, \widetilde{\beta}e^{j3\pi/4}, \widetilde{\beta}e^{j-3\pi/4}, \widetilde{\beta}e^{j-\pi/4}\}\,, \tag{5.12}$$

where we have $i \in \{0,1,2,3\}$ and $n \in \{1,2,\ldots,\eta\}$. Therefore, the $(\eta \times 4)$-element probability matrix Pr_{L1} required for decoding L_1, which is the input of Decoder 1 in Figure 5.2, may be expressed as:

$$\mathrm{Pr}_{L1}(n,i) = \mathrm{Pr}\left(L_{1,n}^{(i)}|y_{SD}\right) = p\left(y_{SD}|L_{1,n}^{(i)}\right)\mathrm{Pr}\left(L_{1,n}^{(i)}\right)\,. \tag{5.13}$$

In order to reduce the complexity of the entire system, we dispense with iterations between the TTCM decoder and the demapper in Figure 5.2. Hence, $\mathrm{Pr}\left(L_{1,n}^{(i)}\right)$ becomes 1/4, representing an equi-probable scenario.

5.4.2 Detection of L_2 at RN_1

The information output of Encoder 2 in Figure 5.2 is mapped onto L_2, while RN_1 will demap the received signal frame x_1 as the HM-16QAM symbols of Figure 5.3 and will obtain the joint symbol probability of L_1 and L_2 in the HM-64QAM symbol streams for producing an $(\eta \times 16)$-element probability matrix. Then, the Log Likelihood Ratio (LLR) Converter 1 of Figure 5.2 will extract the probability of L_2 from the $(\eta \times 16)$-element probability matrix. Therefore, RN_1 is capable of decoding L_2 even when L_3 is contaminated by errors. When demapping the HM-64QAM symbol as HM-16QAM, Eq. (5.11) may be reformulated as:

$$p\left(y_{SR_1}|x_n^{(i)}\right) = \frac{1}{\pi N_0}\exp\left(-\frac{\left|y_{SR_1}-\sqrt{G_{SR_1}}h_{SR_1}x_n^{(i)}\right|^2}{N_0}\right)$$
$$x_n^{(i)} \in \left\{\widetilde{\beta}\left[S_{4QAM} \pm \sqrt{2}\delta_1 e^{\pm\frac{\pi}{4}j}\right]\right\}\,, \tag{5.14}$$

where $i \in \{0,1,\cdots,15\}$. The HM-16QAM constellation points of $x_n^{(i)}$ are shown as hollow circles in Figure 5.3. We defined $L_2^{(0)}$ as the pair of bits (00) in L_2, $L_2^{(1)}$ as (01), $L_2^{(2)}$ (10) and finally $L_2^{(3)}$ for (11), where the corresponding generation rule is given by:

$$p\left(y_{SR_1} \mid L_{2,n}^{(l)}\right) = p\left(y_{SR_1}|x_n^{(l)}\right) + p\left(y_{SR_1}|x_n^{(l+4)}\right) + p\left(y_{SR_1}|x_n^{(l+8)}\right) + p\left(y_{SR_1}|x_n^{(l+12)}\right)\,, \tag{5.15}$$

where $l \in \{0,1,2,3\}$. The input probability matrix of Decoder 2 is formulated in Eq. (5.15). Hence, the the $(\eta \times 4)$-element probability matrix Pr_{L2} required for decoding L_2 may be expressed as:

$$\mathrm{Pr}_{L2}(n,l) = \mathrm{Pr}\left(L_{2,n}^{(l)} \mid y_{SR_1}\right) = p\left(y_{SR_1}|L_{2,n}^{(l)}\right)\mathrm{Pr}\left(L_{2,n}^{(l)}\right)\,, \tag{5.16}$$

where we have $\mathrm{Pr}\left(L_{2,n}^{(l)}\right) = 1/4$.

5.4.3 Detection of L_3 at RN_2

RN_2 requires the highest receive power, because it has to convey the information of L_3. In order to receive L_3, RN_2 has to fully demap the whole HM-64QAM symbol stream. Hence Eq. (5.11) may be represented as:

$$p\left(y_{SR_2} \mid x_n^{(i)}\right) = \frac{1}{\pi N_0} \exp\left(-\frac{\left|y_{SR_2} - \sqrt{G_{SR_2}} h_{SR_2} x_n^{(i)}\right|^2}{N_0}\right)$$
$$x_n^{(i)} \in \left\{\widetilde{\beta}\left[S_{4QAM} \pm \sqrt{2}\delta_1 e^{\pm\frac{\pi}{4}j} \pm \sqrt{2}\delta_2 e^{\pm\frac{\pi}{4}j}\right]\right\}, \tag{5.17}$$

where $i \in \{0, 1, \cdots, 63\}$. Let $L_3^{(0)}$ denote the pair of bits (00) in L_3, $L_3^{(1)}$ represent (01), $L_2^{(3)}$ (10) and finally $L_3^{(3)}$ for (11). Then the LLR Converter 2 of Figure 5.2 may produce the probability of receiving y_{SR_2} when L_3 is transmitted according to:

$$p\left(y_{SR_2} | L_{3,n}^{(l)}\right) = \sum_{k=0}^{15} p\left(y_{SR_1} | x_n^{(i=4k+l)}\right), \tag{5.18}$$

where $l \in \{0, 1, 2, 3\}$. The $(\eta \times 4)$-element probability matrix generated by the LLR Converter 2 is then fed to Decoder 3 of RN_2, as seen in Figure 5.2. For detecting L_3, the $(\eta \times 4)$-element probability matrix Pr_{L3} may be formulated as:

$$\Pr_{L3}(n,k) = \Pr\left(L_{3,n}^{(k)} \mid y_{SR_2}\right) = p\left(y_{SR_2} | L_{3,n}^{(k)}\right) \Pr\left(L_{3,n}^{(k)}\right), \tag{5.19}$$

where we have $k \in \{0, 1, 2, 3\}$ and $\Pr\left(L_{3,n}^{(k)}\right) = 1/4$. Furthermore, we consider logarithmic probabilities, so that the approximate log MAP algorithm of [6] may be directly employed by the decoder block.

5.5 DCMC Capacity Based System Analysis

The achievable DCMC capacity will be used to calculate the bound of our cooperative communication system in this treatise, as well as the achievable rate of receiving L_1, L_2, L_3 from the triple-layer HM-64QAM symbols. When considering the capacity of a Discrete-Input Continuous-Output Memoryless Channel (DCMC) with input $X = \{x_0, x_1, \ldots, x_{M-1}\}$ (M is constellation size) and output $Y = \{-\infty, +\infty\}$, the transition probability of receiving y given x_k is transmitted is expressed as [213]:

$$p(y|x_k) = \frac{1}{\pi N_0} \exp\left(\frac{-|y - hx_k|^2}{N_0}\right), \tag{5.20}$$

where we have:

$$p(y) = \sum_{k=0}^{M-1} p(y|x_k) p(x_k). \tag{5.21}$$

The mutual information of receiving y when x_k is transmitted is given by $\log_2[p(y \mid x_k)/p(y)]$, hence the average mutual information of getting the output Y with the input X may be derived

as [213, 214]:

$$I(X;Y) = \sum_{i=0}^{M-1} \int_{-\infty}^{+\infty} p(y|x_i)p(x_i)\log_2\left(\frac{p(y|x_i)}{\sum_{k=0}^{M-1} p(y|x_k)p(x_k)}\right) \mathrm{d}y \,. \tag{5.22}$$

So the DCMC capacity[3] C can be formulated as:

$$C_{DCMC}^{ML} = \max_{p(x_i)} I(X;Y) \,, \tag{5.23}$$

where ML is short for maximum likelihood, $I(X;Y)$ is maximized when we have $p(x_i) = 1/M$ ($i \in [0 \sim M-1]$) and Eq. (5.23) may be simplified as [213]:

$$C_{DCMC}^{ML} = \log_2(M) - \frac{1}{M}\sum_{i=0}^{M-1} E\left[\log_2 \sum_{k=0}^{M-1} \exp(\Phi_{i,k}) \mid x_i\right] \,, \tag{5.24}$$

where the unit of C is bits per symbol (bps). $E[A \mid x_i]$ is the expectation of A conditioned on x_i, whereas the term $\Phi_{i,k}$ may expressed similar to that in [213]:

$$\Phi_{i,k} = \frac{-\left|\sqrt{G}h(x_i - x_k) + n\right|^2 + |n|^2}{N_0} \,. \tag{5.25}$$

where h is the fading coefficient, G is the path-gain and n is the AWGN at the receiver.

5.5.1 Channel Capacity of the SN-DN Link

The DN demaps the HM-64QAM symbols from the SN during the first TS as 4QAM symbols for decoding the L_1 information of the HM signal. Therefore, when calculating the channel capacity of the SN-DN link, the number of modulation levels is set to $M = 4$. However, the signal received over the SN-DN link is the HM-64QAM symbol stream. Therefore we have to evaluate the DCMC capacity of the 4QAM partition of our HM-64QAM constellation. We choose the four center points ($\widetilde{\beta}S_{4QAM}$) in each quadrant for calculating the channel capacity of receiving L_1 from the HM-64QAM symbols, which hence will be referred to as the capacity of L_1:

$$C_{HM-64QAM}^{L_1} = 2 - \frac{1}{4}\sum_{i=0}^{3} E\left[\log_2 \sum_{k=0}^{3} \exp(\Phi_{i,k}) \mid x^{(i)}\right] \,, \tag{5.26}$$

where we have $x^{(i)} \in \{\widetilde{\beta}e^{j\pi/4}, \widetilde{\beta}e^{j3\pi/4}, \widetilde{\beta}e^{j-3\pi/4}, \widetilde{\beta}e^{j-\pi/4}\}$ and $\widetilde{\beta}$ is the normalization parameter of the HM-64QAM symbols based on the current HM ratio, as exemplified in Section 5.3.

5.5.2 Channel Capacity of the SN-RN$_1$ Link

For decoding the information contained in L_2 of the HM-64QAM symbols, RN_1 would demap the signal frame $\{x_1\}$ as HM-16QAM symbols, and then the Log-Likelihood Ratio (LLR) converter 1

[3] Some authors refer to this modulation-dependent DCMC capacity as the achievable rate.

(as shown in Figure 5.2) will calculate the soft information of L_2 from the HM-64QAM symbols we received. Therefore, the DCMC capacity that we calculate based on the output of the HM-16QAM De-Mapper block (as seen in Figure 5.2) is the joint capacity of the two independent layers, namely of L_1 and L_2. The DCMC capacity of receiving L_1 and L_2 of HM-64QAM may be expressed as:

$$C_{HM-64QAM}^{L_1,L_2} = 4 - \frac{1}{16}\sum_{i=0}^{15} E\left[\log_2 \sum_{k=0}^{15} \exp(\Phi_{i,k}) \mid x^{(i)}\right] , \tag{5.27}$$

where we have $x^{(i)} \in \left\{\widetilde{\beta}\left[S_{4QAM} \pm \sqrt{2}\delta_1 e^{\pm\frac{\pi}{4}j}\right]\right\}$. We assume that the pair of bits contained in L_1 is (b_5b_4) of Figure 5.3, while (b_3b_2) belong to L_2. Then, based on the chain-rule of mutual information [6, 214], we arrive at:

$$\begin{aligned}
&I(b_5, b_4, b_3, b_2; y) \\
&= I(b_5; y) + I(b_4; y \mid b_5) + I(b_3; y \mid b_5, b_4) + I(b_2; y \mid b_5, b_4, b_3) \\
&= H(b_5) - H(b_5 \mid y) + H(b_4 \mid b_5) - H(b_4 \mid b_5, y) + H(b_3 \mid b_5, b_4) \\
&\quad - H(b_3 \mid b_5, b_4, y) + H(b_2 \mid b_5, b_4, b_3) - H(b_2 \mid b_5, b_4, b_3, y) \\
&= [H(b_5) + H(b_4 \mid b_5)] - [H(b_5 \mid y) + H(b_4 \mid b_5, y)] + \\
&\quad [H(b_3 \mid b_5, b_4) + H(b_2 \mid b_5, b_4, b_3)] - \\
&\quad [H(b_3 \mid b_5, b_4, y) + H(b_2 \mid b_5, b_4, b_3, y)] \\
&= H(b_5, b_4) - H(b_5, b_4 \mid y) + H(b_3, b_2 \mid b_5, b_4) - \\
&\quad H(b_3, b_2 \mid b_5, b_4, y) \\
&= I(b_5, b_4; y) + I(b_3, b_2; y \mid b_5, b_4) .
\end{aligned} \tag{5.28}$$

Therefore, it can be stated that:

$$I(b_3, b_2; y \mid b_5, b_4) = I(b_5, b_4, b_3, b_2; y) - I(b_5, b_4; y) , \tag{5.29}$$

where we have $C_{HM-64QAM}^{L_1,L_2} = \max\{I(b_5, b_4, b_3, b_2; y)\}$, which is the DCMC capacity of receiving both L_1 and L_2. While, $C_{HM-64QAM}^{L_1} = \max\{I(b_5, b_4; y)\}$, which is the DCMC capacity of receiving L_1 from the triple-layer HM-64QAM signal. When considering $I(b_3, b_2; y \mid b_5, b_4)$, we found that the receiving of L_2 will not totally independent from the information contained in L_1. The achievable DCMC capacity of receiving L_2 will only be approached when L_1 is perfectly received, so that we may define that the DCMC capacity of receiving L_2 to be $C_{HM-64QAM}^{L_2} = \max\{I(b_3, b_2; y \mid b_5, b_4)\}$. Hence, the DCMC capacity of the L_2 is given by:

$$C_{HM-64QAM}^{L_2} = C_{HM-64QAM}^{L_1,L_2} - C_{HM-64QAM}^{L_1} . \tag{5.30}$$

5.5.3 Channel Capacity of the SN-RN$_2$ Link

The RN_2 will retransmit the information of L_3 of the HM signal and the output of the HM-64QAM De-Mapper block in Figure 5.2 is a $N \times 64$-element probability matrix and the DCMC capacity of

transmitting the HM-64QAM symbols trough the uncorrelated Rayleigh fast fading channel may be expressed as:

$$C_{HM-64QAM} = 6 - \frac{1}{64}\sum_{i=0}^{63} E\left[\log_2 \sum_{k=0}^{63} \exp(\Phi_{i,k}) \mid x^{(i)}\right] , \tag{5.31}$$

we have $x^{(i)} \in \left\{\widetilde{\beta}\left[S_{4QAM} \pm \sqrt{2}\delta_1 e^{\pm\frac{\pi}{4}j} \pm \sqrt{2}\delta_2 e^{\pm\frac{\pi}{4}j}\right]\right\}$ and $\widetilde{\beta}$ is the normalization parameter of the HM-64QAM symbols based on the current HM ratio. The pair of bits contained in the layers L_1=(b_5b_4), L_2=(b_3b_2) and L_3=(b_1b_0), according to the chain-rule of mutual information [6, 214], we may write:

$$\begin{aligned}
&I(b_5, b_4, b_3, b_2, b_1, b_0; y) \\
&= I(b_5; y) + I(b_4; y \mid b_5) + I(b_3; y \mid b_5, b_4) + I(b_2; y \mid b_5, b_4, b_3) + \\
&\quad I(b_1; y \mid b_5, b_4, b_3, b_2) + I(b_0; y \mid b_5, b_4, b_3, b_2, b_1) \\
&= \{H(b_5) + H(b_4 \mid b_5) + H(b_3 \mid b_5, b_4) + H(b_2 \mid b_5, b_4, b_3)\} - \\
&\quad \{H(b_5 \mid y) + H(b_4 \mid b_5, y) + H(b_3 \mid b_5, b_4, y) + H(b_2 \mid b_5, b_4, b_3, y)\} + \\
&\quad \{H(b_1 \mid b_5, b_4, b_3, b_2) + H(b_0 \mid b_5, b_4, b_3, b_2, b_1)\} - \\
&\quad \{H(b_1 \mid b_5, b_4, b_3, b_2, y) + H(b_0 \mid b_5, b_4, b_3, b_2, b_1, y)\} \\
&= H(b_5, b_4, b_3, b_2) - H(b_5, b_4, b_3, b_2 \mid y) + H(b_1, b_0 \mid b_5, b_4, b_3, b_2) - \\
&\quad H(b_1, b_0 \mid b_5, b_4, b_3, b_2, y) \\
&= I(b_5, b_4, b_3, b_2; y) + I(b_1, b_0; y \mid b_5, b_4, b_3, b_2) .
\end{aligned} \tag{5.32}$$

We have $C_{HM-64QAM} = \max\{I(b_5, b_4, b_3, b_2, b_1, b_0; y)\}$ and $C_{HM-64QAM}^{L_1,L_2} = \max\{I(b_5, b_4, b_3, b_2; y)\}$, hence the DCMC capacity of receiving L_3 is $C_{HM-64QAM}^{L_3} = \max\{I(b_1, b_0; y \mid b_5, b_4, b_3, b_2)\}$, which is given by:

$$C_{HM-64QAM}^{L_3} = C_{HM-64QAM} - C_{HM-64QAM}^{L_1,L_2} . \tag{5.33}$$

5.5.4 Overall System Optimization

In our simulations, the same rate-1/2 encoder is employed by all three SN encoders. Hence we only focus our attention on the specific SNR values, where the DCMC capacity reaches 1 bps. Multiple values of the two HM ratios R_1 and R_2 had been tested. At a given HM ratio pair (R_1, R_2), the minimum receive SNR required $SNR_r^{L_1}$ for decoding the L_1 at the DN, $SNR_r^{L_2}$ of L_2 at the RN_1 and $SNR_r^{L_3}$ of L_3 at RN_2 may be computed. The SNR differences among the three layers are:

$$\mathcal{G}_{SNR}^{L_1,L_2} = SNR_r^{L_2} - SNR_r^{L_1} \text{ [dB]} , \tag{5.34}$$

$$\mathcal{G}_{SNR}^{L_1,L_3} = SNR_r^{L_3} - SNR_r^{L_1} \text{ [dB]} , \tag{5.35}$$

where, $\mathcal{G}_{SNR}^{L_1,L_j}$ is the SNR difference between $SNR_r^{L_1}$ and $SNR_r^{L_j}$, for $j \in \{2, 3\}$. If we set SNR_t^{SN} to be identical to the SNR required for receiving the information of L_1, namely to $SNR_t^{SN} = SNR_r^{L_1}$,

this would guarantee that the BER of decoding L_1 would reach an arbitrarily low value. In this situation, if we want the BER performance of receiving L_2 to become sufficiently low, the channel gain G_{SR_1} of the SN-RN$_1$ link should satisfy:

$$10\log_{10} G_{SR_1} + SNR_r^{L_1} = SNR_r^{L_2} \,. \tag{5.36}$$

If we use the distance-ratio d_{SR_1}/d_{SD} to represent the position of the RN, we arrive at:

$$\mathcal{G}_{SNR}^{L_1,L_2} = 10\log_{10}\left(\frac{d_{SD}}{d_{SR_1}}\right)^3 \,, \tag{5.37}$$

where $\mathcal{G}_{SNR}^{L_1,L_2}$ is given by Eq. (5.34) and hence we have:

$$\frac{d_{SR_1}}{d_{SD}} = 10^{-\frac{\mathcal{G}_{SNR}^{L_1,L_2}}{30}} \,. \tag{5.38}$$

Once the position of the RN is available, the path gain between the RN and DN link can be formulated as:

$$G_{R_1D} = \left(1 - \frac{d_{SR_1}}{d_{SD}}\right)^{-3} \,. \tag{5.39}$$

In the capacity analysis, we observe from Eq. (5.24) that a system employing a rate-1/2 channel coding scheme and 4QAM modulation for communication over uncorrelated Rayleigh fading channels requires $SNR_r = 1.81$ dB to reach a DCMC capacity of 1 bit per symbol. Hence the SNR$_t$ of RN$_1$ (SNR$_t^{RN_1}$) has to satisfy:

$$SNR_t^{RN_1} = 1.81 - 10\log G_{R_1D} \quad [\text{dB}] \,. \tag{5.40}$$

Similarly, the SNR$_t$ of RN$_2$ (SNR$_t^{RN_2}$) may be formulated as:

$$SNR_t^{RN_2} = 1.81 - 10\log G_{R_2D} \quad [\text{dB}] \,, \tag{5.41}$$

while the position of RN$_2$ is related to:

$$\frac{d_{SR_2}}{d_{SD}} = 10^{-\frac{\mathcal{G}_{SNR}^{L_1,L_3}}{30}} \,. \tag{5.42}$$

Likewise, the SNR$_t^{SN}$ of the SN should guarantee that:

$$SNR_t^{SN} = SNR_r^{L_1} \,. \tag{5.43}$$

Hence, the average SNR_t of the entire system is given by:

$$\overline{SNR_t} \ [\text{dB}] = 10\log_{10}\left(\frac{10^{(SNR_t^{SN}/10)} + 10^{(SNR_t^{RN_1}/10)} + 10^{(SNR_t^{RN_2}/10)}}{3}\right) \,. \tag{5.44}$$

5.5.5 DCMC Capacity Analysis Based Results

According to the analysis of Section 5.5, we investigated the performance of the cooperative communication system of Figure 5.2, when assuming that a perfect capacity-achieving channel coding scheme is employed. Figure 5.4 shows the DCMC capacity of HM-64QAM, when the HM ratio pair is ($R_1 = 1.5, R_2 = 0.6$). From Eq. (5.26), the DCMC capacity of the system transmitting HM-64QAM symbols which are received as 4QAM symbols of L_1 may be derived. By contrast, the DCMC capacity of receiving L_1 and L_2 from the HM-64QAM signal is determined by Eq. (5.27), while Eq. (5.31) formulates the DCMC capacity of receiving the HM-64QAM symbol streams. The DCMC capacity of receiving only L_2 (or L_3) information from the triple-layer HM-64QAM symbol is expressed by Eq. (5.30) (or Eq. (5.33)).

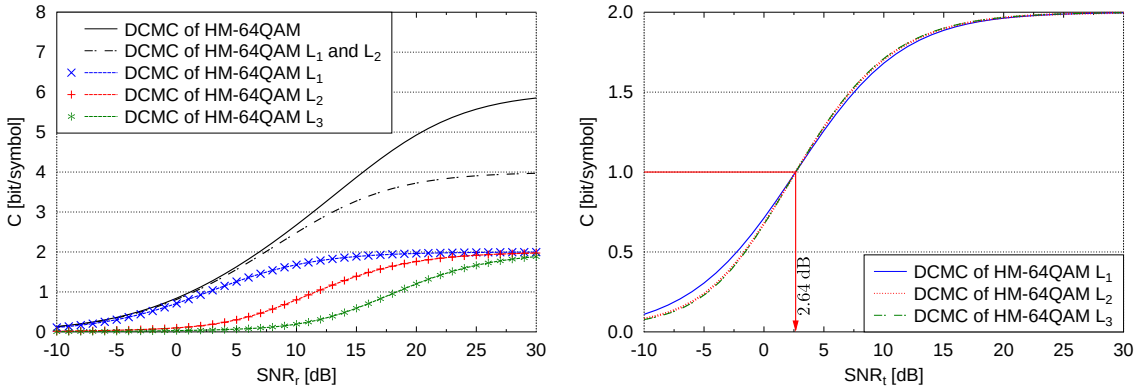

(a) The DCMC capacity versus SNR_r when receiving the triple-layer HM-64QAM signal.

(b) The DCMC capacity versus SNR_t at the SN when broadcasting the triple-layer HM-64QAM signal, where the reduced path-loss between the two SN-RNs links are considered.

Figure 5.4: DCMC capacity versus SNR for the schematic of Figure 5.2 based on the equations from Eq. (5.26) to Eq. (5.41), given the HM-64QAM ratio pair of ($R_1 = 1.5, R_2 = 0.6$). The number of samples when calculating the DCMC capacity is 10^5. The channel is an uncorrelated Rayleigh fading channel.

From the results in Figure 5.4a, the SNR_r values required for receiving the information of L_1, L_2 and L_3 from the HM symbol are 2.64 dB, 11.60 dB and 18.35 dB. Therefore, with the assistance of the two RNs, SNR_t^{SN} was reduced to 2.64 dB. Now the optimum position of the two RNs and the optimum power consumption of the HM-64QAM system using the ratio pair of ($R_1 = 1.5, R_2 = 0.6$) may be determined. From Eq. (5.34) to Eq. (5.44), the optimum position of RN_1 was formulated to be $d_{SR_1}/d_{SD} = 0.50$ and $SNR_t^{RN_1} = -7.30$ dB, while the optimum position of RN_2 is $d_{SR_2}/d_{SD} = 0.30$ and $SNR_t^{RN_2} = -2.82$ dB. Hence, we have $\overline{SNR_t} = -0.71$ dB according to Eq. (5.44). Observe from the DCMC capacity versus SNR_t^{SN} curves of Figure 5.4b that there is an intersection point among the three capacity curves of L_1, L_2 and L_3. This illustrates that with the aid of a sufficient path gain, the detection of L_2 at RN_1 and the detection of L_3 at RN_2 is achieved together with the detection of L_1 at the DN for the same $\overline{SNR_t}$ value of -0.71 dB. In order to find

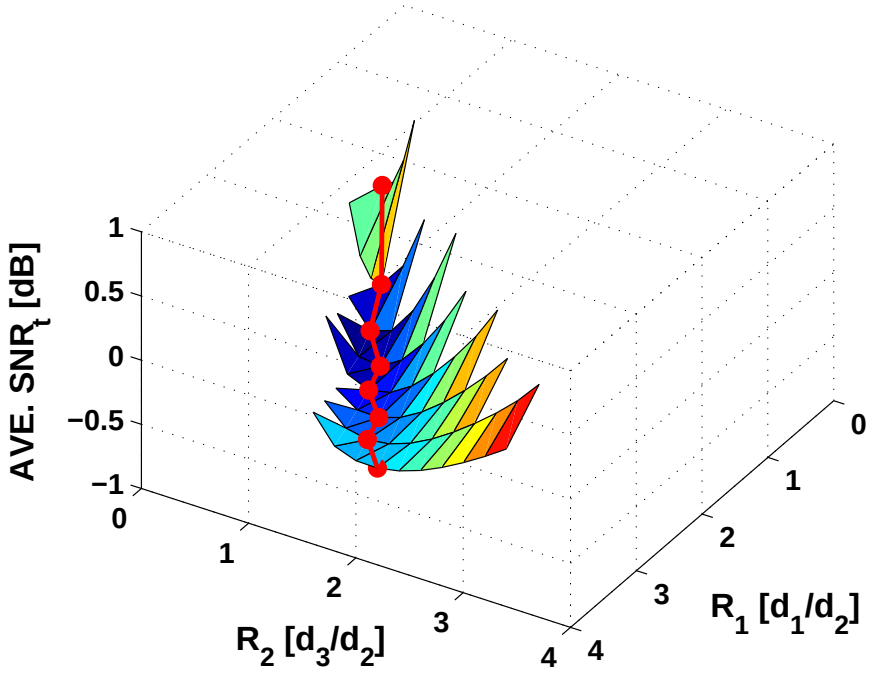

Figure 5.5: The 3D plot of the power consumption surface of the entire system shown in Figure 5.2, when perfect capacity-achieving codes are assumed to be used. Hence the system operates exactly at the DCMC capacity. The results are based on equations from Eq. (5.26) to Eq. (5.44), and the number of samples when calculating the DCMC capacity is 10^5. The channel is an uncorrelated Rayleigh fading channel and the results are summarized in Table 5.1.

the optimum HM-64QAM ratio pair, multiple groups of (R_1, R_2) have been investigated in the same way and Figure 5.5 was generated.

The resultant three-dimensional $\overline{SNR_t}$ versus (R_1, R_2) plot is shown in Figure 5.5. The doted line in the power-dissipation surface shows the minimum $\overline{SNR_t}$ based on specific value of HM-64QAM ratio pair (R_1, R_2), where the corresponding data is shown in Table 5.1. We can observe that the optimum HM-64QAM ratio pair for our cooperative system is $(R_1 = 1.5, R_2 = 0.6)$ and the minimum $\overline{SNR_t}$ of -0.71 dB is considered to be the lower performance bound of our cooperative communication system. Hence, the lower performance bound of our cooperative communication system shown in Figure 5.2 is $\overline{SNR_{t\,min}} = -0.71$ dB, while the throughput of the system is 1 bps. As mentioned, for a single link system assisted by a rate-1/2 channel coding scheme using square 4QAM mapping, which has the same throughput as our system, the SNR$_t$ required for achieving the DCMC capacity of 1 bps is about 1.81 dB. This means that in order to transmit three independent symbols frames, the system requires three TSs and the $\overline{SNR_t}$ necessitated is 1.81 dB, which is 1.81+0.71=2.52 dB higher than that of our optimized cooperative communication system.

$\mathbf{R}_1$	$\mathbf{R}_2$	$\mathbf{SNR}_r^{L_1}$ [dB]	$\mathbf{SNR}_r^{L_2}$ [dB]	$\mathbf{SNR}_r^{L_3}$ [dB]	Pos. $\mathbf{RN}_1$ [$\mathbf{d}_{SR_1}/\mathbf{d}_{SD}$]	Pos. $\mathbf{RN}_2$ [$\mathbf{d}_{SR_2}/\mathbf{d}_{SD}$]	$\overline{\mathbf{SNR}_t}$ [dB]
0.5	0.1	3.58	10.94	18.68	0.57	0.31	-0.16
1.0	0.4	2.94	10.80	18.00	0.55	0.31	-0.63
1.5	0.6	2.64	11.60	18.35	0.50	0.30	-0.71
2.0	1.0	2.38	12.50	19.82	0.46	0.26	-0.66
2.5	1.2	2.27	13.50	20.56	0.42	0.25	-0.57
3.0	1.6	2.15	14.42	21.79	0.39	0.22	-0.46
3.5	1.8	2.10	15.32	22.51	0.36	0.21	-0.35
4.0	2.2	2.04	16.13	23.49	0.34	0.19	-0.25

Table 5.1: The DCMC statistics of the average transmission power of the TTCM aided HM-64QAM cooperative schematic of Figure 5.2. The uncorrelated Rayleigh fading channel is considered, while the number of samples when calculating the DCMC capacity is 10^5. Compared to Table 5.3, the target SNR threshold for each link here is given by the SNR, when the capacity reaches 1 BPS. While the related results are shown in Figure 5.5.

5.6 TTCHM-64QAM Cooperative System Design

In Section 5.5, we have detailed the DCMC capacity analysis of our cooperative communication strategy and we have found both the minimum power consumption and the optimum RN position. In practice we do not have any control over the position of mobile relays, but the relay-selection algorithm would appoint a relay close to the optimum location. In this section, the SN will employ half-rate TTCM coding blocks, rather than assuming a perfect capacity-achieving channel code, and we will optimize this practical system. While the parameters in the simulations are shown in Table 5.2.

Coded Modulation	**TTCM**
Modulation Scheme	4QAM, HM-64QAM, SPM-16QAM
Mapper type	Set-Partitioned
Number of iterations	4
Code Rate	1/2
Code Memory	3
Code Polynomial (octal)	$H_{4QAM} = [13\ 06]$
Decoder type	Approximate Log-MAP
Symbols per frame	12,000
Number of frames	10,000
Channel	Uncorrelated Rayleigh fading channel
Path-loss exponent	3

Table 5.2: Simulation parameters of the schematic in Figure 5.2 and employed in the simulations results of Figure 5.6 to Figure 5.13.

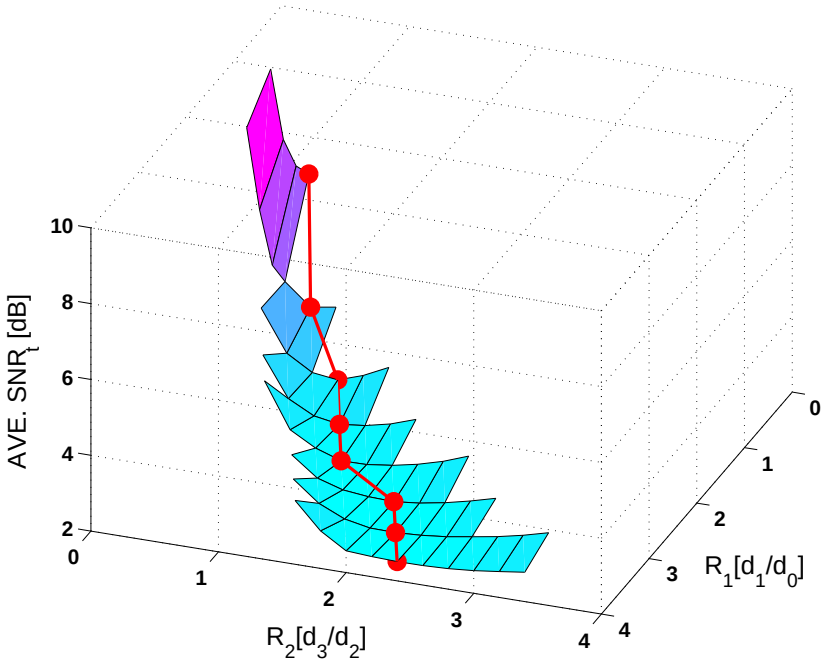

Figure 5.6: The 3D plot of the simulation based power consumption surface of the entire system of Figure 5.2. While the related parameters are shown in Table 5.2 and the related simulation results are summarized in Table 5.3.

$\mathbf{R}_1$	$\mathbf{R}_2$	$\mathbf{SNR}_r^{L_1}$ [dB]	$\mathbf{SNR}_r^{L_2}$ [dB]	$\mathbf{SNR}_r^{L_3}$ [dB]	Pos. $\mathbf{RN}_1$ $[\mathbf{d}_{SR_1}/\mathbf{d}_{SD}]$	Pos. $\mathbf{RN}_2$ $[\mathbf{d}_{SR_2}/\mathbf{d}_{SD}]$	$\overline{\mathbf{SNR}_t}$ [dB]
0.5	0.4	10.81	13.30	32.23	0.83	0.19	6.51
1.0	0.6	7.98	13.52	23.46	0.65	0.30	3.85
1.5	1.0	6.46	14.22	24.99	0.55	0.24	2.88
2.0	1.2	5.91	15.88	23.59	0.47	0.26	2.54
2.5	1.4	5.48	17.69	23.51	0.39	0.25	2.42
3.0	2.0	5.06	17.63	26.46	0.38	0.19	2.41
3.5	2.2	4.93	19.03	26.16	0.34	0.20	2.43
4.0	2.4	4.85	20.46	26.29	0.30	0.19	2.51

Table 5.3: The statistics of the average transmission power of the TTCM aided HM-64QAM cooperative schematic of Figure 5.2. The related simulation parameters are shown in Table 5.2, where the related resulted are shown in Figure 5.6. While, compare to the Table 5.1, the target SNR threshold for each link here is defined as the value, when the BER performance of the Monte-Carlo simulations reaches 10^{-6}

In order to establish a database for the system, we first simulated the BER versus SNR performance of L_1, L_2 and L_3 of the HM-64QAM scheme based on different values of the HM ratio pair (R_1, R_2). In this investigation, an uncorrelated Rayleigh fading channel is considered and a block length of 12,000 symbols is employed, while the number of turbo iterations is fixed to four. Note however that since Encoder 2 and 3 of Figure 5.2 used at the RN_1 and RN_2 are linked with a conventional 4QAM modem, $SNR_t^{RN_1}$ and $SNR_t^{RN_2}$ are given by:

$$SNR_t^{RN_1} = 4.23 - 10\log_{10} G_{R_1D} \quad [\text{dB}], \tag{5.45}$$

$$SNR_t^{RN_2} = 4.23 - 10\log_{10} G_{R_2D} \quad [\text{dB}], \tag{5.46}$$

where a SNR_r of 4.23 dB is required for achieving BER$= 10^{-6}$ for our TTCM/4QAM single link. The three dimensional $\overline{SNR_t}$ versus (R_1, R_2) is shown in Figure 5.6. while it can be observed that the minimum $\overline{SNR_t}$ is 2.41 dB when $(R_1 = 3.0, R_2 = 2.0)$, which is 2.41+0.71=3.11 dB higher than the idealistic lower bound of the system found in Section 5.5.5. The doted line in Figure 5.6 illustrates the minimum $\overline{SNR_t}$ based on specific values of (R_1, R_2). The corresponding data is shown in Table. 5.3.

5.7 Amalgamated HM and SPM for Cooperative Communications

In this section, a linear SPM scheme is employed by the two RNs for simultaneously transmitting a pair of signal frames to the DN during the second time slot (TS). Hence, two TSs are required for the transmission of all the three layers from the SN to the DN. To be more specific, the information flow of the entire system is illustrated in the block diagram shown in Figure 5.7. In our system, the SN employs three rate-1/2 4QAM-TTCM encoders and combines the three independent codeword sequences into a HM signal stream. Thus, the signal frame $\{x_1\}$ is formed by HM-64QAM symbols. When the transmit power at the source is relatively low, the DN may opt for decoding only the information from Encoder 1 during the first TS, where the information contained in the other two layers would be decoded and retransmitted by the RNs to the DN. In order to maintain a low complexity for the entire system, two RNs are activated for assisting the transmissions and each of the two RNs is used for retransmitting only one information layer of the triple-layer HM-64QAM symbols to the DN. With aid of the pre-coding and SPM schemes of Figure 5.7, the two RNs become capable of transmitting simultaneously. Hence, the system now needs two TSs to complete its transmissions between the SN and DN. More specifically, each RN will only deal with a single layer of the triple-layer HM-64QAM scheme, hence the signal frames they transmit are all 4QAM frames. In this way, both the processing complexity of the entire system and the transmit power of the RN remains moderate.

It can be observed that the transmission during the first TS of the cooperative schematic shown in Figure 5.7 is the same as that shown in Figure 5.2. During the second transmission TS, the schematic in Figure 5.7 employs twin-SPM for transmitting the information of L_2 and L_3 simultaneously from the two separate RNs, which has a similar structure of the system in Figure 3.1 of

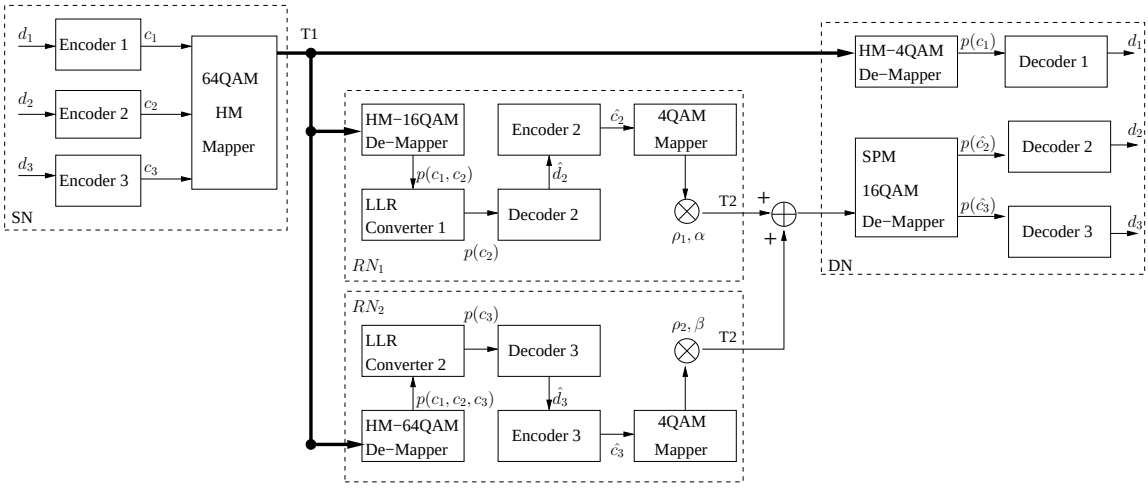

Figure 5.7: The system diagram of a twin-relay HM and SPM aided cooperative system.

Chapter 3. However, the schematic of Figure 3.1 employs single RN, and the SPM based signal formed by the two independent signal sequences will be sent to DN only by the single RN during the second TS. In the schematic of Figure 5.7, twin-RN relaying is employed, where both RNs may contain a single layer information. Hence, the SPM weighting factor pair (α, β) then will be deployed to the two RNs separately. Additionally, in order to help the DN detect the two signal sequences, the two RNs also needs to compensate the channel fading during their transmission. Therefore, the detection of the SPM based signal of the system of Figure 5.7 will turn out to be better than that of the schematic of Figure 3.1, because the channel fading is not compensated by the RN in the schematic of Figure 3.1.

We have to mention however that the system proposed in Figure 5.7 requires further research, since we exploited the idealized simplifying assumption that the two RNs not only have reliable information on the success or failure of correct reception at each nodes in the system, but also have accurate CSI. Practically, finding a pair of appropriate RNs among the candidates in the right location and arrange for them to operate collaboratively will require substantial information exchange across the entire networks, especially when the size of the cooperative network is large. Nonetheless, before the second TS's transmission, the two RNs and the DN also have to inform each other when the corresponding information will be transmitted as well as of the associated SPM weight. The DN may also have to synchronise both the time slot and the carrier phases of the signal sequences of the pair of RNs at different distances. In our investigations in this section, we will construct a four-node system and assume that each node of the network will have the required information concerning the entire network and that the transmissions during the second TS will not be influenced by synchronisation problems. We focus our attention on the performance of an idealized strategy and will consider a realistic system model by gradually eliminating our idealized simplifying assumptions in our future work.

5.7.1 Pre-processed Linear SPM

By employing the SPM [78] scheme at the two RNs in the networks, the symbols received at the DN during the second TS, which are sent by the two RNs, may be expressed as:

$$y_{RD} = \rho_1 \alpha \sqrt{G_{R_1D}} h_{R_1D} x_2 + \rho_2 \beta \sqrt{G_{R_2D}} h_{R_2D} x_3 + n_{RD} \,, \tag{5.47}$$

where ρ_1 and ρ_2 are the pre-coding parameters and (α, β) is the SPM ratio pair. The assumption is that every node in the cooperative network has perfect CSI. Hence, given a specific path-loss and a RN position, we may both compensate the effect of the path-loss as well as that of the Rayleigh fading with the aid of transmit pre-coding. Specifically, the ρ_1 and ρ_2 pre-coding parameters should satisfy:

$$\rho_1 = \frac{h^*_{R_1D}}{|\, h_{R_1D} \,|^2 \sqrt{G_{R_1D}}} \,, \tag{5.48}$$

$$\rho_2 = \frac{h^*_{R_2D}}{|\, h_{R_2D} \,|^2 \sqrt{G_{R_2D}}} \,. \tag{5.49}$$

Hence, during the second TS, the signal received by the DN may be written as:

$$y_{RD} = \alpha x_2 + \beta x_3 + n_{RD} \,, \tag{5.50}$$

where we observe from Eq. (5.50) that the reception of the signal at the DN is identical to that of detecting a twin-layer linear SPM signal received over AWGN channels. Note that the performance of a specific modulation scheme in the AWGN channel is directly determined by the Euclidean distance among the constellation points. The relationship between α and β is given by [78]:

$$\alpha^2 + \beta^2 = 1 \,. \tag{5.51}$$

If we only focus our attention on the relationship between the Euclidean distance d_{min} and α, we have:

$$d_{min} = \begin{cases} \frac{1}{\sqrt{2}} \min\left(2\sqrt{1-\alpha^2}, 2\left(\alpha - \sqrt{1-\alpha^2}\right)\right) & \left(\alpha \geq \sqrt{1/2}\right) \\ \frac{1}{\sqrt{2}} \min\left(2\alpha, 2\left(\sqrt{1-\alpha^2} - \alpha\right)\right) & \left(\alpha < \sqrt{1/2}\right) \,. \end{cases} \tag{5.52}$$

Theoretically the largest Euclidean distance is achieved, when α is $\sqrt{1/5}$ or $\sqrt{4/5}$. Hence, we anticipate that the best performance of an uncoded twin-layer linear SPM scheme would appear when α equals to $\sqrt{1/5}$ or $\sqrt{4/5}$. However, when TTCM is used, it depends on d_{min} of the entire TTCM set partitioning scheme [6].

5.7.2 SPM Aided Triple-layer TTCHM-64QAM Cooperative System Design

In practice we do not have any control over the position of mobile relays, but the relay-selection algorithm would appoint a relay close to the optimum location. In this section, we will optimize this practical system regarding the position of the RN, as well as the HM ratio pair (R_1, R_2) and the SPM weighting pair (α, β). Additionally, in this investigation, the simulations are carried out

by IT++ and the number of iterations of our rate-1/2 TTCM decoder is $\zeta = 4$, the block size is $\eta = 12,000$ symbols. Using a large number of iterations allows the TTCM decoder to more closely approach capacity and a large block length assists in avoiding error propagation, but also imposes an increased complexity. In the simulations, we observed that no substantial BER performance improvement is achieved for more than four iterations ($\zeta > 4$) or for a block size of $\eta > 12,000$ symbols.

A. An Optimum SPM Ratio

In our simulations, the pair of signal sequences received from RN_1 and RN_2 will be multiplied by a specific SPM ratio α or β and be received by the DN simultaneously. Here, we only focus our attention on the performance of receiving a single signal sequence having a SPM ratio α in the simulations and the related results are shown in Figure 5.8a and Figure 5.8b.

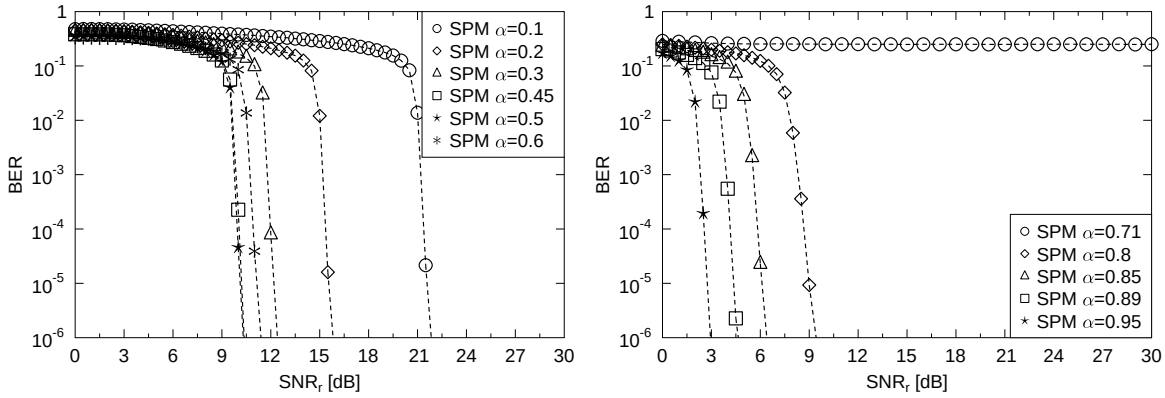

(a) $\alpha < \sqrt{1/2}$ (b) $\alpha > \sqrt{1/2}$

Figure 5.8: The BER versus SNR performance of the TTCM aided twin-layer SPM scheme for the transmission between the RNs and DN of the schematic of Figure 5.7. Both of the two signal sequences are encoded by rate-1/2 TTCM encoder. The performance of a single signal sequence is studied when using $\alpha = \{0.1, 0.2, 0.3, 0.45, 0.5, 0.6, 0.71, 0.8, 0.85, 0.95\}$. The parameters in the simulations are shown in Table 5.2.

From the combined signal sequences, we set the signal associated with a larger SPM ratio α to be the dominant signal and the signal with a smaller SPM ratio β to be the auxiliary signal. Based on the simulation results of Figure 5.8a and Figure 5.8b, we may observe that as expected, for the dominant signal, a larger SPM ratio would result in a better BER performance. However, for the auxiliary signal, the best BER performance appears at the SPM ratio of 0.45 ($\sqrt{1/5} \approx 0.45$) or 0.5. We have found from our simulations the SNR_r value required for achieving BER=10^{-6} for different values of the SPM ratio α, as shown in Figure 5.9. Note that 0.7071 ($\sqrt{1/2} \approx 0.7071$) is a bound, where we have $\alpha = \beta = \sqrt{1/2}$, which would collapse the 16-point constellation to a 9-point constellation making unambiguous decoding to be impossible. Figure 5.9 shows that when

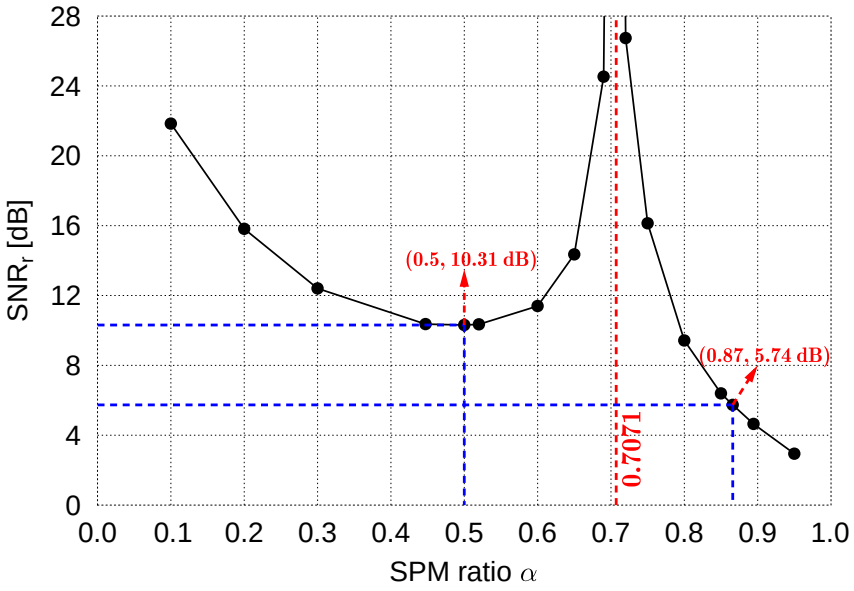

Figure 5.9: The SNR$_r$ versus SPM ratio performance of the TTCM aided twin-layer SPM scheme for the transmission between the RNs and DN of the schematic of Figure 5.7. Both of the two signal sequences are encoded by rate-1/2 TTCM encoder. The performance of a single signal sequence is studied when using $\alpha = \{0.1, 0.2, 0.3, 0.45, 0.5, 0.6, 0.71, 0.8, 0.85, 0.95\}$, while the SNR$_r$ threshold here is defined as the value, when the BER performance of the Monte-Carlo simulations reaches 10^{-6}. The parameters in the simulations are shown in Table 5.2.

$\alpha = 0.5$, the SNR$_r$ required for receiving the auxiliary signal from the SPM-16QAM signal is about 10.31 dB which is the lowest value of receiving the auxiliary signal. Meanwhile, when $\alpha = 0.5$, the corresponding SPM ratio β will be $\sqrt{1-\alpha^2} \approx 0.87$, and the SNR$_r$ required for receiving the dominant signal from the SPM-16QAM signal using $\beta = 0.87$ is about 5.74 dB. Hence, based on the results of Figure 5.9, we find that the optimum SPM ratio pair is $(\alpha = 0.87, \beta = 0.5)$ (we assume $\alpha > \beta$ in this treatise). In this combination, the SNR$_r$ required for receiving the two signal sequences is the lowest. Consequently, the SNR$_t$ required at the two RNs would also be the lowest at the given RN positions.

B. SNR$_t$ of the two RNs

In order to evaluate the power-efficiency of our cooperative communications scheme, we have to calculate the average SNR$_t$ ($\overline{SNR_t}$) defined as the SNR$_t$ per TS. Based on the statistics seen in Figure 5.9, we opted for the SPM ratio pair of $(\alpha = 0.87, \beta = 0.5)$ and hence we have $\text{SNR}_r^{DN} =$ 10.31 dB. Next, we have to find the relationship among $\text{SNR}_t^{RN_1}$, $\text{SNR}_t^{RN_2}$ and SNR_r^{DN}. Let us denote the SNR by γ, which is expressed as $10\log_{10}(\gamma)$ in dB. Furthermore, since L_2 of the triple-layer HM-64QAM symbols has a higher priority than that of L_3, the signal frame $\{x_2\}$ transmitted from RN$_1$ will be multiplied by a higher SPM weighting factor of $\alpha = 0.87$, while another SPM

weighting factor of $\beta = 0.5$ is used for the signal frame $\{x_3\}$ at RN_2. Hence we have:

$$E\left[\gamma_t^{RN_1}\right] = E\left[\frac{|\ \alpha\rho_1 x_2\ |^2}{N_0}\right] , \tag{5.53}$$

where

$$E\left[|\ x_2\ |^2\right] = 1\,. \tag{5.54}$$

Therefore, it can be observed that:

$$\begin{aligned} E\left[\gamma_t^{RN_1}\right] =& E\left[\frac{\alpha^2|\rho_1|^2}{N_0}\right] \\ =& \alpha^2 E\left[\frac{|\ h_{R_1D}^*\ |^2}{|\ h_{R_1D}\ |^4\ G_{R_1D}N_0}\right] \\ =& \frac{\alpha^2}{G_{R_1D}N_0} E\left[\frac{1}{|h_{R_1D}|^2}\right] , \end{aligned} \tag{5.55}$$

where h obeys the Rayleigh distribution of [1]:

$$f(h) = \frac{2h}{\Omega}\exp\left(-\frac{h^2}{\Omega}\right) . \tag{5.56}$$

Note that the mean square value of h is given by $\Omega = 1$, Let $Z = |h|^2$, then the distribution of the variable Z may be expressed as [1]:

$$f_Z(z) = \frac{1}{\Omega}\exp\left(-\frac{z}{\Omega}\right) . \tag{5.57}$$

Let us denote the Cumulative Distribution Function (CDF) as $F_Z(\Gamma) = \Pr(Z < \Gamma)$, which can be expressed as:

$$F_Z(\Gamma) = \Pr(Z < \Gamma) = 1 - \exp\left(-\frac{\Gamma}{\Omega}\right) , \tag{5.58}$$

where Pr denotes probability. Upon introducing $\Gamma' = 1/\Gamma$, we may further express Eq. (5.58) as:

$$\Pr(Z < \Gamma) = \Pr\left(\frac{1}{Z} > \frac{1}{\Gamma}\right) = 1 - \Pr\left(\frac{1}{Z} < \Gamma'\right) . \tag{5.59}$$

Hence, it can be observed that:

$$\Pr\left(\frac{1}{Z} < \Gamma'\right) = \exp\left(-\frac{1}{\Omega\Gamma'}\right) . \tag{5.60}$$

If we let $\Theta = \frac{1}{Z}$, the PDF of the variable Θ may be expressed as [222]:

$$f_\Theta(\theta) = \frac{1}{\Omega\theta^2}\exp\left(-\frac{1}{\Omega\theta}\right) . \tag{5.61}$$

Therefore, the expectation $E\left[\frac{1}{|h|^2}\right]$ may be derived as:

$$E\left[\frac{1}{|h|^2}\right] = \int_{\Theta_{low}}^{\Theta_{up}} \frac{\Theta}{\Omega\Theta^2}\exp(-\frac{1}{\Omega\Theta})\mathrm{d}\Theta\,, \tag{5.62}$$

where Θ_{low} and Θ_{up} are the lower and upper limits of the integration. Let us define $\xi = \frac{1}{\Theta}$, then Eq. (5.62) may be converted to:

$$-\frac{1}{\Omega}\int_{1/\Theta_{up}}^{1/\Theta_{low}} \frac{1}{\xi}\exp\left(-\frac{\xi}{\Omega}\right)\mathrm{d}\xi = \frac{1}{\Omega}\left[E_i\left(\frac{-1}{\Omega\Theta_{up}}\right) - E_i\left(\frac{-1}{\Omega\Theta_{low}}\right)\right] , \tag{5.63}$$

where E_i is the Euler function:

$$E_i(u) = \int_{-u}^{\infty} \frac{e^{-t}}{t} \mathrm{d}t \,. \tag{5.64}$$

Theoretically, we have $|h| \in [0, +\infty)$, which gives us $\Theta_{low} = 0$ and $\Theta_{up} = +\infty$. When $\Theta_{low} = 0$, we may have $E_i\left(\frac{-1}{\Omega\Theta_{low}}\right) = 0$. However, if $\Theta_{up} = +\infty$, the term $E_i\left(\frac{-1}{\Omega\Theta_{up}}\right)$ becomes infinite and we are unable to derive the value of $E\left[1/|h|^2\right]$. To resolve this dilemma, we defined an outage threshold, which is given by $[|h|^2]_{\min} = 0.03$, as discussed in [223]. According to Eq. (5.57), the probability of $\Pr(|h|^2 \geqslant 0.03) \approx 0.97$ indicates that our system will curtail its transmissions, when the fading obeys $|h|^2 < 0.03$. Hence, we may have $\frac{1}{\Theta_{up}} = [|h|^2]_{\min} = 0.03$. In this situation, we have $E\left[1/|h|^2\right] = 2.96$. Hence, Eq. (5.55) may be expressed as:

$$E\left[\gamma_t^{RN_1}\right] = \frac{2.96\alpha^2}{G_{R_1D}N_0} \,. \tag{5.65}$$

Note that this assumption will lead to a 3% throughput reduction for the entire system. Additionally, we have:

$$E\left[\gamma_r^{DN}\right] = E\left[\frac{|\, \alpha x_2 + \beta x_3 \,|^2}{N_0}\right] = \frac{1}{N_0} \,. \tag{5.66}$$

Therefore, we find that:

$$E\left[\gamma_t^{RN_1}\right] = \frac{2.96\alpha^2}{G_{R_1D}} E\left[\gamma_r^{DN}\right] \,, \tag{5.67}$$

which may be expressed in dB as:

$$E\left[SNR_t^{RN_1}\right] = E\left[SNR_r^{DN}\right] + 10\log_{10}\left(\frac{2.96\alpha^2}{G_{R_1D}}\right) \,. \tag{5.68}$$

Similarly, the relationship between $SNR_t^{RN_2}$ and SNR_r^{DN} may be formulated as:

$$E\left[SNR_t^{RN_2}\right] = E\left[SNR_r^{DN}\right] + 10\log_{10}\left(\frac{2.96\beta^2}{G_{R_2D}}\right) \,. \tag{5.69}$$

Finally, $\overline{SNR_t}$ may be expressed as:

$$\overline{SNR_t} = 10\log_{10}\left(\overline{\gamma_t}\right) = 10\log_{10}\left(\frac{\gamma_t^{SN} + \gamma_t^{RN_1} + \gamma_t^{RN_2}}{2}\right) \,. \tag{5.70}$$

5.7.3 Simulation Results

Based on the discussions in Section 5.7, we characterized our cooperative communications system for multiple values of the HM ratio pairs (R_1, R_2) for the sake of generating the power dissipation surface of the cooperative system, which is shown in Figure 5.10.

Explicitly, 64 pairs of (R_1, R_2) have been simulated, where R_1 is chosen from $\{0.5, 1.0, 1.5, 2.0, 2.5, 3.0, 3.5, 4.0\}$ and for each R_1, multiple R_2 values were selected based on the constraints illustrated in Section 5.3. Given a specific HM ratio pair (R_1, R_2), the receive SNR required for adequately receiving L_1, L_2 and L_3, namely $\mathrm{SNR}_r^{L_1}$, $\mathrm{SNR}_r^{L_2}$ and $\mathrm{SNR}_r^{L_3}$ respectively, may be derived for a target BER of 10^{-6}. More specifically, the optimum position of the two RNs and the optimum

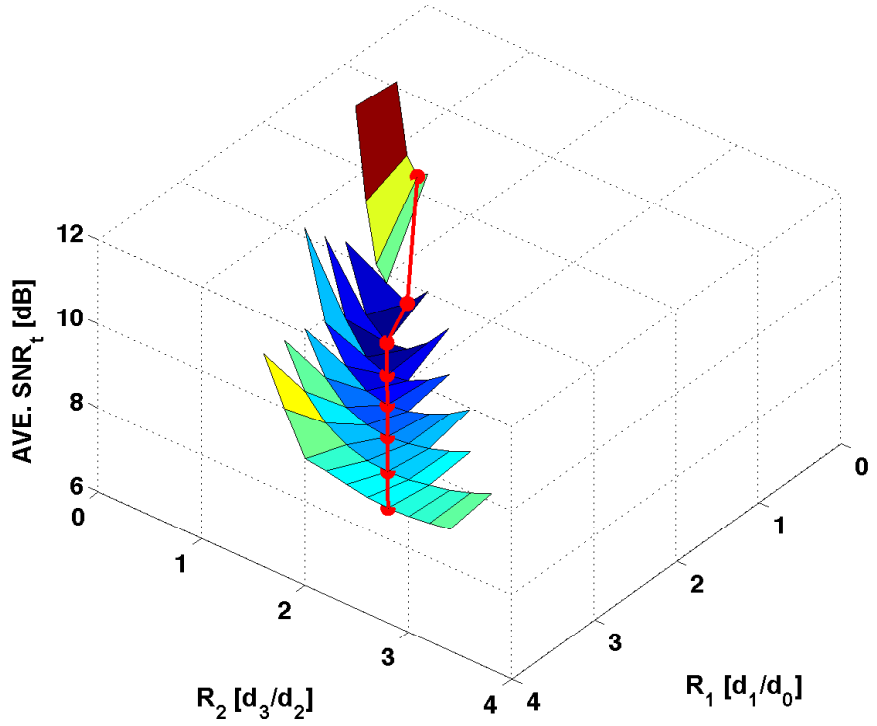

Figure 5.10: The 3D plot of the simulation-based average transmit power dissipation surface of the entire cooperative system of Figure 5.7 versus the HM-64QAM ratio pair (R_1, R_2). The two RNs employ SPM schemes associated with the SPM weighting pair of $(\alpha = 0.87, \beta = 0.5)$. While, the parameters in the simulations are shown in Table 5.2 and the simulation results are summarized in Table 5.4.

average transmit SNR ($\overline{SNR_t}$) of the entire system may be calculated according to $\text{SNR}_r^{L_1}$, $\text{SNR}_r^{L_2}$ and $\text{SNR}_r^{L_3}$ based on the discussions in Section 5.4 and Section 5.6. Hence, we can compute the optimum $\overline{SNR_t}$ for each of the HM ratio pairs (R_1, R_2), as shown in Figure 5.10. The bold line marked by dots in Figure 5.10 illustrates the lowest power consumption point for a specific HM ratio pair (R_1, R_2) and the corresponding data is recorded in Table 5.4.

It can be observed from the results of Figure 5.10, that the best performance of our cooperative communication system obeying this arrangement is achieved, when the HM ratio pair is given by $(R_1 = 1.5, R_2 = 0.8)$ and the SPM weighting factor pair is $(\alpha = 0.87, \beta = 0.5)$. The optimum $\overline{SNR_t}$ per TS is 6.94 dB, where in this situation, the positions of RN_1 and RN_2 are $d_{SR_1}/d_{SD} = 0.53$ and $d_{SR_2}/d_{SD} = 0.31$, where SNR_t^{SN} is 6.81 dB, $\text{SNR}_t^{RN_1}$ is 4.01 dB and $\text{SNR}_t^{RN_2}$ is 4.08 dB, as shown in Table 5.4. The throughput per TS for this scheme is $3/2 \times 0.97 = 1.455$ bps owing to the 3% throughput reduction imposed by the threshold of $[|h|^2]_{min} = 0.03$.

A. EXIT Chart Analysis

The Extrinsic Information Transfer (EXIT) chart is capable of visualizing the input/output characteristics of the constituent MAP decoders in terms of the achievable average mutual information

$\mathbf{R}_1$	$\mathbf{R}_2$	**Pos. RN**$_1$ [$\mathbf{d}_{SR_1}/\mathbf{d}_{SD}$]	**Pos. RN**$_2$ [$\mathbf{d}_{SR_2}/\mathbf{d}_{SD}$]	$\mathbf{SNR}_t^{SN}$ [**dB**]	$\mathbf{SNR}_t^{RN_1}$ [**dB**]	$\mathbf{SNR}_t^{RN_2}$ [**dB**]	$\overline{\mathbf{SNR}_t}$ [**dB**]
0.5	0.3	0.82	0.33	11.18	-8.81	3.88	8.94
1.0	0.6	0.65	0.30	7.98	-0.04	4.27	6.96
1.5	0.8	0.53	0.31	6.81	4.01	4.08	**6.94**
2.0	1.2	0.47	0.26	5.91	5.61	5.12	7.32
2.5	1.6	0.42	0.22	5.42	6.71	5.76	7.76
3.0	2.0	0.38	0.19	5.06	7.52	6.20	8.14
3.5	2.4	0.35	0.17	4.91	8.10	6.50	8.46
4.0	2.8	0.33	0.16	4.79	8.58	6.73	8.74

Table 5.4: The average transmission power $\overline{SNR_t}$ per TS of the HM-64QAM and SPM based cooperative system of Figure 5.7. The SPM weighting pair is ($\alpha = 0.87, \beta = 0.5$) and the simulation parameters are shown in Table 5.2. The target SNR threshold here is defined as the value, when the BER performance of the Monte-Carlo simulations reaches 10^{-6}. While the related simulation results are shown in Figure 5.10.

transfer [193, 195]. It may be used for predicting whether a soft decision based decoder is capable of decoding the information with an arbitrarily low BER based on the available mutual information provided by the symbol-to-bit demapper. Since we do not invoke iterations between the demapper and the TTCM decoder in our symbol-based scheme, we need a sufficiently high receive SNR$_r$ for guaranteeing that the mutual information gleaned from the demapper is sufficiently high for the decoder to attain a low BER. More specifically, the EXIT curves of the HM-64QAM and SPM-16QAM demappers are illustrated in Figure 5.11.

In Figure 5.11, the notation 'Inner' iteration represents the information exchange between the demapper and decoder, while 'Outer' iteration refers to the information exchange between the two components of the TTCM decoder. Since there are no iterations between the demapper and the TTCM decoder, we may observe in Figure 5.11 that the inner curve is a straight line. Specifically, the inner curve shows the mutual information received by the decoder from the demapper, which is increased upon increasing the receive SNR. In order to guarantee that the decoder becomes capable of decoding the information with an arbitrarily low BER, an open EXIT chart tunnel has to be maintained between the 'Inner' and 'Outer' curves all the way to the $(x, y) = (2, y)$ point, where we have $x = I_A^{(i)} = I_E^{(o)}$ and $y = I_E^{(i)} = I_A^{(o)}$. Note that the subscript i and o denote 'Inner' and 'Outer' respectively, whilst I_A and I_E denote the *a priori* and *extrinsic* information. When the HM-64QAM ratio pair is ($R_1 = 1.5, R_2 = 0.8$) and the number of TTCM iterations is $\zeta = 4$, the receive SNR required for achieving a BER of 10^{-6} for each HM layer is: $\text{SNR}_r^{L_1} = 6.81$ dB, $\text{SNR}_r^{L_2} = 15.15$ dB and $\text{SNR}_r^{L_3} = 21.87$ dB. It also can be observed in Figure 5.11 that there are open tunnels between the three 'Inner' curves upon receiving triple-layer HM symbols and the ζ =4-iteration 'Outer' curve. Note that the 'Inner' curve of receiving L_3 of the HM scheme is closer to the 'Outer' curve compared to the other two 'Inner' curves of receiving L_1 and L_2. When L_1 of the HM scheme is detected at the DN, each HM-64QAM symbol received will be detected

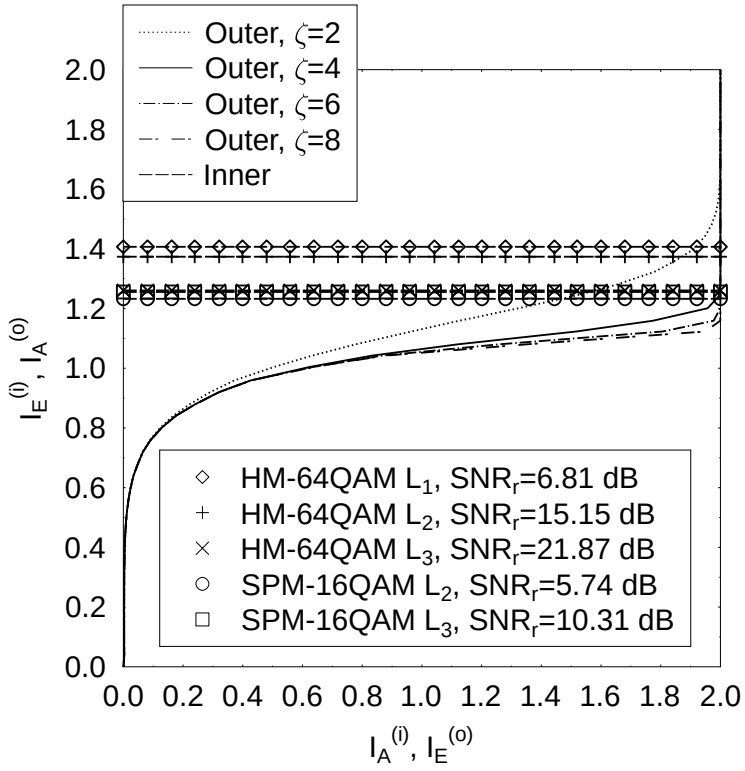

Figure 5.11: The symbol based EXIT chart of our rate-1/2 TTCM aided triple-layer HM-64QAM scheme and twin-layer SPM-16QAM scheme in schematic of Figure 5.7. The number of iterations for the rate-1/2 TTCM decoder is given by $\zeta \in \{2,4,6,8\}$. The HM-64QAM ratio pair is $(R_1 = 1.5, R_2 = 0.8)$ and the SPM weighting coefficient pair is $(\alpha = 0.87, \beta = 0.5)$. The SNR_r threshold defined as the value when the Monte-Carlo simulations reaches 10^{-6} for the target scheme/link. The related simulation parameters are shown in Table 5.2.

as a 4QAM symbol. Similarly, L_2 of the HM scheme will be detected in the form of 16QAM symbols at RN_1. This HM-specific simplifying demapping assumption shifts the 'Inner' curves corresponding to L_1 and L_2 upwards to higher values than the 'Inner' curve recorded for receiving L_3. Hence, we infer that we can reduce the SNR required for receiving L_1 and L_2 to let the two 'Inner' curves to be closer to the ζ =4-iteration based 'Outer' curve. However, according to the simulations, even though there might be an open EXIT tunnel, the integrity of L_1 and L_2 will be degraded, if we reduce the SNR_r.

Additionally, the 'Inner' curves associated with receiving the pre-coding based twin-layer SPM-16QAM scheme are also shown in Figure 5.11. In the simulations, the L_2 and L_3 of the triple-layer HM-64QAM will be mapped to base layer and auxiliary layer of the SPM symbols, respectively. It can be observed in Figure 5.11 that the SNR_r required for achieving a BER of 10^{-6} for both layers of our twin-layer SPM scheme can provide open tunnels between the two 'Inner' curves and the ζ =4-iteration 'Outer' curve. Moreover, both 'Inner' curves are very close to the ζ =4-iteration 'Outer' curve, since the DN fully detects the SPM-16QAM symbols for the sake of receiving the

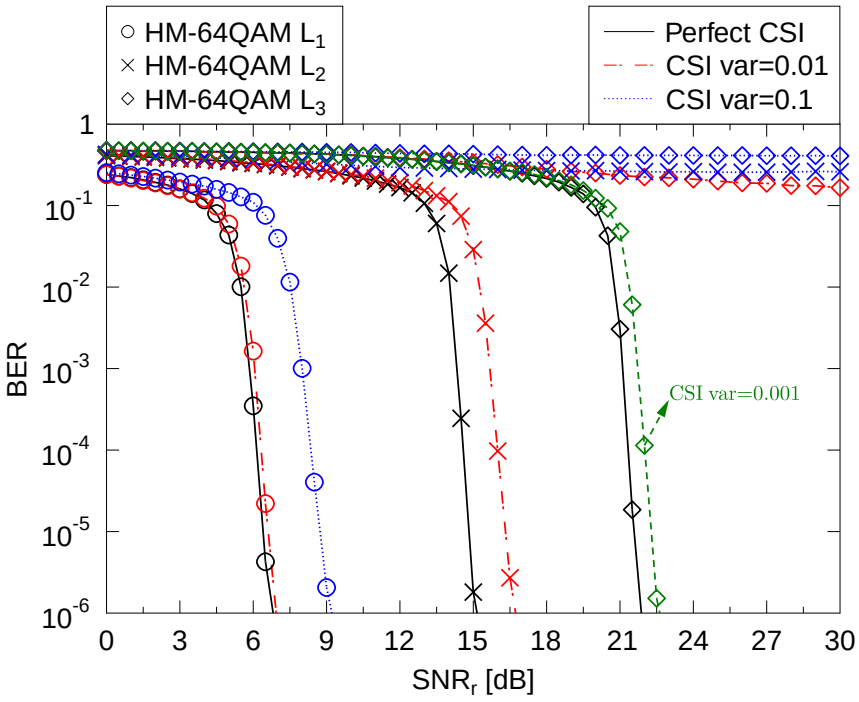

Figure 5.12: BER versus SNR performance of the TTCM aided triple-layer HM-64QAM scheme for the transmission between the SN and RNs of the schematics of Figure 5.2 and Figure 5.7 with imperfect CSI, where the HM-64QAM ratio pair is $(R_1 = 1.5, R_2 = 0.8)$. Explicitly, simulation parameters are shown in Table 5.2 and the simulation results are summarized in Table 5.5.

soft-information of L_2 and L_3. We have investigated the optimum number of iterations for the TTCM decoder. It can be observed from Figure 5.11 that increasing ζ beyond 4 only gives us a marginal gain, while significantly increasing the decoding complexity. Hence we have opted for $\zeta = 4$ for our design.

B. Imperfect CSI for Receiving Triple-layer HM and Pre-coding Based Twin-layer SPM

When considering the impact of imperfect CSI at all nodes in cooperative communications, the performance of our coherent scheme is expected to be degraded. To investigate the robustness of our triple-layer coded HM-64QAM and pre-coding based twin-layer coded SPM-16QAM schemes, we model the CSI estimation errors by a Gaussian process superimposed on each channel coefficient at the two RNs and DN, where the CSI estimation error variance is denoted by $\widetilde{\sigma}$.

The BER performance of receiving triple-layer coded HM-64QAM recorded for diverse CSI estimation error variances $\widetilde{\sigma}$ is shown in Figure 5.12. We can observe that a CSI estimation error of $\widetilde{\sigma} = 0.01$ only slightly impedes the performance of receiving L_1, but will cause a 2 dB SNR degradation (at a BER of 10^{-6}) for receiving L_2. However, the system excessively degrades L_3 for $\widetilde{\sigma} = 0.01$. By contrast, a CSI estimation error of $\widetilde{\sigma} = 0.1$ would impose a 5 dB SNR degradation on the performance of L_1, whilst the cooperative communication system will have been completely lost for L_2 and L_3 in this situation. It is shown in Figure 5.12 that a CSI estimation error variance

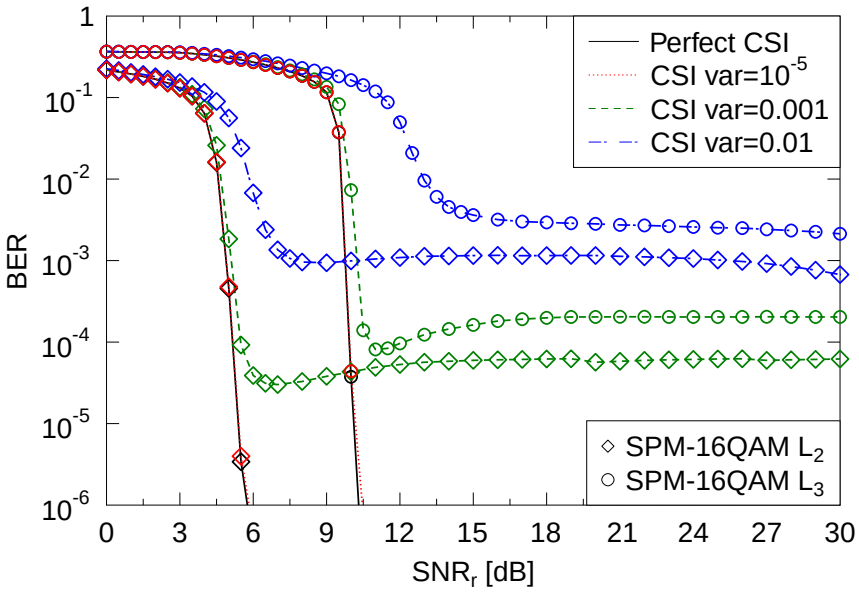

Figure 5.13: BER versus SNR performance of the twin-layer coded SPM-16QAM scheme for the transmission between the RNs and DN of the schematic of Figure 5.7 with imperfect CSI. The SPM-16QAM weighting pair is $(\alpha = 0.87, \beta = 0.5)$. Explicitly, the simulation parameters are shown in Table 5.2 and the simulation results are summarized in Table 5.5.

below $\widetilde{\sigma} = 0.001$ is required for receiving L_3. Hence, we find that the robustness of each layer in the HM-64QAM symbols against imperfect CSI is different, where L_1 is the most robust layer, while L_3 has the highest sensitivity to CSI errors.

The performance of our pre-coding based coded SPM scheme associated with CSI estimation errors are shown in Figure 5.13. If there is CSI estimation error for the R_1N (R_2N) and the DN link, the resultant ρ_1 in Eq. (5.48) and ρ_2 in Eq. (5.49) become:

$$\rho_1 = \frac{\widetilde{h}^*_{R_1D}}{|\widetilde{h}^*_{R_1D}|^2 \sqrt{G_{R_1D}}}, \tag{5.71}$$

$$\rho_2 = \frac{\widetilde{h}^*_{R_2D}}{|\widetilde{h}^*_{R_2D}|^2 \sqrt{G_{R_2D}}}. \tag{5.72}$$

Hence, the pre-coding based twin-layer coded SPM-16QAM symbols received by the DN during the second TS is expressed as:

$$y_{RD} = \frac{\alpha \widetilde{h}^*_{R_1D} h_{R_1D}}{|\widetilde{h}^*_{R_1D}|^2} x_2 + \frac{\beta \widetilde{h}^*_{R_2D} h_{R_2D}}{|\widetilde{h}^*_{R_2D}|^2} x_3 + n_{RD}. \tag{5.73}$$

More specifically, we have:

$$\widetilde{h}_{R_1D} = h_{R_1D} + \Delta_1, \tag{5.74}$$

$$\widetilde{h}_{R_2D} = h_{R_2D} + \Delta_2, \tag{5.75}$$

where Δ_1 is the CSI estimation error imposed on h_{R_1D}, and Δ_2 is the CSI error contaminating h_{R_2D}. In order to simplify our discussions, we assume that both Δ_1 and Δ_2 obey the Gaussian distribution

		Required SNR$_r$ (dB) at BER of 10^{-6}				
CSI error		$\widetilde{\sigma}=0$	$\widetilde{\sigma}=10^{-1}$	$\widetilde{\sigma}=10^{-2}$	$\widetilde{\sigma}=10^{-3}$	$\widetilde{\sigma}=10^{-5}$
Triple-layer	L_1	6.81	9.22	6.94	6.86	6.83
HM-64QAM	L_2	15.15	error-floor	16.73	15.31	15.19
	L_3	21.87	error-floor	error-floor	22.63	21.94
Twin-layer	L_2	5.74	error-floor	error-floor	error-floor	5.83
SPM-16QAM	L_3	10.31	error-floor	error-floor	error-floor	10.46

Table 5.5: The SNR threshold of the cooperative schematic shown in Figure 5.7. These values are tabulated from Figure 5.12 and Figure 5.13. While the related simulation parameters are shown in Table 5.2.

with zero mean and a variance of $\widetilde{\sigma}_1=\widetilde{\sigma}_2=\widetilde{\sigma}$. It can be seen from Figure 5.13 that our pre-coding based twin-layer coded SPM-16QAM scheme is sensitive to the CSI estimation errors. Explicitly, an error floor around BER of 10^{-4} exists for the detection of L_2 and L_3 of the twin-layer SPM scheme when $\widetilde{\sigma}=0.001$. Upon increasing the CSI estimation error variance $\widetilde{\sigma}$, the performance of the pre-coding based coded SPM scheme will be dramatically reduced. The error floor will be eliminated at BER of 10^{-6} by employing sophisticated channel estimation schemes, which could reduce $\widetilde{\sigma}$ below a level of 10^{-5}, as shown in Figure 5.13. The statistics shown in Figure 5.12 and Figure 5.13 are summarized in Table 5.5.

C. Comparisons to Other Systems

Figure 5.14 compares our rate-1/2 TTCM aided triple-layer HM-64QAM scheme to that of the same system relying on a rate-1/2 LDPC code [15]. In order to reveal the different performances of a bit-based LDPC code and of the symbol-based TTCM scheme. It can be observed that the bit-based LDPC scheme performs slightly worse than the symbol based TTCM scheme, even though the number of LDPC decoder iterations is much higher than that of the TTCM decoder, indicating that symbol-based scheme has a lower convergence SNR than an equivalent bit-based scheme, as detailed in [216].

The BER performance curves of the non-cooperative conventional rate-1/2, rate-2/3, rate-3/4 TTCM schemes and of our HM-16QAM aided scheme in Section 3.3 are shown in Figure 5.15. The throughputs of the four schemes are 1 bps, 2 bps, 3 bps and 1.5 bps (the scheme in Section 3.3 requires 2 TSs for cooperative transmission). Note that the throughput of the optimized scheme proposed in this treatise is 1.455 bps. By contrast, the achievable throughput of the system proposed in this treatise is $3\times 0.97=2.91$ bps, when the channel SNR is sufficiently high for the DN to detect all the three layers of the HM symbols in a single TS without the assistance of the RN. The SNR$_t^{SN}$ required for achieving a BER of 10^{-6} for the non-cooperative rate-2/3 8PSK is 13.40 dB, while that of the optimized scheme in Section 3.3 is 12.09 dB. By contrast, the SNR$_t^{SN}$ of the optimized scheme proposed in this treatise is 6.81 dB and $\overline{SNR_t}$ is 6.94 dB per TS. Additionally, the simulation results of [96] show that in order to transmit a twin-layer HM-16QAM signal with

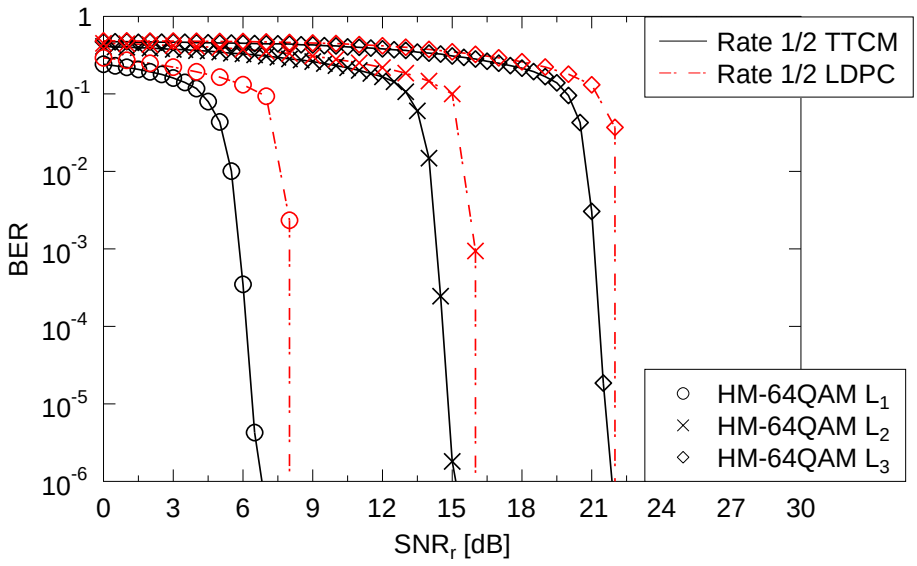

Figure 5.14: The BER versus SNR performance of the transmission between SN and RNs for our triple-layer HM-64QAM based cooperative schematics of Figure 5.2 and Figure 5.7, when using TTCM and LDPC encoders. The triple-layer HM-64QAM ratio pair is ($R_1 = 1.5, R_2 = 0.8$), the related simulation parameters and results are summarized Table 5.6.

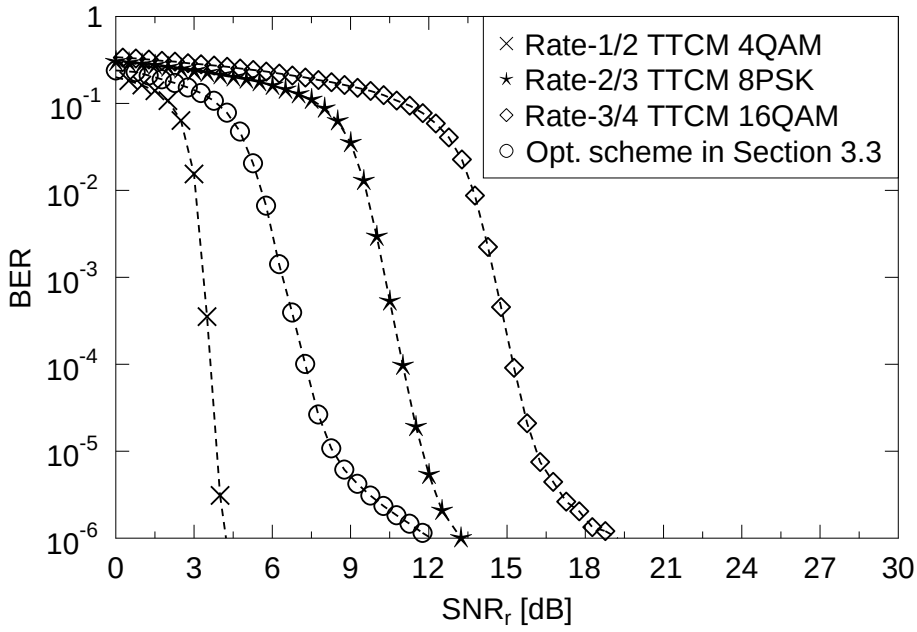

Figure 5.15: The BER versus SNR performance of non-cooperative Rate-1/2 4QAM TTCM, Rate-2/3 8PSK TTCM, Rate-3/4 16QAM TTCM schemes as well as the optimized scheme in Section 3.3. The simulation parameters and the related simulation results are summarized in Table 5.6.

Channel	**Uncorrelated Rayleigh**			
Code	TTCM, LDPC			
Modulation	MISO, HM-16QAM, SPM-16QAM, 4QAM 8PSK			
Code Rate	$R_c^{4QAM} = 1/2$, $R_c^{8PSK} = 2/3$, $R_c^{16QAM} = 3/4$			
Code Polynomial (octal)	$H_{4QAM} = [13\,06]$, $H_{8PSK} = [11\,02\,04]$, $H_{16QAM} = [11\,04\,02]$			
Decoder Type	Approximate Log-MAP			
Decoder Iteration	$\zeta_{TTCM} = 4$, $\zeta_{LDPC} = 20$			
Block Size	12,000			
Frame Size	10,000			
	Required SNR_r (dB) at BER of 10^{-6}			
	Receive L_1	Receive L_2	Receive L_3	Receive entire symbol
TTCM aided HM-64QAM	6.81	15.15	21.87	21.87
LDPC aided HM-64QAM	8.19	16.18	22.25	22.25
Opt. scheme in Section 3.3	–	–	–	12.09
TTCM-4QAM	–	–	–	4.23
TTCM-8PSK	–	–	–	13.40
TTCM-16QAM	–	–	–	19.24

Table 5.6: The simulation parameters and SNR threshold for the simulations shown in Figure 5.14 and Figure 5.15. Compare with the major parameter Table 5.2, the parameters of the code polynomial for the conventional Rate-1/2, 2/3, 3/4, of the number of iterations of the LDPC decoder have been added into this table, where the frame size, block size, channel settings are all the same as those in Table 5.2.

the aid of two rate-1/2 H264/AVC encoders over an AWGN channel for achieving a BER of 10^{-6}, their SNR_t^{SN} should be higher than 14 dB, which is about 7.19 dB higher than that of our optimized scheme transmitting a triple-layer HM-64QAM signal over uncorrelated Rayleigh channels. It can be observed that the scheme optimized in this treatise reduced the SNR_t^{SN} and $\overline{SNR_t}$ of the cooperative system. While, the statistics shown in Figure 5.14 and Figure 5.15 are summarized in Table 5.6.

5.8 Summary and Conclusions

In this chapter, the DCMC capacity of our specifically designed HM schemes has been formulated and the DCMC capacity of each individual layer of our HM-64QAM scheme was also derived. The key results of this chapter as well as in Chapter 2 , Chapter 3 , Chapter 4 are summarized in Table 5.7. While the end-to-end SNR per bit consumed of the cooperative communications proposed in this chapter is summarized in Table 5.8.

Note that since the path-loss exponent used in this chapter is $\alpha = 3$, whilst in the other chapters it is $\alpha = 2$, hence in Table 5.7 we only focussed our attention on the required SNR_t^{SN} of each scheme. It can be stated that the cooperative schemes proposed in Chapter 4 and Chapter 5 may indeed reduce SNR_t required at the SN of a cooperative scheme, despite the fact that the throughput

Code Employed	System Employed	Parameter Employed	Designed for minimized power consumption						Max bps
			$\mathbf{SNR}_t^{SN}$	$\mathbf{SNR}_t^{RN_1}$	$\mathbf{SNR}_t^{RN_2}$	$\overline{\mathbf{SNR}_t}$	TS	bps	
'Perfect'	Figure 5.2	–	2.64 dB	-7.30 dB	-2.82 dB	-0.71 dB	3	1	3
TTCM	Figure 5.2	Table 5.2	5.06 dB	-2.03 dB	1.42 dB	2.41 dB	3	1	3
TTCM	Figure 5.7	Table 5.2	6.81 dB	4.01 dB	4.08 dB	6.94 dB	2	1.46	2.91
'Perfect'	Figure 4.2	–	2.46 dB	–	–	–	2	1	2
TTCM	Figure 4.2	Table 4.2	4.98 dB	–	–	–	2	1	2
TTCM	Figure 3.1	Table 3.2	3.17 dB	–	–	–	2	0.5	2
TTCM	Figure 3.15	Table 3.6	17.47 dB	–	–	–	2	1.5	3
TTCM	Figure 3.16	Table 3.6	20.93 dB	–	–	–	2	2.5	5
TTCM	Figure 3.27	Table 3.8	17.69 dB	–	–	–	2	3	6
TTCM	SISO 4QAM	Table 2.2	4.23 dB	–	–	–	1	1	1
TTCM	SISO 8PSK	Table 2.2	13.04 dB	–	–	–	1	2	2
TTCM	SISO 16QAM	Table 2.2	19.24 dB	–	–	–	1	3	3

Table 5.7: The SNR threshold values of the schematics investigated in Chapter 2, Chapter 3, Chapter 4 and in this chapter. The specific simulation parameters for each system are detailed in the table. The target performance of all the simulation based schemes in the table is based on a BER of 10^{-6}. The terminology 'Perfect' in the table indicates that the channel coding scheme employed is 'perfect channel capacity achieving' as discussed in Section 4.4 and Section 5.5. Note that the block size η for the systems in Figure 3.15, Figure 3.16 and Figure 3.27 is $\eta = 1,200$, while for the other schemes in the table is $\eta = 12,000$.

Code Employed	System Employed	Parameters Employed	Designed end-to-end energy spend per bit for minimized power consumption
'Perfect'	Figure 5.2	–	-0.71 dB
TTCM	Figure 5.2	Table 5.2	2.41 dB
TTCM	Figure 5.7	Table 5.2	5.17 dB

Table 5.8: The end-to-end energy spend per bit values of the schematics investigated in this chapter. The specific simulation parameters for each system are detailed in the table.

of the cooperative schemes investigated in Chapter 4 and Chapter 5 may be higher, provided that we have a sufficiently high SNR for receiving the entire information sequence from the SN.

Theoretically, if the system relies on an idealized perfect 'capacity-achieving' rate-1/2 channel coding scheme, our communication strategy becomes capable of reducing the $\overline{SNR_t}$ of the entire system investigated in Section 5.5.5 to -0.71 dB, while the required SNR_t^{SN} may be set to 2.64 dB. Meanwhile, we have also investigated the performance of the system of Figure 5.7 employing both pre-coding and SPM schemes at the two RNs, as detailed in Section 5.7. The results of Figure 5.10 have demonstrated that the best performance of the system is achieved at a HM-64QAM ratio pair of ($R_1 = 1.5, R_2 = 0.8$) and the optimum SPM ratio pair is ($\alpha = 0.87, \beta = 0.5$). Observe in Figure 5.10 that the optimized system requires an $\overline{SNR_t}$ of 6.94 dB per TS. It can be concluded that by employing HM in cooperative communications, SNR_t^{SN} may indeed be reduced. By contrast,

the performance of the cooperative communication system of Figure 5.2 discussed in Section 5.6 only requires an $\overline{SNR_t}$ per TS of 2.41 dB, as evidenced by Figure 5.6. However, the HM-SPM aided scheme only requires 2 TSs for the DN to receive the HM-64QAM signal sequence from the SN, instead of 3 TSs for the HM assisted scheme in Section 5.6. Hence, the efficiency of the cooperative system conceived in Section 5.7 is improved by requiring extra $\overline{SNR_t}$. We note that if there are more RNs to assist the transmission, the Spatial Modulation (SM) concept [224] may be invoked for further reducing the power consumption of the entire system. The benefit of employing SM will be investigated in our future work. In the Chapter 6, we will combine the TTCM aided HM based cooperative schematic with Opportunistic Routing (OR) algorithm in wireless *ad hoc* networks for reducing the power consumption of a cooperative wireless network, where in order to simplify the investigations, the TTCM aided twin-layer HM-16QAM scheme proposed in Chapter 4 will be considered.

Finally, as detailed in Section 4.6 of Chapter 4 and Section 5.7, the proposed schemes relied on a number of idealized simplifying assumptions. In the practical cooperative communications, the path-loss model may have a break-point. Secondly, each node in the cooperative networks should be informed of the network's status, while the synchronization of the different path also requires further consideration. In our future research, we will gradually eliminate the above-mentioned idealized simplifying assumptions.

Chapter 6

Twin-layer Turbo Trellis-Coded Hierarchical Modulation Aided Opportunistic Routing in *Ad Hoc* Networks

6.1 Introduction

In this chapter, we represent an analytical investigation of the performance of a four-node cooperative communication network employing an efficient opportunistic routing algorithm. In line with the Chapter 4, the packets transmitted are assumed to be those of coded twin-layer modulated signal streams. We detail our opportunistic routing protocol and propose a theoretical analysis method as well as a simulation method for investigating the attainable performance of our cooperative network. The performance characteristics evaluated includes the distribution of delay, the outage probability, the transmit power of each node, the average packet power consumption and the system throughput. Our simulation results will demonstrate that upon transmitting the packets formed by the layered modulated symbol streams, the opportunistic routing algorithm conceived is capable of reducing transmit power required by each node of the network compared to that of the system using traditional opportunistic routing. We will also illustrate that the minimum packet power consumption of the system relying on our opportunistic routing algorithm is also lower than that of the system using traditional opportunistic routing.

In embryonic era, wireless *ad hoc* network were referred to as 'packet radio' networks, which were primarily designed by the Advanced Research Project Agency (DARPA) in 1970. The history of wireless *ad hoc* networks is detailed for example in Labiod's book [225]. The most significant benefit of *ad hoc* networks is their distinctively flexible nature. An *ad hoc* network consists of multiple nodes, where all the nodes are connected by 'links'. The communication between any

Year	Author(s)	Contribution
1994	Johnson [227]	Route discovery and route maintenance protocol for *ad hoc* networks
1995	Davies *et al.* [228]	Contention-tree based multiple access method for *ad hoc* wireless networks
1997	Das and Bharghavan [229]	Employ virtual backbone structure into ad hoc networks for route searching
1999	Broch *et al.* [230]	Integrated *ad hoc* nodes into the hierarchical Internet for mobile transmission
2000	Jonsson *et al.* [231]	Connect an *ad hoc* network to the Internet by using mobile IP
2001	Niculescu and Nath [232]	Estimated the approximate location of all nodes in *ad hoc* networks
2002	Gorssglauser and Tse [233]	Investigated the capacity and throughput of an *ad hoc* network
2003	Zorzi and Rao [126]	Conceived a forwarding algorithm for *ad hoc* and sensor network
2004	Younis and Fahmy [234]	Conceived a protocol for supporting scalable data aggregation in *ad hoc* sensor networks
2005	Weber *et al.* [235]	Estimate the capacity of wireless *ad hoc* network with outage constraints
2006	Pelusi *et al.* [236]	Conceived opportunistic data forwarding for *ad hoc* networks
2008	Zhao and Cao [237]	Vehicle-assisted data delivery in *ad hoc* networks
2009	Harri *et al.* [238]	Mobility models were proposed for vehicular *ad hoc* networks
2010	Tonguz *et al.* [239]	A distributed vehicular broadcast protocol was conceived for *ad hoc* networks
2011	Kim and Giannakis [240]	Resource allocation was designed for MIMO *ad hoc* cognitive radio Networks
2012	Bhorkar *et al.* [159]	Adaptive OR was designed for wireless *ad hoc* networks
2013	Huang [241]	The throughput of mobile *ad hoc* networks relying on energy harvesting was studied
2014	Zuo *et al.* [129]	Energy-efficient cross-layer OR algorithms were designed for *ad hoc* networks
2015	Sharma and Kumar [242]	Opportunistic cross layer design for airborn *ad hoc* networks

Table 6.1: Milestones in wireless *ad hoc* networks (1994-2015).

two nodes in the *ad hoc* network may be assisted by all the other nodes in the network relying on specific transmitter power, path-loss, fading and noise. A series of links which connect a series of communication nodes is termed as a 'path'. Since the links among the nodes in the network may become disconnected at any time, a functioning network must be capable of dynamically re-structuring itself with the aid of reliable routing methods invoked for finding beneficial paths [226] for the transmissions. Therefore, the research of the *ad hoc* networks has been mainly focussed on routing algorithms. Table 6.1 summaries the milestones in the research of wireless *ad hoc* networks during the most recent twenty years.

A detailed investigation of position-based routing in mobile *ad hoc* networks was published in 2001 by Mauve [243]. More explicitly, the associated transmission protocols [228, 230–232, 234, 237–240], the routing algorithms [126, 159, 227, 229, 236] as well as the capacity [233, 235, 241] and energy efficiency [129, 241] were lavishly characterized in the open literature. More recently, the family of OR algorithms has inspired increasing research attentions [130–134]. The routing algorithms of multi-hop wireless networks, such as mobile *ad hoc* networks and wireless mesh networks, have attracted substantial research interests [130, 131]. Again, the main tasks of routing are constituted by route selection and packet forwarding. Classic routing algorithms, such

as the dynamic source routing of [142] and the *ad hoc* on-demand distance vector based routing are investigated in detail in [124, 125], where the source may opt for a fixed time-invariant path to the destination, where the entire is decided according to the near-instantaneous channel conditions encountered at the beginning of transmissions [134]. However, these strategies may not adapt well to the dynamically fluctuating wireless channel conditions [129], hence they may lead to excessive link-level retransmissions and ultimately to the waste of network resources [130].

In order to overcome the deficiencies of conventional routing [124–127], meritorious Opportunistic Routing (OR) algorithms have been developed in [90, 126, 129–136, 156, 159, 170, 171, 244, 245], which exploit the broadcast nature of wireless transmissions and the beneficial path diversity of the multi-hop wireless networks [131]. In contrast to conventional routing, OR relies on multiple opportunistic paths for forwarding the packets [134]. The receiver of the next hop in OR is dynamically chosen from all the nodes in the network which are likely to correctly receive the packet. This receiver node is typically the one, which is geographically closest to the Destination Node (DN) [135]. Since multiple forwarding candidates are activated for assisting the packet's passage through the network, the probability of at least one candidate correctly receiving the packet is increased compared to conventional routing [131]. Given the increased reliability of each hop's transmission, both the throughput and the energy-efficiency of the entire system may be improved [129, 131, 156]. The so-called Extremely Opportunistic Routing (ExOR) regime of [132] is one of the primary OR algorithms in the literature [134]. Explicitly, the ExOR algorithm carries the forwarder node-index list information in the header of the broadcast packets and the specific nodes, which have successfully received the packet are likely to be used as the transmitter during the following Time Slot (TS). Apart from the ExOR algorithm, numerous other opportunistic strategies have been developed for solving diverse problems, such as Geographic Random Forwarding (GeRaF) algorithm of [126, 136] and the MAC-agnostic opportunistic routing of [133]. However, the key objective of all OR strategies is more or less the same, namely that of finding the best candidates in the cooperative network for forwarding the signal. At the time of writing, researchers tend to focus their attention on the specific characteristics of OR algorithms, such as their energy consumption [129, 156, 170], their system delay [129, 171] and system capacity/throughput bound [131]. However, despite having numerous research papers on OR, there is a paucity of analytical studies on the performance of cooperative networks relying on OR algorithms [135].

Along a parallel research avenue, the layered modulation schemes such as Hierarchical Modulation (HM) and Superposition Modulation (SPM), which are proposed in Chapter 3 to Chapter 5 in our thesis, have also attracted a lot of research attention. As an integral part of the DVB-T/-H standard [84], HM has been widely employed throughout the Information Technology (IT) industry for upgrading diverse telecommunication services [86, 207]. While, we have investigated the performance of Turbo Trellis-Coded Modulation (TTCM) [6] aided HM in the context of cooperative communications in [57, 185]. The results demonstrated that the employment of our HM scheme is beneficial in cooperative communications, where the information contained in different HM layers may be demodulated separately [184, 185]. The transmit power of the entire cooperative

system communicating with the aid of HM signal streams may be reduced by invoking carefully designed communication protocols. However, since the HM scheme provides Unequal Error Protection (UEP) for the information contained in the different HM layers, receiving the entire HM signals may require a higher average received power than that of the conventional modulation schemes having the same number of modulation levels. The layered transmission techniques have in deed been intensely investigated in the physical layer [84, 97], where the packets transmitted throughout the cooperative network may also be grouped on the basis of the different layers, jointly conveying the different layers modulated symbols. However, the investigations of OR-aided layered modulation are rather scarce.

Against this backdrop, in this chapter, we proposed a four-node wireless cooperative communication network communicating using TTCM-aided twin-layer HM-16QAM signal packets. The layered modulated packets are forwarded through the cooperative network using our OR algorithm. However, instead of conveying the layered modulated packets as a unit, our OR scheme conceived in this chapter exploits the specific features of the HM scheme. More specifically, the twin-layer HM-16QAM signal packets will be partitioned into a pair of sub-packets, and they may become separately broadcast depending the near-instantaneous received power of all the potential receiver node candidates. In this chapter, the specific OR algorithm, which always keeps the layered modulated packets together as an integral unit during its transmission, will be referred to as the Traditional OR (TOR) algorithm. By contrast, our HM aided OR algorithm is termed as Hierarchical Modulated Opportunistic Routing (HMOR). The novel contributions of this chapter are:

- The layered method is combined with an OR algorithm in the network layer, where a new OR scheme conveying twin-layer HM-16QAM signal packets is proposed.
- We mathematically characterize the Frame-Error-Rate (FER) performance of the twin-layer HM aided TTCM scheme as a function of the instantaneous received Signal-to-Noise Ratio (SNR), when communicating over both Additive-White-Gaussian-Noise (AWGN) channels as well as Rayleigh-distributed block fading channels.
- The accuracy of the theoretical analysis of our HMOR algorithm is confirmed by simulations.

The rest of the chapter is organized as follows. Section 6.2 introduces both the system model and our twin-layer HM-16QAM modulation scheme. The theoretical analysis of our four-node cooperative communication network is represented in Section 6.3. Section 6.4 details the simulation-based characterization of our HMOR based cooperative network, while the related performance results are illustrated in Section 6.5.

6.2 System Model

The differences of the TR, TOR and HMOR regimes are illustrated in Fig. 6.1 and Fig. 6.2. The route is decided by the TR algorithms before the commencement of transmissions. By contrast, for

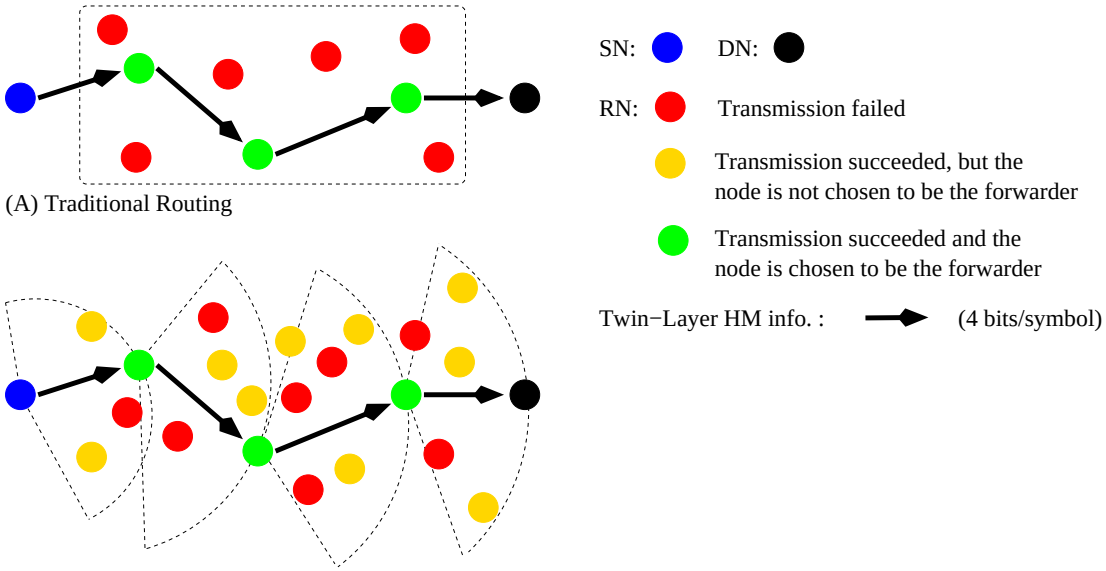

Figure 6.1: Comparison of TR, TOR and HMOR.

the TOR algorithms, multiple receive candidates will be chosen before each broadcast phase and then the specific RN transmitter activated for the sake of forwarding the information during the following TS will be selected according to specific decision algorithms. Even though the transmitted packet is formed by twin-layer HM-16QAM symbols, both the TR and the TOR algorithms will always deliver the layered modulated packets as an inseparable integral payload unit.

In contrast to this inseparable delivery philosophy, our HMOR algorithm may partition the packets into a pair of sub-packets, namely L_1 and L_2. The route selection algorithm of our HMOR algorithm is the same as that of the TOR algorithms, but when the packet becomes partitioned into L_1 and L_2, the entire network may be configured to focus on forwarding the high-priority base-layer L_1 first. When L_1 is received by the DN, the network will start the transmission of L_2. By partitioning the twin-layer HM-16QAM based packet into a pair of sub-packets, the packets that are forwarded through the network will require a lower receive power due to the reduced constellation size. Hence the transmit power of each node in the network may be reduced.

The family of routing algorithms has been lavishly documented in [223, 246]. In order to simplify the discussions, our analysis provided in this chapter is mainly focussed on a cooperative system assisted by two RNs. The general system model is illustrated in Figure 6.3. Although the entire system only has two hops, our transmission algorithm can be readily extended to a larger network. Explicitly, this simple network already characterizes most of the typical situations of a large network having more than three hops. Note that the first RN (RN_1) is near to the SN and the second RN (RN_2) is near to the DN. During the first TS, the SN will broadcast a signal frame to all the other nodes of the cooperative network, where both RN_1 and RN_2 are willing to forward the information to the DN. Additionally, the pair of RNs also collaborate with each other during the transmissions. The original signal frame received from the SN contains a pair of independent

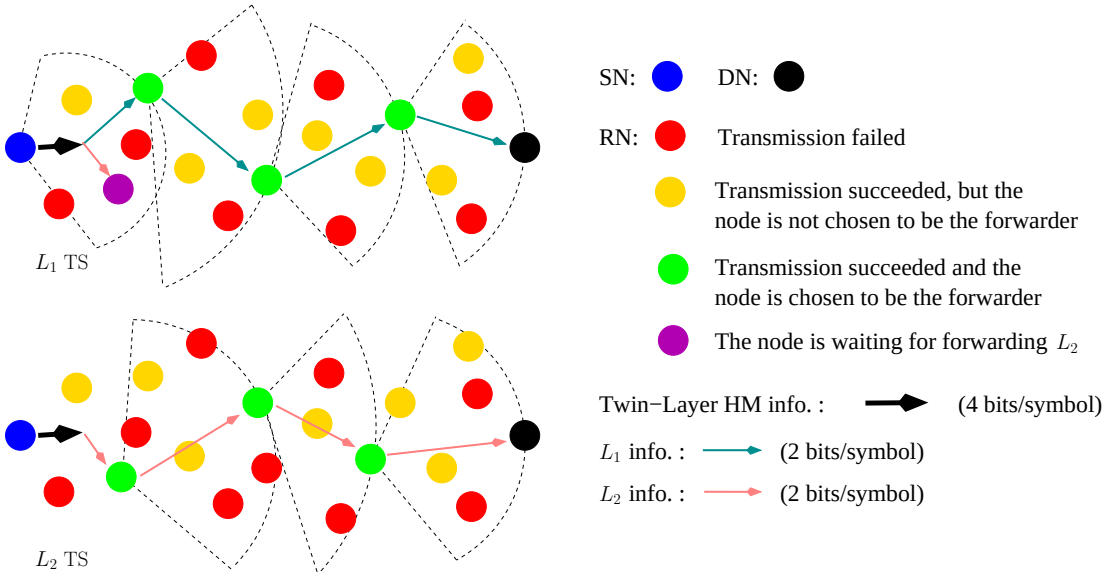

Twin−Layer HM aided OR (HMOR)

Figure 6.2: Comparison of TR, TOR and HMOR.

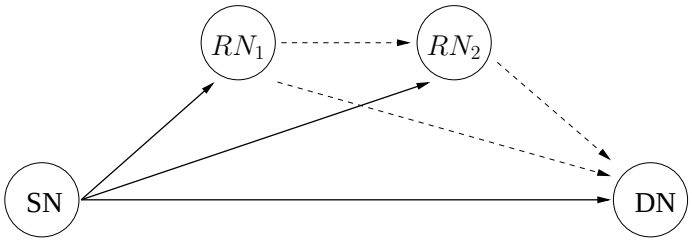

Figure 6.3: The model of our twin-relay assisted cooperative system.

layers, which are originally conveyed together by the HM scheme. We denote the layer having a higher protection priority as L_1, while that having a lower protection level as L_2. According to the specific features of the HM scheme, the SNR required by receiver for decoding L_1 is lower than that of L_2. Hence, upon receiving the twin-layer HM signals, we assume that if the node in the cooperative network is capable of successfully receiving L_2, it is also capable of receiving L_1 at an adequate integrity.

The constellation map of our HM-16QAM scheme is shown in Figure 6.4, which was repeated from Figure 3.29 for convenience. Further details of our twin-layer HM scheme are also available in Chapter 4 and [185]. We define the four bits of a HM-16QAM symbol as $(b_3b_2b_1b_0)$, where L_1 is defined by (b_3b_2), while (b_1b_0) are contained in L_2. Both of the two layers are encoded by a rate-1/2 TTCM encoder. Hence, there is one information bit and one parity bit in each layer. The generation rule of the twin-layer HM-16QAM symbols may be formulated as:

$$S_{HM-16QAM} = \frac{1+R_1}{\sqrt{1+(1+R_1)^2}} \left[S_{4QAM} \pm \frac{1}{(1+R_1)} e^{\pm \frac{\pi}{4} j} \right], \tag{6.1}$$

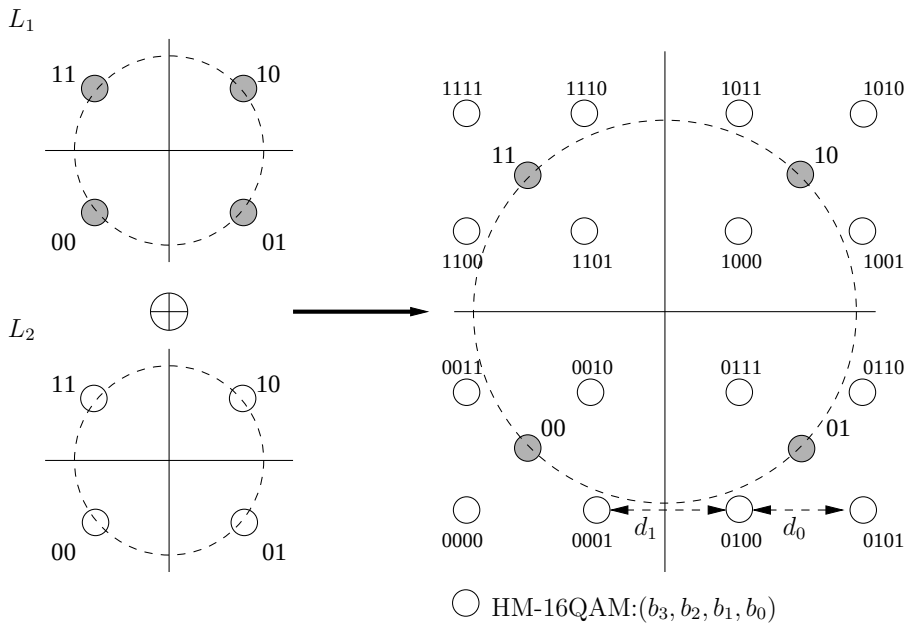

Figure 6.4: The constellation map of the HM scheme, where $R_1 = d_1/d_0$.

where S_{4QAM} denotes the conventional square 4QAM constellations and the HM-16QAM ratio $R_1 = d_1/d_0$ is defined in line with Chapter 3 for controlling the shape of the HM-16QAM constellations, which has the constraint of $R > 0$, as detailed in [185] and Chapter 3. We have found in Chapter 4 that the optimum performance of the system of Figure 4.2 is achieved, when the HM-16QAM ratio is $R_1 = 3.0$, while the rate-1/2 TTCM decoder has $\zeta = 4$ decoding iterations and the transmission packet size is $\eta = 12,000$ symbols. Note that, we opt $\eta = 12,000$ in Chapter 4 for the sake of achieving a better performance in the physical layer. However, in wireless transmissions, a transmission packet length of $\eta = 12,000$ symbols may be excessive for assuming that the fading channels' envelop remains constant during each packet's transmission in a specific link. Hence, in this study, the settings of the HM ratio R_1 and the rate-1/2 TTCM encoder/decoder will keep the same as those in Chapter 4, but the packet length is changed to $\eta = 1,200$ symbols.

6.3 Theoretical Analysis

Again, the system considered communicates over Rayleigh-distributed block fading channels, where all nodes of the cooperative network are assumed to benefit from perfect Channel State Information (CSI). The related simulation parameters are shown in Table 6.2. Furthermore, the symbols used in this chapter are defined as follows:

- $¶_t$: the transmit power.
- $\widetilde{h}$: the instantaneous channel fading value.
- $\overline{\gamma}$: the average receive SNR, which is $\overline{\gamma} = \frac{¶_t \kappa}{N_0 d^\alpha}$, where $\kappa = \left(\frac{c}{4\pi f_c}\right)^2$ is a constant, while c

Coded Modulation	**TTCM**
Modulation Scheme	4QAM, HM-16QAM
HM ratio R_1	3.0
Mapper type	Set-Partitioned
Number of iterations	4
Code Rate	1/2
Code Memory	3
Code Polynomial (octal)	$H_{4QAM} = [13\ 06]$
Decoder type	Approximate Log-MAP
Symbols per frame	1,200
Number of frames	10,000
Channel	AWGN channel Rayleigh-distributed block fading channel
Path-loss exponent	2

Table 6.2: Simulation parameters used in the TTCM-aided twin-layer HM base HMOR schematic of Figure 6.3.

is the speed of light, $f_c = 2.4\ GHz$ is the carrier frequency according to the WIFI standards, d denotes the distance and α is the path-loss exponent. Specifically, we consider the classic free-space path-loss model [1, 206], where we have $\alpha = 2$ and N_0 is the noise power, which is set to -110 dBm in our simulations.

- γ: the instantaneous receive SNR, which is given by $\gamma = \widetilde{h}\overline{\gamma}$.
- N_t: the number of maximum transmission attempts for each node in the cooperative network.

6.3.1 FER Derivation

Evaluating the FER metric is vital for determining whether the information is received successfully or not, which depends on many numerous factors, including the AWGN, the channel fading, the path-loss, etc. Although we can directly infer the FER performance of a specific channel coding scheme in a given scenario with the aid of Monte-Carlo simulations, in order to investigate our OR-assisted cooperative scenario, we have to characterize the FER as a function of the receive SNR γ. A similar technique has been conceived for a single-layer transmission scenario in [129]. In this chapter, we employ the TTCM aided twin-layer HM scheme of Figure 6.4. We firstly generate the FER versus SNR curve for transmission over AWGN channels using simulations and then invoke the schemes designed in [247] to find accurately matching polynomials for characterizing the FER versus SNR curve. As seen in Table 6.2, the coding rate of the TTCM scheme used in this chapter is set to $R_c = 0.5$, with a block length of $\eta = 1,200$ symbols, while the octally represented generator polynomials of the rate-1/2 TTCM encoder are $[13\ \ 06]$. According to the simulation-based FER

versus SNR curve of the AWGN channel, the following three-segment FER versus SNR model is constructed for representing the performance of the twin-layer TTCM aided transmission over AWGN channels:

$$FER_{AWGN}(\overline{\gamma}) \approx \begin{cases} 1 & \text{if } 0 \leqslant \overline{\gamma} < \eta_1, \\ \sum_{k=1}^{4} a_k (\overline{\gamma})^{4-k} & \text{if } \eta_1 \leqslant \overline{\gamma} < \eta_2, \\ a_5 e^{-10a_6 \log_{10}(\frac{\overline{\gamma}}{\Delta})} & \text{if } \overline{\gamma} \geqslant \eta_2. \end{cases} \tag{6.2}$$

In AWGN channels we have $\widetilde{h} = 1$, hence, $\gamma = \overline{\gamma}$. Explicitly, we divide the FER_{AWGN} versus SNR simulation curve of Eq. (6.2) into three segments according to the received SNR thresholds η_1 and η_2. During the fitting process carried out by Matlab, the appropriate values of η_1 and η_2 may be obtained. Additionally, Δ is a variable we used for simplifying the Matlab-based curve-fitting process. Then the FER versus SNR performance encountered over Rayleigh-distributed block fading channels may now be expressed as:

$$FER_{Rayleigh}(\widetilde{h}\overline{\gamma}) = \int_0^{\infty} e^{-\widetilde{h}} FER_{AWGN}(\widetilde{h}\overline{\gamma}) \mathrm{d}\widetilde{h} \,. \tag{6.3}$$

Hence, we have the following scenario:

- When $0 \leqslant \widetilde{h}\overline{\gamma} < \eta_1$, we arrive at:

$$FER^{I}_{Rayleigh} = \int_0^{\frac{\eta_1}{\overline{\gamma}}} e^{-\widetilde{h}} \mathrm{d}\widetilde{h} = 1 - e^{-\frac{\eta_1}{\overline{\gamma}}} \,. \tag{6.4}$$

- For $\eta_1 \leqslant \widetilde{h}\overline{\gamma} < \eta_2$, we have:

$$\begin{aligned} FER^{II}_{Rayleigh} &= \int_{\frac{\eta_1}{\overline{\gamma}}}^{\frac{\eta_2}{\overline{\gamma}}} \sum_{k=1}^{4} a_k (\widetilde{h}\overline{\gamma})^{4-k} e^{-\widetilde{h}} \mathrm{d}\widetilde{h} \\ &= \sum_{k=1}^{4} a_k \overline{\gamma}^{4-k} \int_{\frac{\eta_1}{\overline{\gamma}}}^{\frac{\eta_2}{\overline{\gamma}}} \widetilde{h}^{4-k} e^{-\widetilde{h}} \mathrm{d}\widetilde{h} \\ &= \sum_{k=1}^{4} a_k \overline{\gamma}^{4-k} \left[\gamma_f(5-k, \frac{\eta_2}{\overline{\gamma}}) - \gamma_f(5-k, \frac{\eta_1}{\overline{\gamma}}) \right] , \end{aligned} \tag{6.5}$$

  where $\gamma_f(s,x) = \int_0^x t^{s-1} e^{-t} \mathrm{d}t$, which is the lower incomplete gamma function.

- Finally, for $\widetilde{h}\overline{\gamma} \geqslant \eta_2$, we arrive at:

$$\begin{aligned} FER^{III}_{Rayleigh} &= \int_{\frac{\eta_2}{\overline{\gamma}}}^{\infty} a_5 e^{\left(-10a_6 \log_{10}(\frac{\widetilde{h}\overline{\gamma}}{\Delta})\right)} e^{-\widetilde{h}} \mathrm{d}\widetilde{h} \\ &= a_5 e^{-10a_6 \log_{10}\left(\frac{\overline{\gamma}}{\Delta}\right)} \left(\frac{\eta_2}{\overline{\gamma}}\right)^{\left(1-\frac{10a_6}{\ln 10}\right)} \times \\ &\quad G^{2,0}_{1,2}\left[\frac{\eta_2}{\overline{\gamma}} \,\middle|\, \begin{matrix} \frac{10b}{\ln 10} \\ \frac{10b}{\ln 10} - 1, 0 \end{matrix} \right] , \end{aligned} \tag{6.6}$$

  where, we have $G^{2,0}_{1,2}\left[x \,\middle|\, \begin{matrix} \nu \\ \nu - 1, 0 \end{matrix} \right] = E_\nu(x) = \int_1^{\infty} \frac{e^{-xt}}{t^\nu} dt$, which is the Meijer-G function defined in [248, 249].

	Parameters
Transmitting	$\eta_1 = 1.1480e+00,\ \eta_2 = 1.4125e+00,\ \Delta = 1$
Rate-1/2 4QAM	$a_1 = 9.6418e+01,\ a_2 = 3.7845e+02,\ a_3 = 4.9016e+02$
TTCM	$a_4 = -2.0888e+02,\ a_5 = 7.8800e+03,\ a_6 = 7.3000e+00$
Transmitting L_1	$\eta_1 = 1.1480e+00,\ \eta_2 = 1.6218e+00,\ \Delta = 1$
TTCM aided	$a_1 = 3.9603e+01,\ a_2 = -1.7931e+02,\ a_3 = 2.6689e+02$
Twin-layer HM-16QAM	$a_4 = -1.2998e+02,\ a_5 = 9.2100e+03,\ a_6 = 5.2000e+00$
Transmitting L_2	$\eta_1 = 1.9500e+01,\ \eta_2 = 2.4547e+01,\ \Delta = 15$
TTCM aided	$a_1 = 1.5429e-02,\ a_2 = -1.0273e+00,\ a_3 = 2.2521e+01$
Twin-layer HM-16QAM	$a_4 = -1.6192e+02,\ a_5 = 8.0000e+05,\ a_6 = 7.6000e+00$

Table 6.3: Curve-fitting parameters for the FER versus SNR performance of receiving rate-1/2 TTCM 4QAM scheme, and of receiving L_1 and L_2 of the TTCM aided twin-layer HM-16QAM scheme given HM ratio of $R = 3.0$. The related parameters for the channel coding schemes employed are shown in Table 6.2.

Therefore, the FER versus SNR performance for transmission over Rayleigh-distributed block fading channels is given by:

$$FER_{Rayleigh}(\gamma\overline{\gamma}) = FER^{I}_{Rayleigh} + FER^{II}_{Rayleigh} + FER^{III}_{Rayleigh}\ . \tag{6.7}$$

Quantitatively, in our simulations of Figure 6.5, there are six FER versus SNR curves that have to be matched. We have two curves for the FER versus SNR performance of the rate-1/2 TTCM coded 4QAM scheme for transmission over both AWGN channel and Rayleigh-distributed block fading channels, another two curves for receiving L_1 of the twin-layer rate-1/2 TTCM aided HM scheme over the two channels, and the last two curves for receiving L_2 of the twin-layer rate-1/2 TTCM aided HM scheme over the two channels. The related curve-fitting parameters are shown in Table 6.3.

It can be observed from Figure 6.5a and Figure 6.5b that our mathematical FER versus SNR curve fitting schemes indeed match the simulation curves of the FER versus SNR performance over both AWGN and Rayleigh-distributed block fading channel. Therefore, we have successfully characterized the FER performance as a function of the instantaneous receiver SNR. By computing the FER versus SNR performance curves for both the AWGN and Rayleigh-distributed block fading channel, we arrive at the nodes' successful reception probability based on their near-instantaneous receiver SNR. Therefore, both their power-efficiency and delay may now be quantified. In the following section, we have listed the ten possible states in our cooperative transmissions regime and the basic transmission activation rules among the nodes for the theoretical performance analysis of our system.

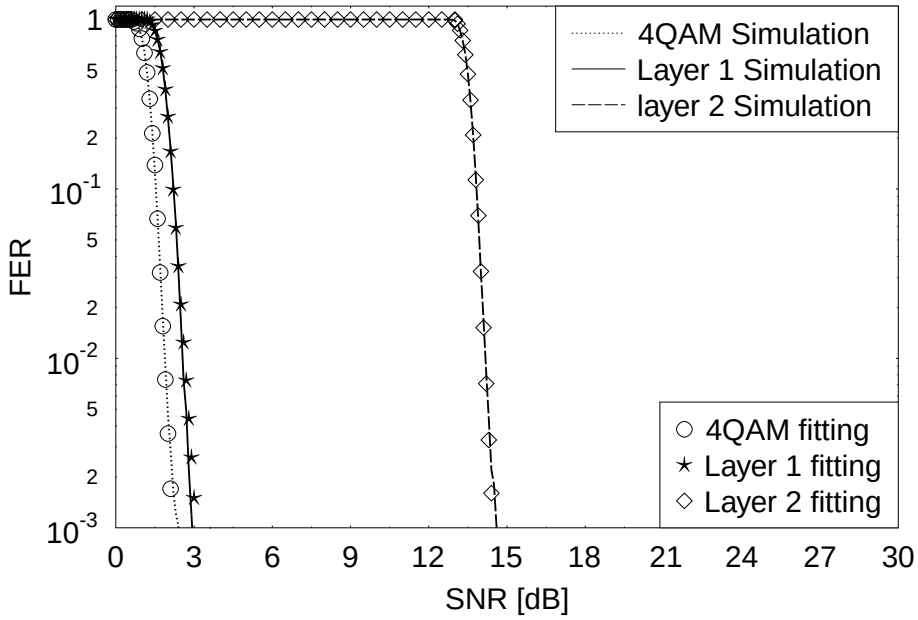

(a) AWGN channel

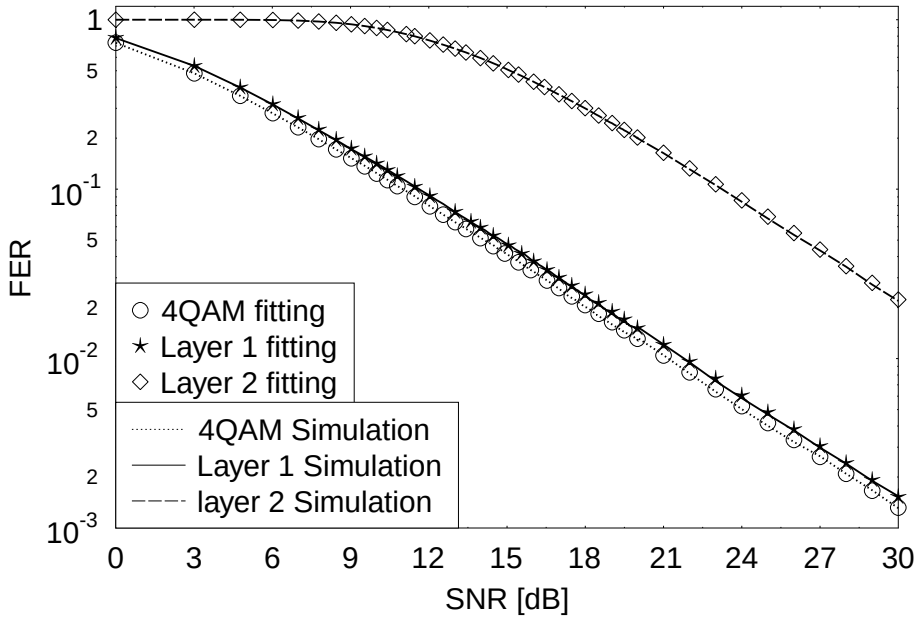

(b) Rayleigh-distributed block fading channel

Figure 6.5: The BER versus FER performance of receiving rate-1/2 TTCM 4QAM scheme, and of receiving L_1 and L_2 of the TTCM aided twin-layer HM-16QAM scheme given HM ratio of $R = 3.0$. The curve-fitting parameters are shown in Table 6.3 and the related simulation parameters are shown in Table 6.2.

State	SN	RN_1	RN_2	DN
S_1	L_1,L_2			
S_2	L_2	L_1		
S_3		L_1,L_2		
S_4	L_2		L_1	
S_5		L_2	L_1	
S_6			L_1,L_2	
S_7	L_2			L_1/Null
S_8		L_2		L_1/Null
S_9			L_2	L_1/Null
S_{10}				L_1/Null,L_2/Null

Table 6.4: The ten states of the TTCM aided twin-layer HM-16QAM based twin-relay assisted cooperative communication system of Figure 6.3. Explicitly, the L_1 and L_2 indicate the information received by each of the four nodes in specific state.

6.3.2 Legitimate System States and State Transitions

Let us now characterize our four-node cooperative communication network in terms of its ten states of $\{S_i\}$, where we have $i \in \{1,2,...,10\}$. The ten states are shown in Table 6.4, whilst their state-transitions will be discussed below with reference to Figure 6.6.

As shown in Table 6.4, each state illustrates the current buffer status of each node in the network. We define the node nearest to the DN that receives L_1 or L_2, as the 'Frontier' of L_1 or L_2, where only the node which is the 'Frontier' of L_1 or L_2 or both may be chosen to be the transmitter for forwarding the packet during the following transmission. Since after every transmission the 'Frontier' of L_1 or L_2 are unique, we use the 'Frontier' of L_1 and L_2 to define the specific receiver state of the system and produce Table 6.4. Due to the specific layer-based decoding feature of the HM scheme, L_1 having a higher protection level requires a lower receiver SNR than that of L_2. Therefore, the position of the particular RN, which successfully received L_2 will never be beyond the position of that RN, which successfully received L_1. Hence, if there are n nodes in the network, the total number N_{state} of the legitimate system states may be expressed as:

$$N_{state} = 1 + 2 + ... + n = \frac{n(n+1)}{2} . \tag{6.8}$$

Note that during any transmission phase, only one of the nodes in the network is activated for transmission, which corresponds to a Time Division Multi Access (TDMA) scheme, where the transmissions at each node are divided into transmission TSs. Therefore, only a single node is forwarding the information. For a specific node, if a packet encounters a transmission outage N_t times, then the packet will be discarded. To be more specific, the transitions among the legitimate system states are presented in Figure 6.6 and the details of the ten states of the four-node network are described below with the aid of frequent references to Figure 6.6:

- **State S_1**: it is the initial 'switch-on' state or the state, when all the other nodes in the co-operative network failed to receive even a single layer information from the SN. Hence, the SN may have to retransmit both the L_1 and L_2 layers during the following TS. Note that if the current state is S_1, the next state may be any one of all the legitimate states. We have to mention that if the current state is the same as the following state, this implies that the transmission attempt of the current state has failed, hence the packet has to be retransmitted, as seen in Figure 6.6.

- **State S_2**: only RN_1 is capable of receiving L_1. Here, we allow RN_1 to have the necessary priority to transmit its L_1 first, during the forthcoming TS. Only when the DN has received L_1 or if L_1 is discarded, because if the number of transmission attempts exceeds N_t, then SN will be allowed to retransmit L_2. Therefore, the next state arrived at from S_2 may be S_2, S_4 or S_7, as portrayed in Figure 6.6.

- **State S_3**: both L_1 and L_2 are received by the RN_1. Hence, during the following TS, SN could remain silent, while RN_1 may attempt to forward L_1 and L_2 to the DN. Therefore, the observe also in Figure 6.6 that next state transition from S_3 may be S_3, S_5, S_6, S_8, S_9 or S_{10}.

- **State S_4**: RN_2 is capable of receiving L_1, while both RN_1 and RN_2 failed to receive L_2 and DN also receives nothing. In this situation, since RN_2, which is nearer to the DN successfully decoded L_1, during the next TS, the system will only allow RN_2 to forward L_1 to DN. After RN_2 completed its transmission, SN will commence its retransmission of L_2. Hence the state S_4 may be followed by S_4 or S_7, as visualized in Figure 6.6.

- **State S_5**: RN_2 is capable of receiving L_1, while RN_1 successfully decodes both L_1 and L_2, but DN fails to receive anything. Then RN_2 will attempt to transmit L_1 to DN in the following TS, and after it completed its transmission, RN_1 will be activated in order to forward L_2 without L_1. The following state upon emerging from S_5 of Figure 6.6 will be S_5 or S_8.

- **State S_6**: RN_2 is capable of receiving both layers L_1 and L_2, while DN received nothing. In this situation, RN_2 will forward both of L_1 and L_2 to DN during the following TS, while the SN and RN_1 will remain silent until the system starts to transmit its next package. As seen in Figure 6.6, the following state upon emerging from S_6 will be S_6, S_9 or S_{10}.

- **State S_7**: this state may be reached from S_1, S_2, S_4 and S_7, depending on two situations, namely on whether DN has received L_1 and on whether the system has discarded L_1 due to N_t failed transmission attempts. Let us consider the transition $S_4 \rightarrow S_7$ for instance. If the previous state is S_4, then RN_2 may forward L_1 to DN, provided that DN successfully receives L_1. Then the system will traverse to state S_7, since DN received L_1 and the entire system will only attempt to forward L_2 to DN from SN during the following TS. However, if RN_2 failed to successfully transmit L_1 to DN, the following state will still be S_4. Then RN_2 will try to retransmit L_1, but if reception failures occur for N_t times, then RN_2 has to discard L_1 and allow SN to retransmit L_2. Hence, a state transition of Figure 6.6 will be enforced from S_4

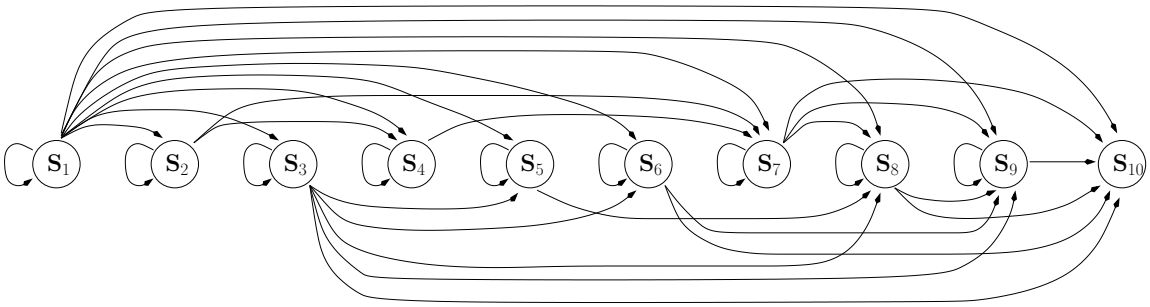

Figure 6.6: The state transition diagram of the ten legitimate system states of the cooperative schematic of Figure 6.3.

to S_7 with DN marked by the flag L_1 lost, as the 'Null' in Table 6.4. The state transitions emerging from S_7 may be S_7, S_8, S_9 or S_{10}.

- **State S_8**: similar to S_7, DN may either have successfully received L_1 or L_1 may have been discarded, which depends on the previous state. Meanwhile, L_2 will be forwarded to DN by RN_1 during the following TS. The following states reached from S_8 may be S_8, S_9 or S_{10}.

- **State S_9**: similar to S_7, in the following TS, only RN_2 is activated to forward L_2 to DN. The next state upon departure from S_9 be S_9 or S_{10}, as observed in Figure 6.6.

- **State S_{10}**: the final state for each packet's transmission, while, whether that layer L_1 or L_2 may be successfully received by the DN or be discarded still depends on the previous state.

6.3.3 Single-Step State-Transition Probability

During the transmissions, SN and RN may have to transmit two types of signals. More specifically, when they have to forward all of the twin-layer information, they would transmit the HM-16QAM symbols streams. By contrast, when they only have to forward single-layer information (L_1 or L_2), they would transmit rate-1/2 4QAM TTCM coded symbols. Note that since the transmissions are based on packets and the number of symbols in a packet is identical to that of the frame length of the TTCM encoder, the FER performance of the TTCM decoder is identical to the packet error rate. Hence, according to the analysis of Section 6.3.1, we define the following state-transition probabilities:

- P^{4QAM}: The probability of successfully receiving the rate-1/2 TTCM 4QAM symbols, which is given by $P^{4QAM} = 1 - FER^{4QAM}(\gamma)$.

- P^{L_1}: The probability of successfully receiving L_1, when the HM-16QAM signals were transmitted, which is formulated as $P^{L_1} = 1 - FER^{L_1}(\gamma)$.

- P^{L_1,L_2}: The probability of successfully receiving both L_1 and L_2, when the HM-16QAM signal was transmitted (as mentioned before, when the node is capable of receiving L_2, it may also be able to successfully receive L_1). It is expressed as $P^{L_1,L_2} = 1 - FER^{L_1,L_2}(\gamma)$.

- $P^{[0/2]}$: The probability of transmitting the twin-layer HM-16QAM signals, but both L_1 and L_2 were received unsuccessfully. This may be characterized by $P^{[0/2]} = 1 - P^{L_1}$.

- $P^{[1/2]}$: The probability of transmitting the twin-layer HM-16QAM signals, but only L_1 is received successfully, which may be expressed as $P^{[1/2]} = P^{L_1} - P^{L_1,L_2}$.

- $P^{[2/2]}$: The probability of transmitting the twin-layer HM-16QAM signals, where both L_1 and L_2 are successfully received, which is given by $P^{[2/2]} = P^{L_1,L_2}$.

- $P^{[0/1]}$: The probability of transmitting only a single layer, namely L_1 or L_2 by using the rate-1/2 TTCM 4QAM scheme, which was not received successfully. This may be characterized by $P^{[0/1]} = 1 - P^{4QAM}$.

- $P^{[1/1]}$: The probability of successfully receiving the transmitted single-layer (L_1 or L_2) information based on the rate-1/2 TTCM 4QAM scheme, yielding $P^{[1/1]} = P^{4QAM}$.

Therefore, based on Section 6.3.2, we may derive a set of single-step state-transition probabilities based on the transmit power $\P_t$ of each node, as shown in Table 6.5, where we have $\overline{P} = 1 - P$. The notation $P_{mn}^{[i/j]}$ shown in Table 6.5 represents the probability of transmission from node m to node n, where i layers(s) was(were) successfully received out of the transmitted j layer(s).

6.3.4 Analytical Characterization

In this section, we conceived a method of analysing the attainable performance of our cooperative systems based on the single-step state-transition probability recorded in Table 6.5. Our theoretical analysis aims for characterizing the distribution of all possible system states, where the transition among all states is based the single-step transition probabilities defined in Table 6.5. The FER performance versus the transmit power $\P_t$ formula is based on Eq. (6.7) of Section 6.3.1, which relies on the single-step transition probabilities recorded in Table 6.5. The statistics used for characterizing the performance of the system are defined as follows:

- Delay_{L1} and Delay_{L2} denote the delays before the DN receives L_1 and L_2, respectively.

- P_{outage}^{L1} and P_{outage}^{L2} represent the probabilities of discarding L_1 and L_2, respectively.

- $\overline{PWC}$ denotes the average packet power consumption of the entire system.

- The notation Φ represents the average throughput of the entire system expressed in terms of packets per TS. The TS here is the time duration required for transmitting a packet containing 1,200 symbols. In order to simplify the analysis of the system, we refrain from converting

		TS(n+1)				
		S_1	S_2	S_3	S_4	S_5
TS(n)	S_1	$P_{SR_1}^{[0/2]}P_{SR_2}^{[0/2]}P_{SD}^{[0/2]}$	$P_{SR_1}^{[1/2]}P_{SR_2}^{[0/2]}P_{SD}^{[0/2]}$	$P_{SR_1}^{[2/2]}P_{SR_2}^{[0/2]}P_{SD}^{[0/2]}$	$\overline{P}_{SR_1}^{[2/2]}P_{SR_2}^{[1/2]}P_{SD}^{[0/2]}$	$P_{SR_1}^{[2/2]}P_{SR_2}^{[1/2]}P_{SD}^{[0/2]}$
	S_2	0	$P_{R_1R_2}^{[0/1]}P_{R_1D}^{[0/1]}$	0	$P_{R_1R_2}^{[1/1]}P_{R_1D}^{[0/1]}$	0
	S_3	0	0	$P_{R_1R_2}^{[0/2]}P_{R_1D}^{[0/2]}$	0	$P_{R_1R_2}^{[1/2]}P_{R_1D}^{[0/2]}$
	S_4	0	0	0	$P_{R_2D}^{[0/1]}$	0
	S_5	0	0	0	0	$P_{R_2D}^{[0/1]}$
	S_6	0	0	0	0	0
	S_7	0	0	0	0	0
	S_8	0	0	0	0	0
	S_9	0	0	0	0	0
	S_{10}	0	0	0	0	0
		S_6	S_7	S_8	S_9	S_{10}
TS(n)	S_1	$P_{SR_2}^{[2/2]}P_{SD}^{[0/2]}$	$\overline{P}_{SR_1}^{[2/2]}\overline{P}_{SR_2}^{[2/2]}P_{SD}^{[1/2]}$	$P_{SR_1}^{[2/2]}\overline{P}_{SR_2}^{[2/2]}P_{SD}^{[1/2]}$	$P_{SR_2}^{[2/2]}P_{SD}^{[1/2]}$	$P_{SD}^{[2/2]}$
	S_2	0	$P_{R_1D}^{[1/1]}$	0	0	0
	S_3	$P_{R_1R_2}^{[2/2]}P_{R_1D}^{[0/2]}$	0	$\overline{P}_{R_1R_2}^{[2/2]}P_{R_1D}^{[1/2]}$	$P_{R_1R_2}^{[2/2]}P_{R_1D}^{[1/2]}$	$P_{R_1D}^{[2/2]}$
	S_4	0	$P_{R_2D}^{[1/1]}$	0	0	0
	S_5	0	0	$P_{R_2D}^{[1/1]}$	0	0
	S_6	$P_{R_2D}^{[0/2]}$	0	0	$P_{R_2D}^{[1/2]}$	$P_{R_2D}^{[2/2]}$
	S_7	0	$P_{SR_1}^{[0/1]}P_{SR_2}^{[0/1]}P_{SD}^{[0/1]}$	$P_{SR_1}^{[1/1]}P_{SR_2}^{[0/1]}P_{SD}^{[0/1]}$	$P_{SR_2}^{[1/1]}P_{SD}^{[0/1]}$	$P_{SD}^{[1/1]}$
	S_8	0	0	$P_{R_1R_2}^{[0/1]}P_{R_1D}^{[0/1]}$	$P_{R_1R_2}^{[1/1]}P_{R_1D}^{[0/1]}$	$P_{R_1D}^{[1/1]}$
	S_9	0	0	0	$P_{R_2D}^{[0/1]}$	$P_{R_2D}^{[1/1]}$
	S_{10}	0	0	0	0	0

Table 6.5: The single-step state-transition probability table.

each TS into actual time duration in seconds. Instead, we treat each TS as a unit in this chapter.

Note that, in this study, our system is considered to be assisted by two RNs and the channel is a Rayleigh-distributed block fading channel, where we assume that the instantaneous channel fading envelope remains unchanged throughout a single packet's transmission. In the Matlab simulations, in order to simplify the discussions, we assume that the positions of the four nodes in the cooperative network are fixed to: SN(100,100), RN_1(400,400), RN_2(800,300) and DN(1100,100) (as shown in Figure 6.7), where the coordinates of the nodes are given in the round bracket. According to the 'Frontier' of L_1 and L_2 as described in Section 6.3.2 and Table 6.4, we are able to identify the current system state and predict the next legitimate channel state. Hence, in order to expand our four-node cooperative network to a general n-node network, we have to find the relationship among the system state S, the number of nodes in the network and the 'Frontier' of L_1 and L_2 in a given state S. Firstly, in an n-node cooperative network assisted by our twin-layer HM scheme, the number of possible system states N_{State} is $N_{State} = \frac{n(n+1)}{2}$, as seen in Eq. (6.8). More specifically, we may record the 'Frontier' of L_1 and L_2 in each state S in a pair of $(N_{State} \times n)$-element matrices,

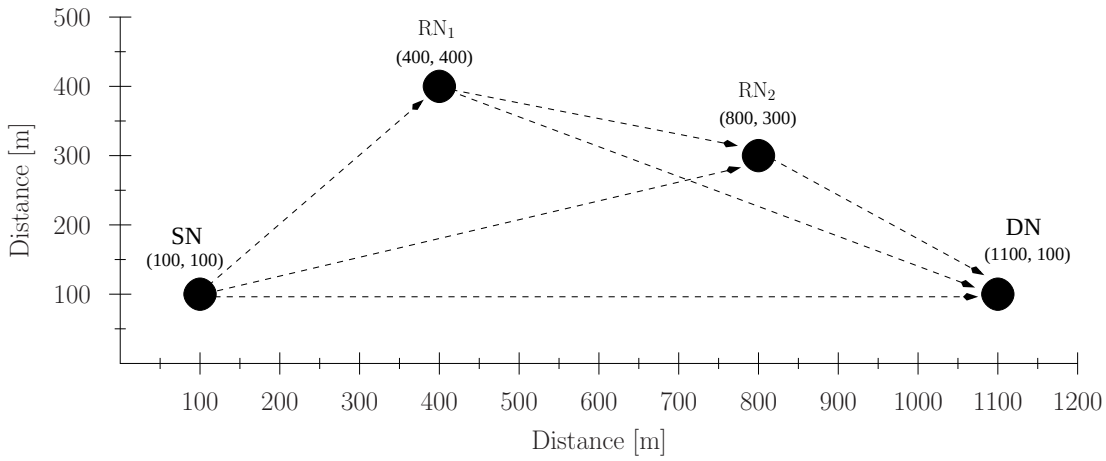

Figure 6.7: The actual hop structure of our four-node cooperative network used in theoretical analysis as well as simulations. The unit of the statistics shown in the figure is meter (m) for distance.

namely in S_{L1} and S_{L2}. Explicitly, the elements in these matrices can be expressed as:

$$S_{L1}(i_1, j_1) = \begin{cases} 1 & \text{if } j_1 = \left\lceil \dfrac{-1+\sqrt{1+8i_1}}{2} \right\rceil \\ 0 & \text{else} \end{cases} \tag{6.9}$$

$$S_{L2}(i_2, j_2) = \begin{cases} 1 & \text{if } j_2 = i_2 - \dfrac{j_1(j_1-1)}{2} \\ 0 & \text{else} \end{cases}, \tag{6.10}$$

where we have $i_1 \in \left\{1, 2, \ldots, \frac{n(n+1)}{2}\right\}$, $\{j_1, j_2\} \in \{1, 2, \ldots, n\}$, n is the number of nodes in the network, while $i_2 \in \left\{\frac{j_1(j_1-1)}{2}+1, \ldots, \frac{j_1(j_1+1)}{2}\right\}$. The element '1' in the matrix indicates that L_1 or L_2 appears at that node within the target state, whereas the rest of the elements will be set to '0'. Hence, when $n = 4$, the matrices S_{L1} and S_{L2} are given by:

$$S_{L1} = \begin{bmatrix} 1 & 0 & 0 & 0 \\ 0 & 1 & 0 & 0 \\ 0 & 1 & 0 & 0 \\ 0 & 0 & 1 & 0 \\ 0 & 0 & 1 & 0 \\ 0 & 0 & 1 & 0 \\ 0 & 0 & 0 & 1 \\ 0 & 0 & 0 & 1 \\ 0 & 0 & 0 & 1 \\ 0 & 0 & 0 & 1 \end{bmatrix}, \quad S_{L2} = \begin{bmatrix} 1 & 0 & 0 & 0 \\ 1 & 0 & 0 & 0 \\ 0 & 1 & 0 & 0 \\ 1 & 0 & 0 & 0 \\ 0 & 1 & 0 & 0 \\ 0 & 0 & 1 & 0 \\ 1 & 0 & 0 & 0 \\ 0 & 1 & 0 & 0 \\ 0 & 0 & 1 & 0 \\ 0 & 0 & 0 & 1 \end{bmatrix}, \tag{6.11}$$

where, for example, the $S_{L1}(10, 4) = 1$ indicates that at the system state S_{10}, L_1 has been successfully received at node 4 of the network, which is the DN node. Meanwhile, we define the

$(N_{state} \times N_{state})$-element single-step transition probability matrix of the ten-state four-node system as Tr, which is recorded in Table 6.5. Our method is generalized in **Algorithm 1** to n nodes. In order to simplify the analysis, the transmissions of L_1 and L_2 will be formulated separately. Therefore, a pair of flag-matrices are generated based on the matrices S_{L1} and S_{L2}, as follows:

$$Nr_{L1} = \begin{bmatrix} 1 & 2 & 2 & 2 & 2 & 2 & 2 & 2 & 2 & 2 \\ 0 & 1 & 0 & 2 & 0 & 0 & 2 & 0 & 0 & 0 \\ 0 & 0 & 1 & 0 & 2 & 2 & 0 & 2 & 2 & 2 \\ 0 & 0 & 0 & 1 & 0 & 0 & 2 & 0 & 0 & 0 \\ 0 & 0 & 0 & 0 & 1 & 0 & 0 & 2 & 0 & 0 \\ 0 & 0 & 0 & 0 & 0 & 1 & 0 & 0 & 2 & 2 \\ 0 & 0 & 0 & 0 & 0 & 0 & 0 & 0 & 0 & 0 \\ 0 & 0 & 0 & 0 & 0 & 0 & 0 & 0 & 0 & 0 \\ 0 & 0 & 0 & 0 & 0 & 0 & 0 & 0 & 0 & 0 \\ 0 & 0 & 0 & 0 & 0 & 0 & 0 & 0 & 0 & 0 \end{bmatrix}, \tag{6.12}$$

$$Nr_{L2} = \begin{bmatrix} 1 & 1 & 2 & 1 & 2 & 2 & 1 & 2 & 2 & 2 \\ 0 & 0 & 0 & 0 & 0 & 0 & 0 & 0 & 0 & 0 \\ 0 & 0 & 1 & 0 & 1 & 2 & 0 & 1 & 2 & 2 \\ 0 & 0 & 0 & 0 & 0 & 0 & 0 & 0 & 0 & 0 \\ 0 & 0 & 0 & 0 & 0 & 0 & 0 & 0 & 0 & 0 \\ 0 & 0 & 0 & 0 & 0 & 1 & 0 & 0 & 1 & 2 \\ 0 & 0 & 0 & 0 & 0 & 0 & 1 & 2 & 2 & 2 \\ 0 & 0 & 0 & 0 & 0 & 0 & 0 & 1 & 2 & 2 \\ 0 & 0 & 0 & 0 & 0 & 0 & 0 & 0 & 1 & 2 \\ 0 & 0 & 0 & 0 & 0 & 0 & 0 & 0 & 0 & 0 \end{bmatrix}. \tag{6.13}$$

These two matrices store the transmission status of the two layers. Let us consider the element $Nr_{L1}(i,j)$ for instance, where i denotes the current state and j represents the next state. When $i < 7$, $Nr_{L1}(i,j) = 0$ indicates that if the current state is S_i, the next state will not be S_j, while $Nr_{L1}(i,j) = 2$ implies that the transition from S_i to S_j is possible and the 'Frontier' of L_1 will change, whereas, $Nr_{L1}(i,i) = 1$ indicates that the 'Frontier' of L_1 will not change during the transition from S_i to S_j, where the counter of the transmission time of the current state will be increased by 1. When we have $7 \leqslant i \leqslant 10$, as mentioned in Section 6.3.2, either L_1 will not be transmitted in the network, or it may be received by the DN or alternatively it might be discarded by the system due to exceeding the maximum number of transmission attempts N_t, which depends on the transmission time instant counters. Hence, we have $Nr_{L1}(i,j) = 0$ for $7 \leqslant i \leqslant 10$. Whilst Nr_{L2} may be deemed to be similar to Nr_{L1} by comparing Eq. (6.12) and Eq. (6.13). Note that DN may only receive L_2 in the final state S_{10}. Therefore, the single-step state transition probability matrix for L_1 can be derived as the Hadamard product of Tr and $\overline{Nr_{L1}}$, which is formulated as:

$$Tr_{L1} = Tr \circ \overline{Nr_{L1}}\,, \tag{6.14}$$

where we have:

$$\overline{Nr_{L1}}(i,j) = \begin{cases} 1 & \text{if } Nr_{L1}(i,j) = 2 \\ Nr_{L1}(i,j) & \text{if } Nr_{L1}(i,j) \neq 2 \ . \end{cases} \tag{6.15}$$

Similarly, we have:

$$Tr_{L2} = Tr \circ \overline{Nr_{L2}} \ . \tag{6.16}$$

Let us now generate a pair of $(N_{state} \times N_t + 1)$ matrices, namely $M1$ (for transmitting L_1) and $M2$ (for transmitting L_2), where the pair of matrices $M1$ and $M2$ will be used to record the transmission and re-transmission among the state-transitions. Specifically, the elements in $M1$ may be expressed as:

$$M1 = \begin{bmatrix} \cdots & \cdots & \cdots & \cdots & \cdots & \cdots & \cdots & \cdots \\ m1(4,1) & m1(4,2) & \cdots & \cdots & \cdots & \cdots & m1(4,7) & m1(4,8) \\ \cdots & \cdots & \cdots & \cdots & \cdots & \cdots & \cdots & \cdots \\ m1(7,1) & \cdots & \cdots & \cdots & \cdots & \cdots & \cdots & \cdots \\ \cdots & \cdots & \cdots & \cdots & \cdots & \cdots & \cdots & \cdots \\ m1(10,1) & 0 & 0 & 0 & 0 & 0 & 0 & 0 \end{bmatrix} . \tag{6.17}$$

The element $m1(k,j)$ in the matrix $M1$ indicates the probability of receiving the information L_1 when the channel state is S_k, while the transmitter in S_k embarks on making the j_{th} attempt to forward the packet L_1. Assuming that we are at the element $m1(4,1)$ at a random TS, this element denotes the successful transmission probability from the previous state to state S_4. According to the transition rule defined in Figure 6.6, the state S_4 may be followed by S_4 or S_7. If we are at $m1(4,1)$ and assume that the next transition of Figure 6.6 is $S_4 \rightarrow S_4$, we may have:

$$m1(4,2) = m1(4,2) + m1(4,1) \times Tr_{L1}(4,4) \ , \tag{6.18}$$

which indicates that our probability $m1(4,1)$ will be added to $m1(4,2)$, where $Tr_{L1}(4,4)$ denotes the transition probability of L_1 based on the transition $S_4 \rightarrow S_4$. If reception failure occurs for six consecutive transitions, we arrive at $m1(4,7)$, where the element '7' indicates that in state S_4 the system makes a 7^{th} effort to forward L_1. If the maximum number of attempts at each node is $N_t = 7$, then $m1(4,7)$ may only have a single final transition. If successful, then we may have:

$$m1(7,1) = m1(7,1) + m1(4,7) \times Tr_{L1}(4,7) \ , \tag{6.19}$$

implying that the probability $m1(4,7)$ will be added to $m1(7,1)$ for the next transition. However, if the transition fails again, we arrive at:

$$m1(4,8) = m1(4,8) + m1(4,7) \times Tr_{L1}(4,4) \ , \tag{6.20}$$

noting that we have $N_t = 7$, while $m1(4,8)$ represents the failure probability of the 7^{th} attempt of S_4 traversing from $m1(4,1)$ to $m1(4,8)$. Hence, the probability $m1(4,8)$ should now be removed from the matrix $M1$, since no more attempts are available for S_4. Note that $m1(10,1)$ represents the probability that DN successfully received both L_1 and L_2 during the current TS. The

processing procedure of the probability matrix $M2$ for the transitions of L_2 is similar to that of L_1, but it is based on the single-transition probability matrix Tr_{L2}. Our theoretical analysis based on $M1$ and $M2$ is detailed in **Algorithm 1**, whilst the corresponding simplified flow-chart based on **Algorithm 1** is illustrated in Figure 6.8.

Again, for $j = N_t + 1$, the related transmission of L_1 or L_2 will be abandoned and the 'Outage' counter will be incremented. In **Algorithm 1**, we have $a = \frac{n(n-1)}{2}$ and $b = \frac{n(n+1)}{2}$, where n is the number of nodes in the cooperative network. Note that when the system's state is S_i ($i \leqslant a$), the system does not receive any information. Meanwhile, during the state-transition from $S_{(a+1)}$ to $S_{(b-1)}$, only L_1 of the twin-layer HM scheme is received successfully by the DN. The final state S_b indicates that both L_1 and L_2 have been successfully transmitted to DN.

The specific segment of **Algorithm 1** spanning from line 2 to 22 calculates the probabilities of all the possible state-transitions of the current TS based on the previous probability matrix $\overline{M1}$ as well as $\overline{M2}$, and the results are recorded in $M1$ and $M2$ as shown by line 3 to 4 of **Algorithm 1**. Note that, during the first TS, we set the probability of successfully receiving L_1 and L_2 to '1'. The segment of **Algorithm 1** spanning from line 23-27 is to calculate the number of TSs that the DN needs for receiving L_1 and L_2, which determines the associated normalized delay. We also mention that, every time we derive Delay_{L1} and Delay_{L2} of the current TS, we have to clear the elements in $M1$ and $M2$ which were used during the calculations, because these probabilities are assumed to represent the information that the DN has successfully received a packet. Hence, they should not remain in the matrix for the ensuing calculations of **Algorithm 1**. The segment of **Algorithm 1** ranging from 28-32 is to calculate the outage probabilities of L_1 and L_2 of the current TS. As we mentioned before, the element in $M1(i,j)$ represents the probability of the state S_i associated with transmitting L_1 for the j^{th} time. Therefore, all the elements in $M1(i,j)$ associated with $j = N_t + 1$ and $i \leqslant a$ represent the outage probability of L_1 during the current TS. Since the elements involved in the $Delay_{L1}$ calculations have been cleared, we may derive the outage probability of L_1 during the current TS, as shown in line 29. As for receiving L_2, since the DN may only receive L_2 in the system state S_b, all the elements in $M2(i,j)$ associated with $j = N_t + 1$ and $i \leqslant b-1$ may be considered to represent the outage probability of L_2. Note that since the elements involved in the $Delay_{L2}$ calculations have also been cleared, the outage probability of L_2 during the current TS may be derived as in line 31 of **Algorithm 1**. Similar by to the delay calculations, the matrix elements $M1$ and $M2$ involved in the outage probability calculations should also be cleared, because in cooperative communications this part of the information will be discarded by the system, when the transmission attempt counter exceeds N_t. Hence, the specific elements in $M1$ and $M2$, which are involved in the outage probability calculations should not remain in the matrix for the calculations during the next TS.

Additionally, when L_1 is discarded by the system, since the transmission attempt counter at the target transmitter exceeds N_t, the current state S_i will be forced to traverse to S_k, where $k \in \{a+1, \ldots, b\}$, if the 'Frontier' of L_2 at state S_k is the same as that at state S_i. Hence, all the elements in $M2(i,:)$ should be copied to $M2(k,:)$, while the elements in $M2(i,:)$ should be cleared after

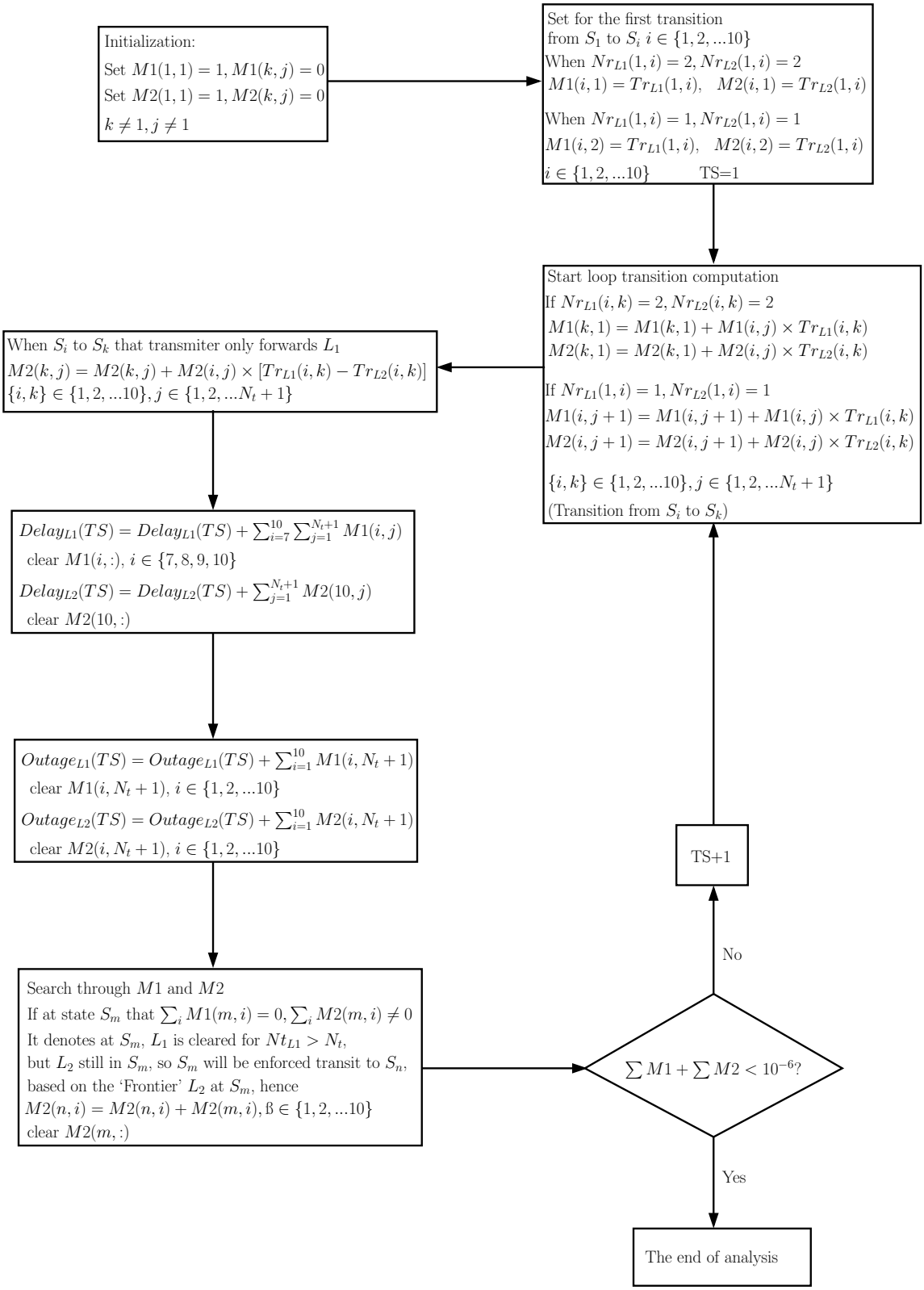

Figure 6.8: The flow-chart of the theoretical analysis of our HMOR algorithm aided four-node cooperative network of Figure 6.7. The flow-chart is based on **Algorithm 1**, where the related simulation parameters are listed in Table 6.2 and the system's schematic is described in Section 6.3.2.

Algorithm 1 Theoretical analysis

while sum($\overline{M1}$)+sum($\overline{M2}$)$> 10^{-6}$ **do**
  if TS==1 **then**
    $M1$(i,1+(Nr_{L1}(1,i)==1))= $1 \times Tr_{L1}$(1,i);
    $M2$(i,1+(Nr_{L2}(1,i)==1))= $1 \times Tr_{L2}$(1,i);
  else
    for i = 1:N_{state} **do**
      for j = 1:N_t **do**
        for k = 1:N_{state} **do**
          % L_1/L_2 broadcasted
          if $Nr_{L1}(i,k)$==2/$Nr_{L2}(i,k)$==2 **then**
            $M1$(k,1)=$M1$(k,1)+ $\overline{M1}$(i,j) $\times$ $Tr_{L1}(i,k)$;
            $M2$(k,1)=$M2$(k,1)+ $\overline{M2}$(i,j) $\times$ $Tr_{L2}(i,k)$;
          else if $Nr_{L1}(i,k)$==1/$Nr_{L2}(i,k)$==1 **then**
            $M1$(k,j+1)=$M1$(k,j+1) + $\overline{M1}$(i,j) $\times$ Tr_{L1}(i,k);
            $M2$(k,j+1)=$M2$(k,j+1) + $\overline{M2}$(i,j) $\times$ Tr_{L2}(i,k);
          end if
          % L_1 is broadcast while L_2 is reserved
          $M2$(k,j)=$M2$(k,j)+ $\overline{M2}(i,j) \times [Tr(i,k) - Tr_{L2}(i,k)]$;
        end for
      end for
    end for
  end if
  % calculate delay
  Delay$_{L1}$(TS) = Delay1(TS) + $\sum_{i=a+1}^{b} \sum_{j=1}^{N_t+1} M1(i,j)$;
  $M1$(i,:)=0, i$\in \{a+1,\ldots,b\}$
  Delay$_{L2}$(TS) = Delay2(TS) + $\sum_{j=1}^{N_t+1} M2(i=b,j)$;
  $M2$(i,:)=0, i=b
  % calculate outage
  Outage$_{L1}$(TS) = out1(TS)+ $\sum_{i=1}^{b} M1(i,N_t+1)$;
  $M1$(i,N_t)=0, i$\in \{1,\ldots,b\}$
  Outage$_{L2}$(TS) = out2(TS)+ $\sum_{i=1}^{b} M2(i,N_t+1)$;
  $M2$(i,N_t+1)=0, i$\in \{1,\ldots,b\}$
  % L_1 is outage and the probability is removed
  if sum($M1$(i,:))==0 &sum($M2$(i,:))$\neq$ 0, i$\in \{1,\ldots,a\}$ **then**
    Find state $S_k \in \{S_{a+1},\ldots,S_b\}$, which the 'Frontier' of L_2 is the same with that of state S_i
    $M2(k,:) = M2(k,:) + M2(i,:)$, $M2(i,:) = 0$
  end if
  % state appearance
  for i = 1: b **do**
    state$_{PMF}$(i) = state$_{PMF}$(i) + max(sum(M1(i,:)),sum(M2(i,:)))
  end for
  $\overline{M1} = M1$; clear $M1$
  $\overline{M2} = M2$; clear $M2$
  TS=TS+1
end while

this copying process, as shown in Line 33-37 of **Algorithm 1**. The probabilities of encountering the specific number of appearances for each state are computed in the segment of **Algorithm 1** spanning from line 38-41. Additionally, the segment ranging from Line 42-44 represents populating the 'new previous probability matrix' $\overline{M1}$ as well as $\overline{M2}$ and clearing $M1$ and $M2$ for the next TS. Note that the loop of **Algorithm 1** is controlled by the total probabilities of remaining in $\overline{M1}$ and $\overline{M2}$. When we have sum($\overline{M1}$)+sum($\overline{M2}$)$< 10^{-6}$, we assumed that the twin-layer information is successfully received by the DN, hence the loop will be terminated. Therefore, we may normalise the distribution of $Delay_{L1}$ and $Delay_{L2}$ as follows:

$$Delay_{L1}(i) = \frac{Delay_{L1}(i)}{\sum Delay_{L1}(i)}\,, \tag{6.21}$$

$$Delay_{L2}(j) = \frac{Delay_{L1}(j)}{\sum Delay_{L2}(j)}\,, \tag{6.22}$$

which are also known as the Probability Mass Function (PMF). According to $Delay_{L1}$ and $Delay_{L2}$, the Cumulative Distribution Function (CDF) of the delay of L_1 and L_2 may be expressed as:

$$CDF_{L1}(k) = \sum_{k}^{i=1} Delay_{L1}(i)\,, \tag{6.23}$$

$$CDF_{L2}(k) = \sum_{k}^{i=1} Delay_{L2}(i)\,. \tag{6.24}$$

Furthermore, the outage probability of L_1 and L_2 may be formulated as:

$$P_{outage}^{L1} = \sum Outage_{L1}(i)\,, \tag{6.25}$$

$$P_{outage}^{L2} = \sum Outage_{L2}(j)\,. \tag{6.26}$$

Hence, the throughput of the entire system may be characterized as:

$$\Phi = \frac{2 - P_{outage}^{L1} - P_{outage}^{L2}}{\sum state_{PMF}}\,, \tag{6.27}$$

where, the $state_{PMF}$ records the appearance of each state throughout the entire transmission process. Meanwhile, in the analysis, instead of assuming that all the nodes in the network has the same transmit power, we are going to find the optimized $\P_t$ for each node. Based on the discussions of Section 6.3.2, at each system state, the transmitter node is given. Explicitly, the node index χ of the transmitter in the n-node network may be inferred from the current state index i as follows:

$$\chi = \begin{cases} \left\lceil \frac{-1+\sqrt{1+8i}}{2} \right\rceil & \text{if } 1 \leqslant i \leqslant \frac{n(n-1)}{2} \\ i - \frac{n(n-1)}{2} & \text{if } \frac{n(n-1)}{2} + 1 \leqslant i \leqslant \frac{n(n+1)}{2}\,. \end{cases} \tag{6.28}$$

Therefore, the total power consumption E_{total} may be expressed as:

$$E_{total} = \sum_{i=1}^{N_{state}} state_{PMF}(i) \times \P_t(\chi)\,. \tag{6.29}$$

Hence, the average power consumption ($\overline{PWC}$) per packet may be formulated as:

$$\overline{PWC} = \frac{E_{total}}{2 - P_{outage}^{L1} - P_{outage}^{L2}} . \tag{6.30}$$

It may be observed that, $\overline{PWC}$ is jointly determined both by E_{total} as well as by outage probabilities P_{outage}^{L1} and P_{outage}^{L2}. During the analysis, our results were generated according to the specific value of N_t. At a specific value of N_t, we have set the $\P_t$ in the range spanning from 10^{-6} W to 0.1 W at all the three nodes in the network, namely at SN, RN_1 and RN_2, for the sake of finding the optimum $\P_t$ for each node for arriving at the minimum per-packet power consumption of $\overline{PWC}$. The search procedure conducted in two rounds. Firstly, we initialise all the nodes to a low power of $\P_t = 10^{-3}$ W and commence the search from RN_2, namely the node nearest to DN, and then moving backwards to SN. After the first round of the search, we may arrive at the optimized $\P_{tSN}^1$, $\P_{tRN1}^1$ and $\P_{tRN2}^1$. All these three values will be the initial values for round two. Then the search process will be repeated for another round. Therefore, we may find the optimized value of $\P_{tSN}$, $\P_{tRN1}$ and $\P_{tRN2}$ for deriving the minimum per-packet power consumption of $\overline{PWC}$. The $\P_{tSN}$, $\P_{tRN1}$ and $\P_{tRN2}$ values derived during the theoretical analysis will also be employed in the simulations for checking whether the results of our theoretical method match the simulation results. In order to provide fair comparisons between our scheme and the TOR scheme, all the results of Section 6.5 will be based on the optimized per-packet power $\overline{PWC}$.

6.4 System Simulations

The flow chart of the simulation for the single packet's transmission is illustrated in Figure 6.9, which is detailed in **Algorithm 2**. **Algorithm 2** illustrates the schedule of our simulations in the context of the cooperative communication system considered. To be more specific, the number of sample-packet transmitted is set to $N_{ST} = 10^5$. As discussed in Section 6.3.2, for every specific state of Table 6.4, the twin-layer information stream of L_1 and L_2 will have reached a specific position in the cooperative networks. Given the current state, according to the transmission rule defined in Figure 6.6 of Section 6.3.2, we activate the corresponding transmission for the following TS. Then, based on the FER versus SNR performance characterized in Section 6.3.1, the success or failure status of L_1 and L_2 during the current transmission may be evaluated. When deciding whether the node is capable of successfully receiving the packet or not, we will generate a random variable $\nu \in u(0,1)$, where $u(0,1)$ represent the uniform distribution within the range $[0,1]$. Explicitly, if we have $\nu \leqslant FER_{target}$, the status of the target node would be considered to be 'failed'. By contrast, if $\nu > FER_{target}$, the transmission between the transmitter and the target node would be successful. Therefore, once we identified the transmission success/failure status based on the current state, the next state to be encountered by our transmissions regime may be predicted, as shown in the segment spanning from line 4 to 8 in **Algorithm 2**.

The segment ranging from line 8 to 14 records the number of TSs the L_1 and L_2 streams required to be conveyed to the DN. Furthermore, line 16 of **Algorithm 2** records the number of events that

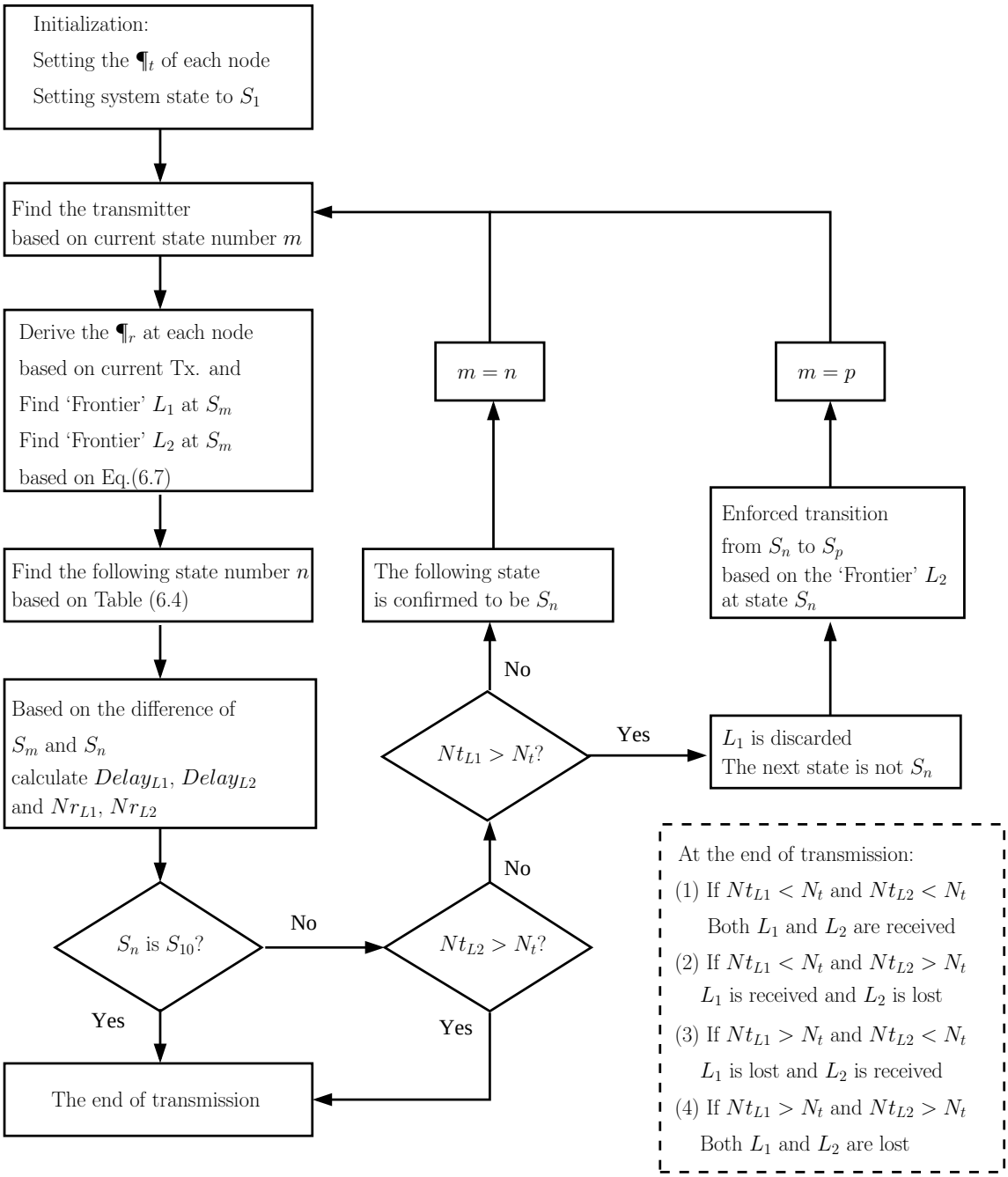

Figure 6.9: The flow-chart of a single packet's transmission in our HMOR algorithm aided four-node cooperative network of Figure 6.7. The flow-chart is based on **Algorithm 2**, where the related simulation parameters are listed in Table 6.2 and the system's schematic is described in Section 6.3.2.

Algorithm 2 Theoretical analysis

for i=1:simulation-time **do**
  current state $S_{current}$ = S_1
  while Brake-flag==0 **do**
    Generate channel fading based on $S_{current}$.
    Derive the instantaneous SNR at each node based on current transmitter. Then, find the correspond FER of receiving L_1 and L_2 at each receiver candidate.
    Judging the next state S_{next} based on Section 6.3.1 and 6.3.2
    Setting up the new transmitter.
    % calculate delay
    if $S_{next} > S_a \& S_{current} \leqslant S_a$ **then**
      Delay_{L_1}(TS)=Delay_{L_1}(TS)+1
    end if
    if $S_{next} = S_{10}$ **then**
      Delay_{L_2}(TS)=Delay_{L_2}(TS)+1
    end if
    % record the times each states appeared
    $State(state_{num}) = State(state_{num}) + 1$
    % calculate transmission time
    if Frontier of L_1 unchanged & transmitter is forwarding L_1 **then**
      $N_{t_{L_1}} = N_{r_{L_1}} + 1$
    else
      $N_{t_{L_1}} = 1$
    end if
    if Frontier of L_2 unchanged & transmitter is forwarding L_2 **then**
      $N_{t_{L_2}} = N_{t_{L_2}} + 1$
    else if Frontier of L_2 unchanged & transmitter is not forwarding L_2 **then**
      $N_{t_{L_2}} = N_{t_{L_2}}$
    else
      $N_{t_{L_2}} = 1$
    end if
    % calculate outage
    if $N_{t_{L_2}} > N_t \& out_{L2} == 0$ **then**
      $out_{L_{2count}} = out_{L_{2count}} + 1$
      $out_{L2} = 1$
    end if
    if $N_{t_{L_1}} > N_t \& S_{next} \leqslant S_a$ **then**
      $out_{L_{1count}} = out_{L_{1count}} + 1$
      Forcing the S_{next} to transfer to $S_{next} \in \{S_{(a+1)}, S_{(a+2)}, \ldots, S_{(b-1)}\}$ based on the current position of L_2 (shown in Section 6.3.2).
    end if
    % end the loop
    if $S_{current} = S_b$ **then**
      Brake-flag=1; break
    end if
    if $S_a < S_{current} < S_b \& out_{L2} == 1$ **then**
      Brake-flag=1; break
    end if
    $S_{current}$ = S_{next}
    TS = TS+1
  end while
end for

each state occurred during the entire transmission process, which will be used for calculating the power consumption of the entire system. The segment ranging from line 17 to 29 of **Algorithm 2** counters the retransmission attempts at the current transmitter. If the '*Frontier*' of L_1 remains unchanged, the value of the counter $N_{r_{L_1}}$ will be incremented by one, otherwise, the $N_{r_{L_1}}$ counter will be set to one. If the '*Frontier*' of L_2 remains unchanged and the transmitter is transmitting L_2, the value of $N_{r_{L_2}}$ will be incremented by one. However, if the '*Frontier*' of L_2 remains unchanged, but the transmitter is not going to transmit L_2 during the following TS, the value of $N_{r_{L_2}}$ will be kept unchanged, otherwise, the $N_{r_{L_2}}$ counter will be set to one. Recall that, the decision concerning the transmitter's specific action and the particular choice of information that the transmitter is going to forward during the next TS were defined in Section 6.3.2. The segment spanning from line 30 to 38 is included in order to decide whether the system has to discard any information. When we have $N_{r_{L_2}} > N_r$, the system will discard L_2, the transmission attempt counter $out_{L_{2count}}$ will be incremented by one, and the flag out_{L2} will be reset to one. As for $N_{r_{L_1}}$, if it exceeds the maximum tolerable number of transmission attempts N_t, while the DN still does not receive anything ($S_{next} \leqslant S_a$), then the new state will have to obey $S_{next} \in \{S_{(a+1)}, S_{(a+2)}, \ldots, S_{(b-1)}\}$, which depends on the '*Frontier*' of L_2. Note that in this situation, the actions of **Algorithm 2** in the segment spanning from line 8 to 11 will not be activated during the next loop. Hence, L_1 will be discarded when the entire loop ends. Furthermore, lines 39 to 45 are related to testing the conditions under which to terminate the loop. Finally, lines 46-47 update the system's state and increment the TS counter for the next loop.

Whist the calculation of the system characteristics carried out during the simulations is different from that in the theoretical analysis, the distributions of $Delay_{L1}$ and $Delay_{L2}$ are the same as those in Eq. (6.21) and Eq. (6.22), respectively. By the same token, CDF_{L1} and CDF_{L1} are also the same as those in Eq. (6.23) and Eq. (6.24). The simulation-based outage probability of L_1 and L_2 is given by:

$$P_{outage}^{L1} = \frac{out_{L_{1count}}}{N_{ST}}, \tag{6.31}$$

$$P_{outage}^{L2} = \frac{out_{L_{2count}}}{N_{ST}}, \tag{6.32}$$

which are different from those in Eq. 6.25 and Eq. 6.26, where again, the total number of packets simulated $N_{ST} = 10^5$. Therefore, the throughput of the system may be expressed as:

$$\Phi = \frac{2 \times N_{ST} - out_{L_{1count}} - out_{L_{2count}}}{TS_{total}}, \tag{6.33}$$

where the total power consumption 'E_{total}' while transmitting N_{ST} packets is the same as that defined in (6.29). The simulation-based average packet-power consumption $\overline{PWC}$ may be formulated as:

$$\overline{PWC} = \frac{E_{total}}{\left(2 - P_{outage}^{L1} - P_{outage}^{L2}\right) \times N_{ST}}. \tag{6.34}$$

6.5 Performance Analysis

In this section, we first compare our twin-layer TTCHM-16QAM aided OR scheme to the TOR scheme. Furthermore, we also compare the performance of a four-node network to a ten-node network, both of them employing our cooperative communication protocol described in Section 6.3.2. Note that in order to make a fair comparison of the systems, the transmit power $\P_t$ of each node has been optimized for achieving the minimum $\overline{PWC}$ for the given value of N_t.

6.5.1 Comparison to Traditional Opportunistic Routing

The TOR scheme has been lavishly documented, for example in [129, 136]. Figure 6.10 represents the optimized $\P_t$ of each single node in the four-node cooperative network. It may be observed from Figure 6.10 that upon increasing N_t, the optimized power $\P_t$ exhibits a slight reduction tendency upto $N_t = 6$, but for $N_t > 6$, it will remain near-constant. Recall that in our cooperative communication protocol, the TTCM aided twin-layer HM-16QAM packet may become partitioned during its transmission. Hence, the optimized power $\P_t$ of each single node of our HMOR scheme is the same as those of the TOR scheme transmitting TTCM coded 4QAM signal packets. Consider $N_t = 7$ for instance, where the optimized power $\P_t$ of each node of our twin-layer HM-16QAM OR and of the TTCM coded 4QAM TOR are:$\P_{tSN} = 0.2512$ mW, $\P_{tRN1} = 0.1585$ mW and $\P_{tRN2} = 0.1$ mW. However, when using the TOR scheme to transmit the TTCM aided twin-layer HM-16QAM packets, we have higher transmit power values, namely, $\P_{tSN} = 3.98$ mW, $\P_{tRN1} = 2.51$ mW and $\P_{tRN2} = 1.58$ mW, when $N_t = 7$. Therefore, Figure 6.10 indicates that, the HMOR scheme is capable of substantially reducing the power $\P_t$ of each single node in the network.

The optimized per-packet power consumption $\overline{PWC}$ of the four-node cooperative communication network is shown in Figure 6.11. The curves seen in Figure 6.11 show the minimum $\overline{PWC}$ that the specific OR scheme may achieve for a given number of transmission attempts of N_t. It may be observed that, for $N_t = 7$, the minimized $\overline{PWC}$ of our four-node based TTCM aided twin-layer HM-16QAM scheme becomes $\overline{PWC}_{min} \approx 0.74$ mW, while $\overline{PWC}_{min}$ of the TOR transmitting TTCM aided 4QAM packets is only slightly lower than that of HMOR scheme, which is about 0.71 mW. However, for $N_t = 7$, the minimum $\overline{PWC}$ that the TOR scheme transmitting TTCM aided HM-16QAM packets may achieve is 12.37 mW.

The throughput of the four-node cooperative network of Figure 6.7 is represented in Figure 6.12. The simulation results are based on the statistics illustrated in Figure 6.10 and Figure 6.11. As expected upon increasing N_t, the throughput of all the schemes is reduced. Based on the minimized average per-packet power-consumption $\overline{PWC}$ and optimized power $\P_t$ of every node in the network, the throughput of our HMOR scheme becomes similar to that of the TOR scheme transmitting TTCM coded 4QAM packets, which is $\Phi \approx 0.22$ $[packet/TS]$ for $N_t = 7$. By contrast, the throughput Φ of the TOR scheme transmitting TTCM aided twin-layer HM-16QAM packets is about 0.41 $[packet/TS]$ for $N_t = 7$. However, the price we paid for the increased throughput is an

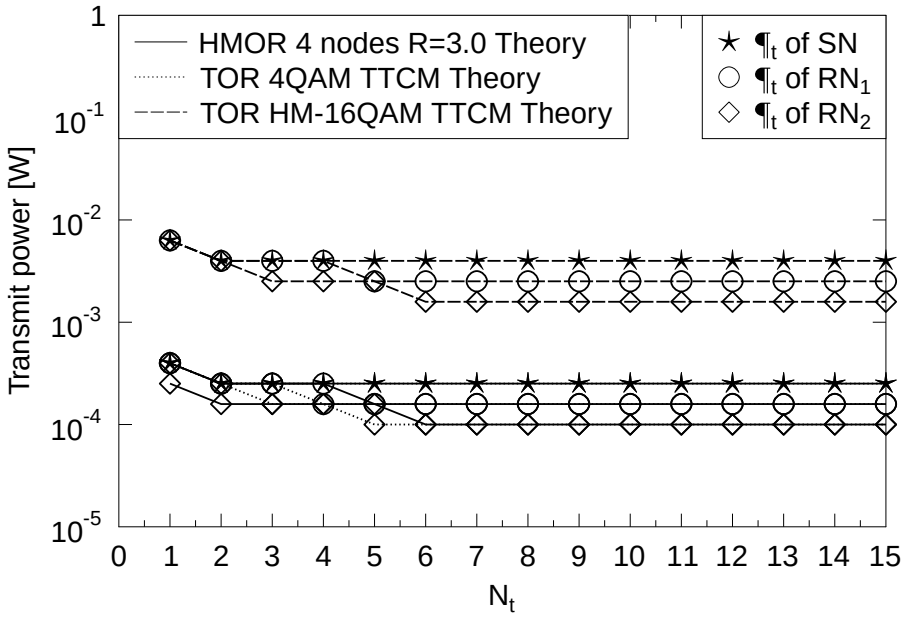

Figure 6.10: The optimized power $\P_t$ of the SN, RN_1 and RN_2 versus the maximum number of transmission attempts N_t of the four-node cooperative communication network considered. The related simulation parameters are listed in Table 6.2, while the system's schematic is described in Section 6.3.2 and the network's topology is seen in Figure 6.7.

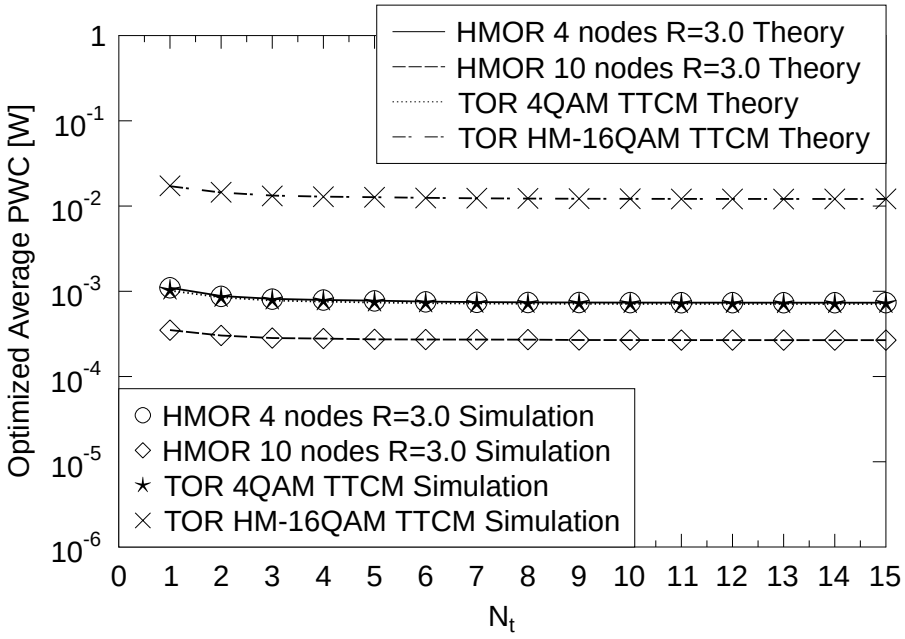

Figure 6.11: The optimized average per-packet power-consumption $\overline{PWC}$ versus the maximum number of transmission attempts N_t of our four-node cooperative communication network. The related simulation parameters are listed in Table 6.2, while the system's schematic is described in Section 6.3.2 and the network's topology is seen in Figure 6.7.

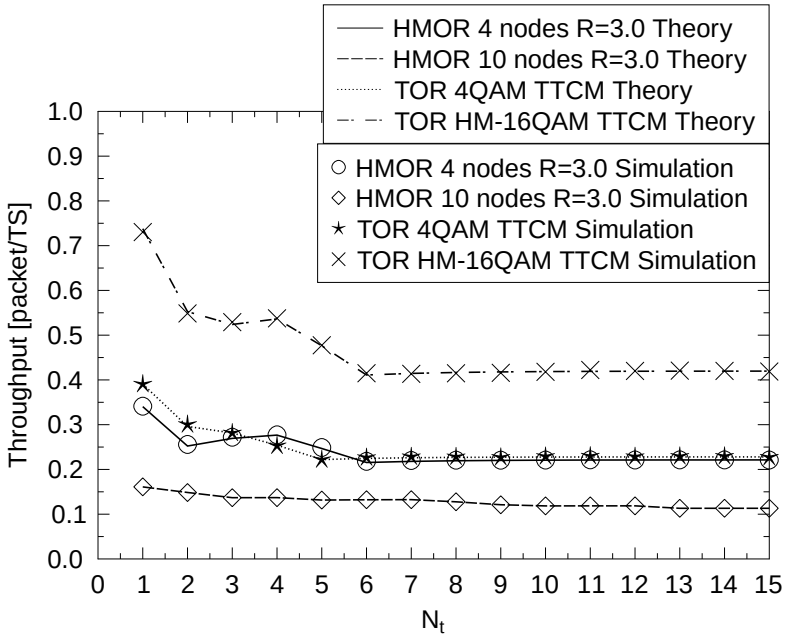

Figure 6.12: The throughput versus the maximum number of transmission attempts N_t of four-node cooperative communication network. The related simulation parameters are listed in Table 6.2, while the system's schematic is described in Section 6.3.2 and the network's topology is seen in Figure 6.7.

about ten times higher power $\P_t$ at each single node of the entire network, as shown in Figure 6.10. Note that, if we set $\P_{tSN} = 3.98$ mW, $\P_{tRN1} = 2.51$ mW and $\P_{tRN2} = 1.58$ mW, the throughput of our HMOR scheme transmitting TTCM aided twin-layer HM-16QAM packets will be increased to 0.894 $[packet/TS]$. In a nutshell, we focussed our attention on the attainable system performance for $N_t = 7$, where the related results portrayed in Figure 6.10 to Figure 6.12 are summarized in Table 6.6.

Code	**TTCM**				
Modulation	4QAM, HM-16QAM				
N_t	7				
Positions of the nodes	SN(100,100), RN_1(400,400), RN_2(800,300), DN(1000,100)				
	$\P_t^{SN}$ mw	$\P_t^{RN_1}$ mw	$\P_t^{RN_2}$ mw	Opt. $\overline{PWC}$ mw	Φ [packet/TS]
HMOR	0.2512	0.1585	0.1000	0.7423	0.2200
TOR 4QAM	0.2512	0.1585	0.1000	0.7133	0.2279
TOR HM-16QAM	3.981	2.512	1.585	12.365	0.4136
HMOR	3.981	2.512	1.585	–	0.894

Table 6.6: The simulation results summarized from Figure 6.10 to Figure 6.12. The related simulation parameters are listed in Table 6.2, while the system's schematic is described in Section 6.3.2 and the network's topology is seen in Figure 6.7.

Figure 6.13 illustrates the outage probability P_{outage} of both our HMOR scheme and that of the TOR scheme. Since HMOR scheme may partition the TTCM aided twin-layer HM-16QAM

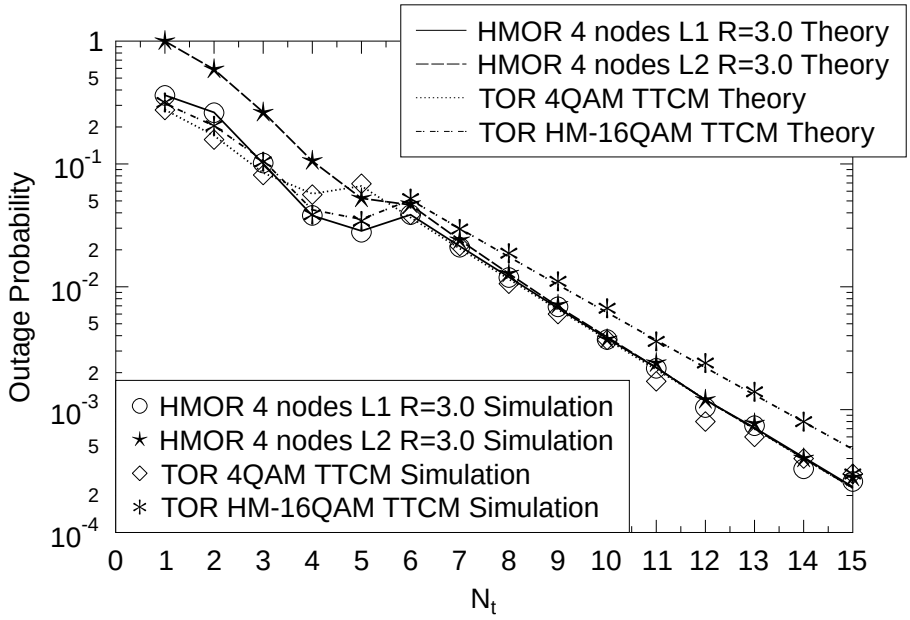

Figure 6.13: The outage probability versus the number of maximum transmission attempts of each node N_t based on different OR schemes. The statistics are all based on the minimized $\overline{PWC}$ for each scheme at a given value of N_t. The related simulation parameters are listed in Table 6.2, while the system's schematic is described in Section 6.3.2 and the network's topology is seen in Figure 6.7.

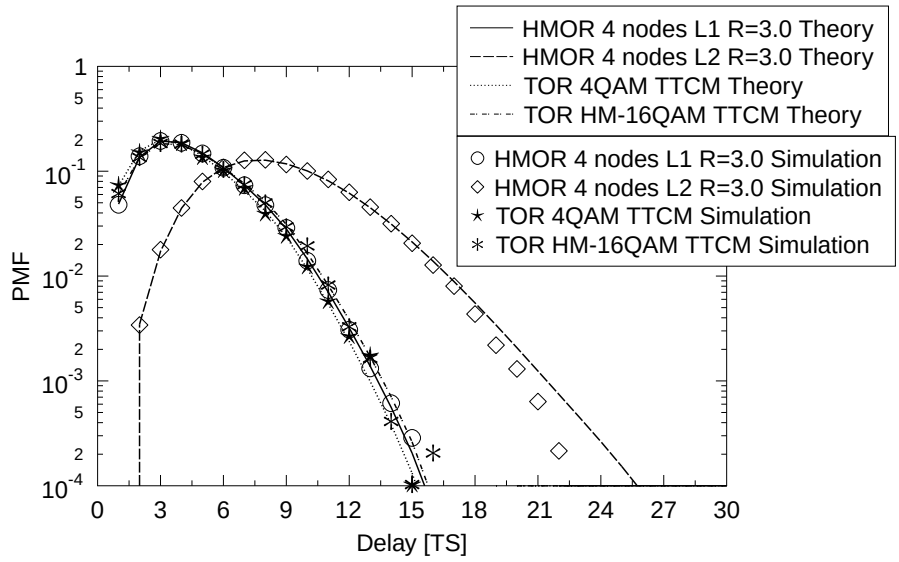

Figure 6.14: The PMF of the four-node cooperative network's delay based on different OR schemes. The statistics are all based on the minimized $\overline{PWC}$ for each scheme given $N_t = 7$. The related simulation parameters are listed in Table 6.2, while the system's schematic is described in Section 6.3.2 and the network's topology is seen in Figure 6.7.

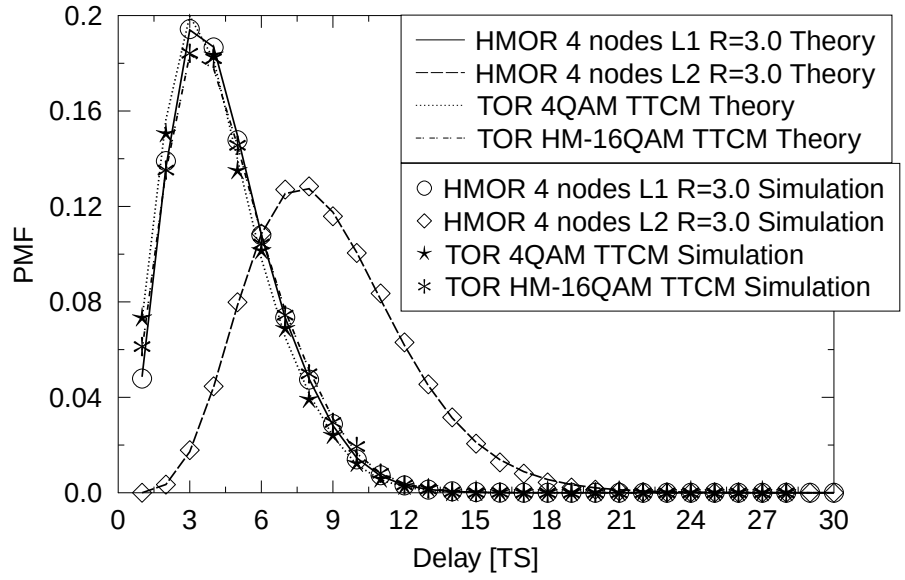

(a) PMF of the delay for $N_t = 7$ based on Figure 6.14

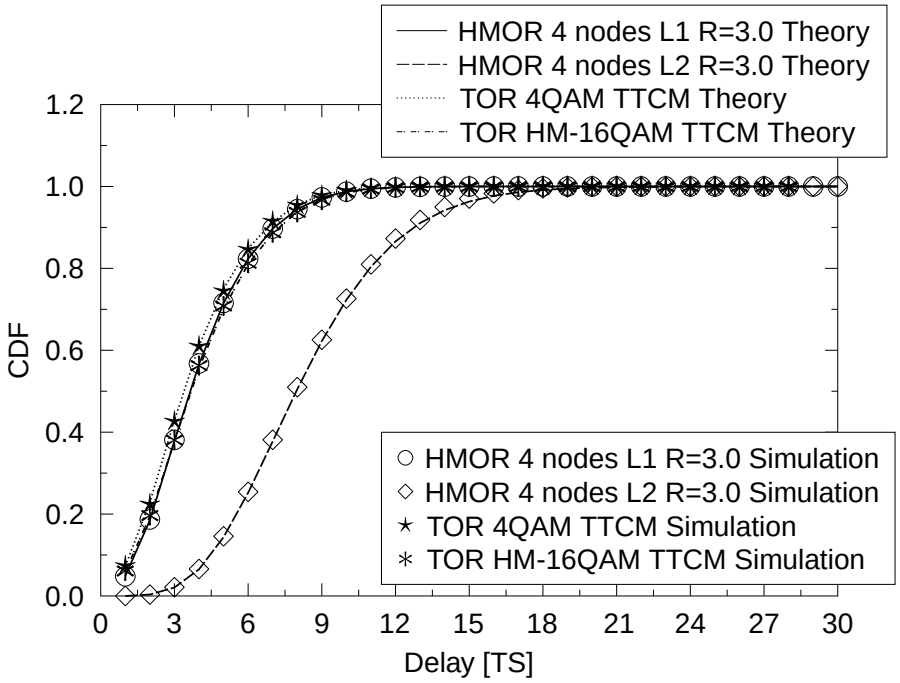

(b) CDF of the delay for $N_t = 7$

Figure 6.15: The PMF and the CDF of the four-node cooperative network's delay based on different OR schemes. The statistics are all based on the minimized $\overline{PWC}$ for each scheme given $N_t = 7$. The related simulation parameters are listed in Table 6.2, while the system's schematic is described in Section 6.3.2 and the network's topology is seen in Figure 6.7.

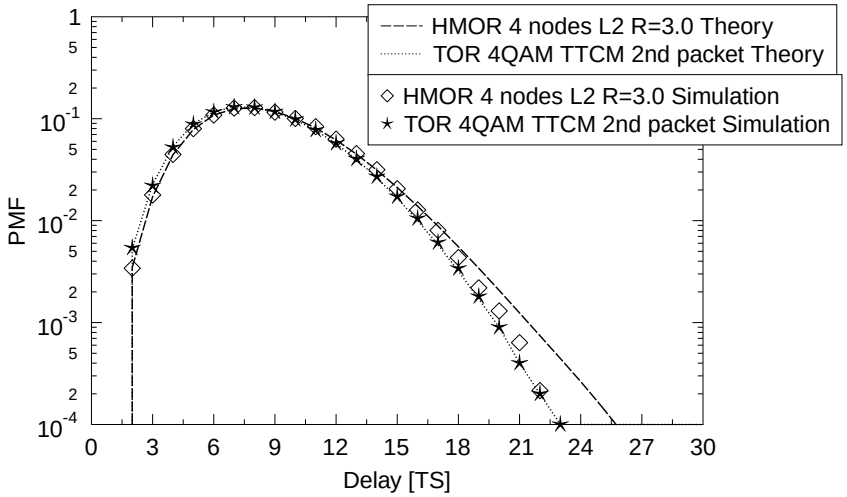

Figure 6.16: The PMF of the four-node cooperative network's delay based on different OR schemes. The statistics are all based on the minimized $\overline{PWC}$ for each scheme given $N_t = 7$. The related simulation parameters are listed in Table 6.2, while the system's schematic is described in Section 6.3.2 and the network's topology is seen in Figure 6.7.

signal into two packets during its transmission, we have to define a pair of outage probabilities, namely P_{outage}^{L1} and P_{outage}^{L2}. It may be observed that upon increasing the number of transmission attempts N_t, the outage probabilities of all the three schemes characterized in Figure 6.13 will be reduced. We also have to mention that the fluctuates of the curves between $N_t = 2$ to $N_t = 6$ in Figure 6.12, Figure 6.13 and Figure 6.19 due to the reduction of the transmission power at each RN, as shown in Figure 6.10. Given the minimized per-packet power-consumption $\overline{PWC}$, when considering $N_t > 6$, the outage probabilities of both L_1 and L_2 of our twin-layer OR scheme, as well as that of the TOR transmitting TTCM aided twin-layer HM-16QAM packets and that of the TOR transmitting single-layer TTCM coded 4QAM packets becomes similar. Figure 6.14 and Figure 6.15a illustrate the PMF of our HMOR scheme's delay for $N_t = 7$. By contrast, the CDF of our HMOR scheme's delay and that of the TOR scheme is represented in Figure 6.15b for $N_t = 7$. Again, all the results shown in Figure 6.15b are based on the minimized $\overline{PWC}$ for each specific OR scheme. It may be observed that the CDF of $Delay_{L1}$ of our twin-layer OR scheme is similar to that of the two traditional schemes. Quantitatively, 99.5% of the packets may be received with a delay of 11 TSs or less. But as shown in Figure 6.10, Figure 6.11 and Figure 6.12, in order to transmit the TTCM coded twin-layer HM-16QAM packets at a lower $\overline{PWC}$ as well as at a reduced $\P_t$ of each node in the network, the price paid by our HMOR scheme is the extended delay of receiving L_2 of the twin-layer HM-16QAM packets at DN. Explicitly, 96.3% of L_2 of the twin-layer HM-16QAM packets may be received with a delay of 15 TSs or less.

Figure 6.17 illustrates our comparison between the TOR algorithm during receiving two packets and of the HMOR algorithm receiving L_2. The system considered is the four-node cooperative wireless *ad hoc* network shown in Figure 6.7. The maximum number of transmission attempts for each node of the cooperative network is set to $N_t = 7$. Note that the power $\P_t$ of each node of the

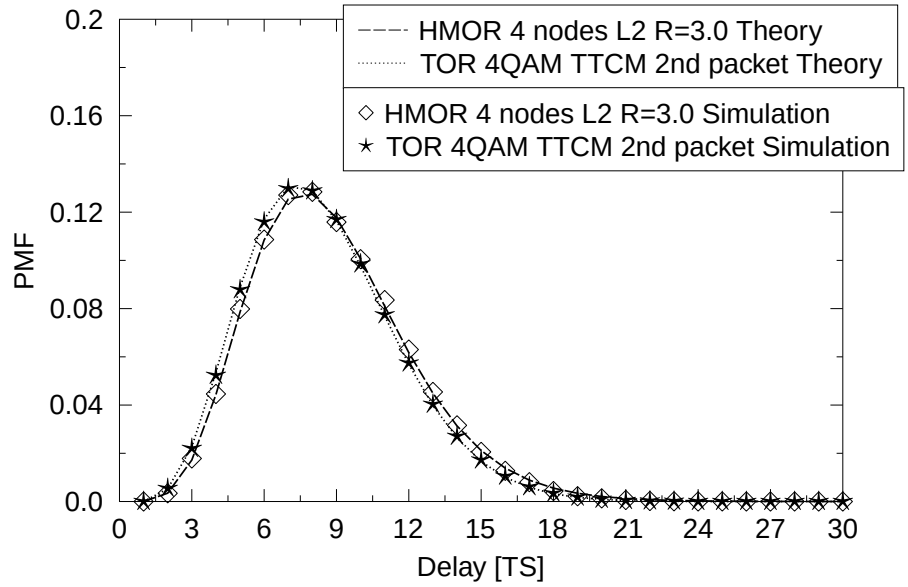

(a) PMF of the delay for $N_t = 7$ based on Figure 6.16

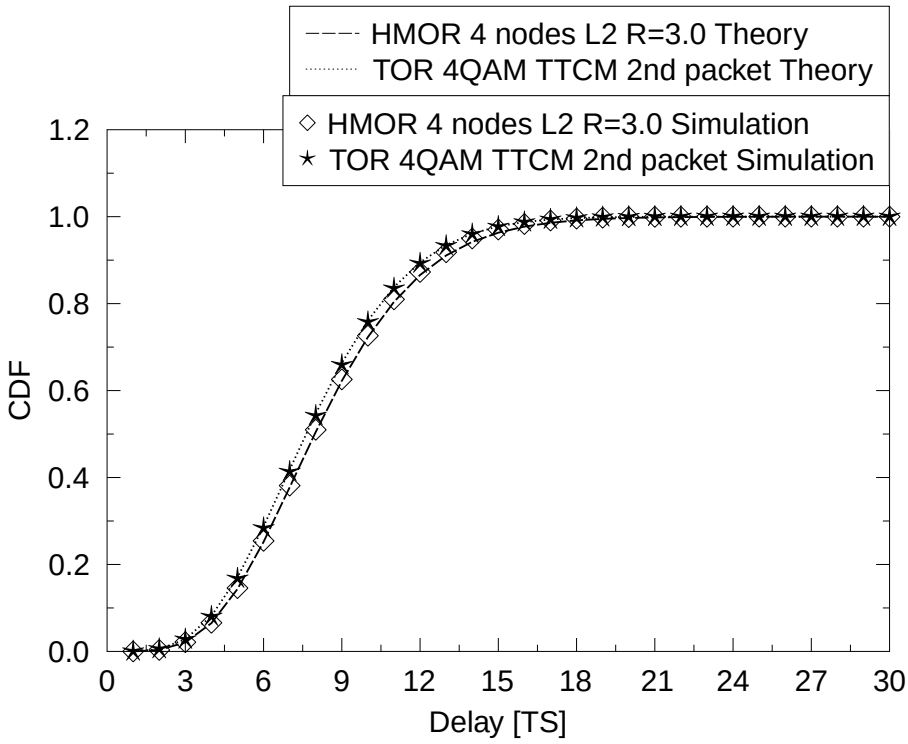

(b) CDF of the delay for $N_t = 7$

Figure 6.17: The PMF and the CDF of the four-node cooperative network's delay based on different OR schemes. The statistics are all based on the minimized $\overline{PWC}$ for each scheme given $N_t = 7$. The related simulation parameters are listed in Table 6.2, while the system's schematic is described in Section 6.3.2 and the network's topology is seen in Figure 6.7.

Code	**TTCM**	
N_t	7	
Constraints on Delay	95% plus of packets received	
Constraints on $\P_t$	The $\overline{PWC}$ of all schemes are minimized	
	Outage Probability P_{outage}	Delay (TS)
HMOR L_1	0.0210	9 (97.33%)
HMOR L_2	0.0239	15 (97.04%)
TOR 4QAM	0.0215	8 (95.36%)
TOR 4QAM (2nd packets)	–	15 (97.66%)
TOR HM-16QAM	0.0296	9 (96.67%)

Table 6.7: The summarized simulation results from Figure 6.13 to Figure 6.17. The related simulation parameters are listed in Table 6.2, while the system's schematic is described in Section 6.3.2 and the network's topology is seen in Figure 6.7.

HMOR algorithm associated with the HM ratio of $R_1 = 3.0$ is similar to that of the TOR algorithm transmitting 4QAM TTCM packets. It may be observed in Figure 6.17b that 97.7% of the second packet of the TOR algorithm transmitting 4QAM TTCM coded packets will be received with a maximum delay of 15 TSs. This is similar to that of $Delay_{L2}$ of our HMOR algorithm associated with the HM ratio of $R_1 = 3.0$. The related results are summarized in Table 6.7.

Additionally, in Figure 6.10 to Figure 6.17, the legend 'Theory' indicates that the results based on our theoretical analysis in **Algorithm 1**, while the legend 'Simulation' indicates that the results are from simulation method outlined in **Algorithm 2**. According to the above figures, it can be observed that our simulation results based on **Algorithm 2** closely match the theoretical results of **Algorithm 1**, which confirm each other.

6.5.2 Increasing the Network Size

In Figure 6.11 and Figure 6.12, we have also presented the performance of a ten-node cooperative network consisting of eight RNs using our HMOR scheme for transmitting TTCM-coded twin-layer HM-16QAM packets. The position of the nodes as well as the related optimized power $\P_t$ ($N_t = 7$) is shown in Table 6.8. Note that the positions of the RN nodes are uniformly distributed between the SN to DN node.

It can be observed from Figure 6.11 that the minimized per-packet power consumption $\overline{PWC}$ of the ten-node network using our HMOR scheme for transmitting twin-layer HM-16QAM packets is even lower than that of the four-node network using the same communication protocol, which is $\overline{PWC} = 0.271$ mW. When the number of relays in the network that was activated for assisting the transmissions is increased, the power $\P_t$ may be reduced as a benefit of the lower distance between the neighbouring nodes. Note that in the ten-node network of Figure 6.18, the eight RNs are uniformly placed between the SN to DN link. However, Figure 6.12 shows that based on the minimized per-packet power consumption $\overline{PWC}$ associated with a specific N_t, the throughput of

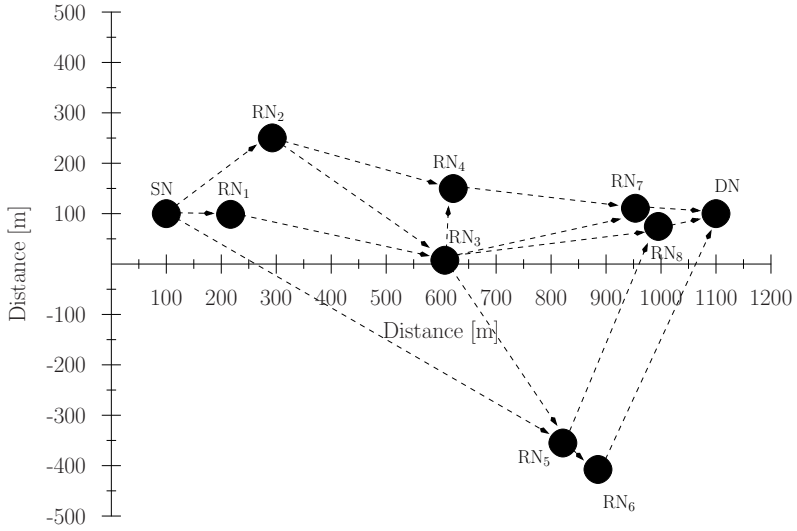

Figure 6.18: The actual hop structure of our ten-node cooperative network used in the theoretical analysis as well as in the simulations. The unit of the distance shown in the figure is meter (m). The positions of the nodes are shown in Table 6.8. Note that only part of the links are displayed for the clear presentation of the figure.

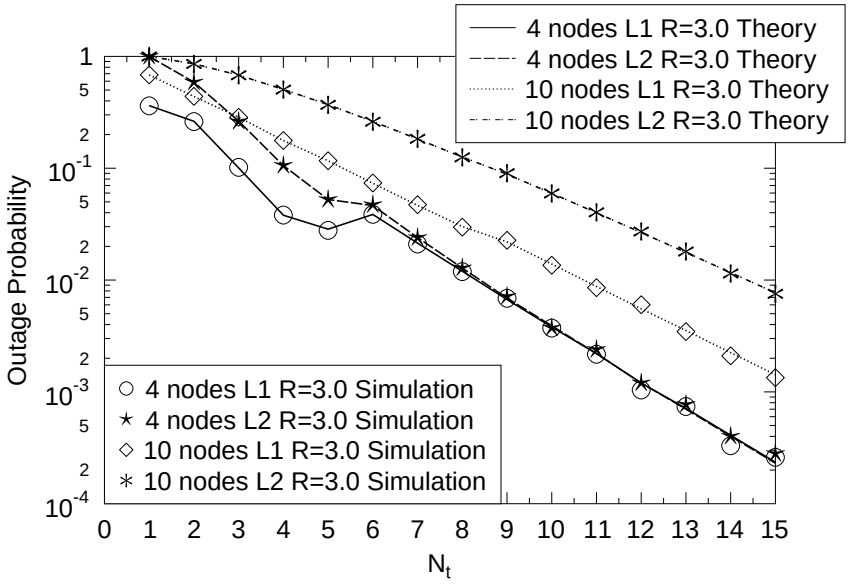

Figure 6.19: The outage probability of the cooperative network based on our HMOR schemes versus the maximum transmission attempts N_t. TTCM aided HM-16QAM signals are transmitted and the HM ratio is $R_1 = 3.0$. The statistics are all based on the minimized $\overline{PWC}$ for each scheme with target value of N_t. The related simulation parameters are listed in Table 6.2 and the system's schematic is described in Section 6.3.2, while the four-node network's topology are seen in Figure 6.7 and the ten-node network's topology is seen in Figure 6.18.

Nodes	Position [m]	$\P_t$ [mw]	Nodes	Position [m]	$\P_t$ [mw]
SN	(100, 100)	0.010	RN_1	(216.9, 98.6)	0.100
RN_2	(292.8, 250.3)	0.100	RN_3	(606.7, 7.5)	0.040
RN_4	(622.0, 149.8)	0.063	RN_5	(821.4, -355.1)	0.016
RN_6	(885.3, -407.6)	0.025	RN_7	(953.4, 110.7)	0.010
RN_8	(995.1, 74.6)	0.016	DN	(1100, 100)	–

Table 6.8: The table of the node positions and the related optimized transmission power $\P_t$ of the ten-node cooperative networks. The related simulation parameters are listed in Table 6.2, while the system's schematic is described in Section 6.3.2 and the network's topology is seen in Figure 6.18.

the ten-node network using our HMOR scheme also becomes lower than that of the four-node network, which is about $\Phi \approx 0.132$ $[packet/TS]$ for $N_t = 7$.

Figure 6.19 indicates that based on the minimized per-packet power consumption $\overline{PWC}$ and for a specific $N_t < 7$, the outage probabilities P_{outage}^{L1} and P_{outage}^{L2} of the ten-node system are consistently higher than those of the four-node system. By contrast, for higher N_t values their outage probabilities are similar to each other. The reason for this trend is that the optimized power $\P_t$ of the ten-node system becomes even lower than that of the four-node system. However, the reduced power $\P_t$ increases the outage probabilities, especially for L_2. Nonetheless, having a sufficiently high number of maximum transmission attempts N_t, the outage probability can indeed be reduced. Figure 6.20 (Figure 6.21a) and Figure 6.21b compares the PMF and the CDF of both $Delay_{L1}$ and $Delay_{L2}$ of the ten-node system to that of the four-node system, when both of the systems operate at $\overline{PWC}$ minimized according to $N_t = 7$. It may be observed that when the number of nodes in the network is increased, and minimized per-packet power consumption $\overline{PWC}$ is used for the entire system, this typically increases the delay of the DN receiving L_1 and L_2 of the twin-layer HM-16QAM packets scheme. When $N_t = 7$, 96.9% of the L_1 packets may be received by the ten-node network within a maximum of 12 TSs delay. By contrast, it may take 19 TSs for the DN to receive L_2. In conclusion, the related simulation results are summarized in Table 6.9.

6.6 Summary and Conclusions

In this chapter, a cooperative network transmitting layered packets has been proposed. We firstly characterized the FER versus SNR performance of receiving both L_1 and L_2 of the TTCM coded twin-layer HM-16QAM signals, as well as that of receiving TTCM coded 4QAM signals for transmission over both AWGN and Rayleigh-distributed block fading channels. Secondly, the cooperative communication protocol of our HMOR scheme of Section 6.3 has been illustrated. Furthermore, we detailed our theoretical analysis and our simulation method conceived for characterizing the HMOR scheme. The simulation results have demonstrated that our theoretical analysis is con-

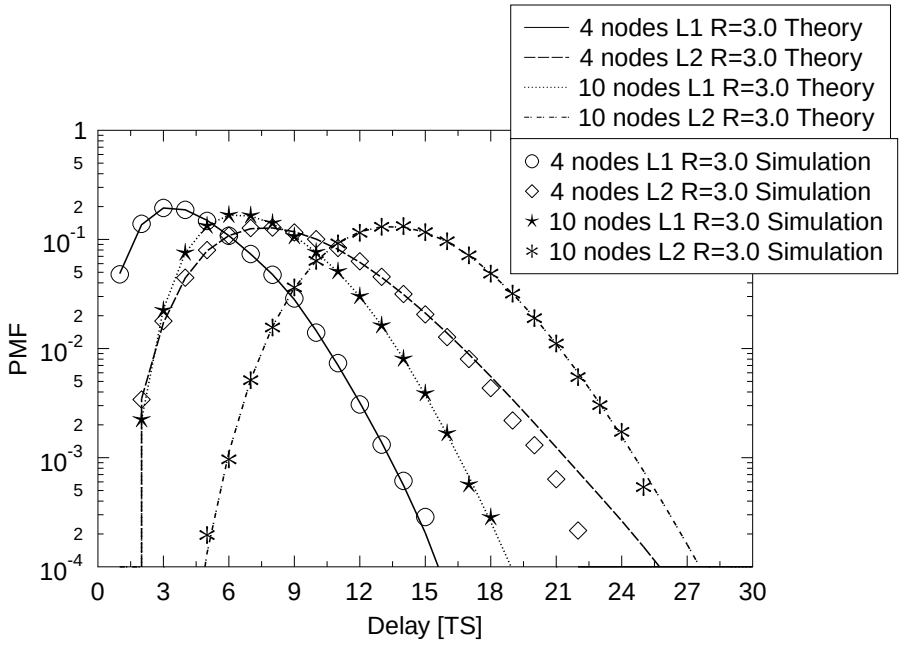

Figure 6.20: The PMF of delay of the cooperative network based on our HMOR schemes with different number of hops. The packet transmitted is TTCM aided HM-16QAM signals and the HM ratio is $R_1 = 3.0$. The statistics are all based on the minimized $\overline{PWC}$ for each scheme given $N_t = 7$. The related simulation parameters are listed in Table 6.2 and the system's schematic is described in Section 6.3.2, while the four-node network's topology is seen in Figure 6.7 and the ten-node network's topology is seen in Figure 6.18.

firmed by our simulations. We have also demonstrated that our HMOR scheme is more flexible and more power-efficient than its TOR benchmark. By partitioning the layered modulated packets according to their specific reception rule, the power $¶_t$ of each single node in the network, as well as the average per-packet power consumption $\overline{PWC}$ of the entire system may be reduced. There is a trade-off between the power-efficiency and delay. Explicitly, our HMOR scheme may require longer time to receive the entire twin-layer packet, whilst the outage probability of the more important information layer L_1 of the twin-layer HM-16QAM packets is reduced. In our future work, buffer-aided cooperative communication will be taken into consideration [250, 251]. Explicitly, the RN may be capable of temporarily storing a number of packets using buffers, where the forwarding process will depend on the instantaneous channel condition. Consequently, the probability of successful transmission among the nodes may be increased and the throughput of the cooperative network may also be improved. Additionally, the HM with three or more layers may also be considered for increasing the data rate of the entire cooperative network.

Meanwhile, the HMOR algorithm proposed in Section 6.2 still has its pros and cons, when employed in practical wireless *ad hoc* networks. The size of the networks should remain relatively small, when employing our HMOR algorithm, because the store-and-forward RN and the partitioned packets require each single node of the network to be informed of the exact reception status of the entire network. Needless to say that this necessitates substantial information exchange across

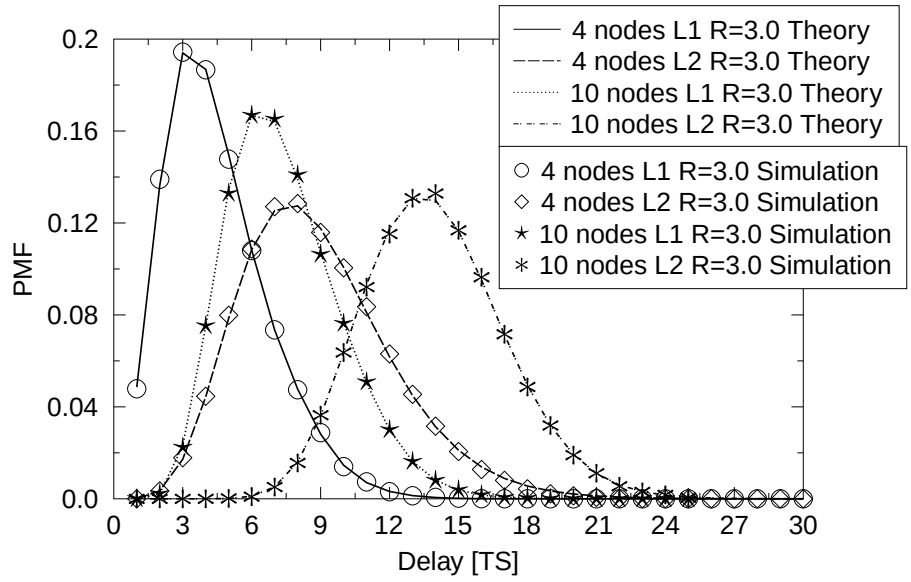

(a) PMF of the delay for $N_t = 7$ based on Figure 6.20

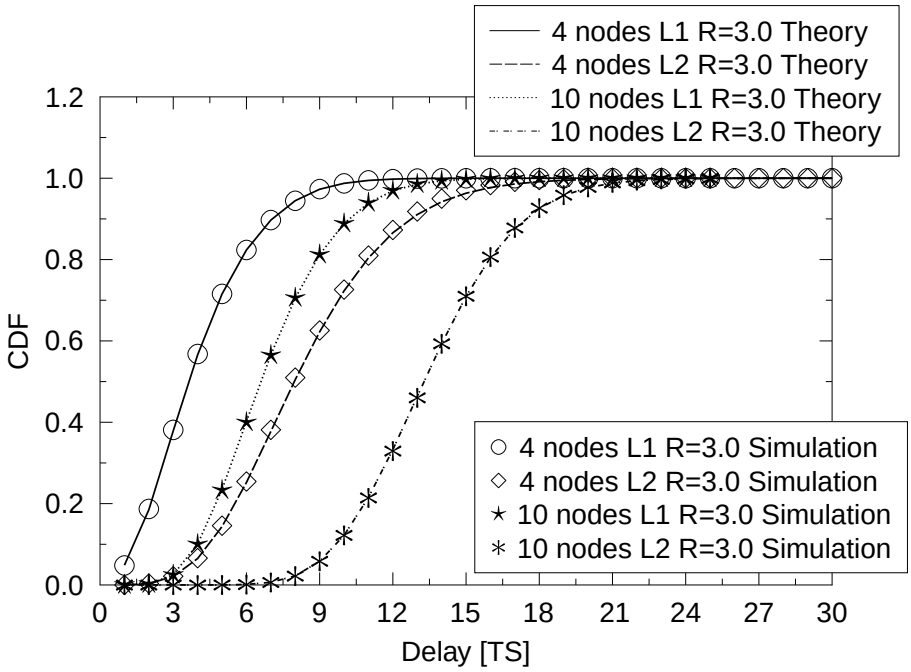

(b) CDF of the delay for $N_t = 7$

Figure 6.21: The PMF and the CDF of delay of the cooperative network based on our HMOR schemes with different number of hops. The packet transmitted is TTCM aided HM-16QAM signals and the HM ratio is $R_1 = 3.0$. The statistics are all based on the minimized $\overline{PWC}$ for each scheme given $N_t = 7$. The related simulation parameters are listed in Table 6.2 and the system's schematic is described in Section 6.3.2, while the four-node network's topology is seen in Figure 6.7 and the ten-node network's topology is seen in Figure 6.18.

Code	**TTCM**	
Modulation	4QAM, HM-16QAM	
N_t	7	
Positions of the nodes	4-node system–Table 6.6 10-node system–Table 6.8	
$\P_t$ of the nodes	4-node system–Table 6.6 10-node system–Table 6.8	
Constraints on Delay	95% plus of packets received	
Constraints on $\P_t$	The $\overline{PWC}$ of all schemes are minimized	
	Opt. $\overline{PWC}$ mw	Φ [packet/TS]
HMOR 4-nodes system	0.7423	0.2200
HMOR 10-nodes system	0.2714	0.1324
	Outage Probability P_{outage}	Delay (TS)
HMOR 4-nodes system L_1	0.0210	9 (97.33%)
HMOR 4-nodes system L_2	0.0239	15 (97.04%)
HMOR 10-nodes system L_1	0.0472	12 (96.92%)
HMOR 10-nodes system L_2	0.1836	19 (95.86%)

Table 6.9: The summary of the results extracted from Figure 6.10 to Figure 6.21. The statistics are all based on the minimized $\overline{PWC}$ for each scheme given $N_t = 7$. The related simulation parameters are listed in Table 6.2 and the system's schematic is described in Section 6.3.2, while the four-node network's topology is seen in Figure 6.7 and the ten-node network's topology is seen in Figure 6.18.

the entire network. Secondly, in practice the transmitter of wireless *ad hoc* networks may only be able to find a limited number of next-hop nodes, because the nodes beyond three hops will be considered as hidden nodes [227, 232]. Hence, the size of the *ad hoc* network employing our HMOR algorithm should remain relatively small. A compelling application of our HMOR algorithm may be found during the transmissions among neighbouring RNs instead of aiming for transmission from SN to DN. To be more specific, similar to the Fish-Eye State Routing (FESR) [252], instead of simply choosing a single RN for forwarding the packet, we allow a group of nodes to form a super-hop for assisting the transmission, where our HMOR algorithm may be beneficially employed.

Chapter 7

Conclusions and Future Research

In this concluding chapter, the main findings of this treatise are summarized in Section 7.1, while our design guidelines are provided in Section 7.2 and ideas for future work are discussed in Section 7.4.

7.1 Summary and Conclusions

In this thesis, the performance of various TTCM aided layered modulation schemes has been investigated in the context of cooperative communications. The SPM (Figure 3.2 of Chapter 3) and HM (Figure 3.13 and Figure 3.14 of Chapter 3) schemes are combined with the TTCM arrangement of Figure 3.1, Figure 3.15, Figure 3.16, Figure 3.27, Figure 4.2, Figure 5.2 and Figure 5.7 for the sake of improving both the flexibility and the power-efficiency of the entire system. To be more specific, the main focus of this thesis is on TTCM aided HM conceived for cooperative communications. Traditionally, researchers employ HM to provide UEP in cooperative communications [92–98]. According to the flexible layered structure of the HM scheme, the SNR required for receiving the higher protected HM layer is lower than that of the lower protected layer. However, we can exploit the HM scheme to reduce the transmit power of the source node and relay node(s) for improving the power-efficiency of the entire system. Specifically, the most appropriate relay positions and HM constellations were identified. Additionally, the SPM scheme of Figure 3.2 was also considered in order to improve the efficiency of the cooperative system. Furthermore, coded HM arrangement of Figure 4.2 was also combined with OR algorithms in the context of the wireless *ad hoc* networks. Our results in Figure 6.11 demonstrated that the power consumption of the entire network may be reduced by our proposed OR algorithms, when the packets transmitted through the network are formed by layered modulation based signals.

In **Chapter 1**, first we introduced the CM schemes. To be more specific, the evolution and history of CM schemes was represented in Section 1.1. Then the history of the two layered modulation schemes, namely of SPM and HM, was summarized in Section 1.2, while the background of OR

algorithms was illustrated in Section 1.3. Furthermore, the motivation of the thesis was presented in Section 1.4, while its structure was shown in Figure 1.3 and its novelty contributions were detailed in Section 1.6.

In **Chapter 2**, we briefly introduced the TCM and TTCM schemes, as well as the EXIT chart based design technique. The simulation results of characterising these schemes were discussed in Section 2.5, where the BER performance of the TCM, TTCM, BICM and BICM-ID schemes when communicating over both AWGN and uncorrelated Rayleigh fading channels were presented in Section 2.5.1. Based on the results of Figure 2.7 and Figure 2.8, as well as on the related statistics recorded in Table 2.3, it may be observed that the TTCM scheme performs better than the other three CM schemes, especially when transmitting over uncorrelated Rayleigh fading channels. In Section 2.5.2, we have investigated the BER performance of TTCM aided transmissions over uncorrelated Rayleigh fading channels, where the effects of using different code rates and varying the number of iterations as well as block sizes were investigated. The related simulation results are recorded in Table 2.4 and Table 2.5. We may observe from Figure 2.10 that upon increasing the number of iterations ζ, the BER performance of the TTCM scheme transmitting over uncorrelated Rayleigh fading channels may be improved. Note that beyond $\zeta = 6$, any further increase of ζ may only lead to slight BER improvements. Observe in Figure 2.11 that a lager block size η may also lead to an improved BER performance. In the remaining chapters, in order to achieve a good BER performance, the TTCM encoder/decoder we employed relies on $\zeta = 4$ and $\eta = 12,000$ unless it is stated otherwise. Finally, our EXIT charts analysis of TTCM aided transmissions was presented in Section 2.5.3.

Chapter 3 was divided into three main parts, namely Section 3.2, Section 3.3 and Section 3.4. In Section 3.2, we combined the SPM and TTCM schemes in the context of cooperative communications. The two main benefits of employing the SPM scheme at the RN are, firstly that the RN may only need a single antenna for the transmission. Secondly, the decoder at the DN may still employ a rate-1/2 TTCM decoder. Hence, the decoding complexity remains moderate. The simulation results were discussed in Section 3.2.7. It was observed from Figure 3.10 that at a BER of 10^{-6}, our SPM scheme is about 3 dB better than the 8PSK TTCM scheme. Furthermore, the results of Figure 3.11 show that with the aid of the PS scheme of Section 3.2.6, the performance of the cooperative system was further improved by about 0.5 dB.

Included in Section 3.3, we combined the bit-based layered modulation HM scheme with TTCM in the contest of cooperative communications. The system model of the HM based single RN aided communication was detailed in Section 3.3.2, the design of set-partitioning based HM was illustrated in Section 3.3.3, while the communication protocol and the demodulation/decoding of the HM signal was discussed in Section 3.3.4. The simulation results of Figure 3.17 to Figure 3.24 demonstrated that our cooperative HM scheme is capable of substantially reduce the SNR required at the DN, when compared to the conventional TTCM scheme. Furthermore, our solution maintained a fair protection for all the information bits contained in the TTCM encoded symbols. In Section 3.4, we proposed an improved scheme by amalgamating the HM and SPM arrangement

with a cooperative regime, where two independent streams were assisted by a single RN. It was observed in Figure 3.27 that by employing the new cooperative strategy, the throughput of the entire system may be doubled compared to that of the systems advocated in Section 3.2 and Section 3.3. Additionally, the SNR required may also be reduced by choosing an appropriate RN position.

In **Chapter 4**, we proposed an improved twin-layer HM scheme to mitigate the limitations of the system conceived in Section 3.3. The HM scheme of this chapter was invoked for merging the two independent coded signal sequences, instead of mapping a codeword into multiple layers. The improved cooperative system was proposed in Section 4.2, while the associate twin-layer HM constellation design and the related demodulation procedure were detailed in Section 4.3. In Section 4.4.4, we characterized the DCMC capacity by a three dimensional plot in Figure 4.6. More specifically, the BER performance of our system was characterized, when assuming that a 'perfect' capacity-achieving channel code is employed, where the minimized $\overline{SNR_t}$ for our HM aided system is 0.77 dB per TS, when employing an HM-16QAM ratio of $R_1 = 1.5$. The entire system required two TSs for completing its transmission session and a transmit SNR_t of 2.46 dB for the SN as well as a transmit SNR_t of -2.02 dB for the RN's transmission during the second TS. In Section 4.5, we provided our simulation results characterizing our TTCM-aided cooperative communication system. The related simulation results were illustrated in Figure 4.8 to Figure 4.11. For the sake of achieving a BER of 10^{-6}, the minimum $\overline{SNR_t}$ of our TTCM aided cooperative system may be achieved, when invoking an HM-ratio of $R_1 = 3.0$, which is $\overline{SNR_{t\,min}} = 3.62$ dB per TS, where the SNR_t required at the SN is 4.98 dB, the SNR_t required at the RN is 1.62 dB and the optimized RN position is $d_{SR}/d_{SD} = 0.26$.

In **Chapter 5**, we proposed an improved triple-layer HM scheme relying on TTCM-aided cooperative communications, where the layered-modulation schemes of HM and SPM were combined for improving both the flexibility and efficiency of the twin-RN assisted system. The system model was detailed in Section 5.2, while the triple-layer HM constellations and the related constraints were illustrated in Section 5.3. Furthermore, Section 5.4 detailed the demodulation/detection of each of the three layers of the triple-layer HM-64QAM scheme. We also characterized the DCMC capacity of each link of the cooperative networks, as detailed in Section 4.4. The DCMC analysis results were recorded in Table 5.1. When assuming that 'perfect' capacity-achieving channel coding is employed, the minimized average transmit SNR ($\overline{SNR_t}$) required to convey the information is -0.71 dB, where the entire system requires three TSs to conclude its transmission session. When a rate-1/2 TTCM code is employed for cooperative communications, the achievable performance was presented in Section 5.6, as shown in Figure 5.3. Figure 5.6 demonstrated that when a rate-1/2 TTCM scheme is employed, the minimized $\overline{SNR_t}$ will be 2.41 dB per TS. On the other hand, in order to improve the efficiency of the cooperative communication system proposed in Figure 5.1, we introduced the SPM scheme at both RN_1 and RN_2. The block diagram of the modified system was depicted in Figure 5.7. The three-dimensional illustration in Figure 5.10 illustrated the relationship among $\overline{SNR_t}$, R_1 and R_2. The related simulation results were recorded in Table 5.4. We observed that for the system proposed in Figure 5.7, the optimized cooperative regime required two TSs and

the minimum required $\overline{SNR_t}$ was 6.94 dB per TS. The improved system of Figure 5.7 was more efficient and exhibited a higher throughput than that of Figure 5.2 at the cost of a higher average transmit $\overline{SNR_t}$.

In **Chapter 6**, we introduced the layered-modulation concept into *ad hoc* networks. The TTCM aided twin-layer HM scheme of Figure 4.2 was combined with the OR algorithms of Section 6.2 and the investigations were focussed on the cooperative network layer. The system model and the related twin-layer HM-16QAM regime were introduced in Section 6.2. In Section 6.3, we theoretically analysed the performance of the twin-layer HM assisted OR algorithm. To be more specific, in Section 6.3.1 we characterized the FER versus SNR function of our twin-layer HM-16QAM regime. Then the legitimate system states of our twin-layer HM based OR algorithm invoked in our four-node network of Figure 6.3 were detailed in Section 6.3.2. Based on the investigations of Section 6.3.1 and Section 6.3.2, we derived the state-transition probabilities of our cooperative system in Section 6.3.3. The analysis of the system was detailed in **Algorithm 1** of Section 6.3.4. By contrast, in **Algorithm 2** of Section 6.4, we proposed the simulation procedures characterizing our cooperative network. The theoretical analysis results and the simulation results were illustrated in Section 6.5, where we found that our OR algorithm is indeed power-efficient. When communicating over wireless *ad hoc* networks, if the packets are layered-modulated signals, by partitioning and appropriately conveying the layered-modulated packets across cooperative networks, the transmit power for each node is reduced. Similarly, the average power consumption per packet may also be decreased. By increasing the number of nodes in the networks, the average power consumption of the system was reduced, albeit at the cost of an increased delay, as evidenced by Figure 6.11 and Figure 6.21.

7.2 Design Guidelines

Although we use TTCM as the channel code throughout the thesis, the HM based design can be generalized to any arbitrary coding schemes. In this section, we will summarize the general design guidelines of the coded HM based cooperative communication schemes investigated throughout Chapter 3 to Chapter 5, followed by the design guidelines of coded HM based OR algorithms conceived for *ad hoc* networks.

1. **Coded HM Design for Cooperative Communications:**

   (a) First, we have to identify, which specific HM features we want to exploit. In Chapter 3, our design objective is to exploit the UEP capability provided by the HM scheme in order to assist the transmission of a single coded information sequence in the context of cooperative communications. By contrast, in Chapter 4 and Chapter 5, our design goal is to assist the transmission of multiple independent information streams with the aid of coded HM schemes. The general idea is to exploit the specific features of the

HM scheme to reduce the SNR_t of the SN and to invoke DAF based RNs for the sake of achieving a cooperative diversity gain.

(b) Then, we appropriately design the RN(s) according to the overall system concept. In the HM based cooperative communication design, we always assume that the highest-priority layer of the multi-layer HM signals may be adequately received by the DN for the sake of maintaining the target-integrity requirement, provided that a sufficient high SNR_r can be achieved at the DN. In that case, the lower-priority layers may be forwarded to the DN by the DAF based RN(s). On the other hand, if the triple-layer HM-64QAM scheme of Chapter 3 is employed, the RN may have to forward two layers of its information to the DN. Nonetheless, in Chapter 4 and Chapter 5, each RN only has to forward a single layer of the information. More explicitly, the soft-information required for the target decoder should be specifically derived, as detailed in Chapter 3 to Chapter 5.

(c) Finally, the optimization of the overall system depends on the choice of HM constellations, on the positions of the RNs, as well as on the required SNR_t of each nodes in the networks. In Chapter 3, Chapter 4 and Chapter 5, the HM constellations may be appropriately modified by employing different HM ratios. Furthermore, the reduced path-loss facilitated by the employment of DAF based RNs may also influence the SNR_r required for adequately receiving the desired signals. Hence, to find the minimum $\overline{SNR_t}$ for the entire system, multiple factors have to be taken into consideration.

2. Coded HM Design for Opportunistic Routing:

(a) Firstly, we determine the specific choice of the cooperative strategies to be used by the wireless *ad hoc* networks, as discussed in Section 6.3. In each transmission TS, only one of the nodes is activated for transmission. The transmission rules should be specially designed, as detailed in Section 6.3.2. After determining the FER versus SNR curve, the performance of the system may be simulated using **Algorithm 2** of Section 6.4 and the related system characteristics may be derived.

(b) Then, we have to determine the legitimate system states and the transition probabilities in the system, as detailed in Section 6.3.2 and Section 6.3.3. More specifically, according to the FER versus SNR function derived in Section 6.3.1, the one-step state-transition probability matrix of the entire cooperative system may be computed, which is illustrated in Table 6.5. Similarly, the related characteristics of the HM based OR algorithm aided *ad hoc* network may be analysed theoretically by using **Algorithm 1**, as detailed in Section 6.3.4.

(c) Finally, we have to compare the simulation results to the theoretical analysis, as discussed in Section 6.5. Then the minimum power consumption of the cooperative net-

work may be derived, as determined by the position of the RNs, as well as by the specific transmit power of each node.

7.3 Design Limitations and Challenges

In our investigations, we stipulated a number of idealized simplifying assumptions, which could be gradually eliminated by future research.

1. **Coded HM Design for Cooperative Communications:**

   (a) As described in Section 4.6 and Section 5.8, in practice, the SN, RNs and DN will not be located on a straight line. Regardless of their positions, we often find that a break-point-based path-loss model is more accurate than having a single fix path-loss exponent.

   (b) All of our investigations are assumed to rely on perfect CSI, but according to the robustness analysis of Chapter 5, we found that the effects of imperfect CSI on our triple-layer HM scheme as well as on the SPM scheme of Chapter 5 are non-negligible. Hence, powerful iterative joint data and channel estimation techniques should be employed, as detailed in [253].

   (c) When considering multiple RNs, as in Chapter 5, our cooperative schemes require that each node in the cooperative network should have accurate CSI as well as be informed of the reception status of all the network nodes. This assumption is relatively hard to satisfy, especially when the size of the cooperative network is large. Hence, it requires further research.

   (d) For the cooperative scheme proposed in Section 5.7 establishing both time and carrier phase synchronization of multiple signal sequences arriving from different distances is also a challenge, which requires substantial extra information exchange between the RNs and DN, which imposes extra power consumption and requires extra transmission bandwidth.

2. **Coded HM Design for Opportunistic Routing:**

   (a) Our HMOR algorithm requires that each node in the network should be informed of the success/failure of the reception of all the other nodes as well as have accurate CSI of the entire system. This will directly increase the complexity of the entire cooperative network. Hence, a large network may not be readily supported.

   (b) In wireless *ad hoc* networks, a transmitter may only be capable of sensing the nodes within a distance of three hops. The nodes that are farther away may be considered as hidden nodes. This problem also limits the size of our HMOR based network. Therefore, a more powerful node detecting algorithm may be required.

(c) The FESR algorithm of [252], may be capable of employing our HMOR algorithm in practical transmissions. Instead of choosing a single node for forwarding the information, multiple already detected nodes may cooperate to form a super-hop for forwarding the information collaboratively. Therefore, our HMOR algorithm may be employed for transmission within the super-hops of a large network.

7.4 Future Research

The HM aided cooperative system conceived in this thesis may be further extended in several directions. In this section, a number of potential future research ideas will be highlighted.

7.4.1 Theoretical Analysis of the DCMC Capacity of the Cooperation Aided Coded HM Scheme

In Chapter 4 and Chapter 5, the DCMC capacity was relied upon for analysing the achievable performance of the coded HM based cooperative scheme. However, the results were derived by simulations only, albeit it is desirable to arrive at a theoretical solution. Recall that the CCMC and DCMC capacities were first considered by Cover and Gamal in [254], where the general upper bound of the CCMC capacity of a half-duplex relay-aided system was derived in [255]. We have appropriately adapted the approach of [256, 257] for deriving the DCMC capacity of our HM aided cooperative communication system. As mentioned in Chapter 4 and Chapter 5, the DCMC capacity is dependent on the specific choice of the modulation scheme, which is more pertinent for the design of practical channel-coded modulation schemes. However, the actual network capacity of even a single-relay based network is an open problem, whilst here we have multiple relays in our system, which are associated with multiple independent transmission links. The theoretical analysis of a complex system like that of Chapter 4 or Chapter 5 would be complex and would require various strong assumptions. Hence, an accurate and yet tractable less complex theoretical analysis would be very attractive.

7.4.2 Near-capacity HM Design for Cooperative Communication

The fundamental goal of the analysis presented in Chapter 4 and Chapter 5 is to quantify the modulation-dependent DCMC capacity of our system in order to analyse the achievable performance of the coded HM scheme. According to the specific cooperative strategy proposed in Chapter 4 and Chapter 5, we aim for finding the minimum energy-consumption based configuration of the system operating at the target rate, assuming that a 'perfect' capacity-achieving channel coding scheme is employed. These results may be considered as the lower bound conceived for guiding the design of HM schemes employing a realistic channel encoder within the same cooperative

framework. In [57], we have employed both TTCM and LDPC codes in another HM based cooperative communication scheme. However, a range of other powerful near-capacity source/channel codes, including turbo codes, Variable Length Code (VLC) [258], polar codes [259] etc may be employed. The constellations of the HM and of the source/channel encoder may be designed jointly for approaching the achievable capacity.

7.4.3 Adaptive HM Aided Cooperative Communications

One of the most significant merits of the HM scheme is its high flexibility, which is particularly beneficial in conjunction with adaptive modulation schemes. The adaptive HM theory was provided by Hossain in [110, 208], where the multiple independent information streams may also be combined by the HM scheme. However, the activated constellation of the transmitted HM-based source signal directly depends on the channel quality. To be more specific, assuming that three independent signal streams are broadcast by the SN, when the channel conditions are good, the SN may activate the triple-layer HM scheme for transmitting all three layers of information simultaneously. However, when the channel conditions are poorer, the SN may activate a twin-layer HM scheme for transmitting the most important two layers of information or even using conventional BPSK/4QAM modulation scheme for transmitting a single layer consisting of the highest-priority information. Hence, the adaptive HM may be deemed to be a convenient application-oriented modulation scheme. Explicitly, the fundamental goal is to guarantee that during each transmission session, the information contained in the transmitted signal may be successfully received by the DN. By incorporating the adaptive HM scheme into our system proposed in Chapter 4 and Chapter 5, both the flexibility and the reliability of the cooperative system may be further improved in order to approach its DCMC capacity more closely.

7.4.4 Spatial Modulation Aided HM in Cooperative Communication

As we mentioned in the conclusion of Chapter 4, Spatial Modulation (SM) may be the most direct and compelling method of improving the performance of the HM based cooperative communication system. In [260], Mesleh *et al.* discussed the performance of the SM scheme in detail, where the information is embedded both into the classic transmitted symbol streams and into the unique transmit antenna indices chosen from a set of transmit antennas according to the information to be transmitted. Note that activating one out of N_t transmit antennas may allow us to convey $\log_2 N_t$ extra bits. Hence, for the same throughput, the SM aided transmitter may employ a lower-order modulation scheme for the activated antenna. This would require a lower SNR_t^{SN} for achieving the same BER, whilst additionally requiring fewer RF chains than the conventional MIMO modulation schemes. Additionally, in contrast to the classic MIMO schemes, such as the Diagonal Bell Laboratories Layered Space-Time (D-BLAST) or the Vertical BLAST (V-BLAST), the Inter Channel Interference (ICI) may be avoided, because only a single transmit antenna of the entire set will be activated by the SM scheme. Furthermore, the need for synchronizing several transmit antennas

may also be avoided. Hence, some of the disadvantages of the classic MIMO schemes may be circumvented.

7.4.5 High-Order HM aided Cooperative Communication in *Ad Hoc* Networks

We have introduced the twin-layer coded HM concept in Chapter 4 for transmission over wireless *ad hoc* networks in Chapter 6. More specifically, the OR algorithm based cooperative system was beneficially assisted by the HM scheme. Both the theoretical analysis as well as the simulation-based study of the resultant cooperative system were presented in detail in Chapter 6. It may be observed that when assuming that the packets transmitted over the networks are layered-modulation signals, the power-efficiency of the entire cooperative network is improved by partitioning the HM-based multiple layer packets into sub-packets during this transmission. However, the HM scheme proposed in Chapter 6 is the simplest twin-layer HM-16QAM scheme. When higher-order HM schemes are considered, the resultant cooperative strategy may become more flexible. On the other hand, when considering a triple-layer HM-64QAM scheme in the context of a four-node cooperative network, the complexity of the cooperative network is increased dramatically. Explicitly, the number of the legitimate states of a triple-layer HM-64QAM aided four-node network may be computed as:

$$N_{state} = \frac{1\times 2}{2} + \frac{2\times 3}{2} + \frac{3\times 4}{2} + \frac{4\times 5}{2} = 20\,. \tag{7.1}$$

Furthermore, the number of the possible states of a triple-layer HM-64QAM aided n-node network may be calculated as:

$$\begin{aligned} N_{state} &= \frac{1\times 2}{2} + \frac{2\times 3}{2} + \cdots + \frac{n\times(n+1)}{2} \\ &= \sum_{i=1}^{n} \frac{i\times(i+1)}{2}\,. \end{aligned} \tag{7.2}$$

Hence, the increased number of states N_{state} and the potential destination target of the nodes in the network results in a complex one-step state-transition probability matrix. Additionally, we should also take into account the position of the nodes, the transmission power of the nodes in the network as well as the specific relay selection algorithms, when analysing the characteristics of the cooperative Network.

7.4.6 Coded HM Based Buffer-aided Multihop Cooperative Communication

Recently, buffer-aided cooperative communications over wireless *ad hoc* networks has drawn a lot of research interests [250, 251, 261]. More explicitly, the RNs are capable of temporarily storing a fixed or a flexible number of packets using buffers. When the channel conditions are poor, the RN may still be able to receive information from the SN and only forward it to DN, when the quality of the RN-DN link has been sufficiently improved. In [167], the authors investigated the performance of a buffer-aided OR algorithm in the context of *ad hoc* networks. They proved that both the throughput and the power-efficiency of the buffer-aided OR algorithm based cooperative

networks are better than that of the traditional OR algorithm based cooperative networks. Note that the conventional OR algorithm aims for searching for the optimum SN-RN, RN-RN, RN-DN links step by step, while the buffer-aided RN is more flexible in terms of deciding, when to transmit and when to receive according to the corresponding channel conditions. Hence, the combination of these two algorithms may be capable of improving the probability of successful transmission across each link. Therefore, both the outage probability and the average packet power consumption may be reduced. However, the buffer-aided OR algorithm is not suitable for delay sensitive systems. The benefits that conventional relaying may offer for delay-sensitive systems is that the conventional relaying avoids the buffering delay [250]. By employing our HM scheme, the higher delay of the buffer-aided OR algorithm may be mitigated, because the delay-sensitive information may be mapped to the higher-protected layer of the HM symbols for the sake of achieving a lower delay, while the delay-tolerant information may be mapped to contained in the lower-protected layer and be forwarded to the DN following the routes decided by the buffer-aided OR algorithm. Therefore, the delay-sensitive and the delay-tolerant information may be transmitted simultaneously, while a high average throughput may be achieved with the aid of an appropriately designed HM scheme.

Appendix A

Appendix

A.1 Noise Power and System Model

In this section, we represent a comparison between the free-space path-loss model and our path-loss model used in Chapter 4.

A.1.1 Noise

In wireless communications, the noise power may be expressed as:

$$N_p = FkTB\,, \tag{A.1}$$

where, F is the noise figure. Typically we have $F = 2$ and in some worst-cast situations $F = 10$. In order to simplify the discussions, we opted for $F = 1$ in Eq. (A.1). $k = 1.38e^{-23}$ is Boltzmann's constant, $T = 290\ K$ is the temperature measured in Kelvin and B is the noise bandwidth (always identical to the bandwidth of the transmission channel). Hence, if the bandwidth of the system is 1 Hz, we have:

$$N_p(\text{dBm/Hz}) = 10\log\left[1.38e^{-23} \times 290 \times 1/0.001\right]\ \text{dBm/Hz}\ = -174\ \text{dBm/Hz}\,. \tag{A.2}$$

Here, we assume that the transmission bandwidth of our system is 20 MHz (Long Term Evolution (LTE) standard), so that the noise power at the receiver is given by:

$$N_0 = N_p + 10\log(2 \cdot 10^7) = -101\ \text{dBm}\,. \tag{A.3}$$

A.1.2 Simplified Path-Loss Model

In order to simplify the analyses, the path-loss model we considered is the free-space 'simplified path-loss model' of [1]. The relationship between the average transmission power P_t and the aver-

age received power P_r satisfies [1]:

$$\frac{P_r}{P_t} = \left[\frac{\sqrt{G_l}\lambda}{4\pi d}\right]^2 , \tag{A.4}$$

where, $\sqrt{G_l}$ is the product of the transmit and receive antenna radiation patterns in the line-of-sight direction. Moreover, for a system employing nondirectional antennas, we have $\sqrt{G_l} = 1$ [1]. Additionally, $\lambda = c/f_c$ is the signal wave length, where c is the speed of light (3×10^8 m/s) and f_c is the carrier frequency, while d is the distance between the transmitter and receiver antennas. Therefore, the path-loss P_L between the source and destination may be expressed as:

$$\begin{aligned} P_L\,[\text{dB}] &= 10\log_{10}\left(\frac{P_r}{P_t}\right) \\ &= -10\log_{10}\left[\frac{\sqrt{G_l}\lambda}{4\pi d}\right]^2 \\ &= 20\log_{10}(d) + 20\log_{10}\left(\frac{4\pi}{\lambda}\right) - 10\log_{10} G_l \\ &= 20\log_{10}(d) + 20\log_{10}\left(\frac{4\pi f_c}{c}\right) - 10\log_{10} G_l \\ &= 20\log_{10}(d) + 20\log_{10}(f_c) - 147.56\,, \end{aligned} \tag{A.5}$$

where $20\log_{10}(\frac{4\pi}{c}) - 10\log_{10} G_l = -147.56$, while the unit of d is 'm' (meter) and the unit of f_c is 'Hz'. Hence, if $f_c = 2$ GHz and the distance between the transmitter and receiver antennas is $d = 1$ km, the path-loss between SN and DN will be $P_L^{SD} = 98.46$ dB.

Accurate path-loss expressions can be derived by the complex ray tracing models of [1]. However, for system design and analysis, often a simple path-loss model is preferred, such as [1]:

$$P_r = P_t\kappa\left[\frac{d_0}{d}\right]^\gamma , \tag{A.6}$$

where κ is a constant defined by:

$$\kappa = \left(\frac{c}{4\pi d_0}\right)^2 . \tag{A.7}$$

Explicitly, d_0 is a reference distance and γ is the path-loss exponent. The value of κ is considered to be the free-space path-loss at a distance of d_0 from the transmitter. In the analysis, we assume that, when the distance between SN and DN is $d_{SD} < d_0$, free-space path-loss associated with $\gamma = 2$ would be considered, because it is assumed that there is no obstacle between the transmit antenna and the receive antenna, In indoor environments, d_0 is assumed to be 1-10 m, while in an outdoor environment d_0 is assumed to be 10-100 m [1]. When $d_{SD} > d_0$, the received power may be derived from Eq. (A.6) and the value of the path-loss exponent is summarised in Table A.1 [1].

In this section, we assume that the path-loss obeys the free-space path-loss model. Hence, the path-loss of each links is given by Eq. (A.5). Meanwhile, according to Eq. (A.6), we also have:

$$P_{r_{SR}} = P_t\kappa\left[\frac{d_0}{d_{SR}}\right]^2 , \tag{A.8}$$

$$P_{r_{SD}} = P_t\kappa\left[\frac{d_0}{d_{SD}}\right]^2 , \tag{A.9}$$

Environment	γ **range**
Urban macrocells	3.7-6.5
Urban microcells	2.7-3.5
Office Building (same floor)	1.6-3.5
Office Building (multiple floor)	2-6
Store	1.8-2.2
Factory	1.6-3.3
Home	3
Free space	2

Table A.1: Typical Path Loss Exponents [1]

where $P_{r_{SR}}$ and $P_{r_{SD}}$ are the signal power received from the SN at RN and DN, respectively. Therefore, we have:

$$G_{SR} = \frac{P_{r_{SR}}}{P_{r_{SD}}} = \left(\frac{d_{SD}}{d_{SR}}\right)^2 , \tag{A.10}$$

which is considered to be the path-gain G_{SR} of the SN-RN link, when we normalise $P_{L_{SD}}$ to 0 dB. Similarly, we also have:

$$G_{RD} = \frac{P_{r_{RD}}}{P_{r_{SD}}} = \left(\frac{d_{SD}}{d_{RD}}\right)^2 . \tag{A.11}$$

However, as described in Section 4.6, in cooperative mobile to mobile communications, the channel often obeys a break-point-based path-loss model [219]. Hence, in our future research, more realistic path-loss models will be considered.

A.1.3 Practical Path-Loss and Our Channel Gain Model

Based on our simulation results provided in Section 4.5, we observe that when the twin-layer HM-16QAM ratio of $R_1 = 3.0$ is used, the power allocation of the entire cooperative system is optimized. From the statistics in Table. 4.3, we can find that in this situation, if the path-loss between the SN and DN is normalized to 0 dB, SNR_t^{SN} should be 4.98 dB, which is identical to the SNR_r^{DN} required for the RN to receive L_1 during the first TS, while the corresponding path gains are $G_{SR} = 11.72$ dB and $G_{RD} = 2.61$ dB. Additionally, the SNR_r^{RN} required to receive L_2 at RN is 16.71 dB and the SNR_t^{RN} required to transmit the L_2 is $SNR_t^{RN} = 4.23 - 2.61 = 1.62$ dB, as shown in Table 4.3. When considering the practical free-space path-loss model used in our system, the receive power P_r^{DN} required at DN to receive L_1 during the first TS may be expressed as:

$$P_r^{DN} = N_0 + SNR_r^{DN} = -101 \text{ dBm} + 4.98 \text{ dB} = -96.02 \text{ dBm} . \tag{A.12}$$

Furthermore, the path-loss between SN and DN is $P_L^{SD} = 98.46$ dB. Hence, the transmission power at the SN is:

$$P_t^{SN} = P_r^{DN} + P_L^{SD} = -96.02 \text{ dBm} + 98.46 \text{ dB} = 2.44 \text{ dBm} , \tag{A.13}$$

where we observe that:

$$P_t^{SN} - N_0 = 2.44 \text{ dBm} + 101 \text{ dBm} = 103.44 \text{ dB} = SNR_t^{SN} + P_L^{SD} . \tag{A.14}$$

On the other hand, the RN position of our optimized cooperative communication system is related to $d_{SR} = 0.26\, d_{SD}$. Hence, when $d_{SD} = 1$ km, we may compute the path-loss P_L^{SR} between the SN and RN as well as that between the RN and DN (P_L^{RD}) using Eq. (A.5):

$$P_L^{SR} = 20\log_{10}(260) + 20\log_{10}(f_c) - 147.56 = 86.94 \text{ dB} , \tag{A.15}$$

$$P_L^{RD} = 20\log_{10}(740) + 20\log_{10}(f_c) - 147.56 = 96.02 \text{ dB} . \tag{A.16}$$

Hence, during the first TS, the receive power P_r^{RN} required at the RN for receiving L_2 is:

$$P_r^{RN} = P_t^{SN} - P_L^{SR} = 2.44 \text{ dBm} - 86.94 \text{ dB} = -84.5 \text{ dBm} . \tag{A.17}$$

We can observe that

$$P_r^{RN} - N_0 = -84.5 \text{ dBm} + 101 \text{ dBm} = 16.5\text{dB} \approx SNR_r^{L^2} . \tag{A.18}$$

During the second TS, in order to guarantee a flawless reception, the $SNR_r^{DN'}$ should be 4.23 dB. Hence, the power received at the RN during the second TS should be:

$$P_r^{DN'} = SNR_r^{DN'} + N_0 = 4.23 \text{ dB} - 101 \text{ dBm} = -96.77 \text{ dBm} , \tag{A.19}$$

where the transmission power of the RN during the second TS may be expressed as:

$$P_t^{RN} = P_r^{DN'} + P_L^{RD} = -96.77 \text{ dBm} + 96.02 \text{ dB} = -0.75 \text{ dBm} . \tag{A.20}$$

We then find that:

$$P_t^{RN} - N_0 = -0.75 \text{ dBm} + 101 \text{ dBm} = 100.25 \text{ dB} \approx SNR_t^{RN} + P_L^{SD} . \tag{A.21}$$

Additionally, the average transmission power $\overline{P_t}$ of the entire system over the two TSs is:

$$\overline{P_t} = 10\log_{10}\left(\frac{10^{P_t^{SN}/10} + 10^{P_t^{RN}/10}}{2}\right) \text{ dBm} = 1.13 \text{ dBm} , \tag{A.22}$$

where it can be shown that:

$$\overline{P_t} - N_0 = 1.13 \text{ dBm} + 101 \text{ dBm} = 102.13 \text{ dB} \approx \overline{SNR_t} + P_L^{SD} . \tag{A.23}$$

The related results are recorded in Table. A.2. We may observe that our path-gain model may be directly converted into the corresponding path-loss model by taking the path-loss P_L^{SD} into consideration.

	Actual path-loss model	**Our simplified path-gain model**
Parameters	f_c=2 GHz f_t=20 MHz N_0=-101 dBm d_{SD}= 1 Km d_{SR}= 260 m d_{RD}= 740 m	G_{SD} = 0 dB d_{SD}=1 d_{SR}=0.26 d_{RD}=0.74
SN-DN 1st TS	P_r^{DN}= SNR_r^{DN}+ N_0= -96.02 dBm P_L^{SD}= 98.46 dB P_t^{SN}= P_r^{DN}+P_L^{SD}=2.44 dBm P_t^{SN}-N_0 = 103.44 dB	SNR_r^{DN} = 4.98 dB G_{SD} = 0 dB SNR_t^{SN} = SNR_r^{DN}= 4.98 dB
	P_t^{SN}-N_0 ≈ SNR_t^{SN} + P_L^{SD}	
SN-RN 1st TS	P_L^{SR}=86.94 dB P_r^{RN}=-84.5 dBm P_r^{RN}-N_0 =16.5 dB	G_{SR}=11.72 dB SNR_r^{RN} = 16.71 dB
	P_r^{RN}-N_0 ≈ SNR_r^{RN}	
RN-DN 2nd TS	$P_r^{DN'}$ = $\text{SNR}_r^{DN'}$+N_0=-96.77 dBm P_L^{RD}= 96.02 dB P_t^{RN}=$P_r^{DN'}$+P_L^{RD}=-0.75 dBm P_t^{RN}-N_0 = 100.25 dB	$\text{SNR}_r^{DN'}$ = 4.23 dB G_{SR} = 2.61 dB SNR_t^{RN} = 1.62 dB
	P_t^{RN}-N_0 ≈ SNR_t^{RN} +P_L^{SD}	
Average	P_t^{SN}= 2.44 dBm P_t^{RN}= -0.75 dBm $\overline{P_t}$ = 1.13 dBm $\overline{P_t}$-N_0 = 102.13 dB	SNR_t^{SN} = 4.98 dB SNR_t^{RN} = 1.62 dB $\overline{SNR_t}$ = 3.62 dB
	$\overline{P_t}$-N_0 ≈ $\overline{SNR_t}$ +P_L^{SD}	

Table A.2: Comparison between actual path-loss model and our simplified path-gain model.

Bibliography

[1] A. Goldsmith, *Wireless Communications*. Cambridge University Press, 1st ed., 2005.

[2] M. K. Simon and M.-S. Alouini, *Digital communication over fading channels*. Wiley-IEEE Press, 2rd ed., 2005.

[3] J. G. Proakis and M. Salehi, *Digital Communications*. McGraw-Hill, 5th ed., 2008.

[4] L. Hanzo, J. Blogh, and S. Ni, *3G, HSPA and FDD versus TDD networking smart antennas and adaptive modulation*. New York: Wiley-IEEE, 2nd ed., 2008.

[5] G. Ungerböck, "Trellis-coded modulation with redundant signal sets. part 1 and 2," *IEEE Communication Magazine*, vol. 25, pp. 5–21, Feb. 1987.

[6] L. Hanzo, T. H. Liew, B. L. Yeap, R. Y. S. Tee, and S. X. Ng, *Turbo coding, turbo equalisation and space-time coding : EXIT-chart-aided near-capacity designs for wireless channels*. Wiley-IEEE Press, 2rd ed., 2011.

[7] G. Ungerböck, *Trellis-coded modulation with redundant signal sets Part 1 and Part 2*, vol. 25. IEEE Communication Magazine, February 1987.

[8] P. Robertson, E. Villebrun, and P. Höher, "A comparison of optimal and sub-optimal MAP decoding algorithms operating in the log domain," *IEEE International Conference on Communications*, vol. 2, pp. 1009–1013, Jun. 1995.

[9] E. Zehavi, "8-PSK trellis codes on Rayleigh channel," *1989 IEEE Military Communications Conference, 1989. MILCOM '89*, vol. 2, pp. 536–540, Oct. 1989.

[10] X. D. Li and J. A. Ritcey, "Bit-interleaved coded modulation with iterative decoding," *IEEE Communications Letters*, vol. 1, pp. 169–171, Nov. 1997.

[11] C. E. Shannon, *A mathematical theory of communication*. Jun. and Oct. 1948.

[12] R. Hamming, "Error detecting and error correcting codes," *Bell System Technical Journal*, pp. 147–160, 1950.

[13] I. Reed, "A class of multiple-error-correcting codes and the decoding scheme," *IRE Professional Group on Information Theory*, vol. 4, pp. 38–49, Sept. 1954.

[14] P. Elias, "Coding for noisy channels," *IRE Convention Record, pt.4*, pp. 37–47, 1955.

[15] R. G. Gallager, "Low-density parity-check codes," *IRE Transactions on Information Theory*, vol. 8, pp. 21–28, Jan. 1962.

[16] L. Bahl, C. Cullum, W. Frazer, and F. Jelinek, "An efficient algorithm for computing free distance (corresp.)," *IEEE Transactions on Information Theory*, vol. 18, pp. 437–439, May. 1972.

[17] L. Bahl, J. Cocke, F. Jelinek, and J. Raviv, "Optimal decoding of linear codes for minimizing symbol error rate (corresp.)," *IEEE Transactions on Information Theory*, vol. 20, pp. 284–287, Mar. 1974.

[18] F. J. MacWilliam and J. A. Sloane, *The theory of error-correcting codes*. North-Holland Mathematical Library, 1977.

[19] H. Imai and S. Hirakawa, "A new multilevel coding method using error-correcting codes," *IEEE Transactions on Information Theory*, vol. 23, pp. 371–377, May. 1977.

[20] J. Wolf, "Efficient maximum likelihood decoding of linear block codes using a trellis," *IEEE Transactions on Information Theory*, vol. 24, pp. 76–80, Jan. 1978.

[21] G. Ungerböck, "Channel coding with multilevel/phase signals," *IEEE Transactions on Information Theory*, vol. 28, pp. 55–67, Jan. 1982.

[22] L.-F. Wei, "Trellis-coded modulation with multidimensional constellations," *IEEE Transactions on Information Theory*, vol. 33, pp. 483–501, Jul. 1987.

[23] D. Divsalar and M. K. Simon, "Multiple trellis coded modulation (MTCM)," *IEEE Transactions on Communications*, vol. 36, pp. 410–419, Apr. 1988.

[24] G. J. Pottie and D. P. Taylor, "Multilevel codes based on partitioning," *IEEE Transactions on Information Theory*, vol. 35, pp. 87–98, Jan. 1989.

[25] A. R. Calderbank, "Multilevel codes and multistage decoding," *IEEE Transactions on Communications*, vol. 37, pp. 222–229, Mar. 1989.

[26] J. Hagenauer and P. Hoeher, "A Viterbi algorithm with soft-decision outputs and its applications," in *IEEE Global Telecommunications Conference*, pp. 1680–1686 vol.3, Nov. 1989.

[27] W. Koch and A. Baier, "Optimum and sub-optimum detection of coded data disturbed by time-varying intersymbol interference [applicable to digital mobile radio receivers]," in *IEEE Global Telecommunications Conference*, vol. 3, pp. 1679–1684, Dec. 1990.

[28] W. T. Webb, L. Hanzo, and R. Steele, "Bandwidth efficient QAM schemes for Rayleigh fading channels," *IEE Proceedings I, Communications, Speech and Vision*, vol. 138, pp. 169–175, Jun. 1991.

[29] E. Zehavi, "8-PSK trellis codes for a rayleigh channel," *IEEE Transactions on Communications*, vol. 40, pp. 873–884, May. 1992.

[30] C. Berrou, A. Glavieux, and P. Thitimajshima, "Near Shannon limit error-correcting coding and decoding: Turbo codes," in *Proceedings of the International Conference on Communications*, (Geneva, Switzerland), pp. 1064–1070, May. 1993.

[31] Y. Kofman, E. Zehavi, and S. Shamai, "Performance analysis of a multilevel coded modulation system," *IEEE Transactions on Communications*, vol. 42, pp. 299–312, Feb./Mar./Apr. 1994.

[32] J. Huber and U. Wachsmann, "Capacities of equivalent channels in multilevel coding schemes," *Electronics Letters*, vol. 30, pp. 557–558, Mar. 1994.

[33] S. L. Goff, A. Glavieux, and C. Berrou, "Turbo-codes and high spectral efficiency modulation," in *IEEE International Conference on Communications*, vol. 2, pp. 645–649, May. 1994.

[34] P. Robertson, E. Villebrun, and P. Hoeher, "A comparison of optimal and sub-optimal map decoding algorithms operating in the log domain," in *IEEE International Conference on Communications*, vol. 2, pp. 1009–1013, Jun. 1995.

[35] D. Raphaeli, "Noncoherent coded modulation," *IEEE Transactions on Communications*, vol. 44, pp. 172–183, Feb. 1996.

[36] P. Robertson and T. Wörz, "Bandwidth-efficient turbo trellis-coded modulation using punctured component codes," *IEEE Journal on selected areas in communications*, vol. 16, pp. 206–218, Feb. 1998.

[37] G. Caire, G. Taricco, and E. Biglieri, "Bit-interleaved coded modulation," *IEEE Transactions on Information Theory*, vol. 44, pp. 927–946, May. 1998.

[38] S. ten Brink, J. Speidel, and R. H. Han, "Iterative demapping for QPSK modulation," *Electronics Letters*, vol. 34, pp. 1459 –1460, July 1998.

[39] S. ten Brink, J. Speidel, and R. Yan, "Iterative demapping and decoding for multilevel modulation," in *IEEE Global Telecommunications Conference*, vol. 1, pp. 579–584, Nov. 1998.

[40] X. Li and J. A. Ritcey, "Trellis-coded modulation with bit-interleavering and iterative decoding," *IEEE Journal on Selected Areas in Communications*, vol. 17, Apr. 1999.

[41] R. H. Morelos-Zaragoza, M. P. C. Fossorier, S. Lin, and H. Imai, "Multilevel coded modulation for unequal error protection and multistage decoding.I. Symmetric constellations," *IEEE Transactions on Communications*, vol. 48, pp. 204–213, Feb. 2000.

[42] M. Isaka, M. P. C. Fossorier, R. H. Morelos-Zaragoza, S. Lin, and H. Imai, "Multilevel coded modulation for unequal error protection and multistage decoding. II. Asymmetric constellations," *IEEE Transactions on Communications*, vol. 48, pp. 774–786, May 2000.

[43] A. Chindapol and J. A. Ritcey, "Design, analysis, and performance evaluation for BICM-ID with square QAM constellations in rayleigh fading channels," *IEEE Journal on Selected Areas in Communications*, vol. 19, pp. 944–957, May. 2001.

[44] J. Hou and M. H. Lee, "Multilevel LDPC codes design for semi-BICM," *IEEE Communications Letters*, vol. 8, pp. 674–676, Nov. 2004.

[45] L. H. J. Lampe, R. F. H. Fischer, and R. Schober, "Multilevel coding for multiple-antenna transmission," in *2002 IEEE International Symposium on Information Theory*, p. 104, 2002.

[46] M. Sikora and D. J. Costello, "A new SISO algorithm with application to turbo equalization," *International Symposium on Information Theory, 2005. ISIT 2005. Proceedings*, pp. 2031–2035, Sept. 2005.

[47] A. Nysaeter and R. Otnes, "On filter-based turbo equalization with serially concatenated trellis coded modulation," *IEEE International Conference on Communications, 2005*, vol. 1, pp. 515–520, May. 2005.

[48] Y. Nana, E. Sharon, and S. Litsyn, "Improved decoding of LDPC coded modulations," *IEEE Communications Letters*, vol. 10, pp. 375–377, May. 2006.

[49] S. X. Ng, O. Alamri, Y. H. Li, J. Kliewer, and L. Hanzo, "Near-capacity turbo trellis coded modulation design based on EXIT charts and union bounds," *IEEE Transactions on Communications*, vol. 56, pp. 2030–2039, Dec. 2008.

[50] S. X. Ng, Y. Li, and L. Hanzo, "Distributed turbo trellis coded modulation for cooperative communications," *in processing of IEEE ICC'09*, Jun. 2009.

[51] Z. Yang, Q. Xie, K. Peng, and J. Song, "Labelling optimization for BICM-ID systems," *IEEE Communications Letters*, vol. 14, pp. 1047–1049, Nov. 2010.

[52] T. T. Nguyen and L. Lampe, "Bit-interleaved coded modulation with mismatched decoding metrics," *IEEE Transactions on Communications*, vol. 59, pp. 437–447, Feb. 2011.

[53] T. Islam, R. Schober, R. K. Mallik, and V. K. Bhargava, "Analysis and design of cooperative BICM-OFDM systems," *IEEE Transactions on Communications*, vol. 59, pp. 1742–1751, Jun. 2011.

[54] T. Cheng, K. Peng, Z. Liu, and Z. Yang, "Improve the performance of LTE turbo coded modulation by irregular mapping," in *IEEE Wireless Communications and Networking Conference (WCNC)*, pp. 597–601, Apr. 2012.

[55] C. Vladeanu, "Spatial modulation with joint antenna index and symbol index turbo trellis coding," *2013 International Symposium on Signals, Circuits and Systems (ISSCS)*, pp. 1–4, Jul. 2013.

[56] W. Liang, S. X. Ng, and L. Hanzo, "Pragmatic distributed algorithm for spectral access in cooperative cognitive radio networks," *IEEE Transactions on Communication*, vol. 62, pp. 1188–1200, Mar. 2014.

[57] H. Sun, S. X. Ng, C. Dong, and L. Hanzo, "Decode-and-forward cooperation-aided triple-layer turbo-trellis-coded hierarchical modulation," *IEEE Transactions on Communications*, vol. 63, pp. 1136–1148, Jan. 2015.

[58] T. B. Wo and P. A. Hoeher, "Superposition mapping with application in bit-interleaved coded modulation," *2010 International ITG Conference on Source and Channel Coding*, pp. 1–6, Jan. 2010.

[59] H. Roder, "Superposition of two modulated radio frequencies," *Proceedings of the Institute of Radio Engineers*, vol. 20, pp. 1962–1970, Dec. 1932.

[60] P. Bergmans and T. M. Cover, "Cooperative broadcasting," *IEEE Transactions on Information Theory*, vol. 20, pp. 317–324, May. 1974.

[61] P. Laurent, "Exact and approximate construction of digital phase modulations by superposition of amplitude modulated pulses (AMP)," *IEEE Transactions on Communications*, vol. 34, pp. 150–160, Feb. 1986.

[62] L. Duan, B. Rimoldi, and R. Urbanke, "Approaching the AWGN channel capacity without active shaping," *1997 IEEE International Symposium on Information Theory. 1997. Proceedings*, Jun.-Jul. 1997.

[63] S. Gadkari and K. Rose, "Time-division versus superposition coded modulation schemes for unequal error protection," *IEEE Transactions on Communications*, vol. 47, pp. 370–379, Mar. 1999.

[64] M. E. Pellenz and J. Portugheis, "Multistage turbo decoding for multilevel superposition coded modulation schemes," *IEEE International Symposium on Information Theory, 2000. Proceedings*, Jun. 2000.

[65] X. Wang and M. T. Orchard, "Design of superposition coded modulation for unequal error protection," *IEEE International Conference on Communications, 2001*, vol. 2, pp. 412–416, Jun. 2001.

[66] G. Karabulut and A. Yongacoglu, "Superposition block coded modulation," *Canadian Conference on Electrical and Computer Engineering, 2003*, vol. 3, pp. 1629–1632, May. 2003.

[67] G. Karabulut and A. Yongacoglu, "Rate design rule for superposition coded modulations," *Canadian Conference on Electrical and Computer Engineering, 2004*, vol. 1, pp. 365–368, May. 2004.

[68] T. W. Sun, R. D. Wesel, M. R. Shane, and K. Jarett, "Superposition turbo TCM for multirate broadcast," *IEEE Transactions on Communications*, vol. 52, pp. 368–371, Mar. 2004.

[69] E. G. Larsson and B. R. Vojcic, "Cooperative transmit diversity based on superposition modulation," *IEEE Communications Letters*, vol. 9, pp. 778–780, Sept. 2005.

[70] Z. G. Ding, T. Ratnarajah, and C. Cowan, "Cooperative multiple access systems using superposition modulation," *IEEE Information Theory Workshop, 2006*, pp. 497–501, Oct. 2006.

[71] K. Ishii, "Cooperative transmit diversity utilizing superposition modulation," *2007 IEEE Radio and Wireless Symposium*, pp. 337–340, Jan. 2007.

[72] C. Hasan and U. Aygolu, "An incremental relaying approach for superposition modulated cooperative transmission," *IEEE Wireless Communications and Networking Conference, 2009*, pp. 1–6, Apr. 2009.

[73] S. Huan, Z. S. Fei, L. Huang, and J. M. Kuang, "Cooperative transmission utilizing high order superposition modulation with iterative detection," *5th International Conference on Wireless Communications, Networking and Mobile Computing*, pp. 1–5, Sept. 2009.

[74] L. Ping, J. Tong, X. J. Yuan, and Q. H. Guo, "Superposition coded modulation and iterative linear MMSE detection," *IEEE Journal on Selected Areas in Communications*, vol. 27, pp. 995–1004, Aug. 2009.

[75] J. Tong, L. Ping, and X. Ma, "Superposition coded modulation with peak-power limitation," *IEEE Transactions on Information Theory*, vol. 55, pp. 2562–2576, Jun. 2009.

[76] R. Zhang and L. Hanzo, "A unified treatment of superposition coding aided communications: Theory and practice," *IEEE Communications Surveys and Tutorials*, vol. 13, pp. 503–520, Jul. 2010.

[77] P. A. Hoeher and T. B. Wo, "Superposition modulation: myths and facts," *IEEE Communications Magazine*, vol. 49, pp. 110–116, Dec. 2011.

[78] H. Sun, S. X. Ng, and L. Hanzo, "Superposition coded modulation for cooperative communications," *2012 IEEE Vehicular Technology Conference (VTC Fall)*, pp. 1–5, Sept. 2012.

[79] M. Noemm, A. Mourad, and P. A. Hoeher, "Superposition modulation with irregular convolutional coding," *2012 IEEE Global Communications Conference*, pp. 2346–2350, Dec. 2012.

[80] Z. P. Xi, J. Zhu, X. Man, and Y. M. Fu, "A novel demodulation approach for modified superposition modulation based on decorrelation," *2013 International Conference on Wireless Communications and Signal Processing*, pp. 1–3, Oct. 2013.

[81] X. Chen, M. X. Xie, and Z. Y. Wang, "An low density parity-check coded adaptive cooperation scheme based on orthogonal superposition modulation," *2013 6th International Congress on Image and Signal Processing*, vol. 3, pp. 1231–1235, Dec. 2013.

[82] S. C. Zhao, X. Ma, and B. M. Bai, "Decoding algorithms of LDPC coded superposition modulation," *IEEE Communications Letters*, vol. 18, pp. 487–490, Mar. 2014.

[83] A. E. Z. Eldin, E. A. A. A. Hagras, and A.-K. H. Mansour, "C4. multi rate single code multi carrier superposition coded modulation (MR-SC-MC-SCM) for multi user communications," *2015 32nd National Radio Science Conference (NRSC)*, pp. 127–138, Mar. 2015.

[84] C. Hellge, S. Mirta, T. Schierl, and T. Wiegand, "Mobile TV with SVC and hierarchical modulation for DVB-H broadcast services," *IEEE International Symposium on Broadband Multimedia Systems and Broadcasting, 2009. BMSB '09.*, pp. 1–5, May. 2009.

[85] S. Wang, S. Kwon, and B. K. Yi, "On enhancing hierarchical modulation," *IEEE International Symposium, Broadband Multimedia System and Broadcasting*, pp. 1–6, Jun. 2008.

[86] R. Y. Kim and Y.-Y. Kim, "Symbol-level random network coded cooperation with hierarchical modulation in relay communication," *IEEE Transactions on Consumer Electronics*, vol. 55, pp. 1280–1285, Oct. 2009.

[87] H. Jiang and P. A. Wilford, "A hierarchical modulation for upgrading digital broadcast systems," *IEEE Transactions on Broadcasting*, pp. 223–229, Jun. 2005.

[88] M. K. Chang and S. Y. Lee, "Performance analysis of cooperative communication system with hierarchical modulation over Rayleigh fading channel," *IEEE Transactions on Wireless Communications*, vol. 8, pp. 2848–2852, Jun 2009.

[89] S. Y. Lee and K. C. Whang, "A collaborative cooperation scheme using hierarchical modulation," *IEEE 68th Vehicular Technology Conference (VTC)*, pp. 1–5, Sep. 2008.

[90] X. H. Zhang, A. Ghrayeb, and M. Hasna, "On hierarchical network coding versus opportunistic user selection for two-way relay channels with asymmetric data rates," *IEEE Transactions on Communications*, vol. 61, pp. 2900–2910, May. 2013.

[91] H. Mukhtar and M. EI-Tarhuni, "An adaptive hierarchical QAM scheme for enhanced bandwidth and power utilization," *IEEE Transactions on Communications*, vol. 60, pp. 2275–2284, Aug. 2012.

[92] K. Ramchandran, A. Ortega, K. M. Uz, and M. Vetterli, "Multiresolution broadcast for digital HDTV using joint source/channel coding," *IEEE Journal on Selected Areas in Communications*, vol. 11, pp. 6–23, Jan. 1993.

[93] S. H. Chang, R. Minjoong, P. C. Cosman, and L. B. Mistein, "Optimized unequal error protection using multiplexed hierarchical modulation," *IEEE Transactions on Information Theory*, vol. 58, pp. 5816–5840, Sept. 2012.

[94] Y. J. Noli, H. C. Lee, and L. Y. Lee, "Design of unequal error protection for MIMO-OFDM systems with hierarchical signal constellations," *Journal of Communications and Networks*, vol. 9, pp. 167–176, Jun. 2007.

[95] Y. C. Chang, S. W. Lee, and R. Komiya, "A low complexity hierarchical QAM symbol bits allocation algorithm for unequal error protection of wireless video transmission," *IEEE Transactions on Consumer Electronics*, vol. 55, pp. 1089–1097, Aug. 2009.

[96] K. M. Alajel, W. Xiang, and Y. F. Wang, "Unequal error protection scheme based hierarchical 16-QAM for 3-D video transmission," *IEEE Transactions on Consumer Electronics*, vol. 58, pp. 731–738, Aug. 2012.

[97] S. S. Arslan, P. C. Cosman, and L. B. Milstein, "Coded hierarchical modulation for wireless progressive image transmission," *IEEE Transactions on Vehicular Technology*, pp. 4299 – 4313, Nov. 2011.

[98] S. S. Arslan, P. C. Cosman, and L. B. Milstein, "On hard decision upper bounds for coded M-ary hierarchical modulation," *2011 45th Annual Conference on Information Sciences and Systems (CISS)*, pp. 1–6, Mar. 2011.

[99] K. Fazel and M. Ruf, "Combined multilevel coding and multiresolution modulation," *Conference Record, IEEE International Conference on Communications, 1993. ICC '93 Geneva*, vol. 2, pp. 23–26, May. 1993.

[100] M. Morimoto, M. Okada, and S. Komaki, "Joint on-board resource sharing and hierarchical modulation scheme for satellite communication," *IEEE Global Telecommunications Conference, 1995*, vol. 3, pp. 14–16, Nov. 1995.

[101] M. Morimoto, M. Okada, and S. Komaki, "A hierarchical image transmission system for multimedia mobile communication," *First International Workshop on Wireless Image/Video Communications, 1996*, pp. 80–84, Sept. 1996.

[102] O'Leary, "Hierarchical transmission and COFDM systems," *IEEE Transactions on Broadcasting*, vol. 43, pp. 166–174, Jun. 1997.

[103] V. Engels and H. Rohling, "Multi-resolution 64-DAPSK modulation in a hierarchical COFDM transmission system," *IEEE Transactions on Broadcasting*, vol. 44, pp. 139–149, Mar. 1998.

[104] D. W. Schill, D. F. Yuan, and J. B. Huber, "Efficient hierarchical broadcasting using multilevel codes," *Information Theory and Networking Workshop, 1999*, Jun. 1999.

[105] A. Seegert, "Broadcast communication on fading channels using hierarchical coded modulation," *IEEE Global Telecommunications Conference, 2000*, vol. 1, pp. 92–97, Nov. 2000.

[106] P. K. Vitthaladevuni and M. S. Alouini, "Ber computation of 4/M-QAM hierarchical constellations," *IEEE Transactions on Broadcasting*, vol. 47, pp. 228–239, Sept. 2001.

[107] P. K. Vitthaladevuni and M. S. Alouini, "A recursive algorithm for the exact BER computation of generalized hierarchical QAM constellations," *IEEE Transactions on Information Theory*, vol. 49, pp. 297–307, Jan. 2003.

[108] J. Pons, P. Duvaut, O. Moreno, and L. Pierrugues, "Enhanced TCM based on a multilevel hierarchical trellis coded modulation (HTCM)," *IEEE Global Telecommunications Conference, 2004*, vol. 4, pp. 2589–2593, Dec. 2004.

[109] B. Barmada, M. M. Ghandi, E. V. Jones, and M. Ghanbari, "Prioritized transmission of data partitioned H.264 video with hierarchical QAM," *IEEE Signal Processing Letters*, vol. 12, pp. 577–580, Aug. 2005.

[110] J. Hossain, P. K. Vitthaladevuni, M. S. Alouini, and V. K. Bhargava, "Adaptive hierarchical modulation for simultaneous voice and multiclass data transmission over fading channels," *IEEE Transactions on Vehicular Technology*, vol. 55, pp. 1181–1194, Jul. 2006.

[111] M. J. Hossain, P. K. Vitthaladevuni, M. S. Alouini, and V. K. Bhargava, "Hierarchical modulations for multimedia and multicast transmission over fading channels," *The 57th IEEE Semiannual Vehicular Technology Conference, 2003. VTC 2003-Spring*, vol. 4, pp. 2633–2637, Apr. 2003.

[112] M. J. Hossain, M. S. Alouini, and V. K. Bhargava, "Hierarchical constellation for multiresolution data transmission over block fading channels," *IEEE Transactions on Wireless Communications*, vol. 5, pp. 849–857, Apr. 2006.

[113] Y. C. Chang, S. W. Lee, and R. Komiya, "A low-complexity unequal error protection of H.264/AVC video using adaptive hierarchical QAM," *IEEE Transactions on Consumer Electronics*, vol. 52, pp. 1153–1158, Now. 2006.

[114] C. Hausl and J. Hagenauer, "Relay communication with hierarchical modulation," *IEEE Communications Letters*, vol. 11, pp. 64–66, Jan. 2007.

[115] S. Wang and B. K. Yi, "Optimizing enhanced hierarchical modulations," *IEEE Global Telecommunications Conference, 2008*, pp. 1–5, Nov.-Dec. 2008.

[116] J. M. Park, S. L. Kim, and J. Choi, "Hierarchically modulated network coding for asymmetric two-way relay systems," *IEEE Transactions on Vehicular Technology*, vol. 59, pp. 2179–2184, Mar. 2010.

[117] M. G. Peng, Y. Liu, and W. B. Wang, "Hierarchical cooperative relay based heterogeneous networks," *IEEE Wireless Communications*, vol. 18, pp. 48–56, Jun. 2011.

[118] S. H. Chang, M. Rim, P. C. Cosman, and L. B. Milstein, "Optimized unequal error protection using multiplexed hierarchical modulation," *IEEE Transactions on Information Theory*, vol. 58, pp. 5816–5840, Sept. 2012.

[119] Z. X. Hu and H. Liu, "A low-complexity LDPC decoding algorithm for hierarchical broadcasting: Design and implementation," *IEEE Transactions on Vehicular Technology*, vol. 62, pp. 1843–1849, Dec. 2012.

[120] X. Wang and L. Cai, "Proportional fair scheduling in hierarchical modulation aided wireless networks," *IEEE Transactions on Wireless Communications*, vol. 12, pp. 1584–1593, Mar. 2013.

[121] H. Meric, J. Lacan, F. Arnal, G. Lesthievent, and M. L. Boucheret, "Combining adaptive coding and modulation with hierarchical modulation in satcom systems," *IEEE Transactions on Broadcasting*, vol. 59, pp. 627–637, Dec. 2013.

[122] B. Mouhouche, A. Mourad, and D. Ansorregui, "Throughput optimization of precoded OFDM with hierarchical modulation," *7th International Conference on Signal Processing and Communication Systems (ICSPCS), 2013*, pp. 1–10, Dec. 2013.

[123] A. Saeed, H. J. Xu, and T. Quazi, "Alamouti space-time block coded hierarchical modulation with signal space diversity and MRC reception in Nakagami-m fading channel," *IET Communications*, vol. 8, pp. 516–524, Mar. 2014.

[124] R. Leung, J. L. Liu, E. Poon, A. L. C. Chan, and B. C. Li, "MP-DSR: a QoS-aware multi-path dynamic source routing protocol for wireless ad-hoc networks," *Annual IEEE Conference on Local Computer Networks, 2001. Proceedings. LCN 2001.*, pp. 132–141, Nov. 2001.

[125] C. E. Perkins and E. M. Royer, "Ad-hoc on-demand distance vector routing," *Second IEEE Workshop on Mobile Computing Systems and Applications, 1999. Proceedings. WMCSA '99*, pp. 90–100, Feb. 1999.

[126] M. Zorzi and R. R. Rao, "Geographic random forwarding (GeRaF) for ad hoc and sensor networks: multihop performance," *IEEE Transactions on Mobile Computing*, vol. 2, pp. 337–348, Oct. 2003.

[127] C. Lott and D. Teneketzis, "Stochastic routing in ad-hoc networks," *IEEE Transactions on Automatic Control*, vol. 51, pp. 52–70, Jan. 2006.

[128] N. Chakchouk, "A survey on opportunistic routing in wireless communication networks," *IEEE Communications Surveys & Tutorials*, vol. PP, Mar. 2015.

[129] J. Zuo, C. Dong, H. V. Nguyen, S. X. Ng, and L. Hanzo, "Cross-layer aided energy-efficient opportunistic routing in ad hoc networks," *IEEE Transactions on Communications*, vol. 62, pp. 522–535, Jan. 2014.

[130] H. T. Liu, B. X. Zhang, H. T. Mouftah, X. Shen, and J. Ma, "Opportunistic routing for wireless ad hoc and sensor networks: Present and future directions," *IEEE Communications Magazine*, vol. 47, pp. 103–109, Dec. 2009.

[131] K. Zeng, W. J. Lou, and H. Q. Zhai, "Capacity of opportunistic routing in multi-rate and multi-hop wireless networks," *IEEE Transactions on Wireless Communications*, vol. 7, pp. 5118–5128, Dec. 2008.

[132] S. Biswas and R. Morris, "ExOR: Opportunistic routing in multi-hop wireless networks," *in Proc. ACM SIGCOMM*, pp. 133–144, 2005.

[133] S. Chachulski, M. Jennings, S. Katti, and D. Katabi, "Trading structure for randomness in wireless opportunistic routing," *in Proc. ACM SIGCOMM*, pp. 169–180, 2007.

[134] Y. H. Li, A. Mohaisen, and Z. L. Zhang, "Trading optimality for scalability in large-scale opportunistic routing," *IEEE Transactions on Vehicular Technology*, vol. 62, pp. 2253–2263, Dec. 2012.

[135] G. Y. Lee and Z. J. Haas, "Simple, practical, and effective opportunistic routing for short-haul multi-hop wireless networks," *IEEE Transactions on Wireless Communications*, vol. 10, pp. 3583–3588, Oct. 2011.

[136] X. C. Jin, R. Zhang, J. C. Sun, and Y. C. Zhang, "TIGHT: A geographic routing protocol for cognitive radio mobile ad hoc networks," *IEEE Transactions on Wireless Communications*, vol. 13, pp. 4670–4681, Apr. 2014.

[137] H. Fussler, J. Widmer, M. Kasemann, M. Mauve, and H. Hartenstein, "Contention-based forwarding for mobile ad-hoc networks," *Ad Hoc Networks*, vol. 2, pp. 337–348, Nov. 2003.

[138] B. Zhao, R. Seshadri, and M. C. Valenti, "Geographic random forwarding with hybrid-arq for ad hoc networks with rapid sleep cycles," *IEEE Global Telecommunications Conference, 2004*, vol. 5, pp. 3047–3052, Nov.-Dec. 2004.

[139] S. Biswas and R. Morris, "Opportunistic routing in multi-hop wireless networks," *ACM SIGCOMM Computer Commun. Rev.*, vol. 34, p. 6974, Jan. 2004.

[140] Y. Yuan, H. Yang, S. Wong, S. Lu, and W. Arbaugh, "ROMER: Resilient opportunistic mesh routing for wireless mesh networks," *in Proc. IEEE Workshop on Wireless Mesh Networks(WiMesh)*, Sept. 2005.

[141] J. LeBrun, C. N. Chuah, D. Ghosal, and M. Zhang, "Knowledge-based opportunistic forwarding in vehicular wireless ad hoc networks," *2005 IEEE 61st Vehicular Technology Conference, 2005. VTC 2005-Spring*, vol. 4, pp. 2289–2293, May.-Jun. 2005.

[142] C. Westphal, "Opportunistic routing in dynamic ad hoc networks: the OPRAH protocol," *2006 IEEE International Conference on Mobile Adhoc and Sensor Systems*, pp. 570–573, Oct. 2006.

[143] E. Rozner, J. Seshadri, Y. Mehta, and L. L. Qiu, "Simple opportunistic routing protocol for wireless mesh networks," *2nd IEEE Workshop on Wireless Mesh Networks, 2006*, pp. 48–54, Sept. 2006.

[144] Z. Zhong, J. Wang, G. Lu, and S. Nelakuditi, "On selection of candidates for opportunistic anypath forwarding," *in Proc. Conference of the ACM Special Interest Group on Data Communication (SIGCOMM)*, 2006.

[145] K. Zeng, W. Lou, J. Yang, and D. B. III, "On throughput efficiency of geographic opportunistic routing in multihop wireless networks," *Mobile Networks Apllications*, vol. 12, pp. 347–357, Dec. 2007.

[146] M. Nassr, J. Jun, S. Eidenbenz, A. Hansson, and A. Mielke, "Scalable and reliable sensor network routing: Performance study from field deployment," *IEEE INFOCOM 2007. 26th IEEE International Conference on Computer Communications*, pp. 670–678, May. 2007.

[147] Y. Lin, B. Li, and B. Liang, "CodeOR: Opportunistic routing in wireless mesh networks with segmented network coding," *IEEE International Conference on Network Protocols, 2008*, pp. 13–22, Oct. 2008.

[148] D. Koutsonikolas, Y. Hu, and C. Wang, "Xcor: synergistic interflow network coding and opportunistic routing," *in Proc. the ACM Annual international Conference on Mobile Computing and Networking(MobiCom)*, Sept. 2008.

[149] V. Conan, J. Leguay, and T. Friedman, "Ieee journal on selected areas in communications," *Fixed point opportunistic routing in delay tolerant networks*, vol. 26, pp. 773–782, Jun. 2008.

[150] K. Zeng, Z. Y. Yang, and W. J. Lou, "Location-aided opportunistic forwarding in multirate and multihop wireless networks," *IEEE Transactions on Vehicular Technology*, vol. 58, pp. 3032–3040, Dec. 2008.

[151] S. B. Yang, F. Zhong, C. K. Yeo, B. S. Lee, and J. Boleng, "Position based opportunistic routing for robust data delivery in MANETs," *IEEE Global Telecommunications Conference, 2009*, pp. 1–6, Nov.-Dec. 2009.

[152] R. Laufer, H. Dubois-Ferriere, and L. Kleinrock, "Multirate anypath routing in wireless mesh networks," *IEEE INFOCOM 2009*, pp. 37–45, Apr. 2009.

[153] Y. F. Lin, B. Liang, and B. C. Li, "SlideOR: Online opportunistic network coding in wireless mesh networks," *2010 Proceedings IEEE INFOCOM*, pp. 1–5, Mar. 2010.

[154] M. Naghshvar and T. Javidi, "Opportunistic routing with congestion diversity in wireless multi-hop networks," *2010 Proceedings IEEE INFOCOM*, pp. 1–5, Mar. 2010.

[155] A. Bletsas, A. G. Dimitriou, and J. N. Sahalos, "Interference-limited opportunistic relaying with reactive sensing," *IEEE Transactions on Wireless Communications*, vol. 9, pp. 14–20, Jan. 2010.

[156] X. F. Mao, S. J. Tang, X. H. Xu, X. Y. Li, and H. D. Ma, "Energy-efficient opportunistic routing in wireless sensor networks," *IEEE Transactions on Parallel and Distributed Systems*, vol. 22, pp. 1934–1942, Feb. 2011.

[157] C. Y. Lee and G. U. Hwang, "Minimum energy consumption design of a two-hop relay network for QoS guarantee," *2010 Wireless Telecommunications Symposium (WTS)*, pp. 1–6, Apr. 2010.

[158] X. Fang, D. J. Yang, and G. L. Xue, "Consort: Node-constrained opportunistic routing in wireless mesh networks," *2011 Proceedings IEEE INFOCOM*, pp. 1907–1915, Apr. 2011.

[159] A. A. Bhorkar, M. Naghshvar, T. Javidi, and B. D. Rao, "Adaptive opportunistic routing for wireless ad hoc networks," *IEEE/ACM Transactions on Networking*, vol. 20, pp. 243–256, Jul. 2011.

[160] Q. Lampin, D. Barthel, I. Auge-Blum, and F. Valois, "QoS oriented opportunistic routing protocol for wireless sensor networks," *2012 IFIP Wireless Days (WD)*, pp. 1–6, Nov. 2012.

[161] Z. H. Wang, Y. Z. Chen, and C. Li, "CORMAN: A novel cooperative opportunistic routing scheme in mobile ad hoc networks," *IEEE Journal on Selected Areas in Communications*, vol. 30, pp. 289–296, Feb. 2012.

[162] S. Guo, L. He, Y. Gu, B. Jiang, and T. He, "Opportunistic flooding in low-duty-cycle wireless sensor networks with unreliable links," *IEEE Transactions on Computers*, vol. 63, pp. 2787–2803, Jul. 2013.

[163] M. J. Xiao, J. Wu, C. Liu, and L. S. Huang, "TOUR: Time-sensitive opportunistic utility-based routing in delay tolerant networks," *2013 Proceedings IEEE INFOCOM*, pp. 2085–2091, Jun. 2013.

[164] W. Y. Shin, S. Y. Chung, and Y. H. Lee, "Parallel opportunistic routing in wireless networks," *IEEE Transactions on Information Theory*, vol. 59, pp. 6290–6300, Jul. 2013.

[165] X. X. Zhong, Y. Qin, Y. Y. Yang, and L. Li, "CROR: Coding-aware opportunistic routing in multi-channel cognitive radio networks," *2014 IEEE Global Communications Conference (GLOBECOM)*, pp. 8–12, Dec. 2014.

[166] M. J. Xiao, J. Wu, and L. S. Huang, "Community-aware opportunistic routing in mobile social networks," *IEEE Transactions on Computers*, vol. 63, pp. 1682–1695, Jun. 2014.

[167] C. Dong, L. L. Yang, J. Zuo, S. X. Ng, and L. Hanzo, "Energy, delay, and outage analysis of a buffer-aided three-node network relying on opportunistic routing," *IEEE Transactions on Communications*, vol. 63, Feb. 2015.

[168] F. Wu, K. Gong, T. R. Zhang, G. H. Chen, and C. M. Qiao, "COMO: A game-theoretic approach for joint multirate opportunistic routing and forwarding in non-cooperative wireless networks," *IEEE Transactions on Wireless Communications*, vol. 14, pp. 948–959, Feb. 2015.

[169] M. Elias, A. Khattab, and K. M. F. Elsayed, "CORB: Context-aware opportunistic resource-based routing for stationary wireless sensor networks," *2015 International Conference on Computing, Networking and Communications (ICNC)*, pp. 166–170, Feb. 2015.

[170] A. M. Popescu, N. Salman, and A. H. Kemp, "Energy consumption analysis of geographic routing in wsns with location error," *18th European Wireless Conference, European Wireless, 2012. EW*, Apr. 2012.

[171] Y. Li, Y. R. Jiang, D. P. Jin, L. Su, L. G. Zeng, and D. P. Wu, "Energy-efficient optimal opportunistic forwarding for delay-tolerant networks," *IEEE Transactions on Vehicular Technology*, vol. 59, pp. 4500–4512, Aug. 2010.

[172] Z. J. Mo, W. F. Su, S. Batalama, and J. D. Matyjas, "Cooperative communication protocol designs based on optimum power and time allocation," *IEEE Transactions on Wireless Communications*, vol. 13, pp. 4283–4296, Apr. 2014.

[173] T. S. Abraham and K. Narayanan, "Cooperative communication for vehicular networks," *2014 International Conference on Advanced Communication Control and Computing Technologies*, pp. 1163–1167, May. 2014.

[174] A. Nosratinia, T. E. Hunter, and A. Hedayat, "Cooperative communication in wireless networks," *IEEE Communications Magazine*, vol. 42, pp. 74–80, Oct. 2004.

[175] Z. Y. Chen and H. Liu, "Spectrum-efficient coded modulation design for two-way relay channels," *IEEE Journal on Selected Areas in Communications*, vol. 32, pp. 251–263, May. 2013.

[176] J. L. Li and A. Stefanov, "Cooperative multiple trellis coded modulation," *IEEE Transactions on Communications*, vol. 57, pp. 688–696, Mar. 2009.

[177] L. Chen, R. A. Carrasco, S. LeGoff, and I. J. Wassell, "Cooperative amplify-and-forward with trellis coded modulation," *IEEE Wireless Communications and Networking Conference, 2009*, pp. 1–5, Apr. 2009.

[178] C. H. Choi, Y. J. Kim, and G. H. Im, "Bit-interleaved coded transmission with multilevel modulation for non-orthogonal cooperative systems," *IEEE Transactions on Communications*, vol. 59, pp. 95–105, Jan. 2011.

[179] Z. Y. Li, M. Peng, and W. B. Wang, "Hierarchical modulated channel and network coding scheme in the multiple-access relay system," *2011 IEEE 13th International Conference on Communication Technology (ICCT)*, pp. 984–988, Sept. 2011.

[180] Z. G. Du, P. L. Hong, K. P. Xue, and J. L. Peng, "Hierarchically modulated coded cooperation for relay system," *2012 IEEE Consumer Communications and Networking Conference (CCNC)*, pp. 812–816, Jan. 2012.

[181] D. K. Kwon, W. J. Kim, K. H. Suh, and H. Lim, "A higher data-rate T-DMB system based on a hierarchical A-DPSK modulation," *IEEE Transactions on Broadcasting*, vol. 55, pp. 42–50, Mar. 2009.

[182] S. X. Ng, J. Y. Chung, and L. Hanzo, "Turbo-detected unequal protection MPEG-4 wireless video telephony using multi-level coding, trellis coded modulation and space-time trellis coding," *IEE Proceedings Communications*, vol. 152, pp. 1116–1124, Dec. 2005.

[183] S. X. Ng, C. Y. Qian, D. D. Liang, and L. Hanzo, "Adaptive turbo trellis coded modulation aided distributed space-time trellis coding for cooperative communications," *Vehicular Technology Conference (VTC 2010-Spring), 2010 IEEE 71st*, pp. 1–5, May. 2010.

[184] H. Sun, Y. R. Shen, S. X. Ng, and L. Hanzo, "Turbo trellis coded hierarchical modulation for cooperative communications," *Wireless Communications and Networking Conference (WCNC)*, pp. 2789–2794, Apr. 2013.

[185] H. Sun, S. X. Ng, and L. Hanzo, "Turbo trellis-coded hierarchical modulation assisted decode-and-forward cooperation," *IEEE Transactions on Vehicular Technology*, vol. 64, pp. 3971–3981, Oct. 2014.

[186] H. Sun, S. X. Ng, and L. Hanzo, "The discrete-input continuous-output memoryless channel capacity of cooperative hierarchical modulation," *IET Communications*, vol. 10, pp. 65–71, Jan. 2016.

[187] H. Sun, C. Dong, S. X. Ng, and L. Hanzo, "Five decades of hierarchical modulation and its benefits in relay-aided networking," *IEEE Access*, vol. 3, pp. 2891–2921, Dec. 2015.

[188] D. Divsalar and M. K. Simon, "The design of trellis coded MPSK for fading channels: set partitioning for optimum code design," *IEEE Transactions on Communications*, vol. 36, pp. 1013–1021, Sept. 1988.

[189] D. Divsalar and M. K. Simon, "The design of trellis coded MPSK for fading channels: performance criteria," *IEEE Transactions on Communication*, vol. 36, pp. 1004–1012, Aug. Spt.

[190] C. Berrou, A. Glavieux, and P. Thitimajshima, "Near shannon limit error-correcting coding and decoding: Turbo-codes," *International Conference on Communications, 1993. Geneva*, vol. 2, pp. 1064–1070, May 1993.

[191] J. Kilewer, S. X. Ng, and L. Hanzo, "On the computation of EXIT characteristics for symbol-based iterative decoding," *2006 4th International Symposium on Turbo Codes Related Top-*

ics; 6th International ITG-Conference on Source and Channel Coding (TURBOCODING), pp. 1–6, Apr. 2006.

[192] P. Robertson, "An overview of bandwidth efficient turbo coding schemes," *International Symposium on Turbo Codes and Related Topics (Brest, France)*, pp. 103–110, Sept. 1997.

[193] S. ten Brink, "Convergence behavior of iteratively decoded parallel concatenated codes," *IEEE Transactions on Communications*, vol. 49, pp. 1727–1737, Aug. 2002.

[194] A. Ashikhmin, G. Kramer, and S. ten Brink, "Extrinsic information transfer functions: model and erasure channel properties," *IEEE Transactions on Information Theory*, vol. 50, pp. 2657–2673, Nov. 2004.

[195] S. X. Ng, J. Wang, and L. Hanzo, "Unveiling near-capacity code design: The realization of shannon's communication theory for MIMO channels," *IEEE International Conference on Communications, 2008. ICC '08.*, pp. 1415–1419, May. 2008.

[196] L. Hanzo, O. Alamri, M. El-Hajjar, and N. Wu, *Near-Capacity Multi-Functional MIMO Systems: Sphere-Packing, Iterative Detection and Cooperation*. Wiley-IEEE Press, 2009.

[197] S. X. Ng, J. Kliewer, O. R. Alamri, and L. Hanzo, "On the design of turbo trellis coded modulation schemes using symbol-based Exit charts," *2006 IEEE 64th Vehicular Technology Conference, 2006. VTC-2006 Fall*, pp. 1–5, Sept. 2006.

[198] S. X. Ng, J. Wang, and L. Hanzo, "Unveiling near-capacity code design: the realization of shannon's communication theory for mimo channels," *IEEE International Conference on Communications, 2008. ICC '08*, pp. 1415–1419, May. 2008.

[199] M. El-Hajjar and L. Hanzo, "EXIT charts for system design and analysis," *IEEE Communications Surveys and Tutorials*, vol. 16, pp. 127–153, May. 2013.

[200] D. Divsalar and M. K. Simon, "The design of trellis coded mpsk for fading channel: set partitioning for optimum code design," *IEEE Transactions on Communications*, vol. 36, pp. 1015–1019, Sept. 1988.

[201] S. X. Ng, T. H. Liew, L. L. Yang, and L. Hanzo, "Comparative study of TCM, TTCM, BICM and BICM-ID schemes," *IEEE Vehicular Technology Conference, (Rhodes, Greece)*, pp. 2450–2454, May. 2010.

[202] S. Huan, Z. Fei, L. Huang, and J. Kuang, "Cooperative transmission utilizing high order superposition modulation with iterative detection," *IEEE Communications Letters*, pp. 1–5, Sept. 2009.

[203] S. X. Ng, K. Zhu, and L. Hanzo, "Distributed source-coding channel-coding and modulation for cooperative communication," *Vehicular Technology Conference Fall (VTC 2010-Fall), 2010 IEEE 72nd*, pp. 1–5, Sept. 2010.

[204] S. Katti, I. Marie, A. Goldsmith, D. Katabi, and M. Medard, "Joint relaying and network coding in wireless networks," *IEEE International Symposium on Information Theory, 2007*, pp. 1101–1105, Jun. 2007.

[205] L. Huang, Z. S. Fei, and J. M. Kuang, "A decode-and-forward relaying scheme based on orthogonal superposition modulation," *11th IEEE International Conference on Communication Technology, 2008. ICCT 2008*, pp. 241–244, Nov. 2008.

[206] H. Ochiai, P. Mitran, and V. Tarokh, "Design and analysis of collaborative diversity protocols for wireless sensor networks," *VTC2004-Fall, IEEE 60th Vehicular Technology Coference*, vol. 7, pp. 4645–4649, Sept. 2004.

[207] S. Wang, S. Kwon, and B. K. Yi, "On enhancing hierarchical modulation," *IEEE International Symposium, Broadband Multimedia System and Broadcasting*, pp. 1–6, Jun. 2008.

[208] M. J. Hossain, M. S. Alouini, and V. K. Bhargava, "Rate adaptive hierarchical modulation-assisted two-user opportunistic scheduling," *IEEE Transactions on, Wireless Communications*, vol. 6, pp. 2076–2085, Aug. 2007.

[209] Z. Y. Li, M. G. Peng, and W. B. Wang, "Hierarchical modulated channel and network coding scheme in the multiple-access relay system," *2011 IEEE 13th International Conference on Communication Technology (ICCT)*, pp. 984–988, Sept. 2011.

[210] A. Sendonaris, E. Erkip, and B. Aazhang, "User cooperation diversity Part I and Part II," *IEEE Transactions on Communications*, vol. 51, pp. 1927–1938, Nov. 2003.

[211] Y. Azar, G. N. Wong, K. wang, and R. Mayzus, "28 GHz propagation measurements for outdoor cellular communications using steerable beam antennas in New York city," *2013 IEEE International Conference on Communications (ICC)*, pp. 5143–5147, Jun. 2013.

[212] S. M. Ross, *Introduction to probability models*. Academic Press., 9th ed., 2007.

[213] S. X. Ng and L. Hanzo, "On the MIMO channel capacity of multidimensional signal sets," *IEEE Transactions on Vehicular Technology*, vol. 55, pp. 528–536, Mar. 2006.

[214] T. M. Cover and J. A. Thomas, *Elements of information theory*. Wiley-Interscience Press, 2rd ed., 2006.

[215] D. J. C. MacKay and R. M. Neal, "Near shannon limit performance of low density parity check codes," *Electronics Letters*, vol. 32, Aug. 1996.

[216] B. Scanavino, G. Montorsi, and S. Benedetto, "Convergence properties of iterative decoders working at bit and symbol level," *IEEE Global Telecommunications Conference, 2001. GLOBECOM'01*, vol. 2, pp. 1037–1041, Nov. 2001.

[217] M. D. Renzo, H. Haas, A. Ghrayeb, S. Sugiura, and L. Hanzo, "Spatial modulation for generalized MIMO: challenges, opportunities, and implementation," *Proceedings of the IEEE*, vol. 102, pp. 56–103, Jan. 2014.

[218] L. Wang and L. Hanzo, "The resource-optimized differentially modulated hybrid AF/DF cooperative cellular uplink using multiple-symbol differential sphere detection," *IEEE Signal Processing Letters*, vol. 16, pp. 965–968, Jul. 2009.

[219] X. C. Zhang and J. G. Andrews, "Downlink cellular network analysis with multi-slope path loss models," *IEEE Transactions on Communications*, vol. 63, pp. 1881–1894, Mar. 2015.

[220] Y. K. Huo, M. El-Hajjar, and L. Hanzo, "Inter-layer FEC aided unequal error protection for multilayer video transmission in mobile TV," *IEEE Transactions on Circuits and Systems for Video Technology*, vol. 23, pp. 1622–1634, Sept. 2013.

[221] Y. Azar, G. Wong, K. Wang, R. Mayzus, J. Schulz, H. Zhao, F. Gutierrez, D. Hwang, and T. Rappaport, "28 GHz propagation measurements for outdoor cellular communications using steerable beam antennas in New York city," *IEEE International Conference on Communications (ICC) in 2013*, p. 51435147, Jun. 2013.

[222] A. Papoulis, *Probability, Random Variables and Stochastic Processes, 4th ed.* McGraw-Hill, Jan. 2002.

[223] C. Dong, L.-L. Yang, and L. Hanzo, "Performance analysis of multihop-diversity-aided multihop links," *IEEE Transactions on Vehicular Technology*, vol. 61, pp. 2504–2516, Apr. 2012.

[224] M. D. Renzo, H. Haas, A. Ghrayeb, S. Sugiura, and L. Hanzo, "Spatial modulation for generalized MIMO: Challenges, opportunities, and implementation," *Proceedings of the IEEE*, vol. 102, pp. 56–103, Jan. 2014.

[225] H. Labiod, *Wireless Ad Hoc and Sensor Networks.* Wiley-IEEE Press, 2010.

[226] W. S. L and Y. C. Tseng, *Wireless Ad Hoc Networking: Personal-Area, Local-Area, and the Secsory-Area Networks.* Auerbach Publications, 2007.

[227] D. B. Johnson, "Routing in *Ad Hoc* networks of mobile hosts," *Mobile Computing Systems and Applications, 1994*, pp. 158–163, Dec. 1994.

[228] R. L. Davies, R. M. Watson, A. Munro, and M. H. Barton, "*Ad-hoc* wireless networking: contention free multiple access," *Fifth IEE Conference on Telecommunications, 1995*, pp. 73–77, Mar. 1995.

[229] B. Das and V. Bharghavan, "Routing in *ad-hoc* networks using minimum connected dominating sets," *IEEE International Conference on Communications, 1997. ICC '97 Montreal, Towards the Knowledge Millennium*, vol. 1, pp. 8–12, Jun. 1997.

[230] J. Broch, D. A. Maltz, and D. B. Johnson, "Supporting hierarchy and heterogeneous interfaces in multi-hop wireless *ad hoc* networks," *Fourth InternationalSymposium on Parallel Architectures, Algorithms, and Networks, 1999*, pp. 370–375, Jun. 1999.

[231] U. Jonsson, F. Alriksson, T. Larsson, and P. Jhansson, "MIPMANET-mobile IP for mobile *ad hoc* networks," *2000 First Annual Workshop on Mobile and Ad Hoc Networking and Computing, 2000*, pp. 15–85, 2000.

[232] D. Niculescu and B. Nath, "*Ad hoc* positioning system (APS)," *IEEE Global Telecommunications Conference, 2001*, vol. 5, pp. 2926–2931, 2001.

[233] M. Grossglauser and D. N. C. Tse, "Mobility increases the capacity of *ad hoc* wireless networks," *Transactions on Networking, IEEE/ACM*, vol. 10, pp. 477–486, Aug. 2002.

[234] O. Younis and S. Fahmy, "HEED: a hybrid, energy-efficient, distributed clustering approach for ad hoc sensor networks," *IEEE Transactions on Mobile Computing*, vol. 3, pp. 366–379, Oct. 2004.

[235] S. P. Weber, X. Y. Yang, J. G. Andrews, and G. de Veciana, "Transmission capacity of wireless *ad hoc* networks with outage constraints," *IEEE Transactions on Information Theory*, vol. 51, pp. 4091–4102, Dec. 2005.

[236] L. Pelusi, A. Passarella, and M. Conti, "Opportunistic networking: data forwarding in disconnected mobile *ad hoc* networks," *IEEE Communications Magazine*, vol. 44, pp. 134–141, Nov. 2006.

[237] J. Zhao and G. H. Cao, "VADD: Vehicle-assisted data delivery in vehicular *Ad Hoc* networks," *IEEE Transactions on Vehicular Technology*, vol. 57, pp. 1910–1922, May. 2008.

[238] J. Harri, F. Filali, and C. Bonnet, "Mobility models for vehicular ad hoc networks: a survey and taxonomy," *IEEE Communications Surveys*, vol. 11, pp. 19–41, Dec. 2009.

[239] O. K. Tonguz, N. Wisitpongphan, and B. Fan, "DV-CAST: A distributed vehicular broadcast protocol for vehicular *ad hoc* networks," *IEEE Wireless Communications*, vol. 17, pp. 47–57, Apr. 2010.

[240] S. J. Kim and G. B. Giannakis, "Optimal resource allocation for MIMO *Ad Hoc* cognitive radio networks," *IEEE Transactions on Information Theory*, vol. 57, pp. 3117–3131, May. 2011.

[241] K. B. Huang, "Spatial throughput of mobile *Ad Hoc* networks powered by energy harvesting," *IEEE Transactions on Information Theory*, vol. 59, pp. 7597–7612, Sept. 2013.

[242] V. Sharma and R. Kumar, "An opportunistic cross layer design for efficient service dissemination over flying *ad hoc* networks (FANETs)," *2nd International Conference on Electronics and Communication Systems (ICECS)*, pp. 1551–1557, Feb. 2015.

[243] M. Mauve, J. Widmer, and H. Hartenstein, "A survey on position-based routing in mobile *ad hoc* networks," *IEEE Network*, vol. 15, pp. 30–39, Nov. 2001.

[244] Z. Kai, Z. Y. Yang, and W. J. Lou, "Opportunistic routing in multi-radio multi-channel multi-hop wireless networks," *IEEE Transactions on Wireless Communications*, vol. 9, pp. 3512–3521, Oct. 2010.

[245] Y. Yan, B. X. Zhang, J. Zheng, and J. Ma, "CORE: a coding-aware opportunistic routing mechanism for wireless mesh networks," *IEEE Wireless Communications*, vol. 17, pp. 96–103, Jun. 2010.

[246] H. Yetgin, K. T. K. Cheung, and L. Hanzo, "Multi-objective routing optimization using evolutionary algorithms," *2012 IEEE Wireless Communications and Networking Conference (WCNC)*, pp. 3030–3034, Apr. 2012.

[247] Q. W. Liu, S. L. Zhou, and G. B. Giannakis, "Cross-layer combining of adaptive modulation and coding with truncated ARQ over wireless links," *IEEE Transactions on Wireless Communications*, vol. 3, pp. 1746–1755, Sept. 2004.

[248] I. Gradshteyn and I. Ryzhik, *Table of Integrals, Series, and Products*. Elsevier Pte Ltd, 7th ed., 2007.

[249] *http://functions.wolfram.com/*.

[250] I. Ahmed, A. Ikhlef, R. Schober, and R. K. Mallik, "Power allocation for conventional and buffer-aided link adaptive relaying systems with energy harvesting nodes," *IEEE Transactions on Wireless Communications*, vol. 13, pp. 1182–1195, Jan. 2014.

[251] N. Zlatanov and R. Schober, "Buffer-aided relaying with adaptive link selectionfixed and mixed rate transmission," *IEEE Transactions on Information Theory*, vol. 59, pp. 2816–2840, Jan. 2013.

[252] M. Schöller, T. Taleb, and S. Schmid, "Neighborhoods as an abstraction for fish-eye state routing," *IEEE 20th International Symposium on Personal, Indoor and Mobile Radio Communications, 2009*, pp. 1396–1400, Sept. 2009.

[253] L. Hanzo, Y. Akhtman, L. Wang, and M. Jiang, *MIMO-OFDM for LTE, WiFi and WiMAX: Coherent versus Non-coherent and Cooperative Turbo Transceivers*. Wiley-IEEE Press, 1st ed., 2010.

[254] T. M. Cover and A. E. Gamal, "Capacity theorems for the relay channel," *IEEE Journal on Information Theory*, vol. 25, pp. 572–584, Sep. 1979.

[255] A. Host-Madsen and J. S. Zhang, "Capacity bounds and power allocation for wireless relay channels," *IEEE Transactions on Information Theory*, vol. 51, pp. 2020–2040, Jun. 2005.

[256] L. K. Kong, S. X. Ng, R. G. Maunder, and L. Hanzo, "Maximum-throughput irregular distributed space-time code for near-capacity cooperative communications," *IEEE Transactions on Vehicular Technology*, vol. 59, pp. 1511–1517, Jan. 2010.

[257] M. F. U. Butt, R. A. Riaz, S. X. Ng, and L. Hanzo, "Distributed self-concatenated coding for cooperative communication," *IEEE Transactions on Vehicular Technology*, vol. 59, pp. 3097–3104, Apr. 2010.

[258] S. F. Chang and D. G. Messerschmitt, "Designing high-throughput VLC decoder. I. concurrent VLSI architectures," *IEEE Transactions on Circuits and Systems for Video Technology*, vol. 2, pp. 187–196, Jun. 1992.

[259] S. B. Korada and R. L. Urbanke, "Polar codes are optimal for lossy source coding," *IEEE Transactions on Information Theory*, vol. 56, pp. 1751–1768, Apr. 2010.

[260] R. Y. Mesleh, H. Haas, S. Sinanovic, W. A. Chang, and S. Yun, "Spatial modulation," *IEEE Transactions on Vehicular Technology*, vol. 57, pp. 2228–2241, Jul. 2008.

[261] N. Zlatanov, R. Schober, and P. Popovski, "Buffer-aided relaying with adaptive link selection," *IEEE Journal on Selected Areas in Communications*, vol. 31, pp. 1530–1542, Oct. 2012.

Subject Index

Author Index

C

D

E

F

G

H

I

J

K

L

M

N

O

P

Q

R

S

T

Y

Z